BLOOD-BORNE CANCER METASTASIS: FROM MECHANISMS TO THERAPEUTICS

A Dissertation

Presented to the Faculty of the Graduate School

of Cornell University

In Partial Fulfillment of the Requirements for the Degree of

Doctor of Philosophy

by

Jiahe Li

August 2015

BLOOD-BORNE CANCER METASTASIS: FROM MECHANISMS TO THERAPEUTICS

Jiahe Li, Ph. D.

Cornell University 2015

Metastasis is the cause of about 90% of cancer-associated deaths, yet the mechanisms governing this clinically important process remain poorly understood. Distant metastases rely on hematogenous dissemination of circulating tumor cells (CTCs). Many studies have shown that CTCs do not mobilize in the circulation alone. Instead, through heterotypic interactions with endothelial cells and different types of blood cells, CTCs acquire the potential to metastasize to distant organs. For successful establishment of metastases, CTCs must adhere and transmigrate through the endothelium layer. Using prostate cancer (PCa) as a model, we discovered and investigated the role of α-1, 3-fucosyltransferase 6 (FT6) gene in PCa bone metastasis. It was found that overexpression of FT6 mediated enhanced adhesion of cancer cells to bone marrow endothelium and subsequent bone metastasis via expression of unique glycan structure on CTCs. This study can potentially lead to effective treatment of bone metastasis in PCa by targeting the FT gene. Moreover, the novel PCa bone metastasis mouse model can provide a platform for screening and identifying new chemical inhibitors to prevent bone metastasis.

The second part of this thesis focuses on development of effective therapeutic strategies for CTC targeting. TNF-related apoptosis-inducing ligand (TRAIL) was chosen as it has been suggested as a potent cytokine in killing CTCs. TRAIL resistance, however, is commonly detected in certain cancer subpopulations. A novel chemical compound, Piperlongumine was found to be capable of sensitizing TRAIL-resistant cancer cells to apoptosis through generation of reactive oxygen species (ROS).

In addition to the drug combination approach, two unique drug delivery platforms specific for CTC targeting were also developed. A large body of experimental evidence makes the case that platelets are physically associated with CTCs to facilitate metastasis in many cancer diseases. Inspired by this phenomenon, we first took a biomaterial approach to functionalize silica particles with platelet membranes and TRAIL. We also genetically modified bone marrow stem cells to produce TRAIL-expressing platelets. Both methods have demonstrated effective reduction of metastases in experimental mouse cancer models.

BIOGRAPHICAL SKETCH

Jiahe Li 李嘉禾 was born to Hanqing Li 李汉青 and Ping Hu 胡苹 in Zhihua Pan, a city in southwest China. Since his childhood, Jiahe enjoyed fishing, growing plants, Kayaking, and many other types of exploration of nature. These experiences have made him become interested in pursuing biological science to better understand the nature. He was enrolled in the biological science in China Agricultural University in Beijing, China in 2005. He ranked #1 in his academic performance in the class throughout four years of undergraduate study. In his sophomore year, to get better education and exposure to scientific research training he decided to study abroad after undergraduate study. With a few US's graduate school offers prior to his graduation from the college, he chose the biomedical engineering program at Cornell University thanks to its strengths in physical science, engineering, and biological science. He spent his first two years in Prof. Xiling Shen's group where he was working on using synthetic biology tools to understand the asymmetric cell division of a bacterium. At the end of his second year, he joined Prof. Michael King's research group after realizing that he was more interested in the biomedical research instead of fundamental study in bacteria. Benefiting from the multidisciplinary research environment in King lab, Jiahe developed two creative therapeutic approaches based on platelets to target and neutralize circulating tumor cells in the bloodstream. He has demonstrated himself as an independent, innovative and collaborative researcher. He is looking forward to a career in academia in the near future.

To my parents and friends, for their endless love and support.

ACKNOWLEDGMENTS

There are so many people to whom I am extremely grateful. First and foremost, I would like to thank my parents Hanqing Li and Ping Hu who have been constant supporters in my endeavors and every big decision since I was born. During my six years of PhD study, I have been back to my home country China only twice. I felt deeply sorry to my parents when they asked me when to come to visit them every time during the phone call. I have been grateful for their understanding of my pressure and stress as a PhD student in a foreign country. I have been doing my best to make them feel proud of their son by sharing every great moment in academics, social life and cycling races.

My girl friend, Jeerapond Leelawattanachai has been my great supporter throughout my PhD study. We met each other at Cornell University when she was a second-year graduate student in the same department. I am a nerdy person who has little romance. Nevertheless, I started to impress her by teaching her experiments and gradually we ended up dating each other. We helped each other both experimentally and in daily life in the following four years. She graduated a year before me and had to go back to her home country Thailand as an earlier agreement with the Thai government for the financial support of her PhD study.

I am extremely grateful to my advisor, Michael King for providing me with the great resource to learn and grow. Thank you to my committee members, Prof. Dave Putnam and Prof. Matthew DeLisa, for their feedback throughout my projects.

I have learned so much from all of the members of the King research group, and I have been motivated by the dedication exhibited by everyone. Thank you to Weiwei Wang and Jong-wei Hsu, both of whom were incredible mentors and friends. Jeff Mattison has been a wonderful lab manager and has given me so much assistance in my PhD studies. Thong Cao has been an energetic and enthusiastic graduate student in the lab and always enjoys discussing research topics with me. Carlos Castellanos, a scientific genius, has been one of the best graduate students I've ever met.

I feel proud of all my undergraduate and master students whom I have been mentoring or working with in the past three years. Charles Sharkey (BS, Chemical Engineering, Cornell University) has demonstrated exceptional work ethic and research talents while working closely with me for three years. He was very helpful and patient when editing my manuscripts. Dantong Huang and James Messing were amazing undergraduates in doing scientific researches who later turned master students in our lab. Qianhui Wu and Sweta Roy (Meng, Biomedical Engineering, Cornell University) impressed me so much with their strong commitment to research in our lab despite huge study pressure from endless homework and classes.

Last but not the least, I would like to thank all my friends and colleagues in Ithaca who have been tremendously helpful for my living and PhD career. Dr. Songming Peng and Dr. Dayong Yang from Prof. Dan Luo's lab, Dr. Pengcheng Bu from Prof. Xiling Shen's lab, Dr. Bing Duan from Prof. Butcher's lab, thank you for your scientific advice for my PhD research. My only social life in bike racing has also made

the completion of the thesis possible given the stress of meeting several deadlines. David Stauffer, Jason Chari, Sammy Mosley, Lenore Pipes, Daniel Stauffer, and all other Ithaca's local bike racers, thank you for training and racing with you together in the amazing finger lake areas.

TABLE OF CONTENTS

LIST OF FIGURES

LIST OF TABLES

CHAPTER 1 INTRODUCTION

* This section is adapted from the following publications:

1. Li J, King MR. Adhesion receptors as therapeutic targets for circulating tumor cells. Front Oncol. 2012; 2:79.
2. Li J, Sharkey CC, Huang D, King MR. Nanobiotechnology for the Therapeutic Targeting of Cancer Cells in Blood. Cellular and Molecular Bioengineering. 2015:1-14.

1.1 Adhesion receptors as therapeutic targets for circulating tumor cells

Circulating tumor cells (CTCs) are cells that leave a primary tumor and circulate in the blood. More than a century ago the Australian physician, Thomas Ashworth first observed circulating tumor cells (CTCs) in the blood of a patient with metastatic cancer. He hypothesized that "the cancer itself being seen in the blood may tend to throw some light upon the mode of origin of multiple tumors existing in the same person." In the past decade, advancing technologies to detect and isolate CTCs have provided unique fluid biopsy information for prognosis, management of chemotherapy dosing and timing as well as monitoring the development of drug resistance over time [1-3]. Driven by these technologies, numerous clinical studies performed for breast, colon, prostate and other epithelial cancers establish a clear connection between average CTC counts and overall survival rate before and during treatment [4-10].

In contrast to the rapid development of tools for CTC detection and isolation, effective therapies that directly remove CTCs from the blood circulation are still underexplored. This is probably attributable to our limited understanding of the heterogeneity of CTCs: in most studies, CTCs are defined as being positive for epithelial cell adhesion molecule ($EpCAM^+$) and cytokeratin 8, 18 or 19 (CK^+) and negative for CD45 ($CD45^-$) [11]. However, almost a third of patients with advanced breast, colorectal and prostate cancers have CTCs that do not meet these criteria [12]. Despite the heterogeneity of CTC markers, some studies have shown that cancer stem cell (CSC) or stem-like cell (CSC-like) markers are frequently expressed by CTCs [13-18]. Such features are especially relevant for targeting CTCs as CSCs are believed to represent a

subpopulation of cancer cells that drive the growth and progression of metastatic cancers [19, 20].

The presence of CTCs in the circulation can in part explain a clinical observation that the removal of a primary tumor is often followed with distant metastasis and/or local recurrence. For example, it was estimated that 20% to 50% patients first diagnosed with primary breast cancer eventually developed metastatic disease in the past [21]. In the case of hepatocellular carcinoma (HCC), liver transplantation is the best treatment for early-stage patients. Unfortunately, every year around 10% of recipients develop post-transplant HCC recurrence, which leads to death in almost all patients [22]. To understand the molecular mechanism, Kim and colleagues developed a tumor self-seeding mouse model whereby the local recurrence mediated by CTCs was investigated using human colorectal, melanoma and breast cancer cells. They found that tumor-derived IL-6 and IL-8 served as CTC attractants whereas the seeder CTCs highly expressed invasion-associated genes (*MMP1*, *FSCN1* and *CXCL1*) to promote infiltration [23]. This finding highlights a highly orchestrated process of local recurrence mediated by CTCs.

CTCs play a predominant role in the metastases to distant organs. In the blood circulation, CTCs are subject to a multitude of stresses including anchorage-dependent survival signaling, immuno-surveilance, and shear stress. For example, CTCs are deprived of integrin-dependent adhesion to extracellular matrix (ECM) components in comparison to nontransformed cells. Whereas such loss of anchorage induces

apoptosis (anoikis) in normal cell types, CTCs are particularly resistant to anoikis by promoting PI3K / Akt proliferation signaling and expression of anti-apoptotic proteins such as BCL2 [24, 25]. Notably, numerous research has demonstrated that CTCs do not mobilize in the circulation alone. Instead, through heterotypic interactions with endothelial cells and different types of haemopotoeic cells, CTCs acquire the potential to metastasize to distant organs (**Figure 1.1**). Therefore, such receptor-mediated adhesion can provide a unique opportunity for neutralizing CTCs either through the blockade of receptors or receptor-targeted drug delivery.

1.1.1 The biology of selectin-mediated hematogenous metastasis

Selectins are transmembrane glycoproteins which were initially found to bind specific glycoproteins on leukocytes. Three structurally related adhesion molecules, L-, E- and P-selectin are composed of an N-terminal C-type lectin domain which confers specific, Ca^{2+}-dependent carbohydrate-binding activity. It is followed by an epidermal growth factor (EGF)-like domain, a variable number of short consensus repeats domains (2, 6 and 9 for L-, E-, and P-selectin, respectively), a single-pass transmembrane domain and a short intracellular C-terminal tail [26]. Despite structural similarity, the three selectins have distinct tissue-specific expression and binding kinetics. L-selectin is constitutively expressed on the surface of almost all types of leukocytes and is cleaved from cell surface upon activation with a variety of cytokines and chemokines [27]. In contrast, the expression of E- and P-selectin is inducible on vascular endothelial cells during the inflammation. Whereas E-selectin depends on de novo mRNA synthesis, P-selectin is stored in Weibel-Palade bodies of endothelial cells. Additionally, platelets

express P-selectin which translocates from α-granules upon platelet activation [28].

The role of selectins in mediating the rolling and trafficking of neutrophils and monocytes to inflammation sites has been well studied. More recently, it has been proposed that CTCs adopt similar strategies to facilitate their initial entrapment in the vessels and the subsequent extravasation. Köhler and colleagues provided the first in vivo evidence that E- and P-selectin are essential for colorectal cancer metastasis. They generated a transgenic immuno-compromised mouse with E- and P-selectin doubly knocked out. Compared to wild-type mice, the double knockout mice with subcutaneously implanted colon cancer cells showed lung metastases reduced in number by 84% [29]. In agreement with earlier in vitro studies, a model was proposed in which the sialylated fucosylated glycans decorated on transmembrane proteins or specific lipids of CTCs mediate the rolling and adhesion to selectin-expressing endothelial cells. The role of selectin ligands in mediating the hematogenous metastasis of CTCs has been reviewed extensively elsewhere [30, 31]. However, this section focuses on therapeutic interventions of selectin binding that have been explored for the prevention of metastasis.

1.1.1.1 Carbohydrate-based inhibitors

Given that all three selectins recognize sialylated fucosylated glycans such as sLe^x, the sLe^x analogs have been shown to significantly prevent neutrophil accumulation and myocardial necrosis after ischemia and reperfusion in animal models [32-34]. This implies that the same analogs may be potent inhibitors for reducing CTC adhesion to

endothelium. Shirota and colleagues investigated the inhibitory effect of a sLe^x analog, GSC-150 on hepatic metastasis of human colon carcinoma in nude mice. They found that liver metastases were significantly attenuated when cancer cells were co-administered with GSC-150 [35]. In addition to sLe^x analogs, novel disaccharides have been generated which function as competitive substrate inhibitors for glycotransferases involved in the synthesis of sLe^x. To this end, a disaccharide compound was able to inhibit sLe^x formation in human monocytic leukemia cells, U937. Its therapeutic effect was further studied in Lewis lung carcinoma in vivo where the experimental metastasis was significantly reduced through the decreased expression of sLe^x [36]. Nevertheless, strategies to abrogate sLe^x-selectin interaction must be considered carefully. Given the turnover rate of selectins or glycotransferases, such carbohydrates may not have a long-lasting inhibitory effect. Moreover, as sLe^x is essential for directing neutrophils and lymphocytes to inflamed tissues, the chronic exposure to sLe^x analogs or metabolic inhibitors can interfere with the normal inflammatory response. Therefore, investigations on the cellular sLe^x synthesis that differentiate CTCs from leukocytes may provide more specific targeting of CTCs while reducing side effects.

1.1.1.2 Gene silencing of fucosyltransferases in CTCs

As the key determinants of selectin ligands, sLe^x and sLe^a are synthesized in the Golgi compartments by sequential actions of N-acetylglucosaminyl-, galactosyl-, sialyl- and fucosyl-transferases. Of note is the terminal step of transferring fucose to N-acetylglucosamine catalyzed by a family of fucosyltransferase (FT) genes [37]. At

least nine FUT genes have been identified in the human genome among which FUT3, 4, 6 and 7 have been well characterized. They are redundant in the synthesis of sialyl lewis carbohydrates but display cell type-specific expression. FUT4 and FUT7 are mainly expressed in blood cell lineages and play a key role in the selectin ligand-mediated migration of leukocytes during the inflammatory response [38]. In contrast, FUT3 and FUT6 are more associated with the progression of cancers, including breast [39, 40], prostate [41], lung [42], liver [43], and gastric cancer [44]. To exploit the therapeutic potential of targeting fucosyltransferases, our laboratory first confirmed that hematopoietic cell lines (HL60 and KG1a) predominantly express FUT4 and FUT7 whereas prostate cancer cell line MDA PCa2b mainly expresses FUT3. Next, siRNA against FUT3 reduced sLe^x expression on prostate cancer cells and significantly inhibited cell rolling and adhesion to a E-selectin-functionalized surface under physiological flow. In addition, the siRNA was able to impair cell growth which may not be directly associated with sLe^x. In fact, two recent studies revealed that the overexpression of FUT4 and FUT6 promoted cell growth by elevating intracellular Akt phosphorylation and suppressing the cyclin-dependent kinase inhibitor p21 in epidermoid carcinoma and hepatocellular carcinoma cells, respectively [45, 46]. Therefore, silencing FUTs via siRNA can simultaneously inhibit the adhesion and clonal expansion of CTCs in the blood circulation. To apply this strategy in vivo, P-selectin-based liposome nanoparticles recently developed in our laboratory can be used to encapsulate siRNAs against FUTs [47]. Although P-selectin recognizes both circulating leukocytes and CTCs, siRNAs against FUTs exclusively expressed in CTCs provide additional targeting specificity.

1.1.2 Therapeutic intervention of CTC-hematopoietic cell interaction

It is estimated that less than 0.01% of CTCs shed from a primary tumor can survive to produce clinically relevant metastases [48]. This suggests that the process of metastasis by CTCs is largely inefficient. Whereas the mechanisms underlying such high rates of attrition remain poorly understood, recent studies identified two important cell adhesion molecules involved in the physical interactions of CTCs with hematopoietic cells: vascular cell adhesion molecule-1 (VCAM-1) and intercellular adhesion molecule-1 (ICAM-1). Such interactions facilitate CTCs in several aspects: (1) survival in the circulation, (2) initial arrest and subsequent extravasation, and (3) eventual growth into overt metastasis [49].

The transmembrane protein VCAM-1 was originally thought to be presented exclusively on endothelial cells in response to tumor necrosis factor-alpha (TNF-α) and interleukin-1 (IL-1) during inflammation [50]. It binds to the leukocyte integrins α4β1 and α4β7 on circulating monocytes, granulocytes and lymphocytes [51, 52]. However, aberrant expression of VCAM-1 was found to be one of eighteen signature genes associated with lung metastasis of breast cancer in both experimental mouse models and patients [53]. Chen and colleagues found that VCAM-1 on breast cancer CTCs tethered to metastasis-associated macrophages which express α4-integrins. Clustering of VCAM-1 on CTCs induces Akt activation and protects CTCs from proapoptotic cytokines such as TRAIL. Notably, either silencing VCAM-1 expression by siRNA or blocking antibody against α4-integrins abolished the pro-survival effect

of VCAM-1[54]. In addition, VCAM-1 was also recently found to be associated with bone metastasis in breast cancer. Prior to this study, a bone-metastatic gene signature including *CXCR4*, *IL11*, *CTGF*, *MMP1* and *OPN* was identified through the reiterative selection of human breast cancer cells MDA-MB-231 in immuno-compromised mice [55]. However, by studying a subpopulation of MDA-MB-231 which experienced a long dormancy prior to bone metastasis, Lu and colleagues discovered that the aberrant expression of VCAM-1 engaged α4-integrins on monocytic osteoclast progenitors to promote the local osteolytic activity in bone [56]. This mouse study was further corroborated by comparing VCAM-1 levels between clinical early and late recurrences of bone metastases. Higher VCAM-1 was significantly associated with early relapse [57].

Like VCAM-1, ICAM-1 is another cell surface glycoprotein which is typically expressed on endothelial cells in response to TNF-α or IL-1 in inflammation. However, the constitutive expression of ICAM-1 on CTCs was found to promote tumor cell transendothelial migration in melanoma [58], pancreatic [59] and breast cancers [60]. To understand this mechanism, in vitro biophysical studies demonstrated that under physiological shear stress ICAM-1 on melanoma CTCs promotes the heterotypic interaction with neutrophils by engaging β2-integrins (CD11a and CD11b) [61, 62]. Moreover, as neutrophils have selectin ligands, such heterotypic interaction facilitates the adhesion and extravasation of melanoma CTCs which otherwise bind inefficiently to the endothelium [63, 64]. Later, our laboratory studied the physical mechanisms of retinoblastoma metastasis. Whereas human RB cell lines RB143 and WERI-Rb27 do

not express E-selectin ligands, they can be recruited to an E-selectin-coated surface through attachment to activated neutrophils. This interaction is also mediated by ICAM-1: β2-integrin [65]. To test the involvement of this heterotypic interaction in vivo, Jin Huh and colleagues compared the lung metastases of human melanoma cells injected alone or in combination with human neutrophils [58]. They found that human neutrophils enhanced CTCs retention in the lung by three-fold. To dissect the molecular mechanism, the cytokine interleukin-8 (IL-8) was found to be a key determinant expressed by melanoma cells to attract neutrophils. IL-8 secretion increased β2-integrin levels on neutrophils and heterotypic aggregation between ICAM-1-positive CTCs and neutrophils. Importantly, siRNA against IL-8 impaired transendothelial migration and lung metastasis by ~50%. In addition to targeting IL-8 as a therapeutic approach, it is possible that blocking antibodies against ICAM-1 or β2-integrins may be also effective [66].

1.1.3 Platelets aggravate CTC metastasis

Platelets are anuclear cytoplasmic bodies released from megakaryocytes in the bone marrow. It is estimated that one liter of blood contains about 400 billion circulating platelets. The primary role of platelets is to maintain haemostasis. This is initiated via platelet activation which results in adhesion and release of a multitude of bioactive factors from platelet granules. In addition to haemostatic regulation, platelets have long been believed to play a critical role in cancer metastasis through the enhancement of CTC survival and adhesion to the endothelium in the circulation. The involvement of platelets in cancer was first recorded in the mid-nineteenth century by the French

clinician Armand Trousseau. He diagnosed patients with migratory thrombophlebitis caused by an occult visceral carcinoma [67]. In fact, preclinical studies in genetic knock-out mice provide evidence that upon immediate entry into the circulation, tissue factor highly expressed by CTCs can signal downstream through FVIIa and FXa to activate a coagulation cascade leading to thrombin generation, fibrin deposition and platelet aggregation around CTCs [68-70]. Such a "platelet cloak" is known to initially trap tumor cells in microvessels [71].

Several mechanisms of platelets in promoting CTC survival have been proposed based on preclinical experiments in mice using a variety of mouse and human carcinoma cell lines. Aggregation of platelets around CTCs protect against immune-mediated clearance of CTCs largely mediated by natural killer (NK) cells. The potential of CTCs to induce platelet aggregation correlates with their enhanced metastatic potential. Bernhard Nieswandt and colleagues demonstrated for the first time that platelets directly impair NK lysis of tumor cells *in vitro* and *in vivo*. In a mouse model of experimental metastasis, they found that tumor seeding in the lung was reduced when platelets were depleted from the host [72]. Further studies reveal that CTC evasion of NK cells is not merely attributed to physical shielding of platelets. NK cell activity is guided by the principles of "missing-self" and "induced-self," which imply that cells lacking expression of MHC class I (missing-self) and/or a stress-induced expression of ligands for activating NK receptors (induced-self) are preferentially recognized and eliminated [73, 74]. While CTCs are often associated with lack of MHC class I, platelets can disrupt "missing self" recognition of NK cells by grafting

MHC I class onto CTCs [75]. Furthermore, platelet-derived transforming growth factor β (TGF-β) can downregualte the activating immunoreceptor natural killer group 2, member D (NKG2D) on NK cells [76].

1.1.3.1 Therapeutic intervention of platelet adhesion to CTCs

As the blood-clotting pathway contributes to platelet adhesion to CTCs, a variety of anticoagulation agents have been tested either alone or together with conventional cancer drugs in preclinical mouse models. Using an experimental metastasis mouse model, Amirkhosravi and colleagues found that the intravenous injection of recombinant mouse tissue factor pathway inhibitor (TFPI) immediately before inoculation of tumor cells reduced metastasis by 83% [77, 78]. Similarly, Cilostazol, a selective inhibitor of phosphodiesterase 3 with anticoagulatory and profibrinolytic effects completely abolished the complex formation of 4T1 tumor cells in the presence of activated platelets *in vitro*. In a spontaneous model of mouse 4T1 breast cancer, the injection of Cilostazol six hours before tumor inoculation reduced pulmonary metastasis by 55%. As platelet aggregation and adhesion to CTCs enhance their survival in the blood circulation, abrogation of the coagulation cascade renders CTCs susceptible to cancer drugs. Wenzel and colleagues invented dual liposomes simultaneously containing the hemostatic inhibitor dipyridamole and the anticancer drug perifosine. The liposomes caused a 90% reduction in the number of lung metastases in a mouse experimental metastasis model [79].

Despite the fact that anticoagulants hold promise for the prevention of metastasis, they

may impair the normal hemostatic function of platelets in the presence of bleeding. Platelet intervention therapies against metastasis must exhibit certain specificity for tumor cell-platelet interactions. Therefore, direct inhibition of platelet adhesion to CTCs may minimize the cardiovascular side effect of anticoagulants. To this goal, heparin and chemically modified heparins have been shown to attenuate the metastasis of human colon carcinoma in a mouse xenograft model [80-82]. The anti-metastatic effect of heparin was initially believed to associate with its anticoagulant activity. Later it was found that competitive binding of heparin to P-selectin on activated platelets abolishes interaction with P-selectin ligands such as sialylated fucosylated mucins expressed on human colon carcinoma cells [80, 82-84]. As the anticoagulant activity of heparin is undesirable in the context of blocking CTC-platelet interactions, polysaccharides isolated from certain sea plants and fungi have shown enhanced inhibition of P-selectin binding without anticoagulant effect. A fucosylated chondroitin sulfate (FucCS) from sea cucumber is 4-8 fold more potent than heparin in the inhibition of LS180 carcinoma cell attachment to immobilized P-and L-selectin. Moreover, administration of FucCS 30 min prior to mouse colon carcinoma MC-38 injection is associated with 2-fold less CTC-platelet aggregates than heparin in the mouse lung. Long-term experiment reveals that FuCS significantly reduced lung metastatic foci by 80% compared to saline control [85].

1.1.3.2 Therapeutic blockage of platelet signaling to CTCs

Certain CTCs express epithelial markers such as EpCAM and cytokeratins, suggesting that the epithelial-mesenchymal transition (EMT) is not necessarily required for CTCs

to access the blood circulation. Instead, a transient contact between platelets and CTCs in the blood circulation is sufficient to induce an EMT gene signature and invasive behavior primarily through the platelet-secreted transforming growth factor-β1 (TGF-β1) [86]. Recently, a small molecule inhibitor, SD-208, has been shown to block the TGF-β receptor I kinase (TβRI) activity. SD-208 successfully prevented the development of TGF-β-induced bone metastases and decreased the progression of established osteolytic lesions in a melanoma mouse model [87]. Therefore, SD-208 possibly represents a viable therapeutic to inhibit platelet-derived TGF-β signaling. In addition to TGF-β, platelet α-granules store abundant proangiogenic factors including vascular endothelial growth factor (VEGF), basic fibroblast growth factor (bFGF), epidermal growth factor (EGF), platelet-derived growth factor (PDGF) and insulin-like growth factor-1 and -2 (IGF-1 and -2) [88]. Given that inhibitors for the proangiogenic factors or their counter-receptors are available as cancer drugs in the treatment of solid tumors [89-91], it is possible that such inhibitors can be used as adjuvant therapies in the context of targeting CTCs.

1.1.4 Novel selectin-based targeting drug delivery to CTCs

Over the past several years, our laboratory has developed a biomimetic approach to isolate CTCs using a selectin-immobilized microtube device [92, 93]. Two factors are responsible for the efficient capture of CTCs by this device. First, the ability of selectins to mediate the rapid tethering and rolling of leukocytes or CTCs under shear is attributed to the fast kinetics between selectins and selectin ligands [94, 95]. The fact that cells can be enriched under flow conditions significantly enhances the

sample-processing rate. Second, the microtube allows for the margination of CTCs toward the wall to interact with immobilized selectins. This margination effect has been well characterized when leukocytes circulate in a flow-dependent interaction with red blood cells [96-98].

Inspired by isolating CTCs under flow conditions, we translated the device to a unique drug delivery platform whereby the immobilization of drug molecules on the surface creates a high localized concentration. One device immobilizes E-selectin-conjugated liposomes onto the surface of a blood-compatible microrenathane (MRE) tube. After encapsulating doxorubicin (DOX), the liposomes could specifically capture cells from the flow and efficiently deliver DOX into adherent cells. Moreover, a halloysite nanotube (HNT)-coated surface further enhanced the targeting and killing of cancer cells, which was attributed to the increased surface area for both E-selectin and DOX.

To provide more specificity to CTCs, two additional approaches have been pursued by our laboratory. One approach was to functionalize the microtube surface with both E-selectin and antibodies against epithelial markers such as EpCAM. Such additional antibodies were able to discriminate between leukocytes and CTCs when cells roll on the surface [93]. The second approach was to replace DOX with molecules that are tumor-specific, such as TNF-related apoptosis-inducing ligand (TRAIL). TRAIL holds promise as a tumor-specific therapeutic as it selectively induces an apoptotic signal by binding to death receptors on the cell surface [99, 100]. To this end, our lab developed a death receptor-mediated apoptosis device to deliver apoptosis signal to captured

CTCs. Notably, with TRAIL and E-selectin on the surface, one hour of rolling exposure was sufficient to kill 30% of leukemia cells (HL60) whereas the viability of normal mononuclear cells was not affected [101].

Conclusion

In haematogenous metastasis, a primary tumor sheds CTCs into the blood circulation which comprise a population of carcinoma cells that can exhibit CSC or CSC-like features. Two hypotheses have been proposed regarding how CTCs establish the initial contact with endothelial cells prior to metastasis. The physical trapping hypothesis is based on the fact that the luminal diameter of capillaries is ~8 μm while the diameter of CTCs ranges from 20 to 30 μm. Thus, CTCs can be simply mechanically trapped in the capillary bed during their first pass through the circulation [102]. However, the findings that certain CTCs display organ-specific tropism (e.g. bone metastases in breast and prostate cancer) challenge this hypothesis [41, 55]. In fact, by displaying selectin ligands on their surface, CTCs in certain cancers acquire the ability to roll and adhere to the endothelium and subsequently exit from the circulation. The identification of selectin-dependent metastasis has made it possible to develop a range of antagonists against selectins or selectin ligands. Such antagonists have proven efficient in reducing experimental metastases in many mouse cancer models. However, they may impair the selectin-dependent trafficking of leukocytes to inflamed areas during the normal inflammatory response. The gene silencing of specific FUTs may confer specificity to CTCs as different FUTs have been shown to differentially express in CTCs versus leukocytes [103]. Nevertheless, the CTC-

endothelium interaction alone is not sufficient for CTCs to overcome damages incurred by hemodynamic shear forces and immuno-surveillance. The survival of CTCs in the blood circulation also depends on the interactions with hematopoietic cells such as macrophages, neutrophils and platelets which require distinct adhesion receptors. Though the abrogation of individual adhesion receptors has shown promising results in a variety of mouse cancer models, it may be clinically relevant to develop a cocktail therapy which simultaneously targets multiple interactions between CTCs and other cell types.

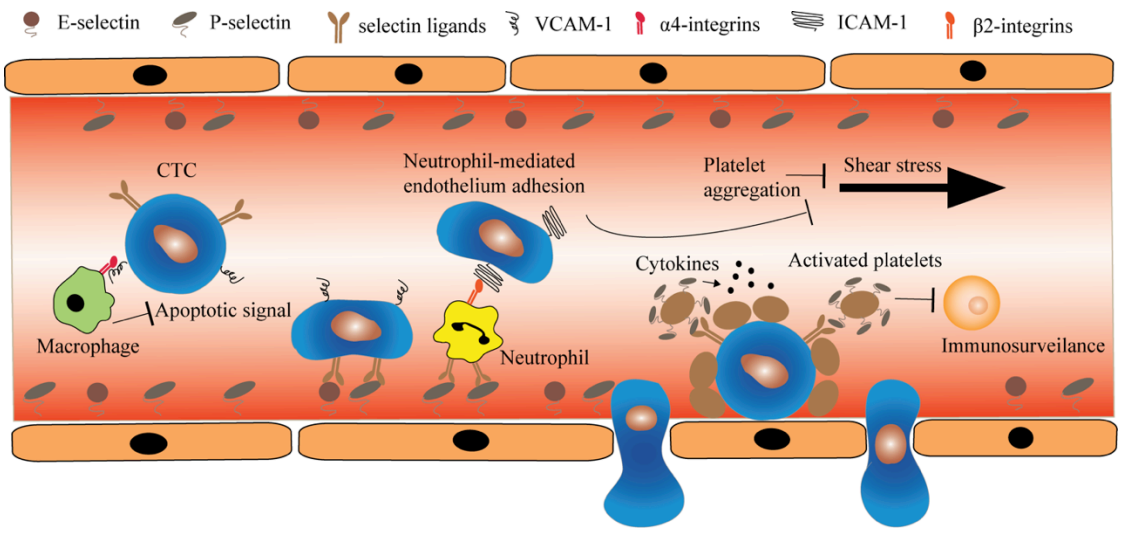

Figure 1.1. The heterotypic cell interactions between CTCs and hematopoietic cells in the circulation. Through heterotypic interactions with endothelial cells and different types of hematopoietic cells, CTCs acquire the potential to metastasize to distant organs.

1.2 Nanobiotechnology for the therapeutic targeting of cancer cells in blood

Metastasis contributes to more than 90% of cancer-associated mortality [104]. It is generally hypothesized that primary tumors shed circulating tumor cells (CTCs) via the lymphatics to neighboring lymph nodes or through hematogenous dissemination to distant organs. The presence of CTCs in the blood represents a poor prognosis in a variety of carcinomas [49, 102, 105]. Nevertheless, the effective treatment for this deadly disease remains clinically challenging. In the case of hematogenous metastasis, CTCs must complete several sequential steps: (1) detachment from the primary tumor, (2) intravasation into the vascular system, (3) survival in the blood circulation, and (4) extravasation into the target tissue [31]. The finding that very few metastases develop despite the release of millions of CTCs into the vasculature daily by large primary tumors suggests that the process of metastasis is very inefficient [106]. This is consistent with a recent experimental demonstration that only a small subpopulation of metastasis-initiating cells (MICs) among human luminal breast cancer CTCs gave rise to distant metastases in mice and the existence of MICs correlated with overall metastatic incidence in patients [107]. Therefore, early metastasis intervention procedures, such as neutralization of CTCs and particularly MICs in circulation, may offer new therapeutic opportunities.

The majority of existing cancer therapies including nanomedicine- and nanoformulation-based therapeutics target solid tumors (primary and metastatic) [108]. The underlying principle of most current nanotechnology-based drug delivery platforms is based on the observation that tumor-associated vasculatures are more

leaky than normal vessels and thus are more permeable to nanoparticles and macromolecules. Additionally, solid tumors retain large molecules due to inefficient lymphatic drainage [109, 110]. While the enhanced permeability and retention (EPR) effect has proven to be a key pharmacokinetic feature for existing nanomedicines, this mechanism is not applicable to potential nanomedicines that target CTCs in circulation. The physical and biological environments surrounding CTCs are drastically different from those of solid tumors. CTCs are exposed to a broad range of fluid shear stresses when transiting in different vascular compartments (arteries, veins and capillaries). Compared to non-transformed epithelial cells, transformed cells are remarkably resistant to varied fluid shear stress (FSS) [111]. In contrast, cancer cells in solid tumors are subjected to high interstitial fluid pressure caused by the stiff extracellular matrix [112, 113]. Additionally, certain CTCs gain the advantage of metastasis via interactions with different blood cells (neutrophils, macrophages, platelets, etc.) whereas solid tumors become aggressive by benefiting from hypoxia or certain tumor-promoting cells such as tumor-associated macrophages [48, 60, 105, 114]. These differences suggest that existing nanomedicines dependent on the EPR effect for targeted drug delivery must be tailored to the specific requirements for the neutralization of CTCs in circulation (**Figure 1.2**).

In this review, we summarize the interactions of CTCs with different host cells during their hematogenous transit and how blocking CTC-host cell interactions via drug molecules have reduced metastases in animal models of cancer. Since the majority of these drugs suffer from fast clearance from circulation, methods to improve their

circulation time through existing nanotechnologies will be discussed. Particularly, novel biomimetic CTC-targeting nanotechnologies are highlighted. Finally, potential CTC neutralization strategies that bridge conventional nanomedicine with technologies that are being utilized for CTC isolation and enumeration are discussed.

1.2.1 Biology of circulating tumor cells

1.2.1.1 Aberrant biological events in CTCs

Solid tumors, at either primary or metastatic locations, can be accessed surgically with sufficient quantity for diagnostic tests and studies involving genomic sequencing, gene expression microarrays, immunohistology and mass spectrometry. In contrast, it remains a challenge to study the biology of rare CTCs in blood with conventional techniques. Efficient CTC isolation together with single-cell RNA-sequencing, exosome sequencing and immunofluorescence staining have enabled the discovery of several intracellular biological events underlying CTC-mediated metastasis. These events include but are not limited to: upregulation of Wnt2 in pancreatic cancer-derived CTCs [115], p53 mutation within CTCs of prostate cancer [116], activation of TGF-β and BMP signaling in CTCs from melanoma [117], and EGFR mutation in lung cancer CTCs [118]. More generally, in nearly all epithelial cancers, a subpopulation of CTCs exist that are characterized by epithelial-to-mesenchymal transition (EMT) markers [119-123]. During EMT, representative epithelial markers such as EpCAM and E-cadherin are downregulated, keratin expression pattern is altered, and mesenchymal markers such as N-cadherin, vimentin and Snail are upregulated in turn [124, 125]. Entry to the mesenchymal state confers specific

properties to CTCs including invasiveness, resistance to anoikis, chemo-resistance and cancer stemness [126-129]. Regardless of changes in signaling pathways and genomic integrity identified in CTCs, it remains to be answered whether these alterations merely mirror tumor progression and evolution occurring at primary and secondary tumors where CTCs are being shed. It has been postulated that subpopulations of metastasis-initiating cells (MICs) and cancer stem cells (CSCs) contribute to metastases in distant organs [13, 107]. It is of clinical significance if targeting of the aberrant signaling pathways could reduce the frequency of MICs and CSCs and thereby lead to better prognosis.

1.2.1.2 Selectin-mediated hematogenous metastasis

Selectins (L-, E-, and P-selectin) are integral membrane glycoproteins. They share several structurally similar domains: an N-terminal C-type lectin domain, an epidermal growth factor (EGF)-like domain, a variable number of short consensus repeats (2, 6, and 9 for L-, E-, and P-selectin, respectively), a single-pass transmembrane domain, and a short intracellular C-terminal tail [26]. L-selectin is constitutively expressed on the surface of leukocytes whereas E- and P-selectin are restricted to inflamed endothelial cells [27]. It has been well accepted that during inflammation, the presence of E- and P-selectin on the endothelium causes the rolling and migration of neutrophils and monocytes which express selectin ligands [130, 131].

Selectin ligands, however, are not limited to leukocytes. Instead, they have been identified on the surface of certain cancer cells. Several lines of evidence support that

both E- and P-selectin facilitate the rolling and adhesion of CTCs in hematogenous metastasis. Köhler and colleagues provided the first in vivo finding that E- and P-selectin are essential for colorectal cancer metastasis. In their study, E- and P-selectin double knockout mice had a 84% reduction of lung metastatic nodules by number compared to wild-type mice after they were subcutaneously implanted with HT29 colon cancer cells [29]. Lung endothelial cells, however, do not constitutively express E- and P-selectin unless they receive inflammatory signals. It is not clear how selectins mediated the adhesion of HT29 cells to the lung endothelium. In contrast to the lungs, endothelial cells in the bone marrow constitutively express E-selectin [132, 133]. Studies have shown that E-selectin ligands on both human and mouse prostate cancer (PCa) cells facilitated bone metastasis in an E-selectin dependent manner [103, 134, 135]. Instead of utilizing the E-selectin knockout mice, these two studies overexpressed α-1, 3 fucosyltransferases (FTs) in E-selectin ligand (ESL)-negative human and mouse PCa cell lines based on the findings that ESL-positive PCa cells highly express FT3, 6 or FT7. Consequently, these engineered PCa cells produced increased incidence of bone metastasis in mice. The role of specific selectin ligands in mediating the hematogenous metastasis of CTCs has been reviewed extensively elsewhere [30, 31, 105]. This review, however, focuses on how nanobiotechnology can be utilized to inhibit the interaction between cancer cells and the endothelium for the prevention of metastasis.

Given that selectins recognize sialylated fucosylated glycans on selectin ligands such as sLe^x, sLe^x analogs have been explored as competitive inhibitors for the binding of

CTC selectin ligands to E- and P-selectin. For instance, a sLe^x analog, GSC-150, was tested for its effect on hepatic metastasis of human colon carcinoma in nude mice. It was found that liver metastases were significantly attenuated when cancer cells were co-administered with GSC-150 [35]. In addition to sLe^x analogs, compounds that can interfere with the synthesis of sLe^x represent another class of selectin inhibitors. Li and colleagues showed that a fluorinated fucose mimetic (2F-Peracetyl-Fucose) could be used to reduce E-selectin-dependent bone metastasis in mice by inhibiting the activity of FT6 [134].

1.2.1.3 Contribution of platelets to CTC-mediated metastasis

The involvement of platelets in cancer was first reported in the mid-nineteenth century by the French clinician Armand Trousseau [136]. He diagnosed patients with migratory thrombophlebitis caused by an occult visceral carcinoma. Mounting evidence has shown that interaction of platelets with tumor cells can promote metastasis through several mechanisms. For instance, interactions with platelets protect CTCs from immune-mediated clearance [72-74], because such adhesion events affect the recognition of CTCs by natural killer cells. Platelet aggregation can result in the grafting of MHC class I ligands onto CTCs, which are typically absent. The newly acquired ligands prevent natural killer cells from identifying the CTCs as "non-self" and spare them from attack [75]. Additionally, activated platelets can induce EMT as well as pro-surival and pro-metastatic signalings in tumor cells, which are associated with enhanced invasiveness and metastatic potential [86, 137, 138].

It has been demonstrated that therapies targeting the interactions between platelets and CTCs can reduce the formation of secondary metastases. One approach to minimizing these interactions has focused on utilizing anti-coagulation agents. Agents such as recombinant mouse tissue factor pathway inhibitor (TFPI) and Cilostazol have been found to reduce the formation of secondary metastases [77, 78, 139]. Unfortunately, the use of anticoagulants may also adversely affect the normal hemostatic function of platelets in the case of bleeding. A more focused approach aims to block the signaling between platelets and CTCs. Invasive behavior can be induced by transforming growth factor-β1 (TGF-β1), which is secreted by activated platelets. Temporary contact with platelets is sufficient to induce invasive behavior in CTCs through TGF-β1 [86]. Blockage of TGF-β1 receptor I (TβR1) kinase activity through the use of SD-208, a small molecule inhibitor, was shown to prevent the development of TGF-β induced bone metastases in a melanoma mouse model [87]. Thus, blocking platelet-CTC signaling is a potentially viable targeted therapy to prevent the formation of additional metastases.

1.2.2 Challenges of targeting CTCs by nanomedicine

Although nanomedicine is a very general concept and represents a broad range of nanoformulations for existing drugs, it manifests itself largely in targeted drug delivery and controlled release. The biological characteristics of CTCs and the physical environment where they reside may pose certain challenges and problems when targeted by nanomedicine (**Table 1.2.1**). Searching for a rare number of CTCs in circulation is likely analogous to the problem of finding a needle in a haystack [140,

141]. This challenge may be solved by adopting the strategies utilized for CTC capture and enrichment. For example, targeting moieties for CTC isolation, such as anti-EpCAM monoclonal antibody, can be functionalized onto nanoparticles for the recognition of CTCs with epithelial origin in circulation [142].

The heterogeneity of CTCs, however, dictates that there is no universal antigen for comprehensive targeting. CTC phenotypes can be categorized into epithelial (epithelial^{+}/mesenchymal^{-}), complete EMT (epithelial^{-}/mesenchymal^{+}), and intermediate EMT (epithelial^{+}/mesenchymal^{+}) [143, 144]. It is possible that all three phenotypes exist in the circulation simultaneously and thus targeting CTCs with epithelial features may become ineffective against those with mesenchymal characteristics [145]. Moreover, CTCs can also be divided into CSCs and non-CSCs according to their tumor-initiating capability, which is not necessarily coupled to the EMT status [146]. This raises the question of whether it is necessary to neutralize all CTCs in circulation to achieve a net reduction in metastasis.

CTCs have been detected both as individual cells and as cellular clusters in blood [147, 148]. Although rare in circulation compared to individual CTCs, CTC clusters show increased invasiveness, are more resistant to anoikis and have a higher likelihood of becoming trapped in microvessels, thereby favoring their survival and extravasation into distant organs [149, 150]. In a study using breast cancer CTCs, it was been found that CTC clusters display a 23- to 50-fold increase in metastatic potential. Moreover, high expression of the cell junction protein plakoglobin was identified as responsible

for this intercellular adhesion [151]. In addition to promoting invasiveness, it is reasonable that, in large cell aggregates, the cells within the core may be less accessible to nanomedicine approaches compared to those at the periphery.

Recently, *ex vivo* culture of breast cancer CTCs has enabled individualized testing of drug susceptibility [152]. Although such a strategy is mainly utilized for the treatment of solid tumors, which are the origin of the CTCs expanded ex vivo, it remains unclear whether the drugs selected from such screening would be effective against CTCs in blood compared to the CTC cell lines expanded in culture medium. In light of several protective effects associated with the adhesion of platelets to CTCs in blood as discussed in Section 1.2.1.3, platelet shielding may not only provide a physical barrier to nanomedicine-mediated drug delivery to CTCs, but also potentially confer drug resistance.

The systemic dissemination of CTCs defines a requirement that nanomedicine vehicles must exist in the circulation for an extended period of time to patrol for metastatic CTCs released from solid tumors. When conventional cancer drugs with systemic cytotoxicity such as doxorubicin and paclitaxel are utilized for CTC neutralization, they should ideally be released only after nanocarriers encapsulating the drugs have been internalized into CTCs to avoid off target effects on normal tissues [153, 154]. In contrast, when more cancer-specific therapeutics such as monoclonal antibodies and tumor necrosis factor−related apoptosis-inducing ligand (TRAIL) are applied to target CTCs, such systemic toxicity may be less of a concern

[99, 100, 155]. In addition to their systemic nature, CTCs are reported to have a relatively short half-life (<24 hours) in circulation [156-158]. This provides a narrow time window for efficient killing of CTCs via nanomedicine approaches. A rational solution to this challenge is to design nanocarriers with extended circulation times. Recently, Michael King's group demonstrated for the first time that leukocytes coated with TRAIL-liposomes were able to efficiently neutralize CTCs in an experimental metastasis mouse model. Such approach utilizes the long circulation time of leukocytes to deliver apoptosis signal to cancer cells with minimal side effect on normal cells such as leukocytes and endothelium [159]. An alternative strategy, however, is to deliver drugs that inhibit intravasation of cancer cells via enhanced tumor cell-matrix interactions [160].

1.2.3 Potential paradigms of conventional nanomedicine in CTC neutralization

Despite the promise of utilizing synthetic compounds for blocking selectin-mediated CTC metastasis or inhibitors for blocking platelet-CTC interactions and signaling, these compounds are likely to be cleared from the body within a short time period via renal filtration due to their relatively low molecular weight (LMW) [161]. Therefore, frequent administration of these molecules is necessary and may become prohibitively expensive for clinical implementation. Nevertheless, the paradigms that have been exploited for nanoparticles and nanoformulations over the past few decades are potentially applicable to extend the circulation time of these LMW compounds. To date, two nanoformulations for treating solid tumors have been approved for clinical use, specifically liposomal doxorubicin (Doxil) and protein-bound paclitaxel

(Abraxane) [162]. One major obstacle to using nanoparticles in vivo is rapid clearance by the mononuclear phagocyte system (MPS). The main strategy for extending the circulation time of nanoparticles is by grafting uncharged hydrophilic polymers onto the surface of particles to create so-called "stealth" particles, with the most commonly used polymer being polyethylene glycol (PEG) [163-165]. By encapsulating sLe^x analogs or fucosyltransferase inhibitors into nanoparticles with PEG-coated surfaces, this is likely to achieve both controlled drug release and extended circulation time. In addition to the intervention of selectin-mediated adhesion of CTCs to endothelium via ESL inhibitor-encapsulated nanoparticles, a coexisting or alternative adhesion event mediated by ICAM-1 (expressed on vascular endothelium) and MUC1 (expressed on some CTCs) has been shown as a potential target for the prevention of metastasis [166, 167]. The Decuzzi lab recently demonstrated that long circulating lipid–polymer nanoparticles encapsulating curcumin were able to substantially reduce the adhesion of highly metastatic human breast cancer cells MDA-MB-231 to TNF-α-treated HUVEC cells in an ICAM-1- and MUC1-dependent manner [168] . It remains to be determined, however, whether such curcumin-encapsulated nanoparticles would be effective in mouse models with experimental and/or spontaneous metastases.

Alternatively, sLe^x or synthetic sLe^x analogs can be functionalized onto the surface of nanoparticles for targeting tumor-associated endothelium. For instance, sLe^x-conjugated liposomes loaded with cisplatin have been shown to accumulate on an E-selectin-expressing endothelium in the vicinity of tumor cells. It was found that sLe^x-conjugated liposomes enabled six-fold higher cisplatin accumulation than non-

conjugated liposomes in tumors [169]. Although this nanoformulation was intended to target solid tumors as opposed to CTCs, an additional benefit may have been to help neutralize CTCs that reseed into solid tumors [23]. Bone-metastatic prostate cancer (PCa) cells bearing ESLs are known to attach more avidly to bone marrow (BM) endothelial cells which constitutively express E-selectin [41, 134]. Therefore, sLe^x-conjugated nanoparticles encapsulating cancer therapeutics can potentially deliver conventional cancer drugs to the BM niche of CTCs for the prevention and treatment of BM metastasis in prostate cancer.

1.2.4 Advanced nanotechnologies in CTC targeting

1.2.4.1 Effect of nanoparticle morphology on their fate in blood circulation

Many nanoparticle designs have been proposed for cancer therapy and diagnosis, with varied biodistribution in blood circulation depending on their administration route, particle size, composition and surface charge [170]. In general, polymeric nanoparticles less than 10 nm in diameter may be easily cleared by the kidneys as blood carries them through the renal system, and particles greater than 100 nm may be easily cleared by phagocytic uptake and hepatic filtration [171]. For the targeting CTCs that extravasate from the vessel wall of the microvasculature, nanoparticles that exhibit the capability to adhere to the vascular wall may be more effective at delivering therapeutic cargo to CTCs [172]. Gentile et al [173] have shown that for spherical particles, large particles will have better margination compared to small particles that are less than 200 nm in diameter. Margination is a biorheological process in which semi-rigid cells and particles are displaced toward the vessel wall in

circulation, providing more opportunities for interactions with the endothelium [173] such as CTC intravasation and extravasation and blockade of these processes. The shape of nanoparticles is an important factor in determining their behavior in the blood circulation, where the adhesive interactions between particles and cells have to counteract the hemodynamic forces exerted by the flowing blood [174]. These two counteracting forces will affect the particles' targeting and attachment abilities within the microvasculature. Various shapes of nanoparticles, such as spherical, hemispherical, discoidal, cylindrical, conical, vase- and rod-shaped, have all been manufactured with emerging nanofabrication technologies and have demonstrated differential behaviors in flow [175, 176].

In flowing blood, a spherical morphology is suited for rotational motion [177], which is important for leukocytes that roll on and interact with the endothelium. In contrast to symmetric spherical particles (including cells), non-spherical particles may align or tumble under flow, with surprising transport properties. For example, red blood cells (RBCs), having a flexible biconcave disc shape with an average diameter of 8μm [178], routinely pass through the reticular meshwork filtering units in the sinusoidal spleen in which the cell slit size rarely exceeds 200 to 500 nm in width, whereas spherical nanoparticles must be less than 200 nm in diameter to do so [175, 179]. In contrast to rigid spheres, biconcave discs are found to deform to other shapes such as parachute and slipper-like morphologies in response to changes in local flow velocity and shear stress, yet they retain the ability to recover their discoidal shape at reduced velocity [178]. Shape flexibility and deformability allow RBCs to pass through vessels

of different dimensions and narrow constrictions, making them an excellent vehicle for traveling in blood. Another important type of blood cell, platelets, normally exhibiting an oblate spheroidal shape, have been shown to assume different morphologies in vitro after prolonged exposure to adhesive surfaces [177]. Activated platelets resemble spheres with a rough surface. The activated platelet shape greatly influences platelet collisions, including the frequency, contact time and available area of collision, as well as the magnitude of shear and normal forces acting on the cells [180].

Inspired by nature's adaptation of non-spherical particles for unique transport properties and cellular interactions in flowing blood, synthetic particles of various shapes have been developed and evaluated for drug delivery in recent years [174]. For instance, Decuzzi et al [176] injected silicon-based particles of quasi-hemispherical, cylindrical and discoidal shapes into tumor-bearing mice and observed different distribution profiles among these particles. They further showed that discoidal particles can maximize accumulation in target organs while reducing sequestration by the liver. Geng et al [181] prepared filomicelle, which are flexible filamentous vehicles that have been shown to effectively and efficiently deliver the anticancer drug paclitaxel to tumors in mice [182], that persists in circulation 10 times longer than their spherical counterpart. Gandra et al [183] modified a filamentous bacteriophage and demonstrated its potential use as a biological nanowire to convey cargos of cancer-targeting peptides and photosensitizing agents. Bruckman et al [184] prepared viral nanoparticles in the forms of rods and spheres, and observed that the nanorods

circulated longer in the bloodstream of mice and were cleared from tissues more slowly compared to nanospheres. Theoretical and experimental calculations further confirmed the distinctive diffusion profiles of these two shapes in the tumor microenvironment [185]. Carbon nanotubes (CNTs) have attracted much attention in drug delivery research due to their long circulation time and the efficient methodologies for chemical modification [186]. For example, Yinghuai et al [187] constructed water-soluble functionalized CNTs as delivery vehicles of cancer therapeutics, BNCT agents, which were found to be concentrated in tumor cells in mice.

These bio-inspired approaches exploiting non-spherical particles for tumor homing are directly applicable for the targeting of CTCs in the bloodstream. Elongated, rod-shaped and filamentous materials possess distinctive transport properties compared to spheres due to their enhanced flexibility and permeability. They also show improved margination toward the vessel wall [185, 188], and are thus potentially more effective at accessing diseased vessels and CTCs [185]. Moreover, the extended circulation lifetime of these particles can increase their probability of interaction with CTCs. Although non-spherical nanoformulations are promising anticancer drug delivery vehicles, they represent an emerging field that requires more extensive evaluations, including focus on mechanical properties, polydispersity, and stability of the carriers. In addition, other design parameters can have significant effects on vascular transport properties as well. For example, size and density are important in particle design. A fine balance among these three factors, shape, size and density, may allow for the

design of particles with enhanced vascular interactions [189] that are able to mimic biomolecules and cells, sensing and interacting with endothelial cells and CTCs in the blood circulation.

1.2.4.2 Biomimetic strategies for drug delivery to CTCs

Red blood cells (RBCs), or erythrocytes, have been exploited as drug delivery vehicles since Inler and colleagues [190] first created enzyme-loaded RBC ghosts in the early 1970s [191]. Their work continues to inspire the design and engineering of biomimetic delivery systems today. Drug delivery vehicles derived from natural RBCs can be divided into four major classes [192]: (1) carrier RBCs, which are natural RBC ghosts carrying therapeutic cargos; (2) synthetic RBC-mimicking particles, which are made of polymers that aim to simulate the mechanical and chemical properties of RBCs; (3) RBC membrane-derived liposomes, which are synthesized from native RBC membranes; (4) RBC-membrane camouflaged nanoparticles (RBC-NPs), which are nanoparticles coated with native RBC membranes.

Although RBC derivatives have not been extensively evaluated in the context of CTCs, their unique biomimetic features suggest they are an excellent type of delivery vehicle for drugs that must work in the bloodstream [191], and exhibit the potential to effectively target CTCs. Both RBCs and CTCs reside in the circulatory system, and can travel to different organs through blood vessels. Therefore, if bioengineered RBCs are capable of recognizing and eliminating CTCs in the vasculature before CTCs are able to extravasate, they could prevent cancer cells from colonizing secondary organs

and reduce metastasis. In addition, human erythrocytes have a life span of 100-120 days [191], a circulation time much longer than that of nanoparticle drug carriers at present. Many types of synthetic nanoparticles sub-100nm in diameter have a circulation half-life on the scale of hours even after PEGylation [193]. The longer blood circulation time of RBC derivatives enhances drug retention in the body and allows for sustained drug release [194], as well as increasing the vehicles' interactions with CTCs.

Another property that makes RBC derivatives an excellent tool for targeting CTCs is their superior biocompatibility. The biocompatibility of nanoparticles is dictated by particle size, surface charge, hydrophobicity-hydrophilicity, as well as the steric effects of their outer coating [195]. Many polymers used for nanoparticle stealth coating, such as PEG, create a hydrophilic shell on the particle surface, thus shielding the nanoparticles from immune recognition and decreasing their rate of elimination [196]. In the early 2000s, however, different groups had reported a phenomenon called "accelerated blood clearance" [197], in which repeated injections of PEGylated liposomes resulted in immune rejection in animal studies [196-199]. This phenomenon raised concerns in the repeated administration of sterically stabilized nanoparticles for drug delivery. In contrast to PEGylation, which provides nanoparticles an outer shell that attenuates immune recognition, RBC derivatives adopt a different mechanism by disguising as the "self", which can potentially be more compatible with the immune system and avoid accelerated blood clearance. Residing in the same environment as macrophages and lymphocytes, RBCs evade the immune system by displaying self-

antigens on their outer membrane [192, 200, 201]. RBC derivatives that incorporate self-antigens, such as CD47 [202], or a complete RBC membrane [192, 194, 203], have shown reduced immunogenicity compared to naked particles. For instance, Gao et al. [47] demonstrated a 4-fold reduction in the uptake of gold nanoparticles (AuNPs) coated with RBC membranes by macrophages in vitro.

Early studies have shown enhanced therapeutic efficacy and reduced immunogenicity in animal cancer models treated with erythrocyte-encapsulated antitumor drugs. In a study by Zocchi et al. [204], murine RBCs were subjected to hypotonic dialysis followed by doxorubicin encapsulation during membrane resealing. Compared to the non-encapsulated drug, mice treated with erythrocyte-encapsulated doxorubicin showed significant inhibition of metastatic growth in liver and lung at a much lower dosage. Doxorubicin encapsulated in RBCs was also administered to dogs with lymphosarcoma [205]. This treatment achieved sustained drug release and induced complete and partial remissions of lymphosarcoma in dogs. Skorokhod et al. [206] administered doxorubicin-loaded erythrocytes to 15 lymphoma patients and reported improved pharmacokinetics compared to those of free doxorubicin, as well as good tolerance in cancer patients. The same research group has also studied the pharmacokinetics of daunorubicin-loaded erythrocytes in patients with acute leukemia [207] and similar findings were reported, thus demonstrating the promising clinical applications of RBC delivery vehicles in treating blood cancers. Another drug used to treat acute leukemia, L-asparaginase, is one of the most widely studied enzymes for RBC encapsulation [208]. Different groups have developed various methods for

preparing asparaginase-loaded RBCs, which have been evaluated for their pharmacokinetics and antitumor activities in mice [209, 210], dogs [211], monkeys [212] and humans [213]. These studies have demonstrated the advantages of using RBC derivatives for targeting CTCs in vivo.

To date, RBC derivatives have not been reported in literature for targeting CTCs that are not of blood cancer origin. Nevertheless, studies involving leukemia or lymphoma animal models and human patients have corroborated the potential use of RBC carriers in targeting non-blood CTCs. Despite the attractive features of erythrocyte derivatives in targeted drug delivery, there are still many clinical challenges. Unlike animals, humans have many different blood groups. To make the technology more versatile for patients, the removal of immunogenic antigens is essential during drug synthesis [194]. In addition, because of their biological origin, RBC derivatives are difficult and expensive to store. They also present great variability, which makes standardization and scale-up challenging [208]. At present, there is no known receptor or ligand on the native RBC membrane that would allow RBC vehicles to interact with CTCs in circulation. A potential solution is to create RBC derivatives carrying antibodies that would specifically recognize CTC surface antigens such as EpCAM, which is present in many types of CTCs. EpCAM expression on CTCs is also found to correlate with metastatic cancer prognosis [214, 215]. Conjugation of various molecules, including antibodies, to RBC membranes can be accomplished through a biotin-avidin linkage [192, 216].

In contrast to RBC biomimetic platforms that primarily seek to improve drug circulation time and biocompatibility, nanoparticles that mimic behaviors of platelets may not only extend the half-life of particles in blood but also bind CTCs with mechanisms similar to natural platelets. A platelet-mimetic approach for metastasis-targeted nanomedicine has been recently developed. In a study from the Gupta group [217], highly metastatic human breast cancer cells MDA-MB-231 were examined for surface expression of platelet-interactive receptors, which were then compared to a weakly metastatic human breast cancer cell line, MCF-7. Interestingly, certain platelet-interactive receptors were found to be significantly overexpressed on the surface of MDA-MB-231 cells such as GPIIb-IIIa-like receptors (which can bind to platelets mediated by fibrinogen), P-selectin (which can bind to platelets mediated by sialoprotein ligands), GPIa-IIa-like receptors (which can bind to platelets mediated by collagen-like molecules), E-selectin (which can bind to sialyl Lewis moieties), integrin αVβ3 (which can bind to fibronectin, vitronectin, etc.), and GPIbα-like proteins (which can bind to von Willebrand factor). In contrast, these receptors were weakly expressed in MCF-7 cells. More importantly, MDA-MB-231 cells showed significantly enhanced binding interactions with active platelets compared to MCF-7 cells. In light of these differences, two specific receptors were selected (GPIIb-IIIa-like integrin and P-selectin), and their corresponding ligands were engineered onto the surface of liposomes to enable platelet-mimetic binding to the cancer cells under physiological flow conditions. Nevertheless, it remains to be answered whether such a platelet-mimetic approach could target real CTCs in a patient's blood. To address this question, both a mouse metastatic cancer model and patient-derived blood containing

CTCs will need to be tested. In addition, the in vivo biodistribution and circulation time of such nanomedicines must be measured. Despite the uncertainties that remain to be addressed, this represents the first paradigm for targeting metastatic CTCs though interactions with platelets.

1.2.5 Integrating CTC isolation technologies with nanomedicine

Enumeration of CTCs in the peripheral blood of cancer patients has shown promise for the diagnosis and monitoring of cancer progression, and it serves as an alternative to conventional imaging methods [218-220]. CTCs of epithelial origin are defined as being positive for epithelial cell adhesion molecule ($EpCAM^+$) and cytokeratin 8, 18, or 19 (CK^+), and negative for CD45 ($CD45^-$) [11]. Therefore, approaches for isolating such CTCs are largely based on the positive selection for epithelial markers [221, 222]. The existence of EpCAM-negative CTCs (i.e., CTCs with EMT signature), necessitates approaches such as negative depletion to select for $CD45^-$ cells [223]. Alternatively, label-independent enrichment methods that are based on size and/or density differences between cancer cells and blood cells have also been developed for CTC enrichment [224, 225]. In addition to cell heterogeneity, the rarity of CTCs in blood relative to white blood cells has made their detection and isolation even more challenging [119, 140, 141]. To solve this problem, nanomaterials have been developed to enable high-density coatings of different capture molecules such as antibodies for improved sensitivity of CTC detection [226]. Recently, silicon nanopillars [227], quartz nanowires [228] and TiO_2 nanofibers [229] have been used to trap CTCs, with enhanced capture efficiency due to the higher aspect ratio of the

nanomaterials. Moreover, when such nanomaterial-based platforms have been integrated with flow-based systems such as microfluidic devices, a significant increase in capture yield is observed via continuous flow of patient blood through the devices [1, 230, 231].

In contrast to the rapid development of CTC isolation technologies, few studies have been performed to enable drug delivery through CTC enrichment devices. It is conceivable that anti-EpCAM-conjugated nanoparticles loaded with cancer drugs could be utilized for targeting CTCs of epithelial state in blood. Moreover, by combining high capture efficiency of 3D nanotopographic features such as silicon nanowires with enhanced drug encapsulation for nanoporous materials, novel nanomedicines can possibly target a subpopulation of CTCs with CSC properties or multi-drug resistance [232-234]. In addition, since mouse models and clinical observations have provided evidence that CTC count correlates with disease progression in cancer patients [23, 142, 218, 235], it is intriguing that an implanted shunt system with similar nanostructure and surface functionalization could be utilized to filter out rare CTCs from the blood circulation. As a proof-of-concept, Rana and King invented a biomimetic approach to capture and kill CTCs in vitro. In this system, a microfluidic device was functionalized with E-selectin, which interacts with CTCs during extravasation through the endothelium. Additionally, the surface was coated with a tumor-specific cytokine, tumor necrosis factor-related apoptosis-inducing ligand (TRAIL), for inducing apoptosis when CTCs were captured from the flow [101, 236]. More recently, the device was further functionalized with naturally occurring

nontoxic halloysite nanotubes for the enhanced capture of CTCs [92, 93]. Nevertheless, several issues need to be addressed to demonstrate the efficacy of this approach in vivo. First, the device must be compatible with the body. As E-selectin and TRAIL are expressed in host cells, it is unlikely that they will induce an immune response. It requires, however, further examination on whether the material that comprises the device and additional nanostructured surface would cause any side effects when interfacing with blood [237]. Secondly, it is necessary to test the isolation efficiency of CTCs in the presence of abundant plasma proteins in the blood. It has been found that owing to high surface free energy, certain nanomaterials adsorb biomolecules upon contact with biological fluids. In particular, plasma proteins may bind to the nanostructured surface to form a biological coating, known as the protein corona [238, 239]. This corona may affect the interaction of the device with the host system [240]. Lastly, it is crucial to evaluate when the device surface becomes saturated with CTCs and requires replacement. Nevertheless, such biomimetic approaches for the delivery of apoptotic signals represents an intriguing proof of concept for future integration of CTC isolation technologies with nanomedicines.

Conclusion

In the past decade, the presence of CTCs has been utilized as an indicator of poor prognosis in several carcinomas. The difficulty of identifying these rare cells in the blood has driven the development of numerous devices for the isolation and characterization of CTCs in clinical settings. It is not until recently, however, that the presence of metastasis-initiating cells (MICs) among CTCs has been experimentally

demonstrated. Therefore, neutralizing MICs or CTCs in the blood may represent a new paradigm for the intervention of metastases in distant organs. In contrast to conventional nanomedicines, which extend the half life of chemotherapeutics in the blood, novel approaches that are inspired by the context of CTCs in circulation have led to a variety of biomimetic nanoparticle or nanoformulation platforms. Integration of nanotechnologies with a deeper understanding of diverse CTC–host cell interactions may offer exciting and promising directions for novel therapeutic interventions in the future.

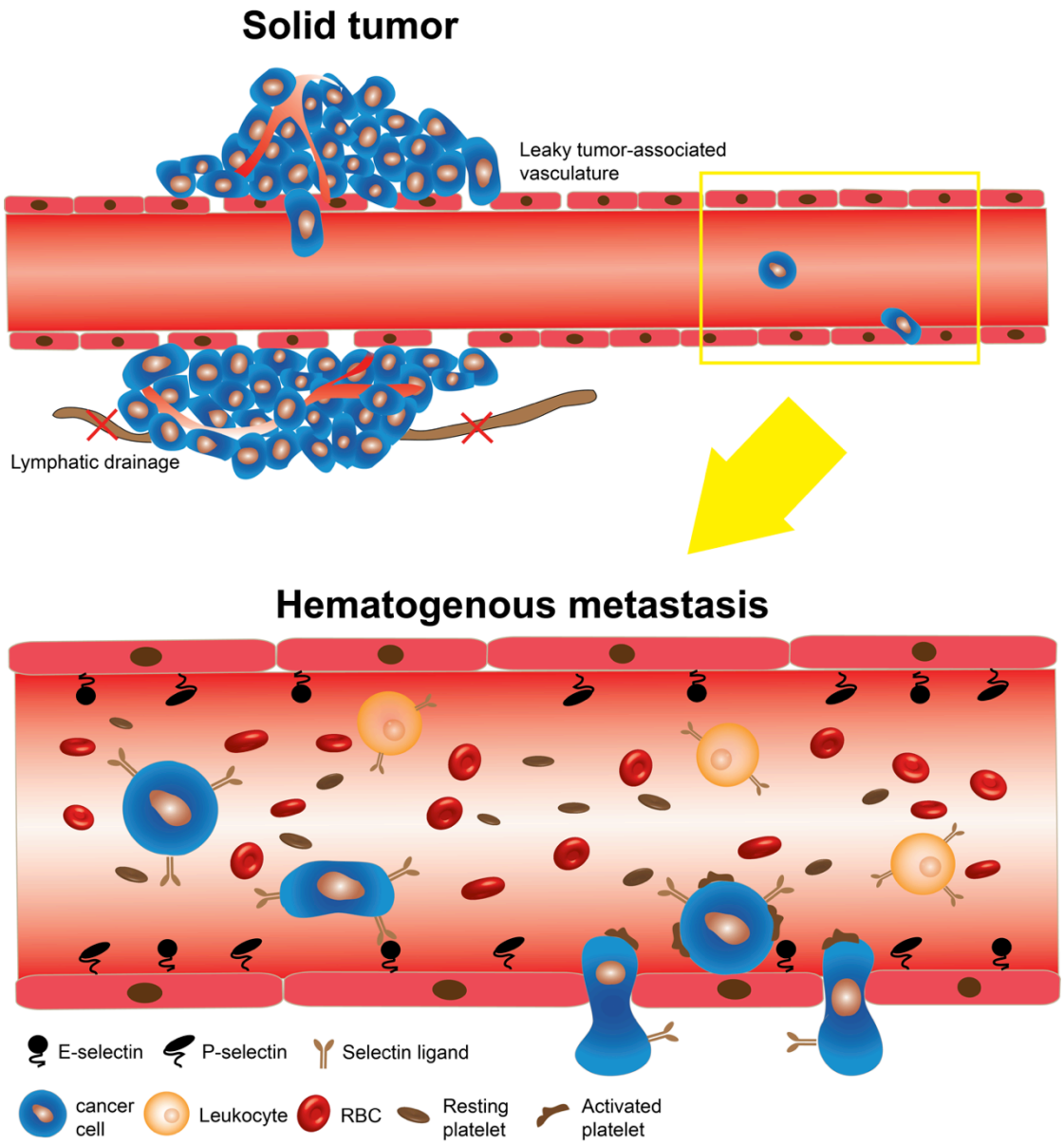

Figure 1.2. Two different contexts for the delivery of nanomedicines: solid tumor versus the blood circulation. Nanomedicine enters a solid tumor through leaky tumor-associated vasculature where dysfunctional lymphatic drainage enables nanomedicine accumulation in the tumor. In contrast, once shed into the blood circulation, CTCs are subjected to environmental changes such as shear stress, and interactions with platelets, endothelial cells and other vascular components.

Table 1.2. Six grand challenges of CTC targeting

CTC properties	Practical Consequences	Ref.
Rarity of CTCs: a needle in a haystack problem	Low efficiency of targeting CTCs	[140, 141]
Heterogeneous subpopulations	Mesenchymal CTCs are not recognized by nanomedicine targeting epithelial cell markers such as EpCAM; Necessity of killing all CTCs versus MICs or CSCs in the circulation; Differential drug resistance	[143-146]
Formation of CTC clusters	Increased invasiveness, resistance to anoikis and trapping in micro-vessels.	[147-151]
Short circulation time of CTCs	Limited exposure time to therapeutics against CTCs in circulation.	[156-158]
Shielding of CTCs by platelets	Physical barrier to penetration of nanomedicine into CTCs; pro-metastatic role via induction of EMT, establishment of early metastatic niches, pro-survival signaling etc.	[86, 137, 138]
Off-target effects associated with systemic drug delivery	Systemic cytotoxicity	[153, 154]

CHAPTER 2: HUMAN FUCOSYLTRANSFERASE 6 ENABLES PROSTATE CANCER METASTASIS TO BONE

* This section is adapted from the following publication:

Li J, Guillebon AD, Hsu JW, Barthel SR, Dimitroff CJ, Lee YF, et al. Human fucosyltransferase 6 enables prostate cancer metastasis to bone. British Journal of Cancer. 2013;109:3014-22.

Prior studies have shown that the interaction between human PCa cells and bone marrow endothelium follows a rolling-and-adhesion cascade mediated by E-selectin ligand (ESL): E-selectin interactions. This adhesion is enabled by elevated expression of human α-1, 3 fucosyltransferases (FTs), key enzymes responsible for ESL activity in human PCa cells and leukocytes. In contrast to human, the incidence of bone metastasis in mice is rare. This may be due to lack of ESL expression found in mouse PCa cell lines. In this study we showed that overexpression of FT3, FT6 or FT7 restored ESLs and enabled mouse PCa cells to roll and adhere in E-selectin-functionalized microtubes, similar to trafficking of circulating PCa cells in bone marrow vessels. We then tested the ability of FT-overexpressing mouse PCa cells to home to bone marrow, in a manner similar to human cells. Following intracardiac inoculation with cells overexpressing one of the FT genes, FT6 cells induced robust bone metastasis in immunocompetent mice. These results indicate that ESLs induced by FTs are sufficient to direct murine PCa cells to bone marrow in an E-selectin-dependent manner. This new bone metastatic mouse model should prove to be useful for future preclinical investigations of PCa bone metastasis.

2.1 Introduction

PCa is the leading cause of cancer death among American men, second only to lung cancer in 2012. When detected at an early stage the five-year survival rate is close to 100%. In contrast, if diagnosed at a late stage with advanced metastatic disease, the five-year survival decreases to 33% [241]. The most common metastatic sites of PCa are lymph nodes, bones, lung and liver [242]. Among these sites, bone is the most

challenging organ for therapeutic intervention as bone metastasis can cause severe skeleton-related diseases such as bone pain, hypercalcemia, fractures and nerve compression syndromes [243, 244].

Metastasis to bone is a multi-step cascade. PCa cells detached from the primary site must first invade a blood vessel, a process called intravasation. Through hematogenous dissemination, a subpopulation of cells attach to bone marrow endothelial cells. This process is mediated by multiple receptor-ligand interactions under shear stress, referred to as a rolling-and-adhesion cascade [245]. This cascade further facilitates PCa cells to breach the bone endothelial layer (transendothelial migration) to establish micrometastases in the bone microenvironment [246].
Bone marrow endothelial cells constitutively express E-selectin which enables homing of hematopoietic stem cells expressing E-selectin ligands (ESLs) to bone marrow [247, 248]. Recent studies have indicated that human PCa cells also express similar ESLs to interact and traverse the vasculature of bone marrow [246, 249, 250]. ESLs are comprised of the tetrasaccharide sialyl Lewis X (sLe^x) attached to the extracellular domain of glycoproteins or glycolipids. The synthesis of sLe^x on such glycoproteins is catalyzed in the Golgi compartment by members of the glycosyltransferase gene family. The final step involves the transfer of fucose to N-acetylglucosamine at the terminal α-2, 3 sialo-lactosamine unit by α-1, 3 fucosyltransferases (FT) 3, 4, 5, 6, and/or 7, depending on the cell type [251]. Gene expression profiling and immunohistology in several human PCa cell lines have shown that the bone metastasis potential correlates well with the expression level of fucosyltransferases [252, 253].

To the contrary, the rare evidence of bone metastasis in mice genetically prone to PCa raises the question of whether mouse PCa cells express ESLs [254]. Moreover, if they are absent in mouse PCa cells, can one develop a new mouse model with robust bone metastasis by increasing expression of functional ESLs?

2.2 Materials and Methods

Cell lines and mice

Mouse prostate adenocarcinoma TRAMP-C1 and TRAMP-C2 were obtained from American Type Culture Collection (ATCC) (Rockville, MD, USA), and cultured in Dulbecco's modified Eagle's medium (Invitrogen, Grand Island, NY, USA) with 4 mM L-glutamine adjusted to contain 1.5 g/L sodium bicarbonate and 4.5 g/L glucose supplemented with 0.005 mg/ml bovine insulin and 10 nM dehydroisoandrosterone, 90%; fetal bovine serum (BD Biosciences, San Jose, CA, USA), 5%; Nu-Serum IV (BD Biosciences), 5%. RM-1 cells are a murine androgen insensitive prostate cancer cell line, which were kindly provided by T Thompson (MD Anderson Cancer Center, Houston, TX, USA) for this study. RM-1 cells were cultured in Dulbecco's modified Eagle's medium supplemented with 10% FBS. Human umbilical vein endothelial cells (HUVEC) were obtained from ATCC and cultured in vascular cell basal medium (ATCC) using the endothelial cell growth kit-BBE (ATCC® PCS-100-040). HUVEC were used up to passage number 6. Six to 8-week old male C57BL/6 mice were purchased from Jackson Laboratory (Bar Harbor, ME, USA). Mice were housed in a SPF barrier animal facility at Cornell University.

Antibodies

The following recombinant proteins or antibodies were employed to characterize ESLs in this study: recombinant mouse E-Selectin/CD62E Fc chimera (R&D Systems, Minneapolis, MN, USA), PE goat anti-human IgG (Santa Cruz Biotech, Santa Cruz, CA, USA), FITC HECA-452 (BD Biosciences), PE anti-mouse PSGL-1 (BD Biosciences), FITC anti-mouse CD44 (BD Biosciences). The following antibodies from BD Biosciences were used as isotype controls: FITC Rat IgG2b, FITC Rat IgM, PE Rat IgG1.

Flow cytometry

Cells were detached with enzyme-free Gibco® Cell Dissociation Buffer (Invitrogen) and suspended at a concentration of 5×10^5 cells in 100 μL cold PBS/1% bovine serum albumin (BSA). Primary antibodies or corresponding isotype control antibodies were incubated with cells for 30 min on ice. Following two washes with 1 ml PBS/1% BSA, fluorescence measurements were collected on an Accuri C6 flow cytometer (BD Biosciences). Data were analyzed using the Flow Express software (De Novo Software, Los Angeles, CA, USA). Cells were gated based on forward and side scatter. For detection of ESLs, recombinant mouse E-Selectin/CD62E Fc chimera was used at a concentration of 10 μg/ml. Cells were suspended at a concentration of 5×10^5 cells in 100 μL cold binding buffer PBS/1% BSA/2 mM Ca^{2+} or control buffer PBS/1% BSA/1 mM EDTA. Incubation was performed for 30 min on ice. Cells were washed with binding buffer or control buffer twice and stained with secondary PE anti-human IgG for 30 min on ice.

Western blotting and immunoprecipitation

For western blotting, whole cell lysates were prepared and separated by 8% SDS-PAGE as previously described [255]. Membranes were incubated with primary antibodies HECA-452 (BD Biosciences), anti-β actin (Santa cruz Biotech) and recombinant mouse E-selectin-Fc (R&D Systems). All primary antibodies were diluted 1:1000. Mouse E-selectin-Fc was diluted to 1 μg/ml in the presence of 2.5 mM $CaCI_2$. Immunoprecipitation was performed to identify E-selectin-reactive membrane protein as previously described [256]. 500 μg precleared proteins were incubated with either 5 μg human IgG isotype or 5 μg mouse E-selectin-Fc. The prepared samples were separated and analyzed by western blotting. Anti-CD44 (Biolegend, San Diego, CA, USA) was used at 1:1000 dilution in the blotting.

Identification of E-selectin-Fc-reactive protein by mass spectrometry

Lysates from empty vector- and FT6-transduced TRAMP-C2 were subjected to immunoprecipitation by E-selectin-Fc. Proteins that interacted with E-selectin-Fc were analyzed by 8% SDS-PAGE. To guide localization, excision and retention of the relevant protein, an E-selectin-Fc-immunostained blot was prepared from the same gel. The stained blot was superimposed with the corresponding gel to excise the fragment in the gel. The fragment was digested with trypsin and analyzed by nano HPLC MS/MS with Orbitrap Elite (Thermo Fisher Scientific Inc. Waltham, MA, USA), and the NCBI database was searched for possible peptide matches. The peptide sequences from empty vector-transduced samples were used as background control to exclude

nonspecific interaction with E-selectin-Fc.

Retroviral production and transduction

Retroviral vectors encoding human α-1,3 FT3, FT6, FT7 and retrovirus packaging helper plasmids pN8e-gag_pol_deltaS and pN8e-VSV-G were utilized. Briefly, retroviral vectors and two helper plasmids were transfected into HEK293T cells by TransIT®-LT1 Transfection Reagent (Mirus Biology, Madison, WI, USA). Virus supernatants were harvested at 48 hr and 72 hr after transfection. Virus supernatants were mixed with target cells in the presence of 8μg/ml polybrene (Santa cruz Biotech) for 24 hr. Afterwards, fresh media was added and cells were selected with 200 μg/ml G418 for 2 weeks.

Tumor cell transendothelial migration assay

The QCM^{TM} Tumor Cell Transendothelial Migration Assay kit (Millipore, Billerica, MA, USA) was used in this study. Briefly, $1x10^5$ endothelial cells in 250 μL endothelial cell culture medium were loaded into each insert. After cells grew to >95% confluence, endothelial cell monolayers were activated with 20 ng/ml of recombinant human TNFα for 4 hr. $1x10^5$ tumor cells were suspended in 250 μL serum-free media and loaded into the insert. Tumor cells were allowed to migrate for 24 hr at 37^{o}C. Cells that migrated to the bottom of the inserts were fixed with 100% methanol, stained with crystal violet and counted on a microscope.

Preparation of E-selectin-functionalized microtube and rolling experiments

50 cm-long microrenathane microtubes with 300 μm inner diameter (Braintree Scientific, Braintree, MA, USA) were first washed with 1× PBS and then coated with 10 μg/ml of recombinant protein G (Millipore, Billerica, MA, USA) for 1 hr at room temperature (RT). Microtubes were incubated with 0.125 μg/ml of recombinant mouse E-selectin/Fc chimera for 2 hr. The surface was then blocked with 5% fat-free milk for 0.5 hr to avoid nonspecific interaction of cells with the tube surface. Tubes were washed with PBS^{++} (PBS saturated with calcium chloride) (Invitrogen) and dissociated monolayer cells at a concentration of 1×10^6 cells/ml in PBS^{++} were perfused through at 2 dyn/cm^2 using a syringe pump (IITC Life Sciences, Woodland Hills, CA, USA). Functionalized microtubes were then secured to the stage of an Olympus IX81 motorized inverted microscope (Olympus America, Melville, NY). A CCD camera (Hitachi, Tokyo, Japan) and DVD recorder (Sony Electronics, Tokyo, Japan) were used to record experiments. Videos were later analyzed using in-house ImageJ (NIH, USA) stack tools to quantify rolling velocities. The number of cells per frame of rolling video was manually counted.

Animal studies

All mice were handled according to the Guide for the Care and Use of Laboratory Animals in compliance with UK-based guidelines. All experimental procedures and protocols were approved by the Institutional Animal Care and Use Committee of Cornell University (Protocol No. 2011-0051). Male C57BL/6 mice (age 8-10 weeks) were anesthetized by 2.5% isoflurane on the day of injections. On day 0, anesthetized animals were injected with 1×10^5 cells suspended in 100 μl sterile DPBS containing

300 μg/ml D-luciferin into the left ventricle of the heart by nonsurgical means via a 29G needle (BD Biosciences). After injection, mice were subject to bioluminescence imaging.

Bioluminescence imaging

Bioluminescent imaging was performed with a CCD camera mounted in a light-tight specimen box (Xenogen, Waltham, MA, USA). Imaging and quantification of signals were controlled by the acquisition and analysis software Living Image® (Xenogen). Anesthetized mice were placed in the IVIS™ Imaging System and imaged from ventral views approximately 10-15 min after intraperitoneal injection of D-luciferin at 150 mg/kg body weight. For experiments on day 0, successful intracardiac injections were indicated by images showing systemic bioluminescence distributed throughout the animal. Only mice with evidence of a satisfactory injection continued in the experiments. Assessment of subsequent metastasis was monitored *in vivo* after one week.

Histology

Mouse hind legs were fixed in 4% formaldehyde in PBS overnight and then decalcified in 10% formic acid in 10% formalin/PBS overnight. Decalcified hind legs were embedded in paraffin after tissue processing (dehydration, clearance and impregnation). Serial sections (5 μm) from each tissue block were cut onto slides and every fifth section was stained with Hematoxylin and Eosin (H&E) as previously described [257]. H&E-stained slides were imaged with an upright Olympus BX-50

microscope equipped with a Moticam 2300 color camera (Cole-Parmer, Vernon Hills, IL, USA).

Statistical analysis

All statistical analyses were performed using GraphPad Prism 5.0a for Mac OS X (San Diego, CA, USA). One-way ANOVA followed by Tukey post test was used to compare statistical significance in the characterization of rolling velocity, number of rolling cells, transendothelial migration and quantification of bioluminescence signals. When analyzing gene expression of FTs in the NCBI database, significance was calculated by Student t-test.

2.3 Results

Mouse PCa cells do not express ESLs

E-selectin is a transmembrane glycoprotein which binds ESLs through its extracellular domain in a Ca^{2+}-dependent manner [258]. Three representative mouse PCa cell lines (TRAMP-C1, TRAMP-C2 and RM1) were examined in this study. TRAMP-C1 and TRAMP-C2 were derived from the transgenic adenocarcinoma mouse prostate model (TRAMP) [259]. This model was generated by overexpressing SV40 which suppresses p53 and Rb to mimic loss of function in tumor suppressor genes. In contrast, the RM1 cell line was developed from the mouse prostate reconstitution model (MPR) [260]. This model overexpresses the oncogene Ras. To test their binding to mouse E-selectin, cells were incubated with dimerized E-selectin-human IgG Fc chimera and fluorescently labeled anti-human Fc. This measurement showed that all three cell lines

express low level of ESLs (**Figure 2.1a**).

Mouse PCa cells express certain glycoprotein ESLs but not sLe^x

The glycoproteins PSGL-1 and CD44 have been identified as ESLs in human PCa, colon cancer and breast cancer [249, 261, 262]. It is not clear whether the lack of functional ESLs is due to the absence of similar glycoproteins, or a lack of sLe^x in mouse PCa cells (**Figure 2.1b**). Antibodies recognizing mouse PSGL-1 and CD44 were applied to TRAMP-C1, TRAMP-C2 and RM1 cells. None of them were found to express PSGL-1, however CD44 is present on the cell surface of all three cell lines (**Figure 2.1c**). These glycoproteins serve as scaffolds to present the tetrasaccharide sLe^x which can directly interact with E-selectin. Using an antibody that recognizes sLe^x (HECA-452), it was found that none of these mouse PCa cell lines express sLe^x (**Figure 2.1c**). Although previous work suggests that mouse ESLs are not recognized by the HECA-452 antibody due to differences in sialic acid composition compared to human ESLs [263], it was found in the present study that the introduction of fucose by overexpression of α-1,3 FTs restored the binding of HECA-452 to mouse cell lines. This validates the use of HECA-452 to identify sLe^x in this work (**Supplemental figure 2.1**). Thus, we may conclude that the lack of sLe^x is likely responsible for the deficiency in E-selectin binding.

FT3, FT6, and FT7 induce functional ESL expression on mouse PCa cells

The final step of sLe^x synthesis on glycoproteins involves the transfer of fucose to N-acetylglucosamine catalyzed by α-1,3 fucosyltransferases (FT). The upregulation of α-

1,3 FT3, 6 and 7 in human metastatic PCa tissues motivates the examination of whether FT3, FT6, or FT7 could be involved directly in the expression of sLe^x in mouse PCa cell lines [135, 253]. cDNA encoding human FT3, FT6 and FT7 were packaged into retroviral particles and transduced into the TRAMP-C1, TRAMP-C2 and RM1 cell lines to establish stable cell clones. Indeed, overexpression of FT3, FT6 or FT7 restored E-selectin-binding in mouse PCa cells compared to empty vector-transduced cell lines (**Figure 2.2**). Thus, overexpression of FTs completes the final step of sLe^x synthesis and enables E-selectin binding in mouse PCa cells.

Characterization of rolling behavior of FT-transduced cells

We next examined E-selectin-binding in a dynamic fluid flow system. A previously established flow-based microtube system was employed to mimic the bone microvascular environment [133, 236, 264, 265]. Briefly, the inner surface of microtubes were coated with mouse E-selectin-Fc chimera (**Figure 2.3a**). To simulate circulating behavior, PCa cells were perfused at physiological wall shear stress (WSS) through the microtube lumen and their rolling behavior was characterized by measuring the rolling velocity and recording the number of interacting cells. In all three cell lines, FT6-transduced cells exhibited the slowest rolling velocity under physiological WSS of 2 dyn/cm^2 (**Figure 2.3b**). The rolling adhesion was Ca^{2+}-dependent, as flushing with 1mM EDTA abolished cell binding as expected for E-selectin adhesion (data not shown). In contrast, cells transduced with empty vector were unable to roll or interact with E-selectin-coated microtubes (**Figure 2.3b**). In addition, FT6-overexpressing cells displayed the highest number of rolling cells

interacting with E-selectin-coated surfaces (**Figure 2.3c**, **Supplemental figure 2.2**). The behavior in this biomimetic in vitro system suggests that ESLs may support the recruitment of CTCs from circulation to bone endothelium *in vivo*.

Transendothelial migration of FT-transduced cells

After CTCs roll and form firm adhesions with the endothelial layer in bone marrow microvessels, CTCs must breach this layer to establish micrometastases, a process referred to as transendothelial migration (TEM). To assess TEM capability, empty vector or FT-transduced TRAMP-C1, TRAMP-C2 and RM1 cells were seeded on confluent monolayers of endothelial cells pre-stimulated with TNF-α to transiently express E-selectin. The potential of TEM was measured by counting cells that migrated through the layer after 24 hr incubation (**Figure 2.4a**). Notably, FT6-transduced cells showed greater TEM ability than empty vector, FT3 and FT7-transduced cells (**Figure 2.4b-d**, **Supplemental figure 2.3**).

FT6 promotes the greatest potential for BM metastasis

We next investigated whether the differential rolling velocity and TEM are sufficient to lead to distinct BM metastases in immune-competent mice. Equal numbers of empty vector or FT-transduced TRAMP-C2 cells stably expressing firefly luciferase were injected into the left ventricle of C57BL/6 mice. The intracardiac route was selected to allow for systemic dissemination of CTCs before becoming entrapped in the microvessels of the lung [266, 267]. One week after cell injection, bone metastases were quantified by measuring luminescence signal in the tibia and femur (**Figure**

2.5a). The bioluminescence signal from the tibias and femurs were normalized to whole-body luminescence signal taken on day 0. Consistent with the in vitro findings, FT6-transduced TRAMP-C2 cells developed the highest metastatic burden in bone (**Figure 2.5b and c**). Further examination of BM invasion by hematoxylin and eosin (H&E) staining revealed that only FT6-transduced TRAMP-C2 cells established significant metastases in the femur proximal to the knee joint (**Figure 2.5d**).

FT6 converts CD44 to a functional E-selectin ligand

To identify candidate ESLs induced by the overexpression of FTs, the glycoproteins from total lysates of FT-transduced TRAMP-C2 cells were examined by Western blotting. Both mouse E-selectin-Fc and HECA-452 identified protein bands of a similar size, indicating that the ESLs formed after overexpression of FTs are positive for sLe^x or sLe^x-like glycan (**Figure 2.6a**). Whereas FT3-transduced cells were not detectable by either E-selectin-Fc or HECA-452, FT6 and FT7 generated unique patterns of ESLs in the blots. It is possible that FT3-induced ESLs are primarily glycolipids or glycoproteins that cannot be readily detected due to the denaturation step of Western blotting. Noting that the slowest rolling velocity and greatest TEM found in vitro as well as the highest incidence of bone metastasis in vivo was observed for FT6, the identify of unique glycoproteins were further investigated in FT6-transduced TRAMP-C2. The distinct fragment produced by FT6 lysate was excised from SDS-PAGE gel after superimposition to the band of a similar size in blots and analyzed by mass spectrometry. An E-selectin-binding, sLe^x-bearing protein, CD44, was identified and further validated through immunoprecipitation by beads conjugated

to E-selectin-Fc (**Figure 2.6b**). Consistent with human studies, CD44 has been found to be a key protein that is involved in the adherence of metastatic prostate and breast cancer cells to bone marrow endothelial cells [268].

FT6 expression correlates with clinical PCa progression

To access the clinical relevance of FT6 in human PCa, the gene expression profile of FT6 was analyzed through public microarray repositories from the NCBI Gene Expression Omnibus (profile #GDS2545, Metastatic prostate cancer HG-U95A). It consists of three categories: (1) normal prostate tissue adjacent to PCa tumor (n=63), (2) primary PCa tumors (n=65) and (3) distant metastasis samples (n=25). We found higher levels of FT6 in primary prostate tumors (p=0.05) and metastatic tumors (p=0.001) in comparison to normal prostate epithelium adjacent to primary PCa tumors (**Figure 2.7b)**. No significant difference was found when examining FT3 and FT7 in the same tissues, except an increase in FT3 expression in distant metastasis samples compared to normal prostate epithelium adjacent to tumors (p=0.04) (**Figure 2.7a and c**).

α-1, 3 FT inhibitor reduces FT6-dependent bone metastasis

The in vivo experiments in this work along with gene expression profiles from clinical samples support the idea that FT6 may be one of key mediators that drives bone metastasis. Thus, it is of therapeutic interest to explore whether the inhibition of FT6 can reduce bone metastasis in our mouse model. To this end, fluorinated fucose mimetic (2F-Peracetyl-Fucose) was utilized to inhibit the activity of FT6 (**Figure**

2.8a). Following three days of incubation with 20 μg/ml 2F-Peracetyl-Fucose, FT6-transduced TRAMP-C2 showed reduced E-selectin binding (**Figure 2.8b**). This concentration did not compromise cell viability (data not shown), consistent with a prior study in which a three-fold higher concentration did not affect the viability of leukocytes [269]. To assay the efficacy of this fucose mimetic in vivo, FT6-transduced TRAMP-C2 cells that received the same treatment or vesicle control (DMSO) were injected into C57BL/6 mice via the left ventricle. One week later, fucose mimetic-treated cells produced significantly fewer and smaller bone metastases compared to DMSO treatment quantified by bioluminescence imaging (**Figure 2.8c and d**). Since 2F-Peracetyl-Fucose is highly cell-permeable and has not been shown to reduce cell viability in prior studies, we reason that it represents a potential therapeutic for the reduction of bone metastasis.

2.4 Discussion

In this work, we aimed to dissect the molecular mechanism of why bone metastasis is a frequent occurrence in the human disease but rare in mouse. Our results indicated that the lack of functional ESLs in mouse cell lines may partly explain this discrepancy. As ESLs are composed of a scaffold protein or lipid decorated by the tetrasaccride sLe^x, we further identified a lack of sLe^x in mouse PCa cells. However, overexpression of human α-1, 3 FTs in mouse PCa cells restored E-selectin binding and led to rolling of PCa cells in E-selectin-coated microtubes under physiological flow conditions. Interestingly, the different FTs (FT3, FT6 and FT7) showed differential rolling velocities and TEM capability *in vitro*. Among the three mouse

PCa cell lines tested (TRAMP-C1, TRAMP-C2 and RM1), FT6-transduced cells showed the slowest rolling velocity and the highest degree of TEM. To correlate these *in vitro* findings with *in vivo* metastatic potential, we inoculated FT-transduced TRAMP-C2 cells labeled with firefly luciferase into the left ventricle of wild-type C57BL/6 mice. Within one week, the FT6-overexpressing cells promoted significant bone metastasis in the tibia and femur as detected by bioluminescence imaging. We further identified CD44 as a primary ESL in cells expressing FT6 but not FT3 or FT7. This correlates with previous studies in human cells where CD44 promoted the adherence of metastatic cancer cells and mesenchymal stem cells to bone marrow endothelial cells [248, 261, 262, 268, 270].

Interestingly, previous work by the Dimitroff lab showed that FT7 rather than FT3 or FT6 promoted trafficking of human PC3 PCa cells to immunodeficient mouse bone marrow [135]. This may reflect inherent species-dependent differences between mouse and human-derived PCa cells. It should be noted that the mouse genome does not include the FT3 or FT6 genes and only FT4 and FT7 are inherently present to support E-selectin-mediated leukocyte rolling [38, 271]. Expression of human FT6 in mouse PCa cells may compensate for this loss during evolution. Despite such inter-species differences, FT6 has been found to be elevated in other human bone metastatic PCa and breast cancer cell lines [253, 272]. Moreover, one of significant findings in this work is that FT6 gene expression correlates best to clinical PCa progression and metastasis as revealed by public microarray repositories from the NCBI Gene Expression Omnibus.

Previous study in breast cancer indicates that ESLs mediate breast cancer cell TEM and that E-selectin blocking antibody can functionally abolish this migration *in vitro* [262]. While it is not clear whether FT plays a role in the TEM of breast cancer cells, it was shown that ESLs prime TEM of human mesenchymal stromal cells (MSCs) and direct them to bone by maintaining ESL expression in MSCs via FT6 [270, 273, 274]. Viewing this previous work in light of the current study, we speculate that therapeutic targeting of ESLs could prevent both E-selectin-mediated trafficking to bone and TEM in the reduction of PCa bone metastasis.

Many cancers have been found to associate with inflammation as exemplified by the infiltration of tumor-associated macrophages and regulator T cells, and inflammation can further aggravate cancer progression [275]. In this study, we utilized the fucose mimetic 2F-Peracetyl-Fucose to inhibit FT enzyme activity, and achieved a significant reduction of bone metastasis in the FT6-induced bone metastasis mouse model. This inhibitor along with other sugar mimetics have been suggested to suppress inflammation by inhibiting the synthesis of ESLs in infiltrating leukocytes without affecting cell viability [269, 276]. We suggest that fucose mimetics may be a potential drug that target the vicious cycle of inflammation and cancer progression. In addition to these sugar inhibitors, siRNA that targets specific fucosyltransferases can also be utilized [252].

This newly developed experimental metastasis model has several advantages over

existing mouse models of bone metastasis: (1) It bypasses complicated surgical implantation of PCa cells in the bone. Moreover, the direct intraosseous implantation bypasses several crucial steps in the metastatic cascade: survival in the bloodstream, rolling and extravasation [277]; (2) Less time-consuming than iterative selection of bone metastatic PCa cells [278]; (3) The use of wild-type mouse allows for study of PCa development in an immunocompetent background which considers the involvement of immune system.

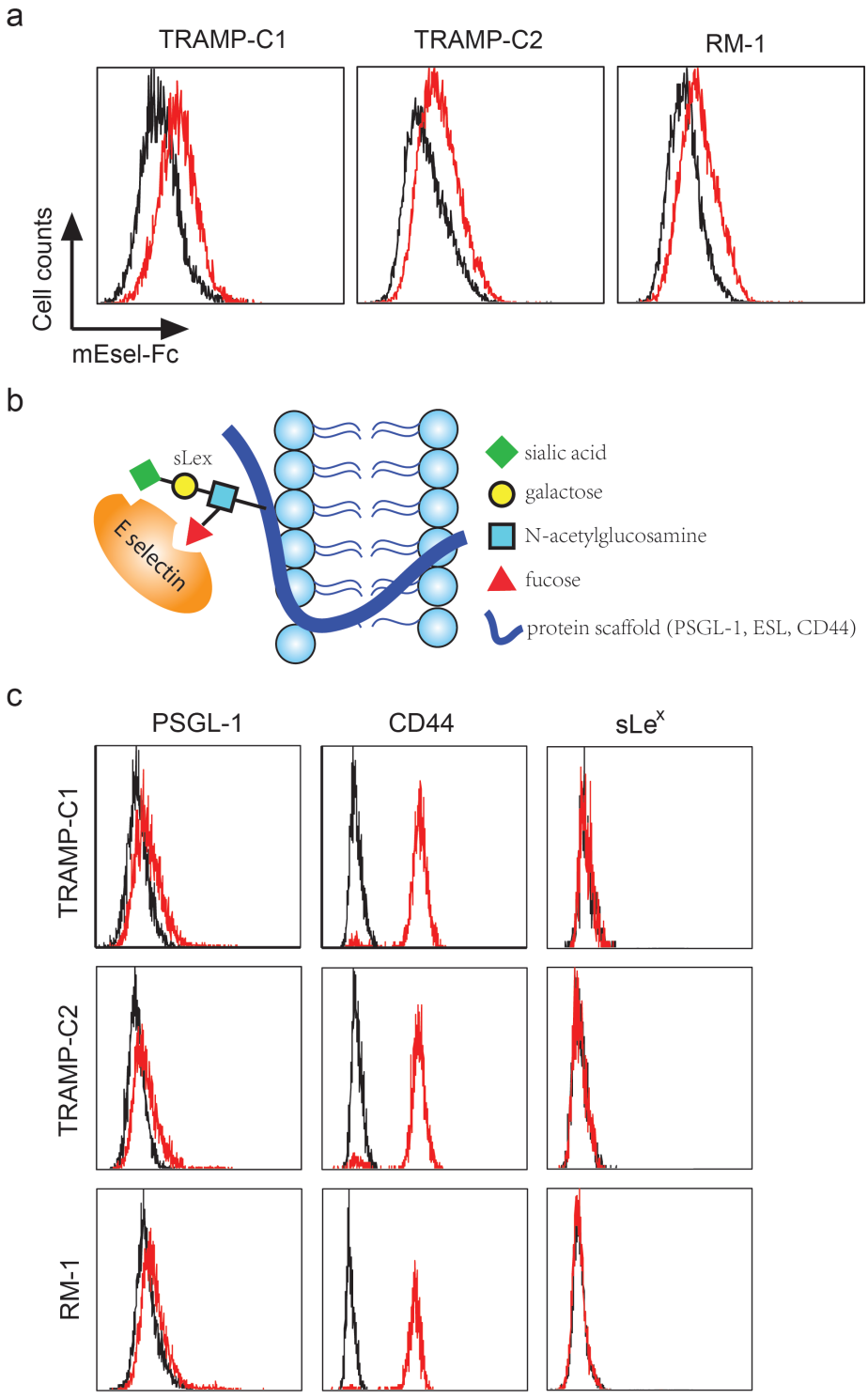

Figure 2.1. Characterization of ESLs in mouse PCa cells. (a) Mouse PCa cells have low binding affinity to E-selectin**.** TRAMP-C1, TRAMP-C2 and RM-1 were assayed

for mouse E-selectin-Fc chimera binding. Staining was performed in the presence of 2 mM Ca^{2+} (red histograms) or 1mM EDTA (black histograms); n=3. Representative histograms from three experiments are shown. (b) A cartoon showing components of ESLs required for the binding of ESLs to E-selectin. (c) Mouse PCa cells express ESL scaffold but lack essential carbohydrate. Mouse PSGL-1, CD44 and sLe^x were assayed with PE-anti-PSGL-1, FITC-anti-CD44 and FITC-HECA452 antibodies (red histograms) or corresponding isotypes (black histograms); n=3. Representative histograms from three experiments are shown.

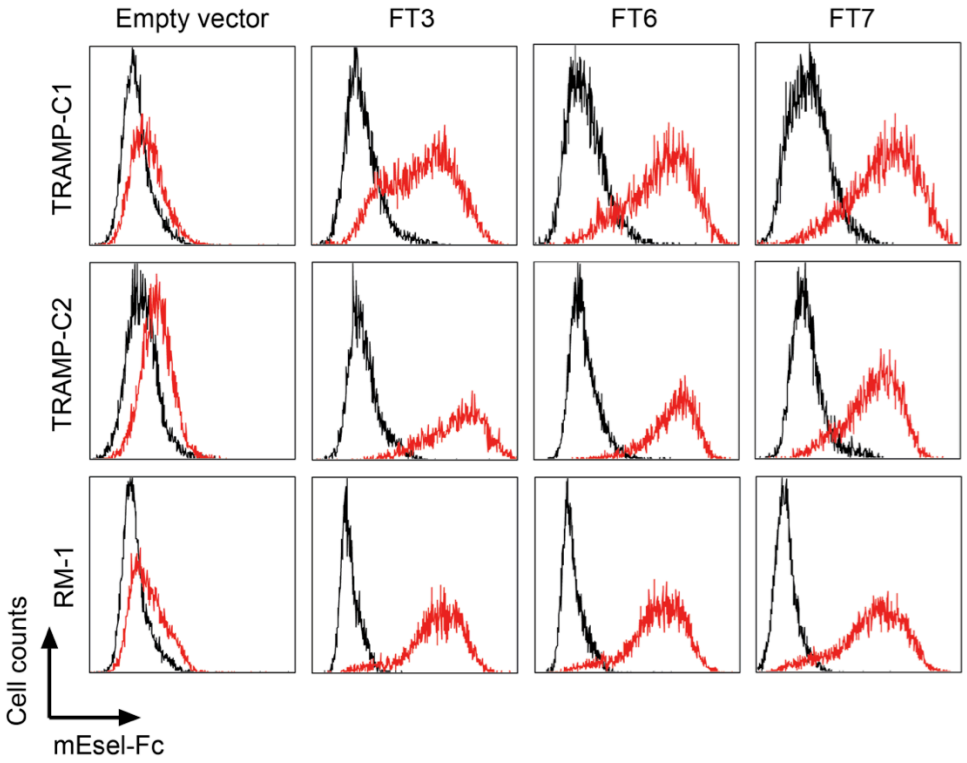

Figure 2.2. α-1,3 FTs are potent inducers of E-selectin-binding in mouse PCa cells. Retrovirus packaged with empty vector (vehicle control), FT3, FT6 and FT7 were transduced into TRAMP-C1, TRAMP-C2 and RM1 cells. Stable cells were established under selection with G418 (400 μg/ml) for two weeks. Afterwards, cells were assayed for mouse E-selectin-Fc chimera binding. Staining in the presence of 2 mM Ca^{2+} (red histograms) or 1mM EDTA (black histograms); n=2. Representative histograms from two experiments are shown.

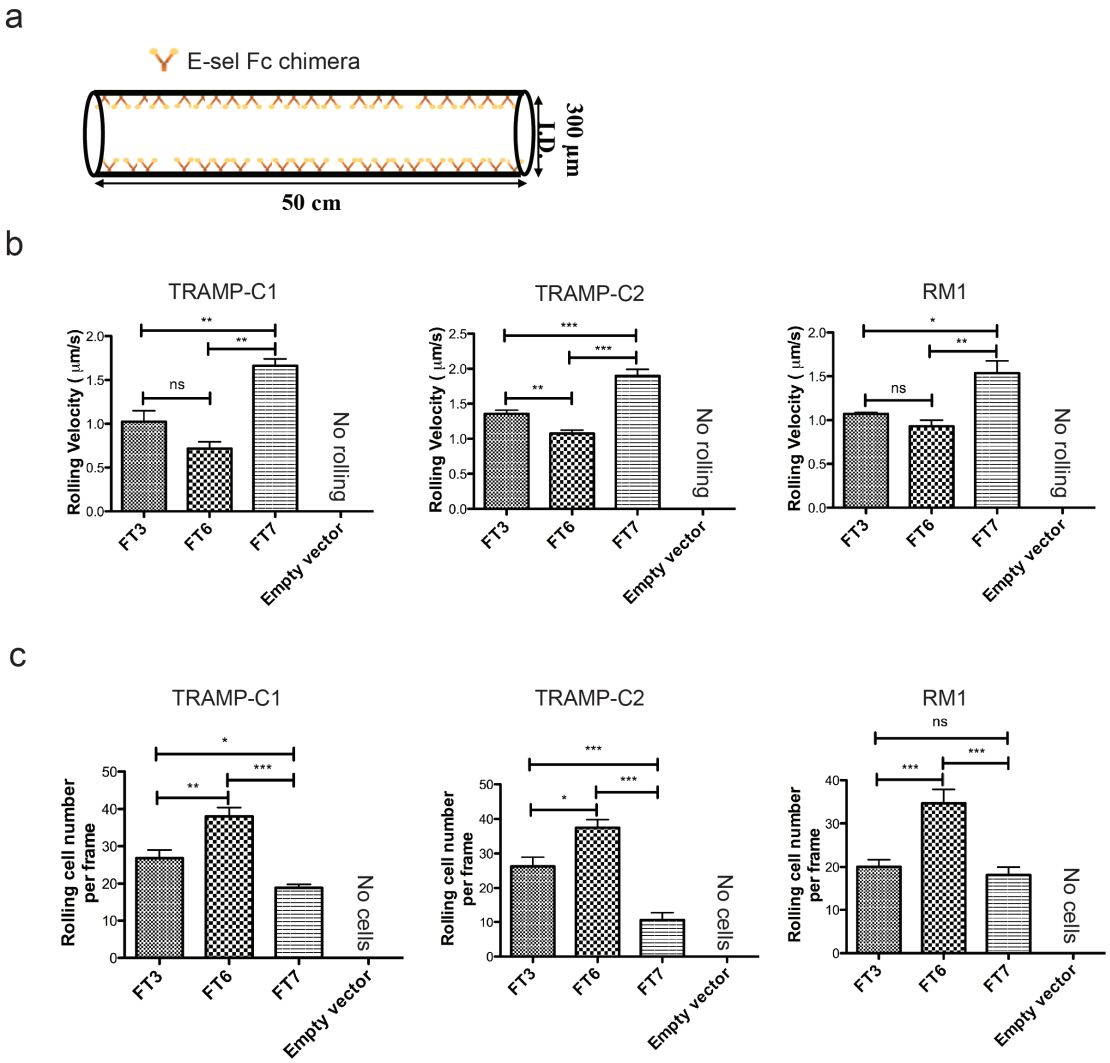

Figure 2.3. α-1,3 FTs mediate robust but distinct mouse PCa cell rolling in E-selectin-coated microtubes. (a) A cartoon of a biomimetic microtube is shown. The inner surface of microtubes were functionalized with protein G and E-selectin-Fc chimera to mimic constitutive E-selectin expression on bone marrow endothelial cells. (b) Cell rolling velocity for α-1,3 FT-transfected TRAMP-C1, TRAMP-C2 and RM-1, respectively. 30 rolling cells were recorded under physiological WSS of 2 dyn/cm^2 from each independent experiment. "No rolling" indicates that empty vector-transfected cells failed to roll on E-selectin surfaces. Results are the mean ± SEM of

three experiments; ** $p<0.01$, *** $p<0.001$. (c) Number of rolling cells interacting with E-selectin-functionalized surfaces per frame under physiological WSS of 2 dyn/cm^2. 10 frames were recorded for each experiment. Results are the mean ± SEM of three experiments; ** $p<0.01$, *** $p<0.001$.

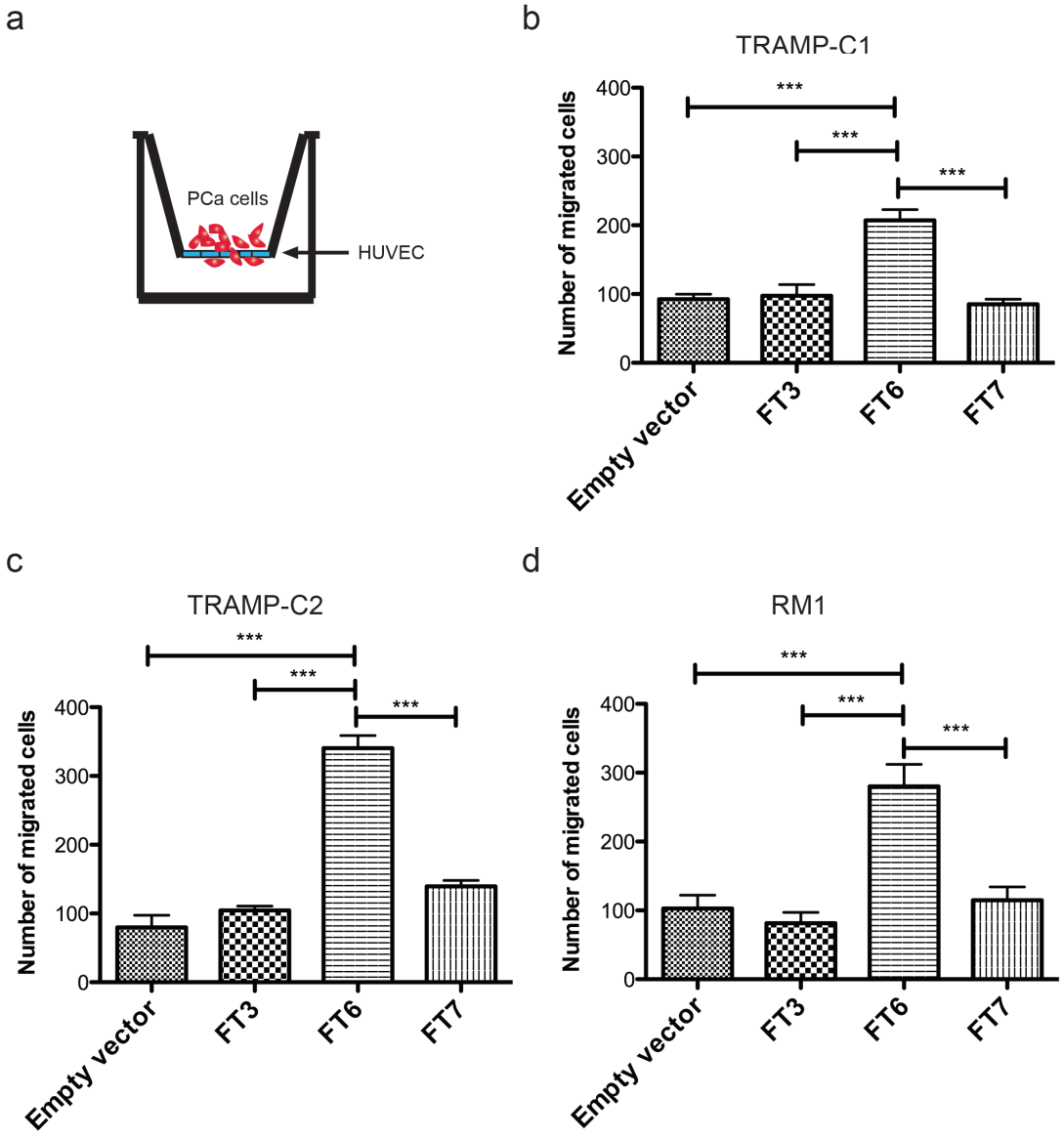

Figure 2.4. α-1, 3 FTs induce differential transendothelial migration. (a) A cartoon depicting the transendothelial migration assay is shown. Nearly confluent HUVEC monolayers were stimulated with TNF-α for 4 hr before PCa cells were seeded. (b-d) Number of cells that migrated through a monolayer of HUVEC after incubation for 24 hr. Results are the mean ± SEM of three experiments; ** $p<0.01$, *** $p<0.001$.

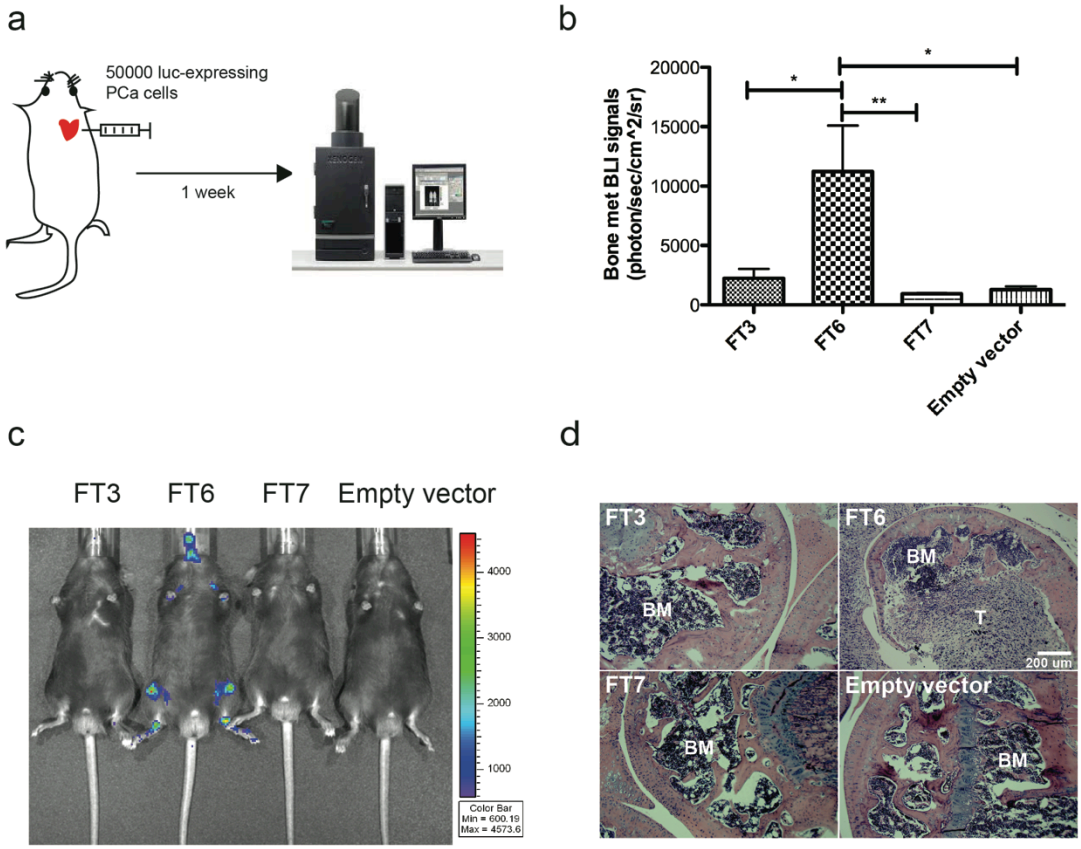

Figure 2.5. FT6 induces the highest incidence of bone metastasis using TRAMP-C2 cells in C57BL/6 mice. (a) A cartoon illustrating the procedures including intracardiac injection and bioluminescence imaging is shown. (b) Quantification of bone metastases in femurs and tibias one week after inoculation of PCa cells. Bioluminescence (BLI) signals collected on day 7 were normalized to whole-body BLI on day 0. FT6 induced statistically significant bone metastasis compared to empty vector, FT3 and FT7 groups. For each group, n=6. The experiment was repeated twice; Results are mean ± SEM from two independent experiments; *$p<0.05$, **$p<0.01$. (c) Representative BLI images taken one week after PCa inoculation. Heat bar is

represented as counts. BLI signals < 600 counts were considered noise and removed per manufacturer suggestion. (d) Representative images of H&E staining from BLI-positive areas. BLI was found to come largely from femurs proximal to knee joints. BM= bone marrow, T= tumor.

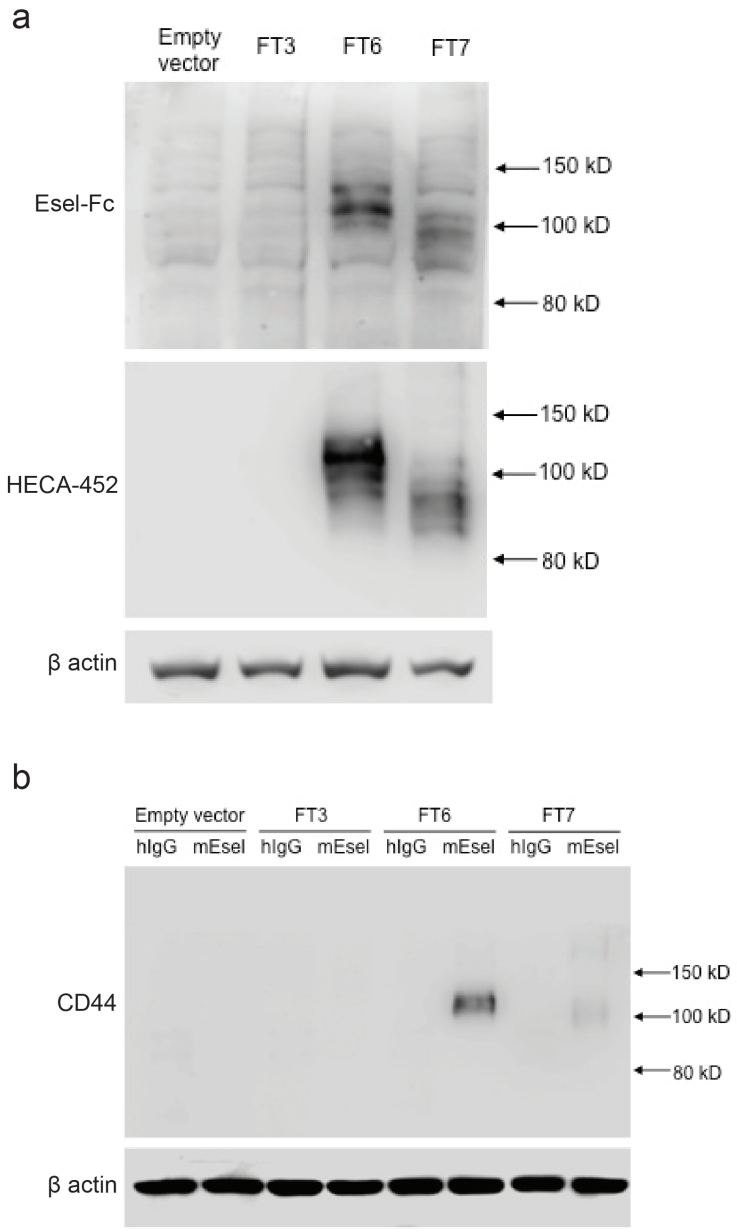

Figure 2.6. CD44 is a primary ESL following FT6 overexpression. (a) Western blotting of membrane proteins from FT3, FT6 and FT7-transduced TRAMP-C2 cells. Distinct patterns were identified after proteins were probed with E-selectin-Fc and anti-sLe^x mAb HECA-452. Empty vector-transduced TRAMP-C2 served as a background control. Anti-β actin was used as loading control. (b) E-selectin-Fc immunoprecipitates from FTs-transduced TRAMP-C2 proteins were subjected to

Western blotting and immunostained with anti-CD44. Human IgG immunoprecipitates were not reactive with anti-CD44 indicating specific interaction between E-selectin and CD44. Only FT6 cells generated a CD44-reactive band showing that FT3 and FT7 were unable to modify CD44 to become a functional ESL.

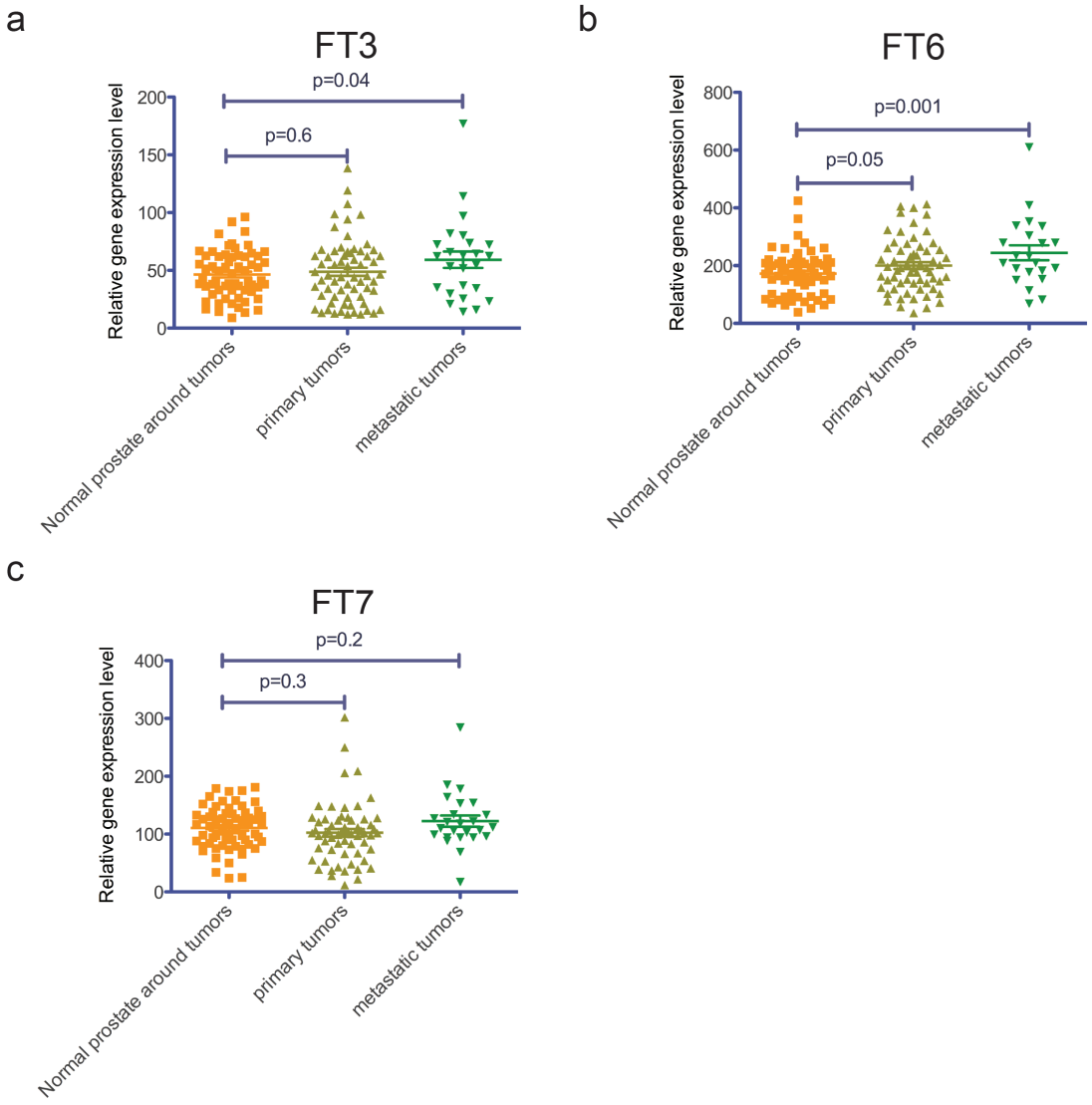

Figure 2.7. Gene expression analysis of FTs in clinical prostate cancer. The NCBI Gene Expression Omnibus (GEO) dataset GDS2545 was utilized for profiling the expression of (a) FT3, (b) FT6 and (c) FT7 in 1) normal prostate 2) normal prostate tissue adjacent to tumor, 3) primary tumors, and 4) metastatic prostate tumor samples, and significance was analyzed by Student t-test.

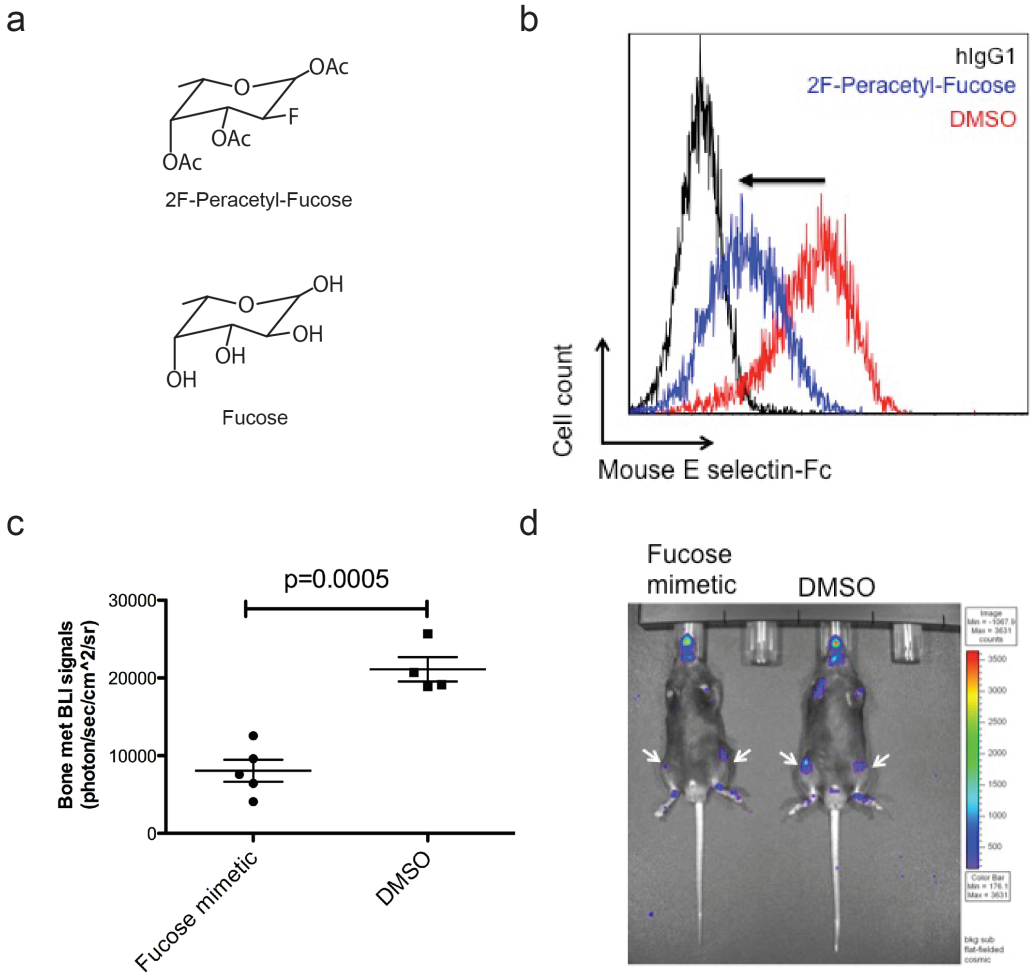

Figure 2.8. Inhibition of FT6 by fucose-mimetic (2F-Peracetyl-Fucose) reduces bone metastasis. (a) Molecular structure of 2F-Peracetyl-Fucose and natural fucose. (b) FT6-transduced TRAMP-C2 cells were treated with 20 μg/ml 2F-Peracetyl-Fucose or 0.2% DMSO for 96 hr. The expression of ESLs was detected by human IgG isotype or mouse E-selectin-Fc at 10 μg/ml. (c) Pretreatment with 2F-Peracetyl-Fucose reduced bone metastasis in vivo. FT6-transduced TRAMP-C2 cells with the same treatment as (b) were injected into the left ventricle of C57BL/6 mice. Bone metastases in femurs and tibias were quantified by BLI one week later. Significance was analyzed by Student t-test. DMSO group, n=5. 2F-Peracetyl-Fucose group, n=4.

(d) Representative image of bone metastases in study (c). Arrows indicate areas of bone metastases.

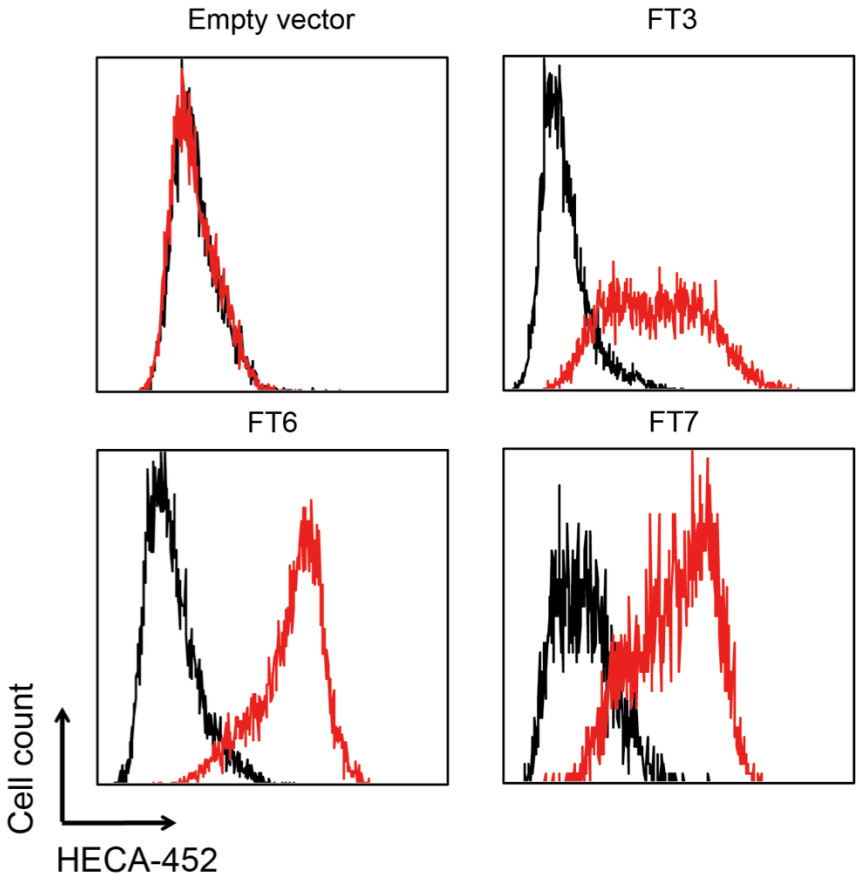

Supplemental figure 2.1. HECA-452-reactive TRAMP-C2 cells after overexpression of FT3, FT6 and FT7. TRAMP-C2 cells were transduced with retrovirus carrying cDNA for FT3, FT6 or FT7. Stable cell lines were selected by G418 and stained with FITC-HECA-452. FITC-Rag IgM was used as isotype control.

TRAMP-C1

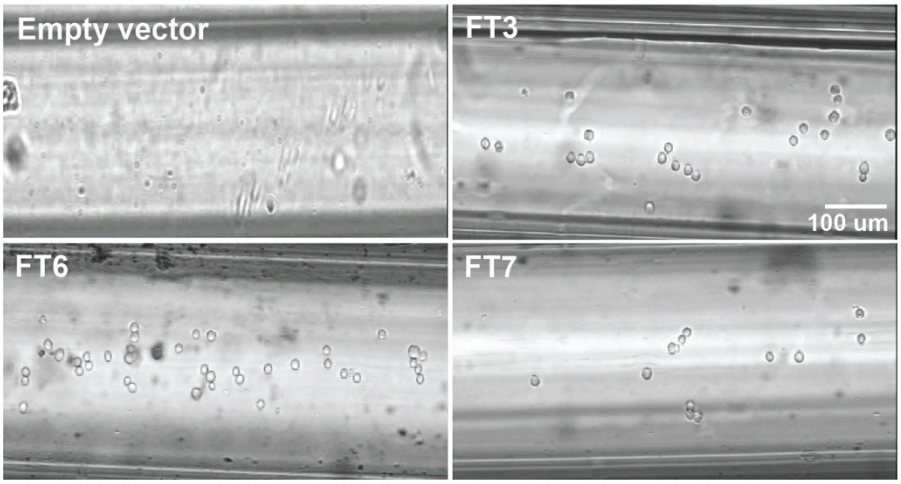

TRAMP-C2

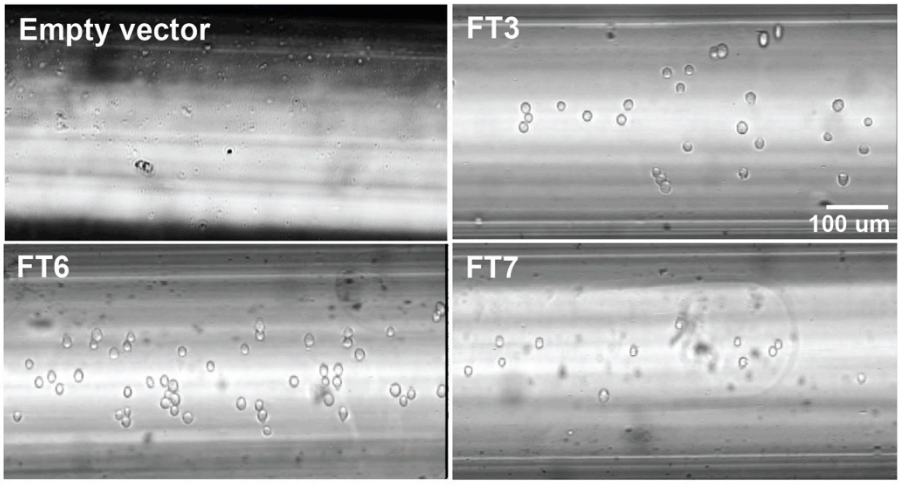

RM1

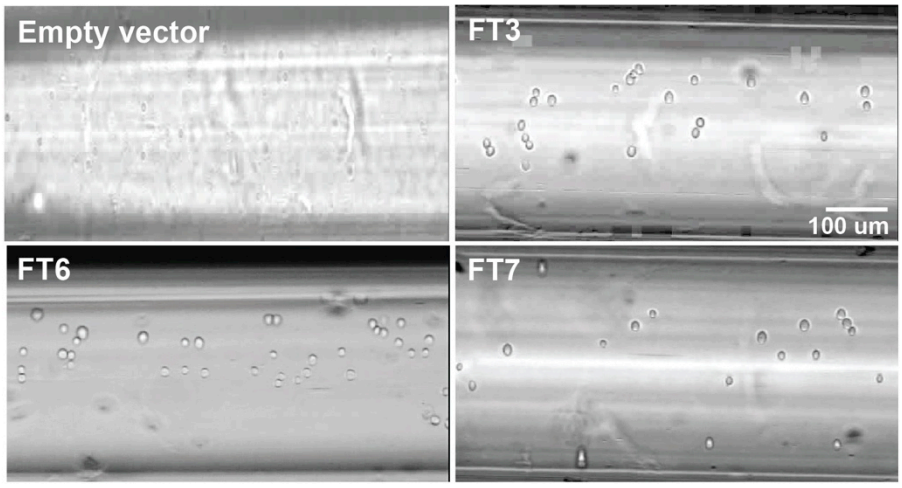

Supplemental figure 2.2. Representative images of rolling cells on E-selectin-coated surfaces. Cells were recorded at physiological WSS of 2 dyn/cm^2. Images were captured (20X objective) on an Olympus IX81 motorized inverted microscope.

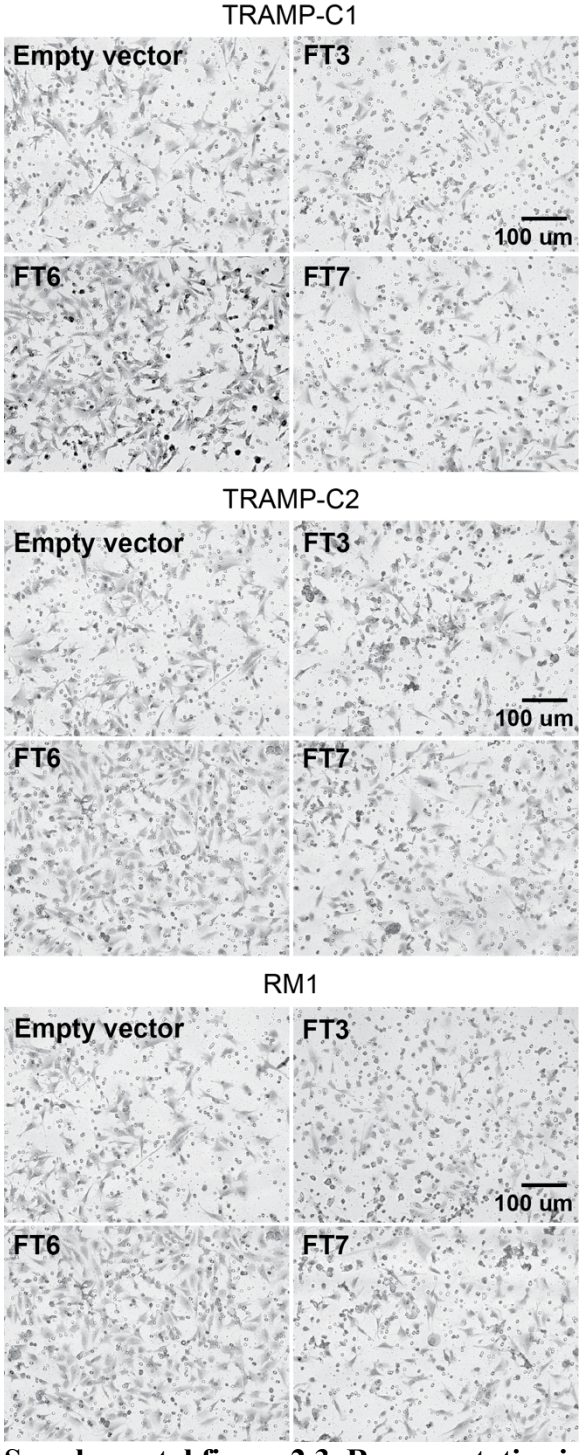

Supplemental figure 2.3. Representative images of cells that have undergone transendothelial migration. At the end of the assay, cells from the top of the inserts

were removed. Cells at the bottom of the inserts were fixed and stained with crystal violet. Images were taken (20X objective) on an Olympus IX81 motorized inverted microscope.

CHAPTER 3 PIPERLONGUMINE AND IMMUNE CYTOKINE TRAIL SYNERGIZE TO PROMOTE TUMOR DEATH

* This section is adapted from the following publication:

Li, J., C.C. Sharkey, and M.R. King, *Piperlongumine and immune cytokine TRAIL synergize to promote tumor death.* Scientific Reports, 2015. **5**: p. 9987.

Malignant transformation results in increased levels of reactive oxygen species (ROS). Adaption to this toxic stress allows cancer cells to proliferate. Recently, piperlongumine (PL), a natural alkaloid, was identified to exhibit novel anticancer effects by targeting ROS signaling. PL induces apoptosis specifically in cancer cells by downregulating several anti-apoptotic proteins. Notably, the same anti-apoptotic proteins were previously found to reduce tumor necrosis factor-related apoptosis-inducing ligand (TRAIL)-induced apoptosis in cancer cells. Therefore, we reasoned that PL would synergize with TRAIL to stimulate potent apoptosis in cancer cells. We demonstrate for the first time that PL and TRAIL exhibit a synergistic anti-cancer effect in cancer cell lines of various origins. PL resulted in the upregulation of TRAIL receptor DR5, which potentiated TRAIL-induced apoptosis in cancer cells. Furthermore, such upregulation was found to be dependent on ROS and the activation of JNK and p38 kinases. Treatment with combined PL and TRAIL demonstrated significant anti-proliferative effects in a triple-negative breast cancer MDA-MB-231 xenograft model. This work provides a novel therapeutic approach for inducing cancer cell death. Combination of PL and TRAIL may suggest a novel paradigm for treatment of primary and metastatic tumors.

3.1 Introduction

Most FDA-approved cancer chemotherapy agents are broadly categorized into "proliferation inhibitory" and "signaling targeted" drugs. Proliferation inhibitory drugs gain their selectivity by targeting rapidly dividing cancer cells. These drugs have been found to inhibit mitosis or prevent DNA replication. For example, paclitaxel and

related drugs that inhibit microtubule polymerization dynamics have proven effective for treating some epithelial cancers (breast, lung, prostate and others) [279]. In contrast, nucleoside analogues or DNA-intercalating agents, such as doxorubicin, target proliferating cells by interfering with the synthesis of genomic DNA [280]. Nevertheless, normal tissues or organs such as bone marrow, gut and hair follicles undergo rapid division making them susceptible to the anti-proliferative effect of these drugs [281-283]. Such toxicities can prevent continuous dosing of the drugs in certain patients with relatively high sensitivity to this side effect.

A second class of drugs inhibits specific signaling pathways that can promote tumor growth [284]. These signaling pathways are commonly amplified in certain cancers through protein overexpression or gene amplification, while these pathways in normal cells are not [285, 286]. One example of this class is tyrosine kinase inhibitor. Trastuzumab, a humanized anti-HER-2 monoclonal antibody, has been approved for treatment of patients with breast cancers that overexpress the human epidermal growth factor receptor-2 (HER-2) protein or that exhibit ErbB2 gene amplification [287]. However, the fact that the overexpression of HER-2 occurs in 25-30% of breast cancers renders the therapy ineffective against the remainder of breast cancer cells that do not rely on HER-2 overexpression [288].

Recently, a new class of chemicals targeting the stress response to reactive oxygen species (ROS) has gained attention due to the chemicals' specificity and broad effect in a variety of cancer types [289]. It is postulated that malignant transformation,

caused by gain-of-function activation in oncogenes or loss-of-function mutations in tumor suppressor genes, results in enhanced cellular stress. Adaptation to this stress is necessary for cancer cell survival while it is not required in normal cells [290]. Using a high throughput small-molecule screening, piperlongumine (PL) was identified as a drug that increases the level of ROS and apoptosis in cancer cells but has little inhibitory effect on either rapidly or slow dividing normal cells [291]. It was later shown that PL also induces autophagy in cancer cells as an alternative strategy of suppression in a caspase-independent cancer cell death [292]. A biochemical examination of PL-induced cell death indicated that it represses various anti-apoptotic proteins including B-cell CLL/lymphoma 2 (BCL2), baculoviral IAP repeat containing 5 (also known as survivin) and X-linked inhibitor of apoptosis (XIAP) in cancer cells [291].

Clinical treatments involving a single drug have proven short-lived due to the emergence of resistant cancer cells. A major strategy for overcoming drug resistance is combination therapy [293-295]. Given the effectiveness of PL in cancer cell lines and preclinical mouse models, it remains to be answered if a synergistic effect or enhanced induction of apoptosis can be achieved when PL is combined with another drug. One reagent explored in this study is tumor necrosis factor-related apoptosis-inducing ligand (TRAIL), which is under clinical trials for cancer therapy [296]. Similar to PL, TRAIL has been found to kill cancer cells while sparing normal cells [100, 297, 298]. It is broadly expressed on lymphocytes, neutrophils and other immune cells as an innate immune cytokine to clear diseased cells. TRAIL can induce apoptosis

immediately following its binding to TRAIL receptors highly expressed in cancer cells of various origins [297]. However, certain cancer cells develop TRAIL resistance through elevated expression of anti-apoptotic proteins that are nevertheless suppressed by PL [291, 299]. In this study, we investigated the effect of these two combined tumor-specific reagents on cancer cells and normal cells. Furthermore, the preclinical efficacy of the combination therapy was evaluated in a triple-negative breast cancer model.

3.2 Materials and Methods

Cell lines and mice

Human colon cancer HT29, prostate cancer DU145, breast cancer MDA-MB-231 and normal primary mammary epithelial cells were obtained from American Type Culture Collection (ATCC) (Rockville, MD, USA). Human colon cancer HCT116 were kindly provided by Dr. Xiling Shen (Cornell University, Ithaca, NY, USA). MDA-MB-231 cells were cultured in DMEM (Invitrogen, Grand Island, NY, USA) with 10% FBS and the other cell lines were cultured in RPMI 1640 (Invitrogen) with 10% FBS. Primary mammary epithelial cells were cultured in Mammary Epithelial Cell medium (ATCC) and were used up to passage number 6. Six to eight-week old female NOD SCID gamma mice were purchased from Jackson Laboratory (Bar Harbor, ME, USA). Mice were housed in a SPF barrier animal facility at Cornell University.

Chemicals and antibodies

Piperlongumine and doxorubicin were purchased from Cayman Chemical Company

(Ann Arbor, MI, USA). Soluble recombinant human TRAIL for *in vitro* work was purchased from PeproTech (Rocky Hill, NJ, USA). His-tagged TRAIL for *in vivo* work was produced and purified as previously described [300]. JNK, ERK and p38 inhibitors were obtained from LC laboratories (Woburn, MA, USA). The following chemicals or kits were used for assaying cell proliferation and apoptosis: MTT (AMRESCO, Solon, OH, USA), Crystal Violet (Acros Organics, Pittsburgh, PA, USA), and TACS® Annexin V-FITC Kit (Gaithersburg, MD, USA). Antibodies for western blotting or flow cytometry were: mouse anti-caspase 3 (Novus Biologicals, Littleton, CO, USA), mouse anti-β actin (Santa Cruz Biotech, Santa Cruz, CA, USA), PE-conjugated anti-DR4 (Santa Cruz Biotech), PE-conjugated anti-DR5 (R&D Systems, Minneapolis, MN, USA), rabbit anti-DR5 (Abcam, Cambridge, MA, USA), goat anti-rabbit IgG-HRP (Santa Cruz Biotech) and goat anti-mouse IgG-HRP (Santa Cruz Biotech). Human DR5 shRNA was purchased from Sigma (St. Louis, MO, USA).

Flow cytometry

Cells were detached with enzyme-free Gibco® Cell Dissociation Buffer (Invitrogen) and suspended at a concentration of 5×10^5 cells in 100 μL cold PBS/1% bovine serum albumin (BSA). Primary antibodies or corresponding isotype control antibodies were incubated with cells for 30 min on ice. Following two washes with 1 mL of PBS/1% BSA, fluorescence measurements were collected using an Accuri C6 flow cytometer (BD Biosciences, San Jose, CA, USA). Data were analyzed using the Flow Express software (De Novo Software, Los Angeles, CA, USA).

Western blotting

Western blotting was performed as previously described [301]. Briefly, whole cell lysates were prepared and separated using 10% SDS-PAGE. Membranes were incubated with primary antibodies and secondary antibodies diluted at 1:1000. Immobilized proteins were detected by using a chemiluminescent HRP substrate (Millipore, Billerica, MA, USA).

Cell proliferation assay

The effect of PL and TRAIL on cell proliferation was assayed by measuring mitochondrial dehydrogenase activity using MTT as the substrate. After the drug treatment, cells were incubated with MTT at a concentration of 0.5 mg/mL, at 37°C for 3 hr. The purple MTT product was solubilized with DMSO and measured at 570nm using a BioTek plate reader (Winooski, VT, USA). The effect of PL and TRAIL was also evaluated qualitatively using a crystal violet cell viability assay. After drug treatment, cells were washed with PBS and fixed with methanol. The fixed cells were incubated with crystal violet at a concentration of 0.5% for 20 min at room temperature. The blue crystal violet product was solubilized with a 1% SDS solution.

Evaluation of synergistic effect by Jin's formula

The synergistic effect of combined PL and TRAIL was analyzed by Jin's formula [302]. The formula is $Q = E_{a+b}/(E_a + E_b – E_a \times E_b)$, where E_{a+b}, E_a and E_b are the average inhibitory effects of the combination treatment, PL only and TRAIL only, respectively. In this method, $Q < 0.85$ indicates antagonism, $0.85 < Q < 1.15$ indicates

additive effects, and Q > 1.15 indicates synergism. The E_{a+b}, E_a and E_b quantities were obtained from MTT assay.

Measurement of ROS production

Cells were first treated with PL, Dox or DMSO for 6 hr and then loaded with 1 μM of CM-H2DCFDA (Invitrogen, Carlsbad, CA, USA) in PBS for 10 min at 37°C. Afterwards, cells were allowed to recover in growth medium for 15 min at 37°C. Cells were analyzed using a flow cytometer. In groups receiving pretreatment of NAc, 1 mM NAc was added 1 hr prior to incubation with PL, Dox or DMSO. Histograms are representative of two separate experiments.

Lentiviral production and transduction

Lentiviral vectors (scrambled control shRNA and shRNA against DR5) and packaging helper plasmids pMD2G and psPAX2 were transfected into HEK293T cells by TransIT®-LT1 Transfection Reagent (Mirus Biology, Madison, WI, USA). Virus supernatants were harvested at 48 hr and 72 hr after transfection. Virus supernatants were mixed with target cells in the presence of 8μg/ml polybrene (Santa cruz Biotech) for 24 hr. Afterwards, fresh media was added and cells were selected with 1 μg/ml puromycin for one week.

Animal studies

All mice were handled according to the Guide for the Care and Use of Laboratory Animals in compliance with US- and UK-based guidelines. All experimental

procedures and protocols were approved by the Institutional Animal Care and Use Committee of Cornell University (Protocol No. 2011-0051). Hairs at the dorsal area of female NOD SCID gamma (NSG) mice were shaved on the day of injection. For examination of DR5 expression induced by PL, 1 million of MDA-MB-231 cells were implanted subcutaneously. When tumors reached 5-8 mm in diameter, vehicle control (DMSO), PL (2.4 mg/kg), TRAIL (2 mg/kg), or a combination treatment were administered intratumorally, twice for two days. 24 hr after the second administration, tumors were collected and subjected to immunohistochemical (IHC) staining for DR5. Rabbit IgG isotype was used as a control for detection of nonspecific IHC staining. For combination therapy, mice were injected subcutaneously with 100 μL sterile PBS containing 1 million MDA-MB-231 cells. When tumors reached 3-5 mm in diameter, mice received the vehicle control (DMSO), PL (2.4 mg/kg), TRAIL (2 mg/kg), or a combination treatment intratumorally at the indicated time points. Tumor dimensions were determined using a caliper, and the tumor volume (mm^3) was calculated by the formula: volume=length × $width^2$× 0.5. Mice were euthanized 3 weeks after the inoculation of cancer cells.

Immunohistochemistry and digital analysis

Sections of 4% paraformaldehyde-fixed paraffin-embedded tumor slides were stained with anti-human DR5 rabbit polyclonal antibody or rabbit IgG control. ABC kit (Vector Laboratories, Burlingame, CA, USA) and DAB kit (Vector Laboratories) were used to develop the signals from antibody staining. Slides were counterstained by hematoxylin (Vector laboratories). Glass slides were scanned with Aperio ScanScope

scanner (Leica Microsystems Inc., Lincolnshire, IL, USA) and were analyzed with automated image analysis algorithm Aperio Positive Pixel Count (Leica Microsystems Inc.) using the default set of parameters. Briefly, in each slide, tumor cell areas were distinguished from neighboring stromal cells by the higher nucleus to cytoplasm ratio (N/C ratio) of cancer cells. In selected tumor areas, averaged intensity of staining was acquired through dividing total intensity by the sum of the numbers of weak positive (N_{wp}), positive (N_p) and strong positive pixels.

Immunofluorescence staining of frozen tumor sections

Freshly collected tumors were embedded in OCT and snap frozen in liquid nitrogen. Tumors were sectioned to a thickness of 10 μm by cryotome and mounted on glass slides. Tissue sections were fixed by ice cold acetone and stained with rabbit anti active caspase 3 (Cell signaling, Danvers, MA, USA) followed by DyLight™ 649 Donkey anti-rabbit IgG (Biolegend, San Diego, CA, USA). Slides were counterstained by DAPI and were imaged on an Olympus fluorescence microscope with Metamorph acquisition software.

Statistical analysis

All statistical analyses were performed using GraphPad Prism 5.0a for Mac OS X (San Diego, CA, USA). A one-way ANOVA followed by Tukey post test was used to compare statistical significance in the characterization of *in vitro* cell proliferation and tumor mass in the xenograft model.

3.3 Results

The synergistic anti-tumor effect of PL and TRAIL

The effect of PL and TRAIL combination treatment on cell viability was tested in colon cancer (HT29 and HCT116), prostate cancer (DU145) and breast cancer (MDA-MB-231) cells. The concentrations of PL and TRAIL were chosen based on previous studies [303, 304]. Following 24 hr of treatment with PL, TRAIL, or a combination of both, the percentage of viable cells significantly decreased compared to the single treatments in a dose-dependent manner measured by MTT assay (**Figure 3.1a-d**) and crystal violet assay (**Supplemental figure 3.1**). Furthermore, PL and TRAIL exerted a synergistic inhibitory effect in these tested cell lines as evaluated by Jin's formula (**Supplemental figure 3.2**). Such synergy was observed when 15 μM PL was combined with 50 or 200 ng/mL TRAIL. Given the role of PL in raising ROS level in transformed cells as previously reported [291], it remained unclear whether PL potentiated TRAIL-induced growth inhibition via ROS. To generalize the mechanism to multiple cell types, we used one prostate cancer cell line (DU145) and one breast cancer cell line (MDA-MB-231). In addition, DU145 and MDA-MB-231 were chosen based on their differential sensitivity to TRAIL. DU145 and MDA-MB-231 cells were pretreated with 1mM ROS scavenger N-acetyl Cysteine (NAc) followed by treatment with PL, TRAIL, or their combination. Whereas NAc abolished the cytotoxic effect of PL, it failed to affect TRAIL activity. Moreover, pretreatment with NAc completely negated the synergistic effect of combined PL and TRAIL, with cell viability close to TRAIL treatment alone (**Figure 3.1e and f)**.

We next determined the effect of PL on ROS levels in these two cancer cell lines through flow cytometry using the redox-sensitive fluorescent probe CM-H2DCFDA. Treatment with PL for 6 hr caused a marked increase in ROS levels in comparison to DMSO treatment. In contrast, pretreatment with 1mM NAC fully reversed the PL-induced ROS elevation (**Supplemental figure 3.3**). Therefore, it is concluded that the observed synergy of combined PL and TRAIL on cancer cells is mediated by ROS.

Given that certain cancer drugs such as doxorubicin (Dox) also generate oxidant stress and may synergize with TRAIL via ROS, we further sought to determine whether the mechanisms of TRAIL sensitization in cancer cells by PL and Dox converge on ROS production. Dox was found to increase ROS in both DU145 and MDA-MB-231 after 6 hr of incubation with cancer cells. In contrast, pretreating cells with 1mM NAc followed by Dox yielded reduced ROS levels equivalent to the basal level seen in cells not treated with Dox. As expected, we further demonstrated that Dox can synergize with TRAIL to inhibit cell proliferation in these two cancer cell lines to an extent close to the PL and TRAIL combination (**Supplemental figure 3.4a**). Such synergy was also found to be ROS-dependent, since pretreating cancer cells with 1mM NAc abolished the synergistic effect of Dox and TRAIL (**Supplemental figure 3.4b**). However, despite the fact that NAc could neutralize the inhibitory effect of a single PL treatment on cell viability (**Figure 3.1e and f**), a single Dox treatment was still effective in reducing cell viability in the presence of NAc (**Supplemental figure 3.4b**). Based on these data, one may conclude that both PL and Dox are dependent on ROS to synergize with TRAIL for enhanced apoptosis induction. Additionally, ROS drives

the toxicity of PL by itself, whereas Dox does not rely on ROS for its own cytotoxicity.

TRAIL enhances PL-induced apoptosis signaling

Although previous studies showed that PL can induce apoptosis selectively in cancer cells, it has not been previously shown whether TRAIL can enhance PL-induced apoptosis. The cleavage of procaspase 3, which indicates the activation of apoptosis signaling, was examined by western blotting in DU145, HCT116 and MDA-MB-231 cancer cell lines. In contrast to minimal cleavage of procaspase 3 by PL, TRAIL significantly enhanced cleavage of procaspase 3 when combined with PL (**Figure 3.2a**). Furthermore, an annexin V/PI assay was performed to differentiate necrotic, late apoptotic and early apoptotic cells after treatments of DMSO, 15 μM PL, 50 ng/ml TRAIL or combined TRAIL and PL in DU145 and MDA-MB-231 cells for 4 hr. In DU145, it was shown that the combined cell deaths (necrosis, late apoptosis and early apoptosis) were induced at 2.7% by PL, 12.8% by TRAIL, and 21.8% via combined PL and TRAIL after subtracting basal cell death in control treatment. For MDA-MB-231, the combined cell death percentages were 13.7% by PL, 17.6% by TRAIL, and 49.5% via the PL and TRAIL combination (**Figure 3.2b**).

PL upregulates death receptor 5 (DR5) via ROS

TRAIL-induced apoptosis signaling is triggered by the engagement of soluble TRAIL with TRAIL receptor DR4 and/or DR5 expressed on cancer cells. Previous studies showed that certain cancers developed TRAIL resistance by downregulating DRs [299]. In light of the enhanced anti-tumor effect of combined PL and TRAIL, it is not

clear whether PL also modulates the expression of DRs in addition to the downregulation of anti-apoptotic proteins as reported previously [291]. Expression of DR4 and DR5 at the transcriptional level was first investigated. Little change of mRNA (less than 2-fold difference) was observed after cells were exposed to 15 μM PL over 6, 12 and 24 hr (**Supplemental figure 3.5**). The surface expression of DR4 and DR5 were examined by flow cytometry in DU145 and MDA-MB-231 following 10 hr of exposure to 15 μM PL. Whereas DR4 expression was unaffected, expression of DR5 was significantly elevated by PL compared to the vehicle control (**Figure 3.3a**). Furthermore, the total DR5 expression was assayed by western blotting. It was shown that PL upregulated DR5 expression in DU145 and MDA-MB-231 in a time- and concentration- dependent manner, although TRAIL by itself also elevated DR5 expression in MDA-MB-231 (**Figure 3.3b**).

To better understand the mechanism of PL-induced DR5 expression, DU145 and MDA-MB-231 were pretreated with 1 mM antioxidant N-acetyl Cysteine (NAc) for 1 hr followed by treatment with 15 μM PL for 24 hr. As shown in **Figure 3.3c**, NAc suppressed PL-mediated upregulation of DR5 by quenching intracellular ROS. To confirm whether up-regulation of DR5 by PL is essential to sensitize tumor cells to TRAIL, DR5 expression was knocked down via shRNA in DU145 cells. It was found that silencing of DR5 significantly reduced the enhancing effect of PL on TRAIL-induced cell death (**Figure 3.3d**). Therefore, PL potentiates TRAIL-induced apoptosis signaling via ROS-mediated DR5 upregulation at the translational level.

PL-induced upregulation of DR5 is mediated through MAPK activation

Mitogen-activated protein kinases (MAPKs) have been reported to act as sensors for ROS generated in various intracellular stress conditions [305, 306]. Thus ROS generated from PL treatment likely elevates DR5 expression via MAPKs. To examine whether MAPKs is responsible for PL-induced upregulation of DR5, specific inhibitors for JNK, p38 and ERK1/2 MAPKs were utilized. Pretreatment of MDA-MB-231 or DU145 cells with JNK inhibitor SP600125 suppressed PL-induced upregulation of DR5 in a dose-dependent manner. Similarly, when cells were pretreated with p38 inhibitor SB202190, a dose-dependent decrease in PL-induced DR5 upregulation was observed. In contrast, ERK1/2 inhibitor PD98059 had no such inhibitory effect (**Figure 3.4a and b**). Similar results were also confirmed in HT29 and HCT116 cell lines (**Supplemental figure 3.6)**. Thus, JNK and p38 protein kinases concomitantly upregulate DR5 in cancer cells treated with PL.

Evaluation of combination therapy in triple-negative breast cancer xenograft model

Triple-negative breast cancer (TNBC) is defined as the absence of staining for estrogen receptors, progesterone receptors, and HER2/neu [307]. TNBC is insensitive to some of the most effective therapies available for breast cancer treatment including HER2-directed therapy such as trastuzumab and endocrine therapies such as tamoxifen or the aromatase inhibitors [308]. It was first tested whether the combination therapy induced cytotoxicity of normal cells. No growth inhibition was observed for PL, TRAIL, or their combination when normal breast epithelial cells were tested *in vitro* (**Figure 3.5a**). To confirm that PL can induce upregulation of DR5

in vivo, vehicle control, PL, TRAIL or combined PL and TRAIL were injected into subcutaneous tumors (5-8 mm in diameter) of MDA-MB-231 in NOD-SCID gamma (NSG) mice on day 0 and day 1. 24 hr after the second injection, tumors were sectioned and subjected to immunohistochemistry staining for DR5 expression. Whereas DR5 was detected at a basal level in vehicle control and TRAIL treatment groups compared to rabbit IgG isotype-stained slides, it was significantly upregulated in groups receiving PL or combined PL and TRAIL (**Figure 3.5b**). After confirming the safety of combination therapy as well as elevation of DR5 by PL *in vivo*, NOD-SCID gamma (NSG) mice were subcutaneously implanted with human TNBC MDA-MB-231 cells. Four days post implantation when the average diameter of tumors grew to 3-5 mm, NSG mice were intratumorally injected with vehicle control, PL, TRAIL or combined PL and TRAIL (combo) at preclinically relevant dosages every other day for a total of five injections. Weekly measurement of tumor size for three weeks indicated significant inhibition of tumor growth when combined PL and TRAIL were administered (**Figure 3.5c and d**). In the meantime, monitoring of the body weight showed no significant weight loss (**Figure 3.5e**). At the end of therapy, apoptotic cells were quantified in tumor sections corresponding to each treatment group via immunofluorescence staining of active caspase 3. It was found that combined PL and TRAIL resulted in the highest number of apoptotic cells (**Figure 3.5f and g**). Thus, PL and TRAIL combination inhibited tumor growth via potent induction of cancer apoptosis similar to *in vitro* observation.

3.4 Discussion

In this study, we provide evidence that PL and TRAIL can synergistically induce apoptosis in cancer cells of various origins. Interestingly, PL was found to enhance the expression of total and membrane-bound DR5, a main TRAIL receptor for TRAIL-induced apoptosis signaling. The upregulation of DR5 was abolished when cancer cells were pretreated with the anti-oxidant N-acetyl cysteine. Furthermore, it was shown that the enhanced DR5 expression caused by PL is dependent on the activation of mitogen-activated protein kinases, JNK1/2 and p38. Thus, we propose two different mechanisms to explain the synergistic effect of combined PL and TRAIL in cancer cells: downregulation of anti-apoptotic proteins, and upregulation of TRAIL receptor DR5 via ROS-mediated activation of MAPKs (**Figure 3.6**).

Although most anti-tumor agents are classified according to their putative mechanism of action, in reality the mechanism of action may be multi-factorial. For example, doxorubicin has been known to generate oxidant stress [309]. Based on our results, we found that both PL and Dox are dependent on ROS to synergize with TRAIL for enhanced apoptosis induction. Additionally, ROS drives the toxicity of PL by itself while Dox does not rely on ROS for its own toxicity. However, such observation should not limit the potential clinical application of PL in combination with TRAIL, although Dox presented similar efficacy when combined with TRAIL. For example, it has been shown that cancer patients experience differential responses to the side effects of Dox in clinical treatments [310, 311]. Although PL has not been evaluated clinically, its safety in preclinical studies including previous publications and our current work suggests PL and TRAIL combination as a viable option when other

TRAIL combination therapies are not effective or are found to cause side effects in certain cancer patients.

TNBC represents one of the most challenging breast cancer subtypes for effective targeted therapy due to the absence of common receptors expressed on other breast cancer subtypes. Whereas resistance to cell cycle inhibition drugs such as doxorubicin and paclitaxel have been detected in TNBC [312], the current study tested the combination of PL and TRAIL in a xenograft mouse model using the TNBC cell line MDA-MB-231. Consistent with the synergistic effect observed *in vitro*, this combination therapy significantly inhibited the growth of MDA-MB-231 even one week after discontinuing the treatment. The presented *in vivo* trials involved intratumoral (i.t.) injection of the therapeutics since this technique has been extensively evaluated over the past few decades [313-317]. An advantage of using this method is that i.t. injections allow for extremely high doses of drug within the tumor with minimal systemic toxicity. Additionally, this approach allows one to directly evaluate the synergistic effect of the PL and TRAIL without the results being affected by the pharmacokinetic factors associated with intravenous injections. We acknowledge, however, that this is also a limitation because the delivery method provides little insight into the therapy's systemic effectiveness. The pharmacokinetics of the combination therapy will be the subject of future work. Despite this the observed synergistic therapeutic activity identifies PL and TRAIL as a promising combination therapy for potentially several types of cancer using an i.t. delivery approach.

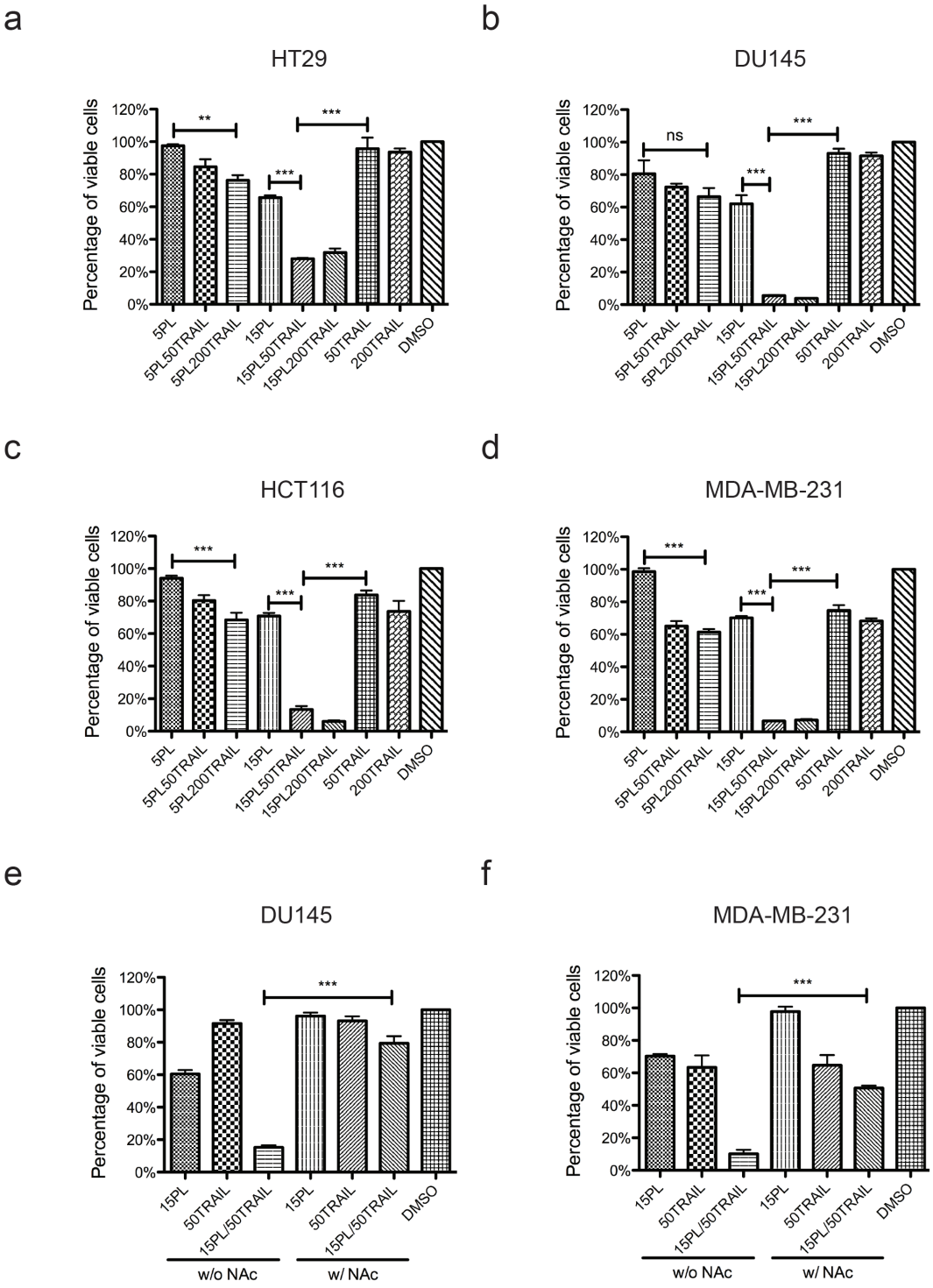

Figure 3.1. The anti-tumor effect of combined PL and TRAIL. Cancer cells were treated with the indicated concentrations of PL (5 or 15 μM) and/or TRAIL (50 or 200

ng/mL) in 48-well plates for 24 hr. Cell viability was measured using MTT assay. The cell lines tested were: (a) HT29 (colon cancer), (b) DU145 (prostate cancer), (c) HCT116 (colon cancer) and (d) MDA-MB-231 (breast cancer). (e, f) PL-induced ROS mediated synergistic anti-proliferation effect of PL and TRAIL. Pretreatment of DU145 and MDA-MB-231 with 1mM NAc significantly increased viability of cells subjected to combined PL and TRAIL, with cell viability close to TRAIL treatment alone. All results are presented as the mean ± SEM, n=3; **, $p<0.01$; ***, $p<0.001$; ns, no significant difference.

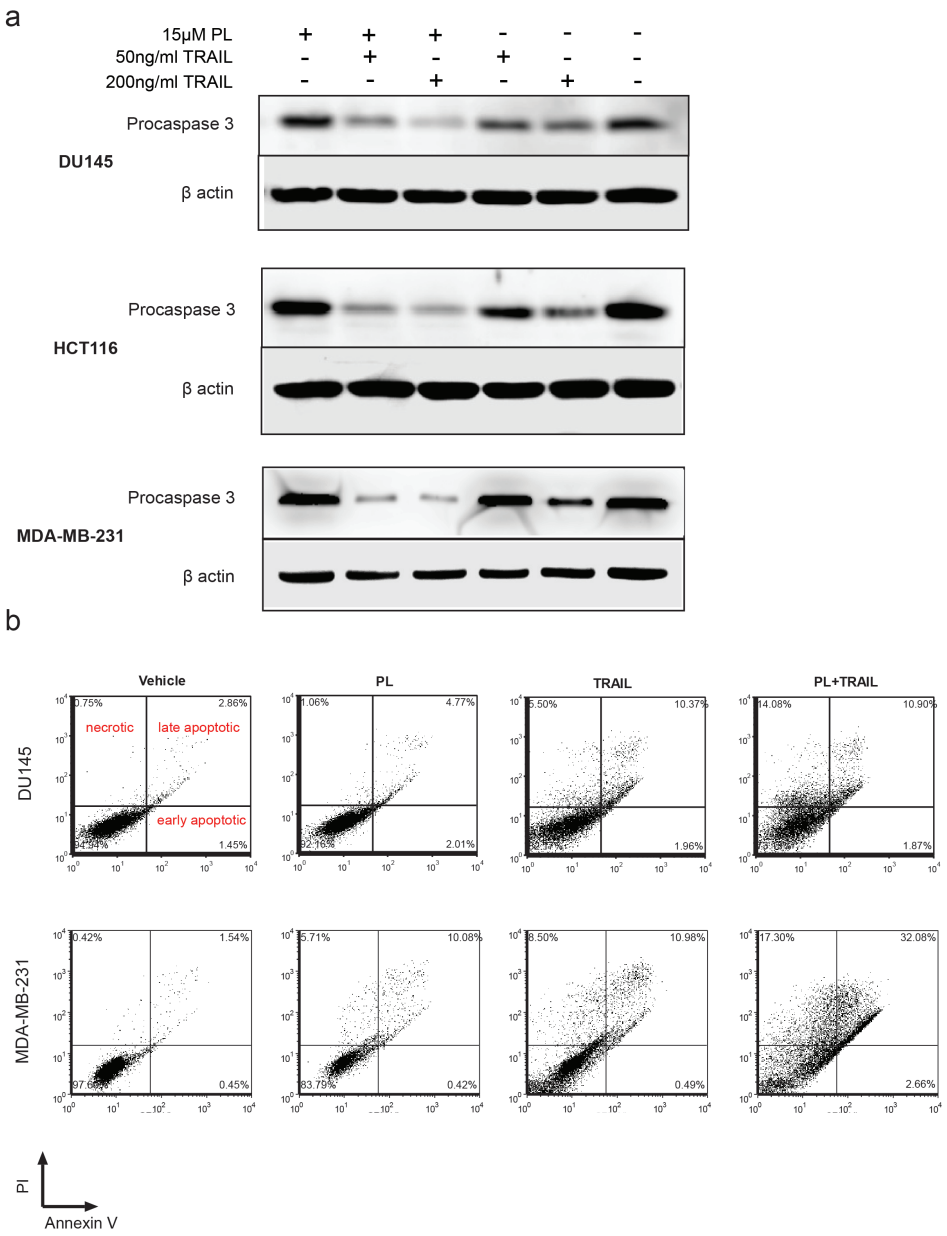

Figure 3.2. Enhancement of PL-induced apoptosis by TRAIL. (a) DU145, HCT116 and MDA-MB-231 were treated with PL and TRAIL for 12 hr. The cleavage of procaspase 3 was detected as an indication of apoptosis. (b) Flow cytometry of Annexin V/PI staining of apoptosis/necrosis. DU145 and MDA-MB-231 cells were treated with DMSO, 15 μM PL, 50 ng/ml TRAIL or combined PL and TRAIL for 4 hr. Representative dot plots from two experiments are shown.

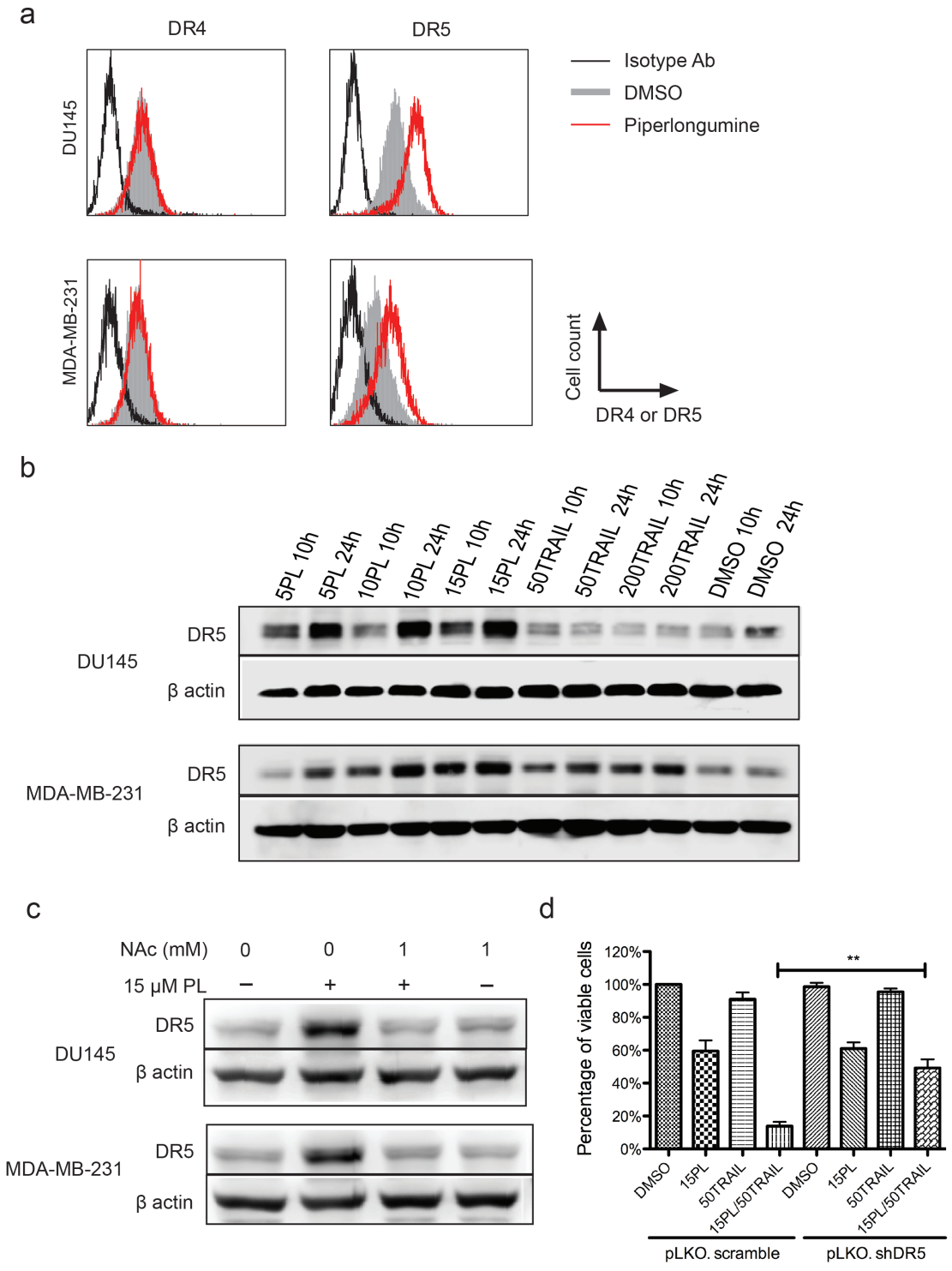

Figure 3.3. Piperlongumine upregulates expression of TRAIL receptor DR5. (a) Expression of membrane-bound DR4 and DR5 in DU145 following treatment with

DMSO or 15 μM PL for 6 hr. In contrast to DR4, DR5 expression was significantly elevated by PL. (b) Total DR5 expression induced by PL or TRAIL in a concentration- and time-dependent manner. DU145 and MDA-MB-231 were treated with PL (5, 10, 15 μM) or TRAIL (50 and 200 ng/mL) for 10 and 24 hr. Total DR5 protein was examined by western blotting. (c) Pretreatment of cancer cells with antioxidant NAc for 1 hr abolished the upregulation of DR5 by PL. The expression of total DR5 was measured by western blotting following incubation with 1 mM NAc and/or 15 μM PL. (d) Silencing DR5 expression reduced the synergistic anti-proliferation effect of combined PL and TRAIL. DU145 cells stably transduced with scrambled shRNA (pLKO. scramble) or DR5 shRNA (pLKO. shDR5) were treated with PL, TRAIL, and their combination at the indicated concentrations. Cell proliferation was measured by MTT assay. Results are mean ± SEM, n=3; **, $p<0.01$.

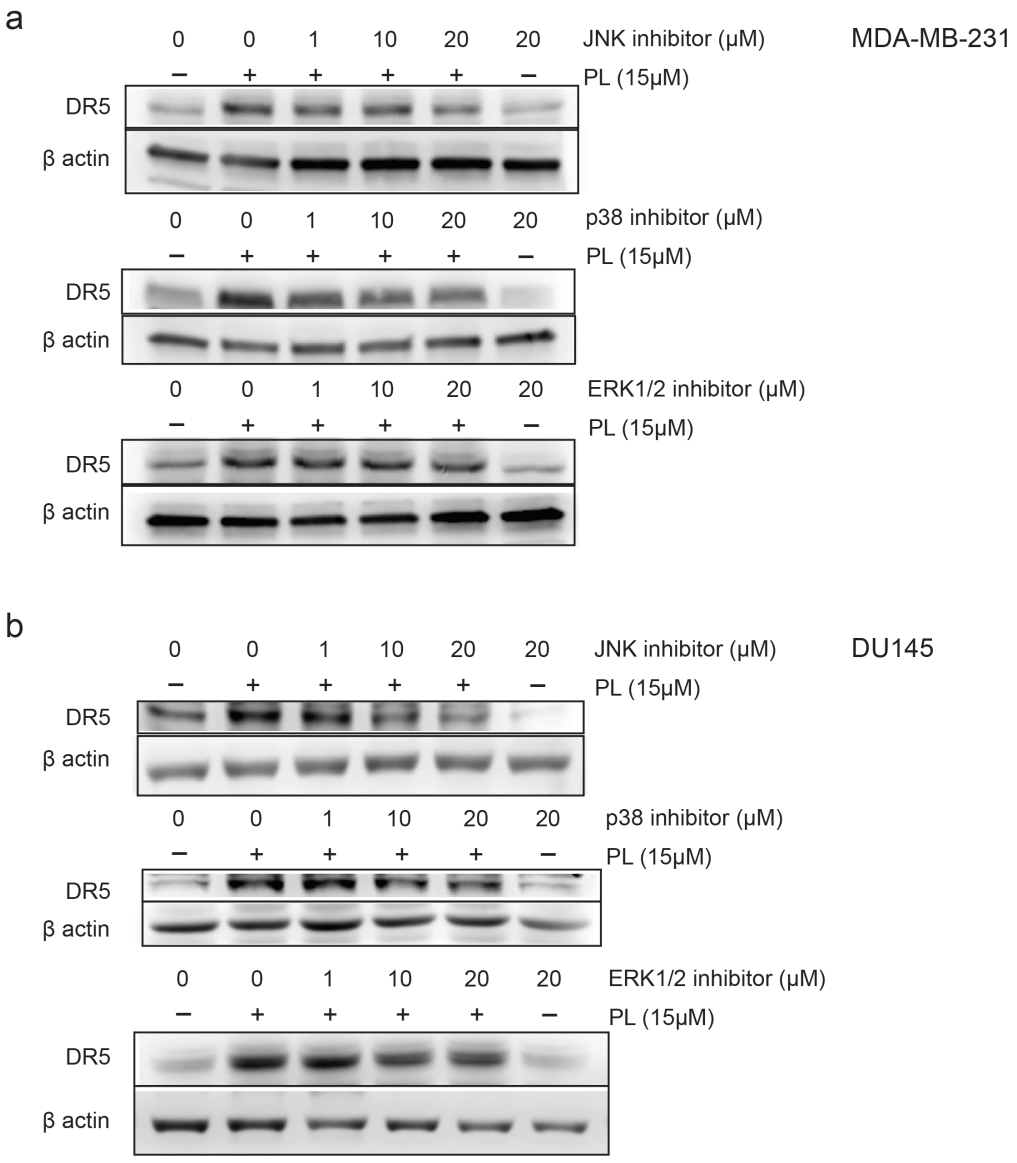

Figure 3.4. Piperlongumine-induced upregulation of DR5 is mediated through MAPK activation. MDA-MB-231 (a) and DU145 (b) were pretreated with the indicated concentration of JNK, p38 or ERK inhibitor for 12 hr followed by 15 μM PL for 24 hr. Expression of total DR5 was examined by western blotting.

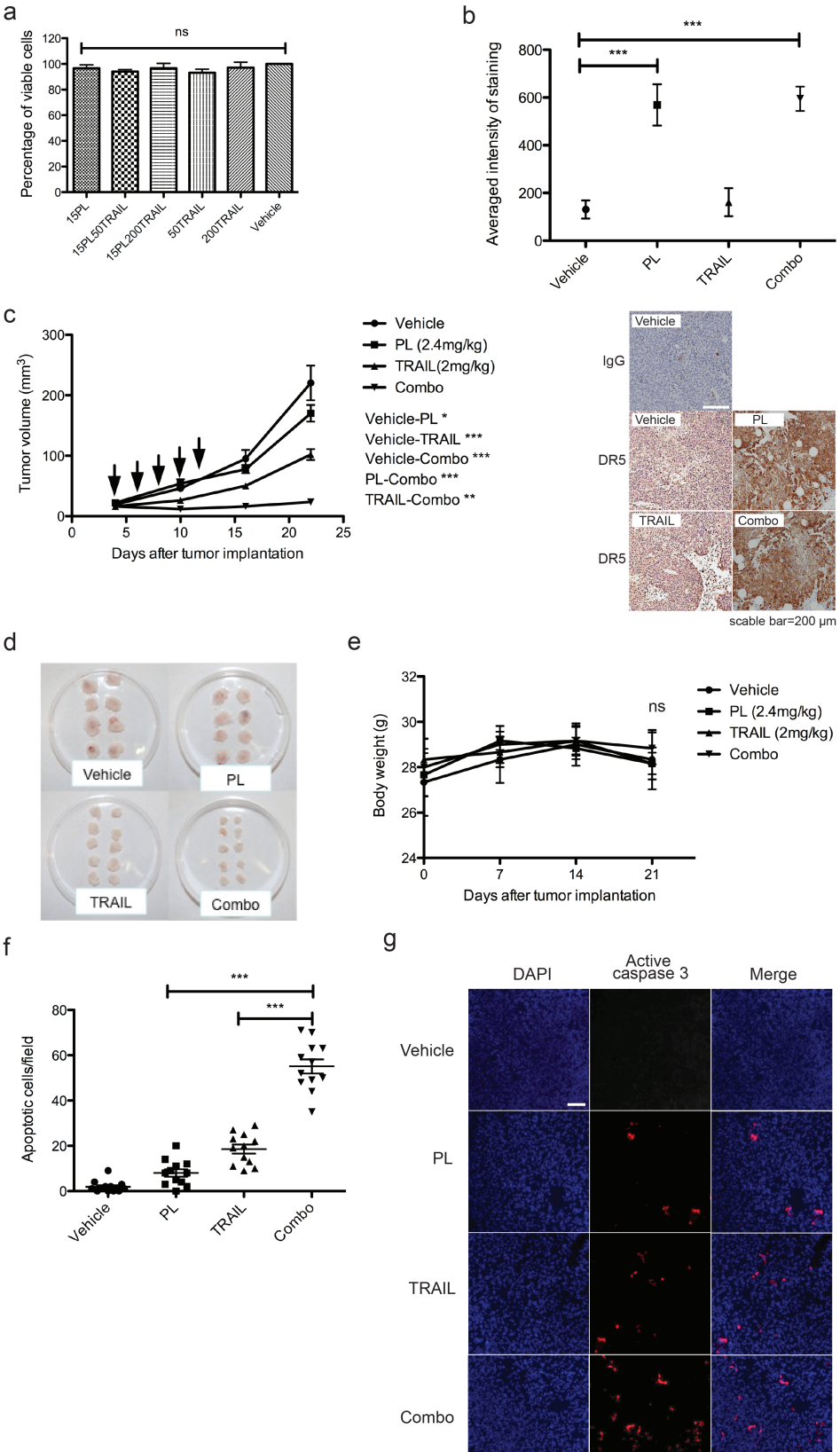
a
ns
Percentage of viable cells
120
100
80
60
40
20
0
15PL
15PL50TRAIL
15PL200TRAIL
50TRAIL
200TRAIL
Vehicle
b
***
***
Averaged intensity of staining
800
600
400
200
0
Vehicle
PL
TRAIL
Combo
c
Tumor volume (mm3)
300
200
100
0
0
5
10
15
20
25
Days after tumor implantation
Vehicle
PL (2.4mg/kg)
TRAIL(2mg/kg)
Combo
Vehicle-PL *
Vehicle-TRAIL ***
Vehicle-Combo ***
PL-Combo ***
TRAIL-Combo **
IgG
Vehicle
DR5
Vehicle
PL
DR5
TRAIL
Combo
scable bar=200 μm
d
Vehicle
PL
TRAIL
Combo
e
Body weight (g)
32
30
28
26
24
0
7
14
21
Days after tumor implantation
ns
Vehicle
PL (2.4mg/kg)
TRAIL (2mg/kg)
Combo
f
***
***
Apoptotic cells/field
80
60
40
20
0
Vehicle
PL
TRAIL
Combo
g
DAPI
Active caspase 3
Merge
Vehicle
PL
TRAIL
Combo
Scale bar=50 μm

Figure 3.5. Evaluation of combination therapy in triple-negative breast cancer xenograft model. (a) Examination of cytotoxicity of combination therapy in normal cells. Human mammary epithelial cells were treated with the indicated concentration of PL, TRAIL, or their combination *in vitro*. Cell proliferation was measured by MTT assay and compared to vehicle control (DMSO). (b) Elevation of DR5 expression in tumors receiving PL. Two doses of vehicle control (DMSO), PL (2.4 mg/kg), TRAIL (2 mg/kg), or combined PL and TRAIL (combo) were intratumorally injected on day 0 and day 1 (n=3). On day 2, tumors were collected for IHC staining of DR5. The averaged staining intensity was calculated by positive pixel count algorithm and representative IHC images are shown. Rabbit IgG was used as a staining control. (c) Measurement of subcutaneous tumor growth over three weeks of therapeutic treatment. When tumor size reached 3-5mm in diameter in NSG mice subcutaneously xenografted with MDA-MB-231, vehicle control (DMSO), PL (2.4 mg/kg), TRAIL (2 mg/kg), or combined PL and TRAIL (combo) were administered every other day for a total of five injections. The downward arrows indicate the day of injections. Tumor mass was measured weekly and calculated as described in Materials and Methods. Results are presented as the mean ± SEM for each group (n=8 or 10). End-point tumor volumes were compared for each pair of treatments by t-test. (d) Tumors removed at the end of therapy were imaged. (e) Measurement of body weight during the therapy. (f) Quantification of the number of apoptotic cells in tumor sections. Tissue sections from four tumors in each treatment group were immunostained for active caspase 3. The number of apoptotic cells per fluorescent image was determined for cells identified as positive for active caspase 3 (n=12). (g) Representative fluorescent

images are shown. Nuclei were stained with DAPI. All results are mean ± SEM. *, $p<0.05$; **, $p<0.01$; ***, $p<0.001$. ns, no significant difference.

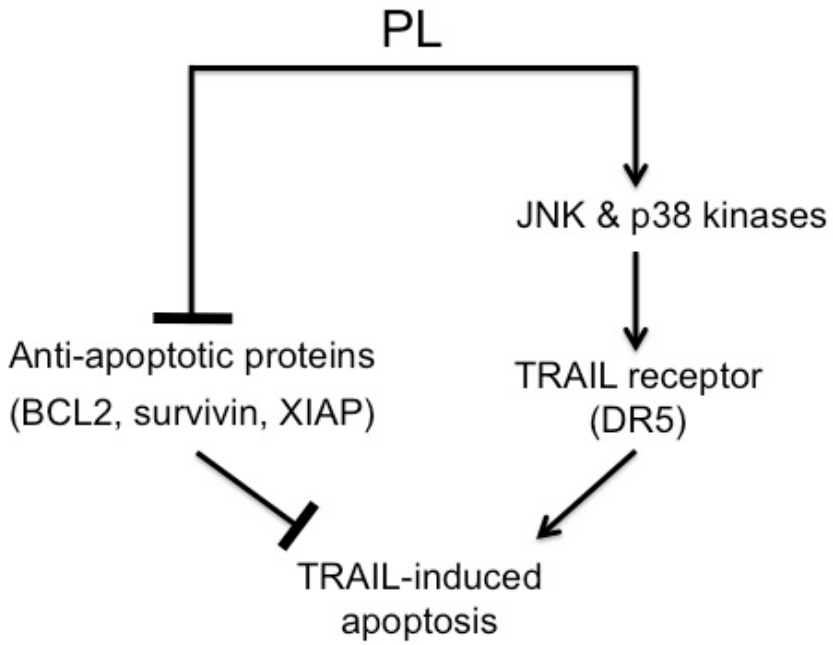

Figure 3.6. Proposed mechanism of enhanced apoptosis induction by combined PL and TRAIL. PL downregulates anti-apoptotic proteins and increases DR5 TRAIL receptor expression via ROS-mediated activation of MAPKs.

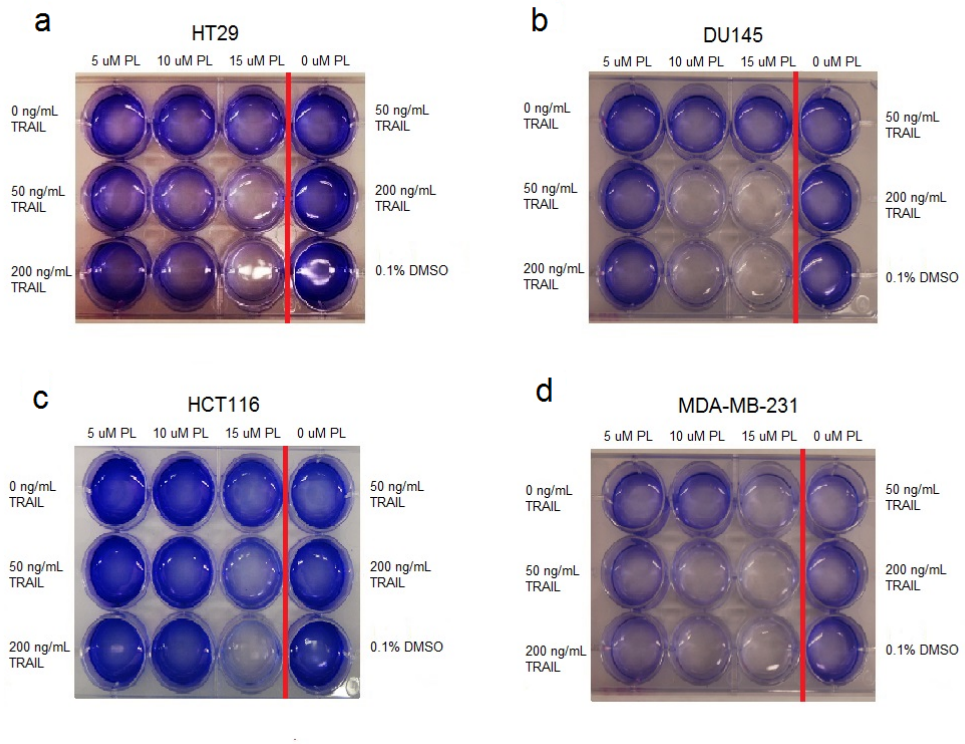

Supplemental figure 3.1. Qualitative anti-tumor effect of combined PL and TRAIL via crystal violet assay. Cancer cells were treated with the indicated concentrations of PL (0, 5 or 15 μM) and/or TRAIL (0, 50 or 200 ng/mL) in 12-well plates for 24 hr at 37°C. Cell viability was measured using crystal violet assay. Cell lines tested were: (a) HT29 (colon cancer), (b) DU145 (prostate cancer), (c) HCT116 (colon cancer) and (d) MDA-MB-231 (breast cancer). Results are qualitatively determined by comparing the darkness of the solution. Darker solution indicates a higher survival rate of the cancer cells receiving the indicated treatment.

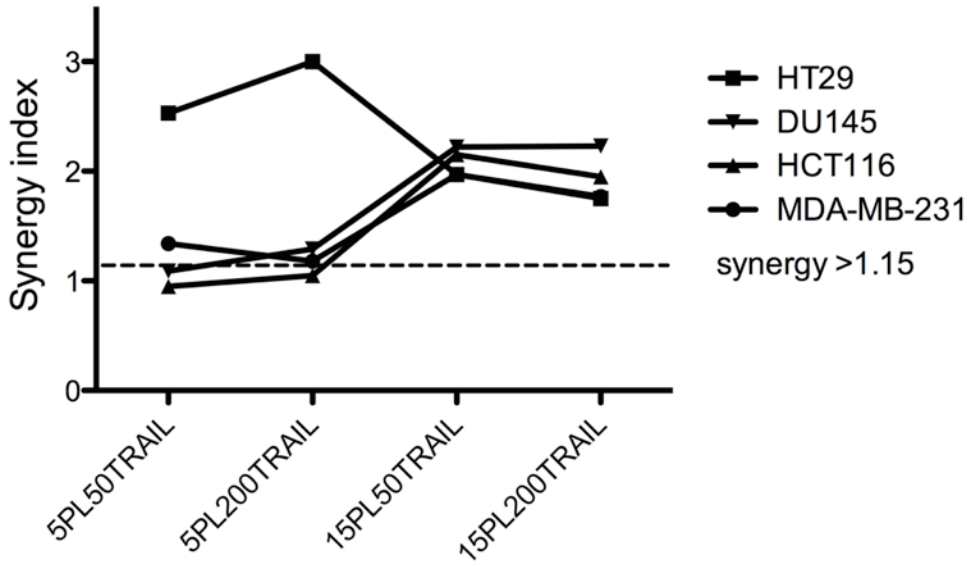

Supplemental figure 3.2. Analysis of synergistic anti-tumor effect of combined PL and TRAIL in cell lines by Jin's formula. The formula is described in Materials and Methods. The inhibitory effects of single and combined treatments were derived from results of MTT assays. PL and TRAIL exerted a synergistic inhibitory effect in the tested cell lines when 15 μM PL was combined with 50 or 200 ng/mL TRAIL (>1.15, synergism).

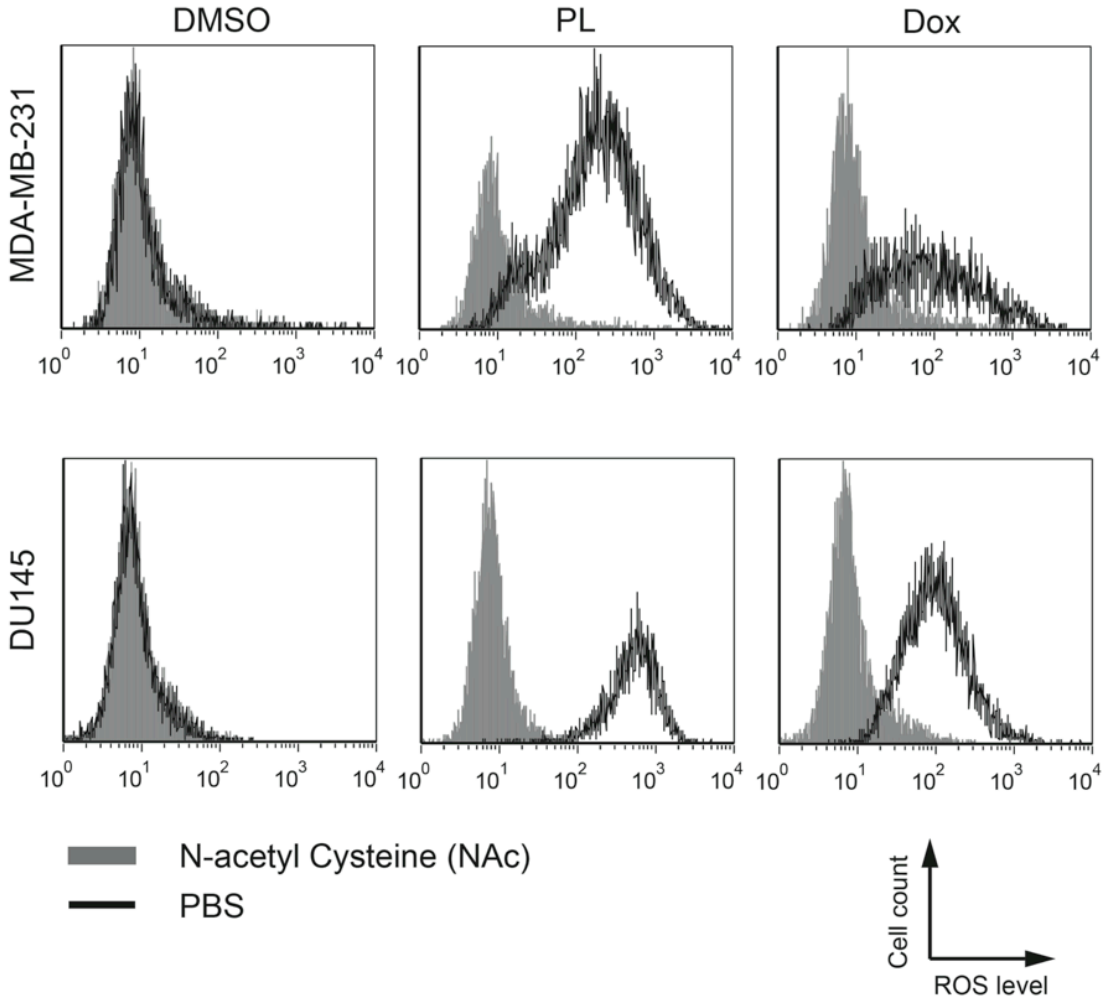

Supplemental figure 3.3. ROS elevation induced by PL or Dox and reversion by NAC. MDA-MB-231 and DU145 cells were treated with 15 μM PL, 15 μM doxorubicin (Dox) or DMSO for 6 hr. Cells were also pretreated with 1 mM NAC for 1 hr, followed by PL or Dox for 6 hr. The ROS levels were quantified through flow cytometry using the redox-sensitive fluorescent probe CM-H2DCFDA.

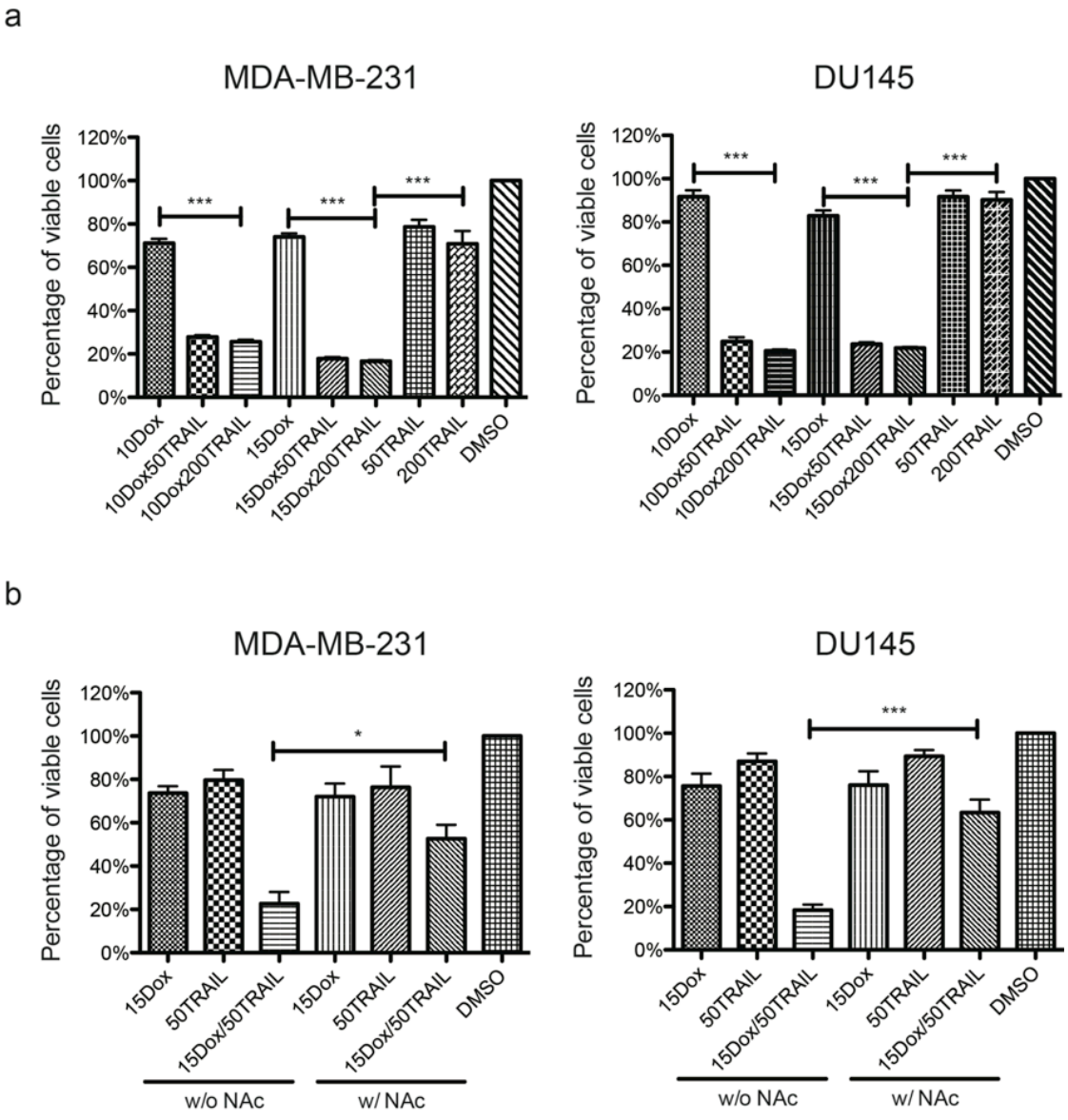

Supplemental figure 3.4. Dox-induced ROS sensitizes cancer cells to TRAIL. (a) Cancer cells were treated with Dox (10 or 15 μM) and/or TRAIL (50 or 200 ng/mL) for 24 hr. Cell viability was measured using MTT assay. (b) Reversion of Dox and TRAIL synergy in apoptosis induction by NAc. Pretreating cancer cells with 1mM NAc significantly increased viability of cells subjected to combined Dox and TRAIL. All results are presented as the mean ± SEM, n=3; *, $p<0.05$; ***, $p<0.001$.

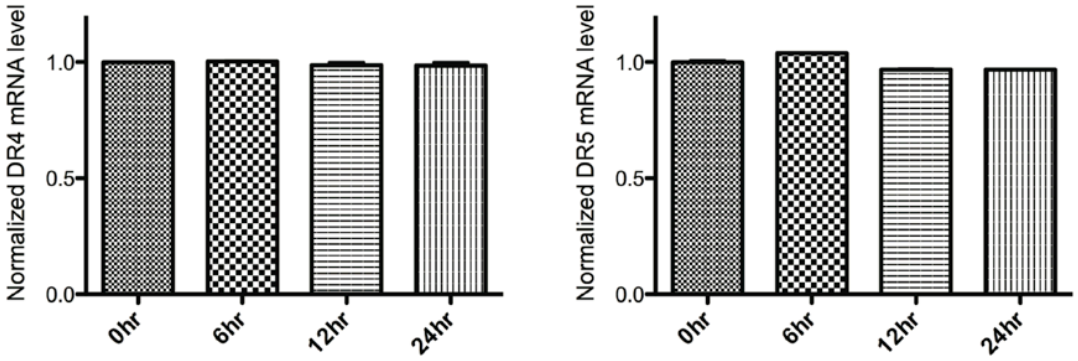

Supplemental figure 3.5. qPCR quantification of DR4 and DR5 mRNAs in DU145 cells. Cells were treated with 15 μM PL over 6, 12 and 24 hr. mRNAs of DR4 and DR5 were normalized to that of β actin. Experiments were repeated twice.

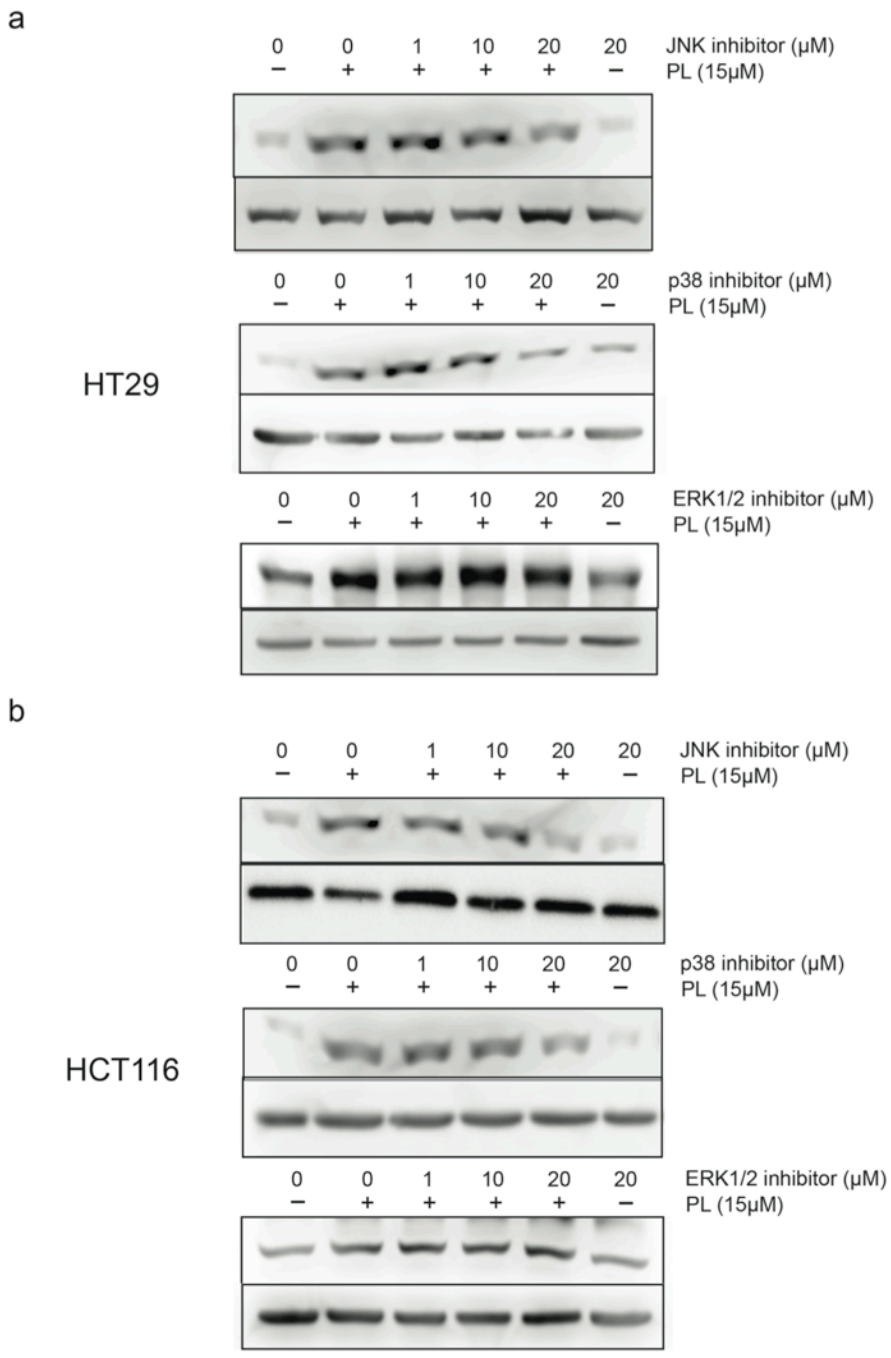

Supplemental figure 3.6. PL-induced upregulation of DR5 is mediated through MAPK activation. HT29 (a) and HCT116 (b) were pretreated with the indicated concentration of JNK, p38 or ERK inhibitor for 12 hr followed by 15 μM PL for 24 hr. Expression of total DR5 was examined by western blotting.

CHAPTER 4 PLATELET MEMBRANE-FUNCTIONALIZED PARTICLES TO TARGET TUMOR CELL-ASSOCIATED MICRO-THROMBI

* This section is adapted from the following manuscript:

Li J, Wun B, Roy S, Wu Q, Sharkey CC, King MR. Platelet membrane-functionalized particles to target tumor cell-associated micro-thrombi. (Submitted)

Circulating tumor cells (CTCs) are responsible for metastases in distant organs via hematogenous dissemination. Fundamental studies in the past decade have suggested that neutralization of CTCs in circulation could represent an effective strategy for preventing metastasis. Learning from current paradigms of targeting cancer cells in a solid tumor, novel therapeutic approaches largely fall into two main targeting categories: unique cancer markers (e.g. overexpression of surface receptors) and tumor-specific microenvironment (e.g. low pH, hypoxia, etc.). While relying on a surface receptor to target CTCs can be greatly challenged by cancer heterogeneity, targeting of tumor microenvironments has the advantage of recognizing a broader spectrum of cancer cells regardless of genetic differences or tumor types. The blood circulation, however, where CTCs transit through, lacks the same tumor microenvironment as that found in a solid tumor. In this study, a unique "microenvironment" was confirmed upon introduction of cancer cells of different types into the blood circulation in mice. It was found that activated platelets and fibrin were physically associated with blood-borne cancer cells forming a micro-thrombi in the vasculature. Inspired by this phenomenon, we further developed a "Trojan Horse" strategy to neutralize CTCs in circulation. Camouflaged by a platelet membrane with surface conjugation of tumor-specific apoptosis-inducing ligand cytokine, TRAIL, biomimetic silica particles were found to incorporate into micro-thrombi and dramatically decrease lung metastases in a breast cancer mouse model.

4.1 Introduction

Metastasis contributes to more than 90% of cancer-associated mortality. It occurs after

primary tumors shed circulating tumor cells (CTCs) via hematogenous dissemination to distant organs [49, 104]. Despite of advancements in the fundamental biology and diagnosis of CTCs, effective neutralization of CTCs for the prevention of metastasis remains clinically challenging. Existing nano-medicines for cancer treatment aim to target solid tumors (primary and metastatic tumors). The underlying principle is largely based on the enhanced permeability and retention (EPR) effect in which nanoparticles and macromolecules drain into tumor-associated leaky vasculatures and are retained in tumors due to inefficient lymphatic drainage [109, 110]. Although it has been proven to be a key paradigm for existing nano-medicines, the EPR effect, however, may not be readily translated to the targeting of CTCs in circulation. The physical environment surrounding CTCs is different from that of solid tumors [318]. In solid tumors, high interstitial fluid pressure represents a major barrier to the delivery of nano-medicine caused by enhanced stiffness of extracellular matrices and leaky tumor-associated vasculature [108, 113]. In contrast, CTCs are exposed to a broad range of fluid shear stresses when transiting in different vascular compartments (arteries, veins and capillaries). The mobile nature of CTCs and varied fluid shear stresses may have a major impact on the effectiveness of nano-medicines against CTCs.

During their transit in the blood circulation, CTCs are subjected to destruction by natural killer cells, neutrophils, macrophages and cytotoxic T cells [75, 319-321]. Nevertheless, CTCs can locally induce thrombosis, including platelet activation and fibrin deposition, to form a protective cloak, which in turn protects CTCs from an

immune attack [75, 322, 323]. These two dueling forces counteract each other to determine the survival of CTCs in the circulation and eventually the likelihood of developing distant metastases. Current immunotherapies that boost the cytotoxicity of immune cells (natural killer cells and cytotoxic T cells) via systemic injection of cytokines such as IL-2 and IFN-α may tip the balance in favor of CTC neutralization. Unfortunately, this strategy under certain circumstances can elicit a life-threatening cytokine storm caused by over-reactivity of the immune system [324, 325]. Alternatively, anti-thrombosis drugs have been demonstrated as an effective means of reducing metastasis in mouse cancer models. These drugs, however, can in principle interfere with the normal hemostatic function of thrombosis, which eventually leads to bleeding disorders [326, 327]. In general, these two different approaches can potentially cause severe side effects by disrupting homeostasis of the immune and hemostatic systems.

To leverage the strength of the immune boosting approach and circumvent the side effects associated with anti-thrombosis therapies, a Trojan horse strategy was developed in this work. Inspired by the adhesion of activated platelets to CTC-associated micro-thrombi, biocompatible silica (Si) particles were functionalized with membrane-derived vesicles from activated platelets. This biomimetic coating allows for targeting of synthetic particles to CTCs. Additionally, the major tumor-killing cytokine, Tumor necrosis factor-related apoptosis inducing ligand (TRAIL) was conjugated to the platelet membrane-coated Si particles. TRAIL is highly expressed on the surface of cancer-killing natural killer cells, activated neutrophils and cytotoxic

T cells [100, 298]. Such a system takes advantage of CTC adhesion to activated platelets and the tumoricidal activity of immune cells to produce a targeted therapeutic effect. Moreover, synthetic particles camouflaged with platelet membrane were incorporated into CTC-induced thrombosis in the vasculature to deliver cancer-killing drugs within CTC thrombi at a high local concentration.

4.2 Methods and Materials

Cell lines and mice

Human breast cancer cell line MDA-MB-231, prostate cancer cell line PC3, and umbilical vein endothelial cells (HUVECs) were obtained from American Type Culture Collection (ATCC, Rockville, MD, USA). MDA-MB-231 cells were cultured in DMEM (Invitrogen, Grand Island, NY, USA) with 10% FBS. PC3 cells were maintained in RPMI (Invitrogen) with 10% FBS and HUVECs were expanded in vascular cell basal medium (ATCC) using the endothelial cell growth kit-BBE (ATCC). HUVECs were used up to passage number 6. Six to eight week old female NOD SCID gamma mice were purchased from Jackson Laboratory (Bar Harbor, ME, USA). Mice were housed in a SPF barrier animal facility at Cornell University.

Chemicals and antibodies

His-tagged TRAIL for *in vivo* work was produced and purified as previously described [328]. The following chemicals or kits were used for assaying cell proliferation and apoptosis: MTT (AMRESCO, Solon, OH, USA) and TACS® Annexin V-FITC Kit (Gaithersburg, MD, USA). Reagents for SEM and TEM were obtained from Electron

Microscopy Sciences (Hatfield, PA, USA): glutaraldehyde, osmium tetroxide and uranyl acetate. APC-conjugated antibodies specific for the extracellular domains of human CD41, CD42b, CD47, CD61 and CD62P in flow cytometry and fluorescence microscopy studies were purchased from Biolegend (San Diego, CA, USA). Primary CD41 antibodies for the extracellular domain (M-148) and cytoplasmic domain (B-9) detection and human CD47 blocking antibody (B6H12) were from Santa Cruz Biotech (Dallas, TX, USA).

Synthesis of silica particles

Monodisperse silica (Si) particles with a diameter of 2-3 μm were synthesized using tetraethyl orthosilicate (TEOS), 29% ammonia and 100% ethanol via the Stöber method. To produce a positively charged surface, Si particles were suspended in ethanol containing 1 mg/ml 3-aminopropyl triethoxysilane (APTES) and stirred overnight. To prepare FITC-labeled Si particles, FITC was first reacted with APTES in the presence of ethanol and ammonia. Afterwards, TEOS was added to FITC dye solution and stirred overnight to form FITC-labeled Si particles. All synthesized Si particles were washed three times with 100% ethanol followed by three times with TBS to remove free substrate. Particles were characterized with dynamic light scattering using a Zetasizer (Malvern Instruments, Malvern, Worcestershire, UK) and LEO 1550 FE-SEM (Zeiss, Atlanta, GA, USA) prior to PMDV coating.

Membrane protein profiling by LC-MS

PMDV-coated particles were washed three times with TBS. On-bead tryptic

proteolysis protocol was performed. Briefly, proteins were reduced by adding 5 mM DTT (45 min, 56°C), and free cysteines were alkylated with iodoacetamide (15 mM, 25°C, 1 hr in the dark). A sample of 0.2 μg porcine sequencing grade trypsin (Promega, Mannheim, Germany) were added and the samples were incubated overnight at 37°C. After digestion, the reaction was stopped with 10 μL of 10% formic acid (FA). The resulting precipitate and particles were removed by centrifugation (13,000 x g, 15 min, 4°C). Supernatant was transferred for LC-MS analysis. Capillary liquid chromatography of tryptic peptides was performed with UltiMate® 3000 RSLCnano LC system (Thermo, Chelmsford, MA, USA). Mass spectrometry analysis of tryptic peptides was performed using Orbitrap Elite (Thermo).

Flow cytometry and fluorescence microscopy

PMDV-coated and uncoated Si particles were suspended at a concentration of 1 million per 100 μL blocking buffer PBS/1% BSA. APC-conjugated primary antibodies were added in the blocking buffer and incubated for 30 min at room temperature. Following three washes with 1 mL of PBS, fluorescence measurements were collected using a Guava flow cytometer (EMD, Billerica, MA, USA). Data were analyzed using the Flow Express software (De Novo Software, Los Angeles, CA, USA). For fluorescence microscopy detection, stained particles were first immobilized on poly-lysine coated glass slides. Images were acquired in an upright Olympus BX-50 microscope.

SEM and TEM

PMDV-coated Si particles were fixed in 2.5% glutaraldehyde and 1% osmium tetroxide. Samples were serially dehydrated in 25%, 50%, 75%, 95% and 100% ethanol. Samples used for SEM were subjected to critical point drying followed by carbon sputter coating. Particles were imaged using a LEO 1550 FE-SEM at an accelerating voltage of 3 kv with a 3 mm working distance. For TEM, after ethanol dehydration, samples were immobilized on carbon-coated copper grids and counterstained briefly with 2% uranyl acetate. Images were taken by a FEI T12 Spirit TEM STEM (Tecnai, Hillsboro, OR, USA) at 120 kv.

Preparation of fibrin-functionalized microtube for in vitro thrombosis model

50 cm-long microrenathane microtubes with an inner diameter of 300 μm (Braintree Scientific, Braintree, MA, USA) were first washed with 1× PBS and then coated with 1 mg/ml human fibrinogen for 1 hr at RT. In negative control microtubes, 1 mg/ml human albumin was used instead. Afterwards, $CaCl_2$ (20 mM) and human α-thrombin (1 U/ml, Enzyme Research Laboratories, IN) in TBS were infused into microtubes and incubated for 1 hr at RT. All microtubes were blocked with 1% BSA to prevent nonspecific adhesion. Functionalized microtubes were then secured to the stage of an Olympus IX81 motorized inverted microscope (Olympus America, Melville, NY). After washing microtubes with TBS, PMDV-coated Si particles and uncoated particles at a concentration of 1×10^6 per ml in TBS plus Ca^{2+}, EDTA or Ca^{2+} plus 1mg/ml fibrinogen were perfused at 4 dyn/cm^2 using a syringe pump (IITC Life Sciences, Woodland Hills, CA, USA). A CCD camera (Hitachi, Tokyo, Japan) and DVD recorder (Sony Electronics, Tokyo, Japan) were used to record experiments for offline

analysis.

Cell proliferation assay

Cell proliferation was assayed by measuring mitochondrial dehydrogenase activity using MTT as the substrate. At experimental end points, cells were incubated with MTT at a concentration of 0.5 mg/mL, at 37°C for 3 hr. The purple MTT product was solubilized with DMSO and measured at 570 nm using a BioTek plate reader (Winooski, VT, USA).

Measurement of ROS production

Cells were first treated with PMDV-coated Si particles, uncoated particles or hydrogen peroxide for 12 hr. This was followed by loading cells with 1 μM of CM-H2DCFDA (Invitrogen, Carlsbad, CA, USA) in PBS for 10 min at 37°C. Afterwards, cells were allowed to recover in growth medium for 15 min at 37°C, and then analyzed using a flow cytometer.

Experimental lung metastasis assays

All mice were handled according to the Guide for the Care and Use of Laboratory Animals in compliance with US- and UK-based guidelines. All experimental procedures and protocols were approved by the Institutional Animal Care and Use Committee of Cornell University (Protocol No. 2011-0051). In the study of cancer cell-induced thrombosis in blood circulation, cells were labeled with CellTracker™ Red CMTPX (Invitrogen) and were injected into 6-8 week-old C57BL/6 or Nod SCID

gamma (NSG) mice via tail vein at 1×10^6 cells per 0.1ml in PBS. After 30 min, mice received 5×10^7 FITC-labeled PMDV-coated Si particles or uncoated particles through retro-orbital injection. Mice were euthanized after 30 min. The lungs were removed, embedded in OCT, and snap frozen in liquid nitrogen. Embedded samples were sectioned to a thickness of 8 μm by cryostat (Tissue-Tek®, Torrance, CA, USA) and mounted on glass slides.

Tail bleeding assay

Tail bleeding time was determined by removing 3 mm of the distal mouse tail and immediately immersing the tail in 37°C PBS. A complete cessation of bleeding was defined as the end point of bleeding time.

Statistical analysis

All statistical analyses were performed using GraphPad Prism 5.0a for Mac OS X (San Diego, CA, USA). A one-way ANOVA followed by Tukey post test was used to compare statistical significance in the characterization of *in vitro* cell proliferation and *in vivo* experiments.

4.3 Results

Observation of cancer cell/fibrin/platelet thrombi in experimental lung metastasis model

Previous studies have provided *in vitro* evidence that multiple types of human cancer cells could activate thrombosis by involving platelet adhesion and fibrin deposition.

Moreover, in experimental metastasis models involving treatments with an antibody or a chemical to interfere with coagulation, mice had a reduced frequency of metastases [326, 327, 329]. Nevertheless, it remains unclear how cancer cells and thrombosis spatially and physically interact in the vasculature. To address this question, an experimental lung metastasis model was chosen for two reasons: 1. The lungs are the most frequently metastatic organs in multiple types of cancer including breast, prostate, melanoma and colon cancers [330-333]. 2. The highly vascularized structure of the lungs allows for facile visualization of CTC-fibrin-platelet emboli in circulation [334]. Fluorescently labeled human breast cancer cells MDA-MB-231 and colon cancer cells COLO 205 were inoculated into the blood circulation of separate NSG immunocompromised mice. After 30 min, the lungs were collected, immediately fixed with formaldehyde, and snap frozen by liquid nitrogen for tissue sectioning. The combined chemical and physical fixation procedure provided a "snapshot" of interplay between cancer cells and blood components. Subsequent immunofluorescence staining for fibrin and activated platelets demonstrated colocalization of cancer cells, fibrin and platelets in lung vasculatures despite their systemic nature (**Figure** 4.**1a and b**). To rule out the species difference, syngeneic mouse metastasis models were tested by injecting C57BL/6-derived colon cancer cells MC38 and melanoma cancer cells B16-F10 into C57BL/6 mice via the tail vein, respectively. The same trend of colocalization patterns were observed (**Figure** 4.**1c and d**). The experimental metastasis models demonstrated that cancer cells physically interacted with fibrin and activated platelets in circulation. This suggests that synthetic particles functionalized with activated platelet-derived membrane components may hijack this interaction for

the targeting of CTCs.

Functionalization of Si particles with platelet membrane

The preparation of platelet membrane-coated Si particles involves two major steps: extraction of platelet membrane-derived vesicles (PMDVs) from activated platelets, and vesicle-particle fusion (**Figure 4.2a**). Platelets were pelleted from platelet-rich plasma (PRP) through differential centrifugation of whole blood. Following three washes to remove plasma proteins, the isolated platelets were fragmented by seven freeze-thaw cycles and sonication to release platelet membrane-derived vesicles. Then, ultracentrifugation with a discontinuous sucrose gradient (5%, 40%, 55%) was performed to separate membrane vesicles from free proteins, intact platelets, and high-density granules. Two distinct lipid layers were formed at the interfaces of the 5%-40% and 40%-55% sucrose layers. To identify which fraction contained PMDVs, a dot blot assay was performed to stain two platelet integral membrane proteins (CD41a and CD47) in each fraction (0.5 mL) of sucrose gradient. It was found that the majority of membrane vesicles existed at the interface between 5% and 40% (**Figure 4.2b**). The z-average diameter of vesicles was 106 ± 32 nm with a zeta potential of -10 mV, close to the surface charge of intact platelets (**Table 4.1**). The morphology of vesicles was characterized and displayed hollow structure under TEM (**Figure 4.2c**).

Previous studies have examined the electrostatically mediated deposition and fusion of negatively charged liposomes on cationic particle support [335, 336]. In light of the negative surface charge of PMDVs, Si particles with diameter close to platelet size

were functionalized with (3-Aminopropyl) triethoxysilane (APTES) to produce a positive charge on the surface. Subsequently, PMDVs were immobilized on the positively charged particle surface by incubating 100 μg PMDVs with 10 million particles. After removing free vesicles from the mixture, the coated particles were characterized by dynamic light scattering and electron microscopy. The coated particles were found to be close to uncoated particles in size. In contrast, the surface zeta potential changed from +25.5 ± 4.6 mV (APTES-particles) to -10.1 ± 1.9 mV (coated particles), close to that of PMDVs and platelets (**Table 4.1**). Furthermore, SEM and TEM imaging revealed a coating of the platelet membrane on the surface of Si particles, in comparison to uncoated ones. Fusion between adjacent proteo-lipid patches and lipid vesicles likely resulted in complete coverage of the particle surface (**Figure 4.2c**).

Detection of platelet membrane proteins on coated particles

Integral membrane proteins are essential for adhesion of activated platelets to CTC-induced fibrin clots. To examine the presence and stability of proteins on functionalized Si particles, membrane proteins were stripped from PMDV-coated Si particles after incubation in TBS at 37 °C for 12, 24, and 48 hr and were resolved by SDS-PAGE. Commassie blue staining of the protein gel confirmed that the compositions of membrane proteins present on Si particles throughout different incubation times were largely identical (**Figure 4.3a**). To profile membrane proteins on PMDV-coated Si particles, an on-bead trypsin digestion was performed, followed by liquid chromatography-mass spectrometry (LC-MS). The top membrane proteins

based on their relative abundance were identified (**Table 4.2**). To further validate protein identity from LC-MS, key proteins involved in platelet adhesion (CD41, CD42b and CD61) and anti-phagocytosis (CD47) were detected on PMDV-coated Si particles by antibodies recognizing the extracellular domain of each membrane protein (**Figure 4.3b and c**). In addition to proteins, glycans (sialic acid and N-acetylglucosaminyl residues) are key post-translational modifications for membrane protein-mediated cell-cell or cell-fibrin adhesion. The presence of sialic acid and *N*-acetylglucosaminyl residues on PMDV-coated Si particles was identified by staining with Alexa Fluor® 488-conjugated wheat germ agglutinin (WGA) and analyzed via flow cytometry and immunostaining (**Figure 4.3d and e**). To investigate the orientation of native proteins on PMDV-coated Si particles, CD41, a single-pass type I membrane protein composed of a N terminal extracellular domain, a transmembrane region and a C terminal cytoplasmic domain, was selected due to its simple structure as well as abundant expression on the platelet membrane. Two antibodies recognizing extracellular and cytoplasmic domains of CD41 were used in flow cytometry. It was found that the majority of CD41 was present in an extracellular-outward orientation with a 4:1 ratio of extracellular-to-cytoplasmic domains on the outer surface of PDMV-coated Si particles (**Supplemental figure 4.1**).

Platelet membrane coating reduces phagocytic uptake of particles

The largest populations of macrophages in the body are located in the liver and lungs [337]. Since the liver and lung are two major sites of distant organ metastases, macrophage-mediated phagocytosis of synthetic particles may present a major barrier

to efficient delivery to CTCs in liver and lung microvessels. The ability of platelet membrane camouflage to reduce particle phagocytosis was studied using the human macrophage cell line THP-1. First, THP-1 cells were differentiated into macrophage-like cells using 100 ng/ml phorbol 12-myristate 13-acetate (PMA) for 48 hr. In preparation for the phagocytosis assay, FITC-labeled uncoated and PMDV-coated Si particles were incubated with human plasma to allow for opsonization by serum proteins at 37°C for 30 min. Afterwards, differentiated cells were incubated with an equivalent number of two different Si particles respectively at 37°C for 2 hr. After enzymatic removal of surface-bound particles by trypsin, THP-1 cells with internalized particles were quantified using flow cytometry. It was found that the PMDV coating significantly reduced particle phagocytosis in comparison to uncoated particles (**Figure 4.4a and b**). Additionally, fluorescent microscopy confirmed that more uncoated Si particles were internalized into the cytoplasm of THP-1 cells (**Figure 4.4c**). Notably, after opsonization, uncoated and coated particles exhibited a surface zeta potential of -9.2 ± 1.1 mV and -10.8 ± 1.7 mV, respectively, which rules out the influence of charge difference on particle adhesion and internalization in the THP-1 phagocytosis assay (**Supplemental table 4.1**). To investigate the mechanism of reduced phagocytosis in PMDV-coated Si particles, absorption of IgG to uncoated and coated Si particles was compared, since the extent of antibody (especially IgG) opsonization to exogenous materials has been found to correlate with the level of macrophage-mediated phagocytosis [338]. Using FITC-labeled anti-human IgG antibody, it was shown that uncoated Si particles absorbed more IgG than PMDV-coated ones (**Figure 4.4d**). The differential opsonization with IgG likely explained the

reduced phagocytosis for coated Si particles. In addition to differential IgG opsonization, CD47 was also found to be essential for reduced phagocytosis in PMDV-coated Si particles. Treating coated particles with CD47 blocking antibody was able to increase phagocytosis of coated particles in THP-1 cells (**Figure 4.4e**).

Adhesion of PMDV-coated Si particles to fibrin under flow

Upon release of CTCs into circulation, tissue factor on the cells convert prothrombin (inactive) to thrombin (active) in plasma, which in turn induce platelet activation, fibrin deposition and recruitment of activated platelets to fibrins [322]. To investigate the capability of PMDV-coated Si particles to target fibrin in a microvessel under flow conditions, a previous protocol for preparing fibrin-immobilized polystyrene beads was adopted to prepare an *in vitro* thrombosis model in microtubes [339]. Briefly, after immobilizing 1mg/ml fibrinogen on the microtube surface, thrombin was added to form fibrin. Particles were perfused at a defined shear stress controlled by a syringe pump and the adhesion events were recorded with a CCD camera mounted on a microscope (**Figure 4.5a**). To compare the adhesion dynamics of PDMV-coated Si particles to that of activated platelets, equal density of particles or cells suspended in tris-buffered saline (TBS) plus Ca^{2+} were perfused through fibrin-functionalized microtubes under physiological wall shear stresses in veins (4 and 8 dyn/cm^2). It was found that adhesion events of both particles and platelets increased over time but decreased with increasing shear stress. In addition, PMDV-coated Si particles adhered slightly less efficiently to fibrin surfaces than activated platelets (**Figure 4.5b**).

To confirm that the binding of PMDV-coated Si particles was fibrin-dependent, it was verified that the albumin-coated surface failed to induce particle adhesion in microtubes. Moreover, replacement of Ca^{2+} with EDTA abolished the adhesion of particles to fibrin surface (**Figure 4.5c**). This observation was consistent with the fact that the adhesion of activated platelets to fibrin is Ca^{2+}-dependent.

To simulate physiologically relevant conditions, PMDV-coated Si particles were suspended in TBS containing 0.4 mg/ml soluble fibrinogen which, in principle, binds to the same $\alpha_{II\beta}/\beta_3$ (CD41/CD61) integrins on activated platelets as fibrin. Interestingly, despite the presence of competitive fibrinogen in suspension, under flow conditions PMDV-coated Si particles were able to bind to immobilized fibrin with comparable efficiency as in TBS Ca^{2+} (**Figure 4.5d).** Furthermore, a more physiologically relevant condition was tested by suspending PMDV-coated Si particles in platelet-poor plasma (PPP). It was found that this more complex environment did not interfere with the active adhesion of particles to fibrin-coated surface under flow (**Figure 4.5d and e**). It is possible that activated $\alpha_{II\beta}/\beta_3$ (CD41/CD61) integrins on PMDV-coated Si particles tend to bind to surface-bound fibrin more efficiently than the free form of fibrinogen. Nevertheless, such observations mirror the adhesion of activated platelets to thrombi in the presence of abundant fibrinogens in plasma. Moreover, the potential of PMDV-coated Si particles to adhere to fibrin in a complex body fluid environment suggests that they could be utilized to target thrombi induced by cancer cells or certain cardiovascular disease states.

Conjugation of TRAIL to PMDV-coated Si particles induces apoptosis in cancer cells

TRAIL is highly expressed on the surface of natural killer cells, activated neutrophils, and cytotoxic T cells and is largely responsible for the anti-tumor effect of immune cells. In contrast, TRAIL expression was not detectable on the surface of human or mouse platelets (**Supplemental figure 4.2**). We next explored whether conjugation of TRAIL to the surface of PMDV-coated Si particles could induce apoptosis in cancer cells. TRAIL was conjugated to coated Si particles via a NHS-biotin/streptavidin linkage and the maximum loading yield without particle aggregation was found to be ~1 μg per mg of Si particles (~10^7 Si particles) by Bradford and ELISA assays. TRAIL conjugation density was varied at 0.2, 0.5 and 1 μg per mg of particles for *in vitro* incubation with MDA-MB-231 (breast cancer) and PC3 (prostate cancer) cells. In addition, cancer cells were incubated with TRAIL-conjugated particles at different particle-to-cell ratios. It was found that the reduction of cell viability by TRAIL-conjugated Si particles was dependent on both TRAIL coating density and particle-to-cell ratio (**Figure 4.6a**). In contrast, when the HUVEC endothelial cells, which also serve as a normal cell control, were incubated with PMDV-coated particles with 1 μg TRAIL per mg of silica at different particle-to-cell ratios, no growth inhibition was detected relative to PMDV-coated particles without TRAIL (**Figure 4.6b**). Furthermore, to examine whether the NHS-biotin/streptavidin crosslinking would compromise TRAIL activity, PMDV-coated particles with 1 μg TRAIL per mg of silica were incubated with cancer cells at different particle-to-cell ratios and compared to an equivalent amount of soluble TRAIL for each ratio. It was found that the surface conjugation did not compromise the cytotoxicity of TRAIL on cancer cells (**Figure**

4.6c). The ability of TRAIL-conjugated Si particles to adhere to immobilized fibrin under flow was also tested. TRAIL conjugation at 0.2, 0.5, and 1 μg per mg of Si particles did not interfere with particle adhesion (**Figure 4.6d**).

Killing of CTCs in lung vasculature by TRAIL-conjugated PMDV-Si particles

To investigate the ability of PMDV-camouflaged Si particles to target CTCs in circulation, 10^5 red fluorescently labeled MDA-MB-231 cells were injected via tail vein into NSG mice. 30 min after injection, mice received retro-orbital injections of 5 x 10^6 FITC-labeled PMDV-Si particles or uncoated Si particles. Shortly after injection, lungs were collected, immediately fixed with formaldehyde and snap frozen by liquid nitrogen for tissue sectioning. Fibrin was stained in sections for localization of cancer cell-induced thrombosis in the lung vasculature. Three-color fluorescence imaging detected co-localization of cancer cells, fibrin and PMDV-Si particles (**Figure 4.7a**). Uncoated particles failed to target CTC-fibrin thrombi in lung vasculatures (**Figure 4.7b**).

The ability of PMDV-coated Si particles to co-localize with CTCs suggested a Trojan horse strategy of delivering cancer-specific cytotoxic drugs such as TRAIL to neutralize CTCs in circulation. To test this idea, an experimental lung metastasis model was utilized by inoculating MDA-MB-231 cells expressing firefly luciferase via tail vein. TRAIL-conjugated PMDV-Si particles (1 μg TRAIL per mg of silica) were injected at 30, 90 and 120 min after injection of cancer cells at a particle-to-cell ratio of 50 : 1. Three control groups were established to compare the efficacy of

targeted TRAIL delivery via PMDV-Si particles: TBS, PMDV-coated Si particles and soluble TRAIL (**Figure 4.8a**). Longitudinal bioluminescence imaging was performed at week 2 and 4 after injection of cancer cells (**Figure 4.8b and c**). Quantification of bioluminescence in lungs indicated ~40 fold reduction of lung metastases in the experimental group compared to TBS and PMDV-Si particle controls. Moreover, TRAIL-conjugated PMDV-Si particles showed ~8 fold reduction compared to soluble TRAIL (**Figure 4.8d**). Following mouse sacrifice at week 4, the lung metastases were examined histologically through H&E staining and immunohistochemistry using an anti-luciferase antibody. In vehicle control groups (TBS and PMDV-Si particle), the lungs developed metastases throughout entire lobes with severely compromised airways, whereas the soluble TRAIL treatment group showed scattered large tumor nodules. In contrast, the TRAIL-conjugated PMDV-Si treatment was associated with much smaller and fewer tumor nodules than those in the soluble TRAIL group (**Figure 4.9a and b**). The identity of tumor cells in lung lobes was further confirmed with an anti-luciferase antibody (**Figure 4.9c**).

The biological safety of TRAIL-conjugated PMDV-Si particles in vivo

Previous studies indicated that a major side effect for TRAIL is induction of hepatocyte apoptosis associated with high dosages of TRAIL [344, 345]. Therefore, *in vivo* liver toxicity was first tested in tumor-free NSG mice with the same dose and frequency (i.e. 0, 30, and 90 min time points) as described above. After 24 hr, livers were collected and were subjected to TUNEL staining for apoptotic cells. As with vehicle controls (TBS and PMDV-Si particles), neither soluble TRAIL nor TRAIL-

conjugated PMDV-Si particles induced detectable apoptosis in liver. DNase I treatment of liver section was used as a positive control for TUNEL staining (**Supplemental figure 4.3a and b**). In addition to TUNEL assay, no necrotic areas were found in H&E staining of liver sections from soluble TRAIL or TRAIL-conjugated PMDV-Si particles compared to those from vehicle controls (TBS and PMDV-Si particles) (**Supplemental figure 4.3c and d**).

A tail bleeding test was also performed to examine whether TRAIL-conjugated PMDV-coated Si particles would interfere with blood coagulation *in vivo*. Tumor-free NSG mice receiving the same dose and frequency (i.e. 0, 30, and 90 min time points) retro-orbitally as described above were subjected to tail bleeding immediately after the last administration of particles or controls. No significant difference of bleeding time was detected in PMDV-coated Si particles or TRAIL-conjugated PMDV-coated Si particles relative to vehicle control (TBS) (**Supplemental figure 4.3e**). This suggests that the treatment will have no significant effect on coagulation.

4.4 Discussion

In the past decades, numerous studies have identified receptor-ligand interactions between activated platelets and cancer cells, including but not limited to P selectin ligands (cancer cells)-P selectin (platelets), $\alpha_{II\beta}/\beta_3$ integrins (both cancer cells and platelets)-fibrinogen (in plasma), and $\alpha_2\beta_1$ integrins (both cancer cells and platelets)-collagen (extracellular matrix) [114, 346]. Inspired by these molecular interactions, nanotechnologies have sought to mimic activated platelets by conjugating antibodies

or peptide sequences that recognize cancer cells [347, 348]. Nevertheless, existing platelet biomimetic strategies represent a bottom-up approach and may have certain limitations: the bottom-up approach is largely inadequate in duplicating a complex protein makeup of natural platelets on a synthetic substrate. The heterogeneity and complexity of cancer biology, however, suggest that not all cancer cells or cancer types utilize the same receptor-ligand interaction for platelet-cancer cell adhesion. Therefore, mis-targeting or off-targeting can be associated with this strategy. In addition, the cost of producing target antibodies or peptides at a clinical grade may become prohibitively expensive when these biomimetic formulations require scale up.

In contrast to the bottom-up strategy, a top-down approach that utilizes platelet membrane-derived vesicles (PMDVs) to coat synthetic particles may have several advantages: (1) Our study demonstrated that PMDVs in principle maintain a whole makeup of membrane proteins and glycans from platelet membranes that are relevant to CTC targeting. Moreover, molecules involved in self-recognition (e.g. CD47) of host cells for overcoming macrophage-mediated phagocytosis are also displayed on PMDV-coated Si particles; (2) The facile access to sufficient human platelet-rich plasma (PRP) which is routinely collected clinically for platelet transfusions allows for scaling up of such a platform at relatively low cost.

Conventional methods seek to introduce polymeric conjugates (e.g. PEG) to avoid opsonization leading to reduced phagocytosis [349]. In contrast, it has been shown that the CD47 protein expressed by host cells mediates anti-phagocytosis through

interactions with signal regulatory protein-α (SIRPα) expressed on macrophages [350]. Therefore, a more biologically inspired approach has been developed by conjugating synthetic particles with CD47 or the minimal interacting peptide of CD47 to reduce phagocytosis and extend the half-life of particles in blood circulation [351]. In addition to CD47, it remains unclear if host cells also utilize other proteins to antagonize the macrophage-mediated phagocytosis. Therefore, a top-down biomimetic strategy utilized in PMDV coating of Si particles may be of interest when other potential proteins for anti-phagocytosis remain unidentified.

Future investigations could engineer particles with a platelet-like disc shape (e.g. plateloid silica particles) for functionalization with platelet membrane. Plateloid particles without any targeting moiety have been demonstrated to exhibit more efficient tumoritropic accumulation in solid tumors by taking advantage of hydrodynamic forces and interfacial interactions with tumor-associated endothelium [352]. Nevertheless, it hasn't been studied whether such an advantage would also apply for targeting of CTCs in circulation. It is likely that disc-shaped particles coated with platelet membrane are more resistant to fluid shear stress when targeting fibrin-associated CTCs. In addition, an ultrasoft hydrogel with great deformability has been recently demonstrated to simulate the behavior of platelets to collapse at fibrin networks with optimal clotting effect [353]. Combining these two physical features (disc shape and deformability) with platelet membrane functionalization might form the basis for particles that more closely resemble the physical properties of platelets in the future.

	Size (nm)	Zeta potential (mV)
Platelets	2320 ± 185	-9.8 ± 3.1
Platelet-derived vesicles	106 ± 12	-10.5 ± 2.4
Si particles	2008 ± 34	-20.8 ± 3.2
APTES Si particles	2085 ± 48	25.5 ± 4.6
Membrane-coated Si particles	2293 ± 92	-10.1 ± 1.9

Table 4.1. Particle characterization

Name	Functions	Receptors
THBS1	Platelet adhesion	Fibrinogen, fibronectin, laminin, and collagen
Integrin α2b (CD41)	$\alpha_{IIb}\beta_3$ complex, platelet adhesion and aggregation	Fibrinogen, fibronectin, vWF
Integrin β, β_3 (CD61)	$\alpha_{IIb}\beta_3$ complex, platelet adhesion and aggregation	Fibrinogen, fibronectin, vWF
GP Ib α (CD42b)	GPIb-V-IX complex, platelet adhesion	vWF
GP Ib β (CD42c)	GPIb-V-IX complex, platelet adhesion	vWF
GP IX	GPIb-V-IX complex, platelet adhesion	vWF
GP V	GPIb-V-IX complex, platelet adhesion	vWF
GP VI	Initial platelet adhesion	Collagen
MHC-1	Host recognition, self compatibility	CD8 receptor
CD47	Anti-phagocytosis	Signal regulatory protein-α (SIRPα)
P-selectin	Platelet adhesion	PSGL-1 (decorated with sLe^x)

Table 4.2. Top platelet membrane integral proteins identified by LC-MS

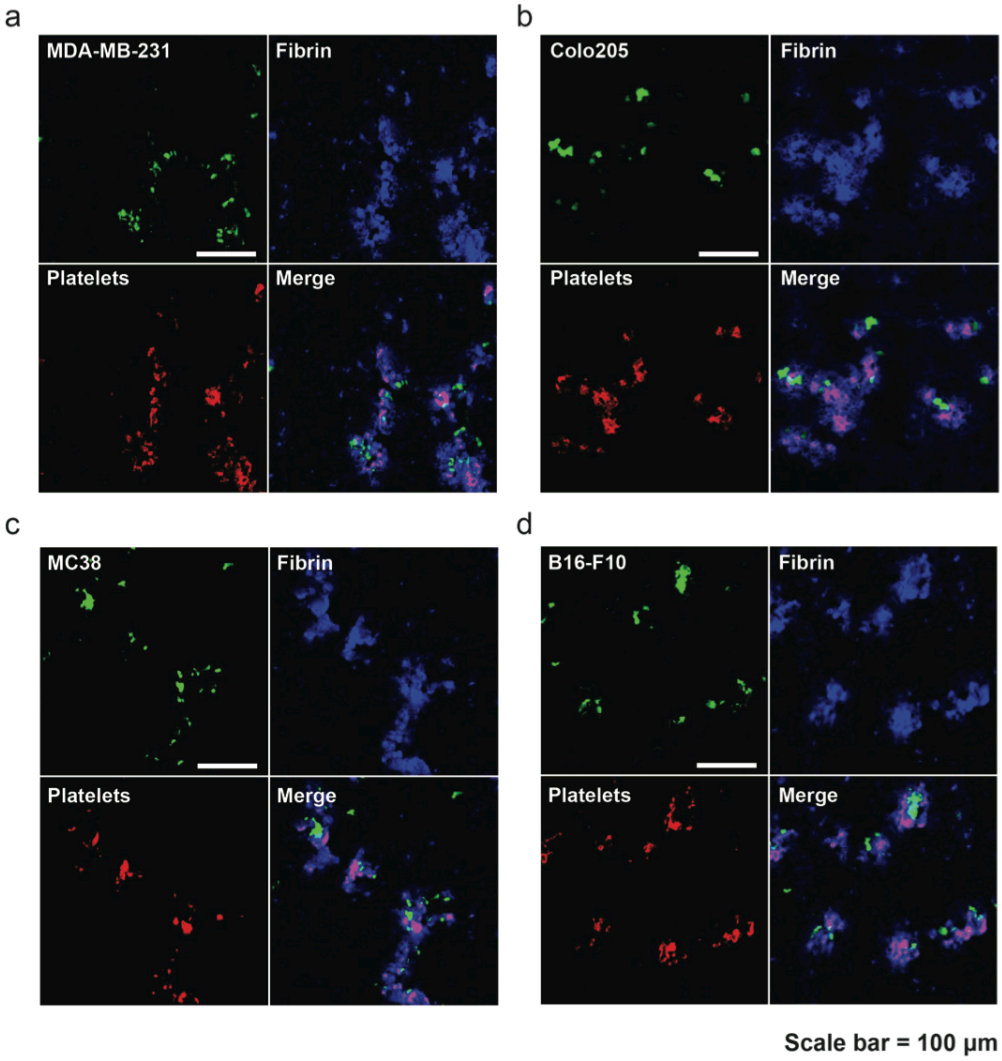

Figure 4.1. Co-localization of cancer cells/fibrin/platelets in lung vasculature. Immunofluorescence staining of activated platelets and fibrin in lung sections with circulating CTCs. Calcein-AM-labeled human cancer cells (a) MDA-MB-231 and (b) COLO 205 were intravenously injected into NSG immunocompromised mice. After 30 min, lung sections were prepared for immunofluorescence staining of fibrin and activated platelets. In a syngeneic metastasis model, C57BL/6-derived cancer cells (c) MC38 and (d) B16-F10 were injected into C57BL/6 followed by staining of fibrin and activated platelets in lung sections.

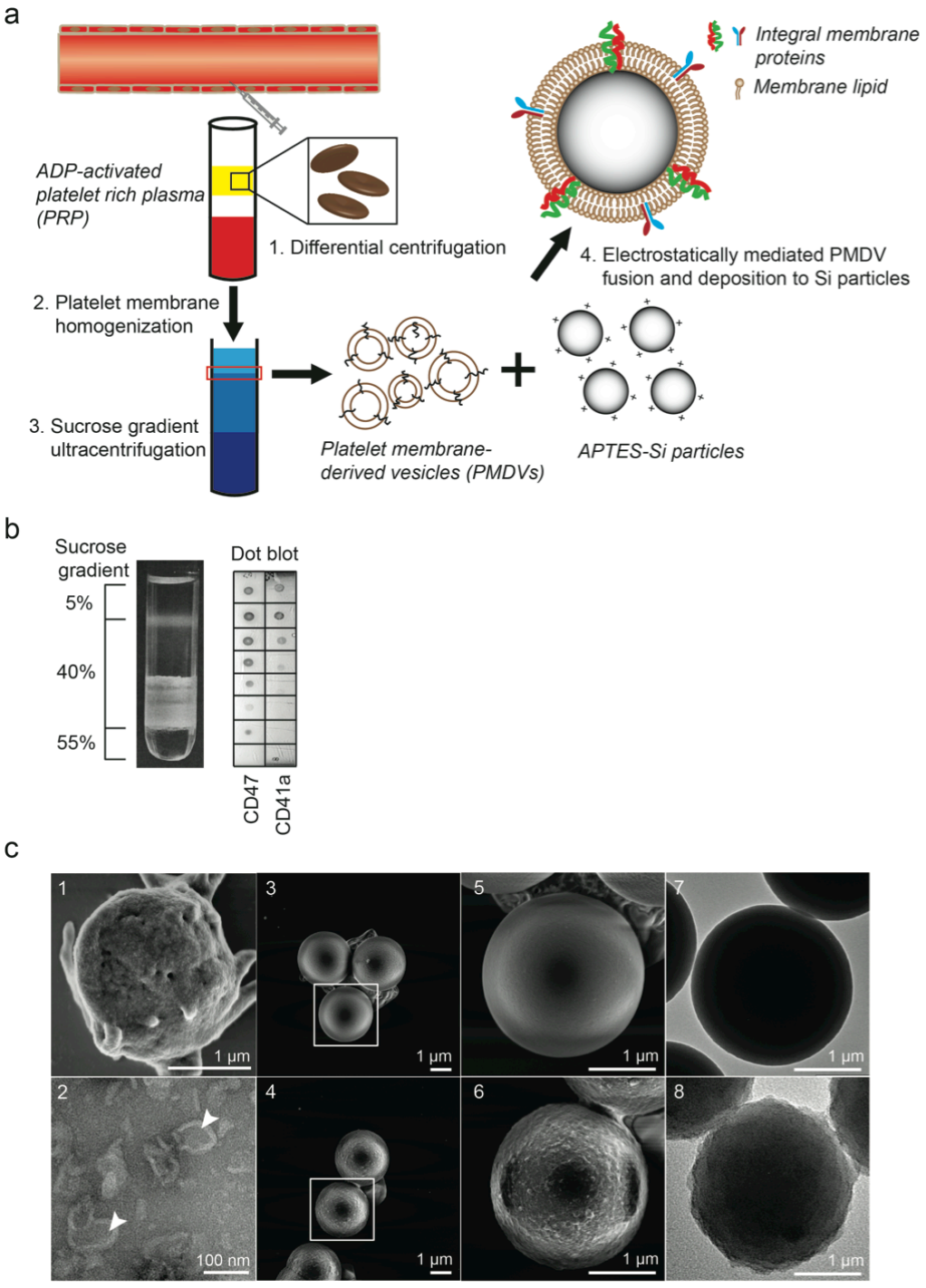

Figure 4.2. Functionalization and characterization of PMDV-coated Si particles

(a) Schematic of preparing platelet membrane-coated Si particles. (b) Detection of membrane protein-associated lipid layer in discontinuous sucrose gradient solution by

dot blot assay. Lipid fractions were identified as translucent layers in between two sucrose concentrations. (c) SEM and TEM characterization. SEM images: (1) Activated platelets, (3, 5) APTES-Si particles, (4, 6) PMDV-coated Si particles. TEM images: (2) PMDVs, (7) APTES-Si particles, (8) PMDV-coated Si particles. Arrow head indicates hollow structure of PMDVs.

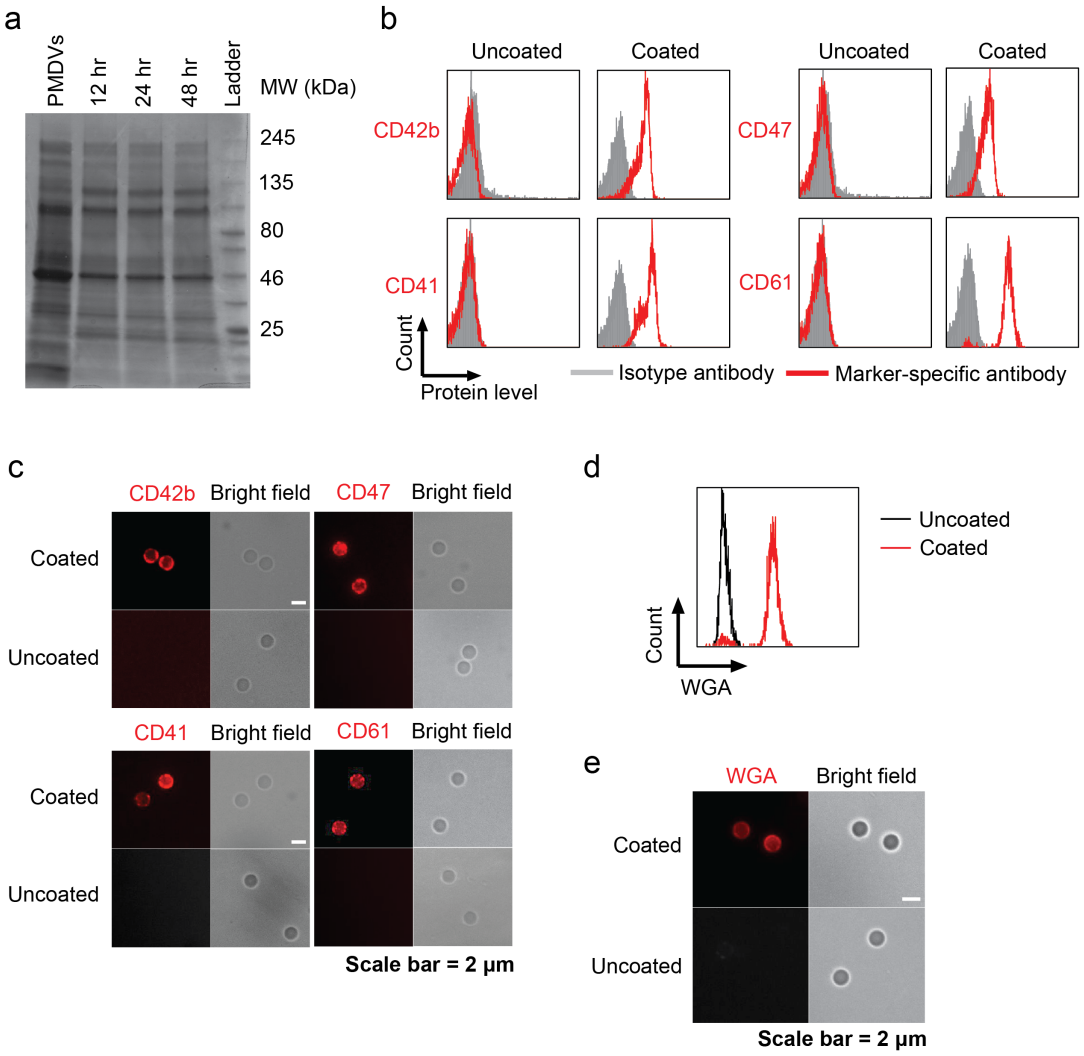

Figure 4.3. Presence of glycoproteins and glycans on PMDV-coated Si particles. (a) Stability of PMDV-coated Si particles. Membrane proteins were stripped after incubation of coated particles in TBS at 37 °C for 12, 24, and 48 hr. Afterwards, proteins were separated and stained by Commassie blue in SDS-PAGE. PMDVs were loaded as a positive control. (b) Detection of platelet membrane glycoproteins CD42b, CD47, CD41, and CD61 by flow cytometry. (c) Immunofluorescence staining of CD42b, CD47, CD41, and CD61 in PMDV-coated or uncoated Si particles. Far-red and bright field images were presented. (d) Detection of sialic acid and N-

acetylglucosaminyl glycans on PMDV-coated Si particles. Sialic acid and N-acetylglucosaminyl residues were identified by fluorescently labeled wheat germ agglutinin (WGA) in both flow cytometry and immunofluorescence staining.

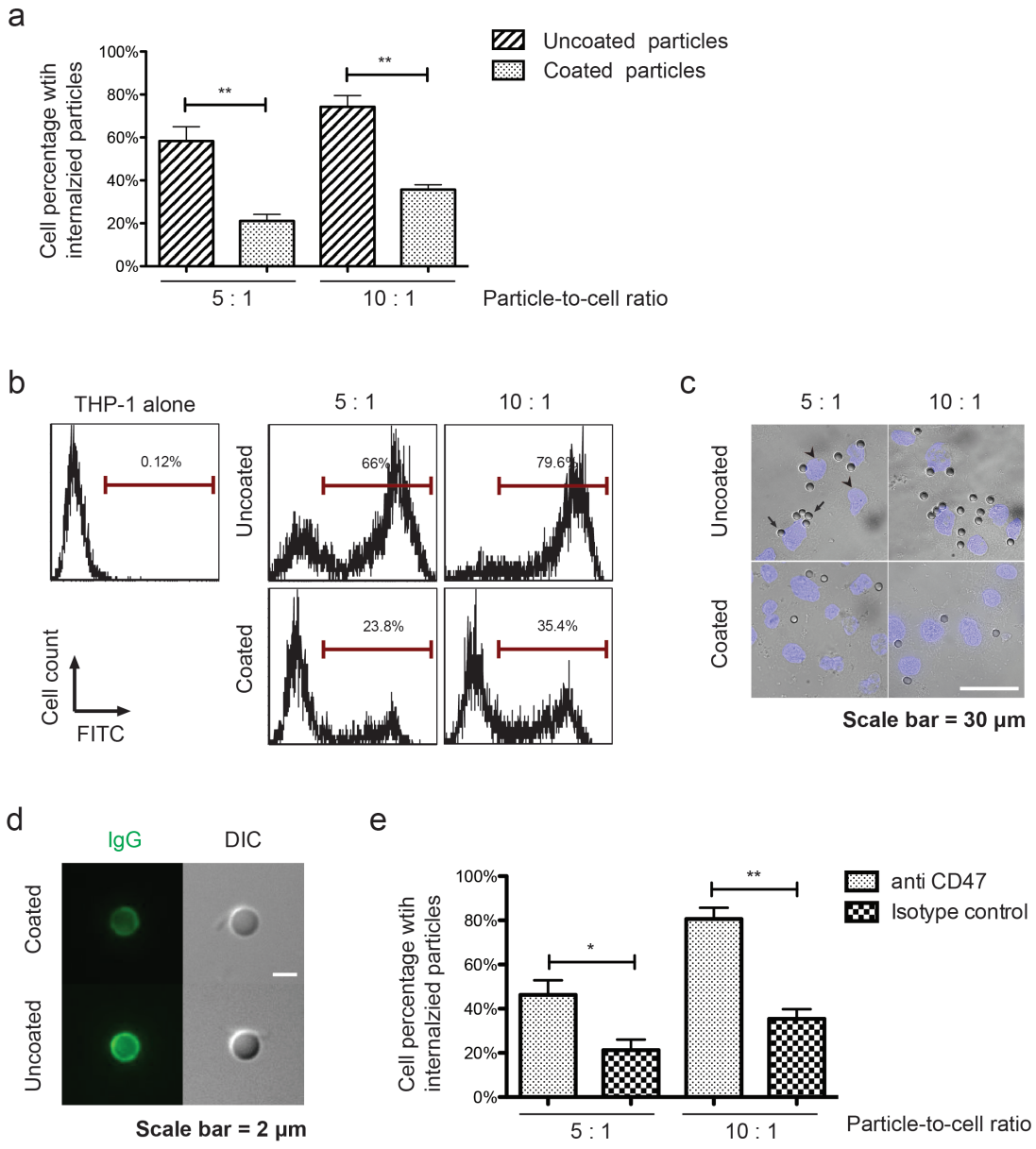

Figure 4.4. Reduction of macrophage-mediated phagocytosis. (a) Internalization of uncoated and PMDV-coated Si particles in phagocytic cells. FITC-labeled Si particles were incubated with PMA-differentiated THP-1 at particle-to-cell ratios of 5:1 and 10:1. Cells with internalized particles were quantified by flow cytometry after removal of surface bound particles by trypsin. Results are presented as the mean ± SEM, n=3; **, $p<0.01$. (b) Representative flow cytometry histograms of phagocytic THP-1 cells

with internalized Si particles. (c) Representative images of phagocytic THP-1 cells with internalized Si particles. After removing surface bound Si particles by trypsin, cells were cytospun onto glass slides. Nuclei were stained by DAPI (blue). Arrows: Si particles; arrowheads: nuclei. (d) Differential opsonization of human IgG to the surface of uncoated and PMDV-coated Si particles. After 30 min incubation with human serum, washed particles were stained with FITC-labeled anti-hIgG Fc. Particles were imaged through green fluorescent and DIC channels. (e) CD47 was partially responsible for reduced phagocytosis of PMDV-coated Si particles. FITC-labeled PMDV-coated Si particles were preincubated with anti-CD47 blocking antibody and subsequently added to PMA-differentiated THP-1 cells. Cells with internalized particles were quantified by flow cytometry. Results are presented as the mean ± SEM; n=3; *, $p<0.05$; **, $p<0.01$.

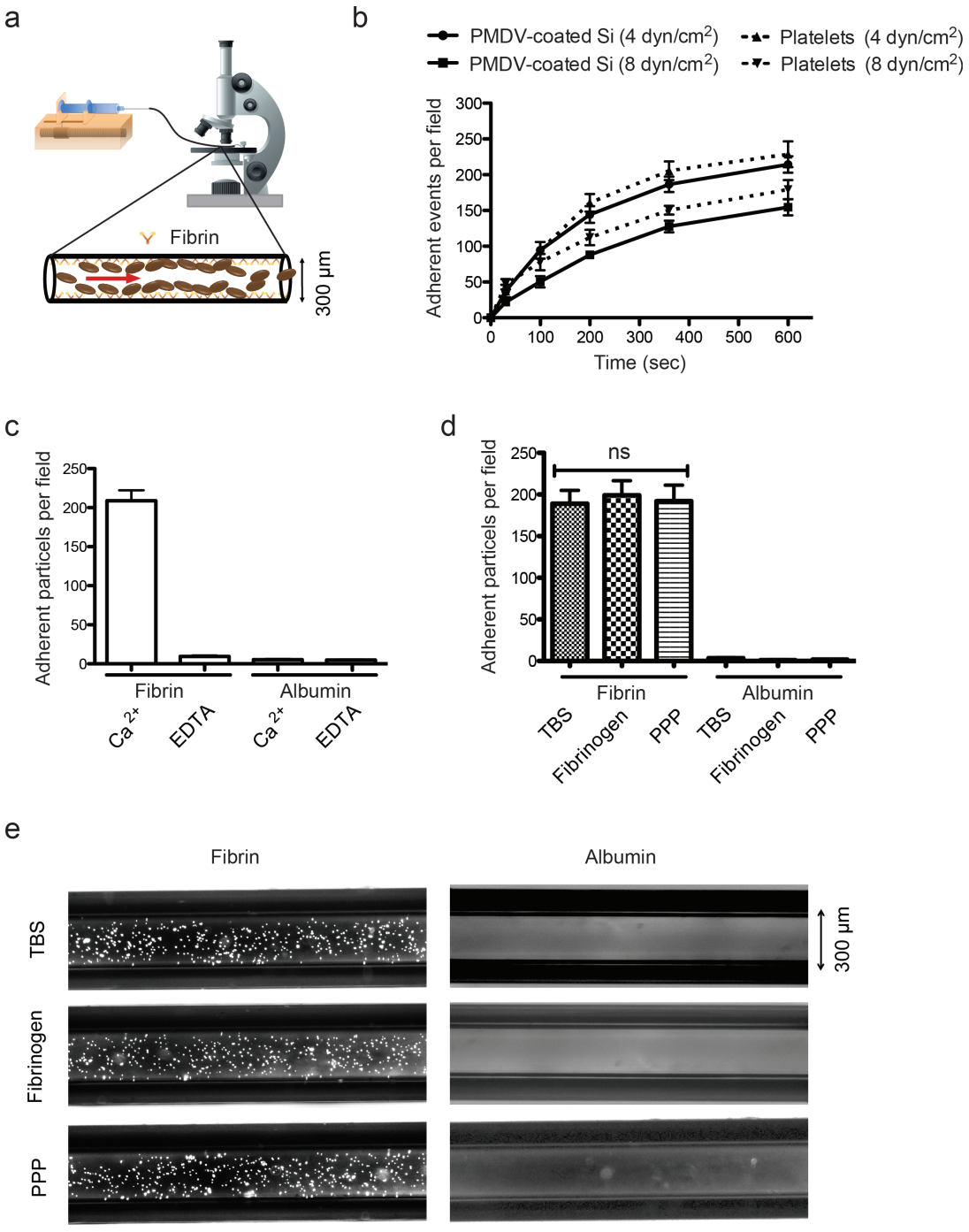

Figure 4.5. Adhesion of PMDV-coated Si particles to immobilized fibrin under flow. (a) Schematics of a microtube with inner surface coated with fibrins to simulate blood clot. 10^6/ml PMDV-coated Si particles were perfused through microtubes at 4 dyn/cm^2 via a controlled syringe pump. (b) Adhesion of coated particles and activated

platelets to a fibrin-functionalized surface under flow. (c) Comparison of adherent particles in Ca^{2+}- or EDTA-containing buffer under flow. For negative control, albumin was coated on the surface in the absence of fibrin. (d) Comparison of particle adhesion to fibrin-coated microtubes under flow in tris-buffered saline (TBS), TBS containing 1 mg/ml soluble fibrinogen, or platelet poor plasma (PPP). TBS buffer was supplemented with Ca^{2+}. Results are presented as the mean ± SEM, ns=no significant difference. (e) Representative fluorescent images of adherent particles in fibrin-coated microtubes were taken after removing unbound particles via TBS washing.

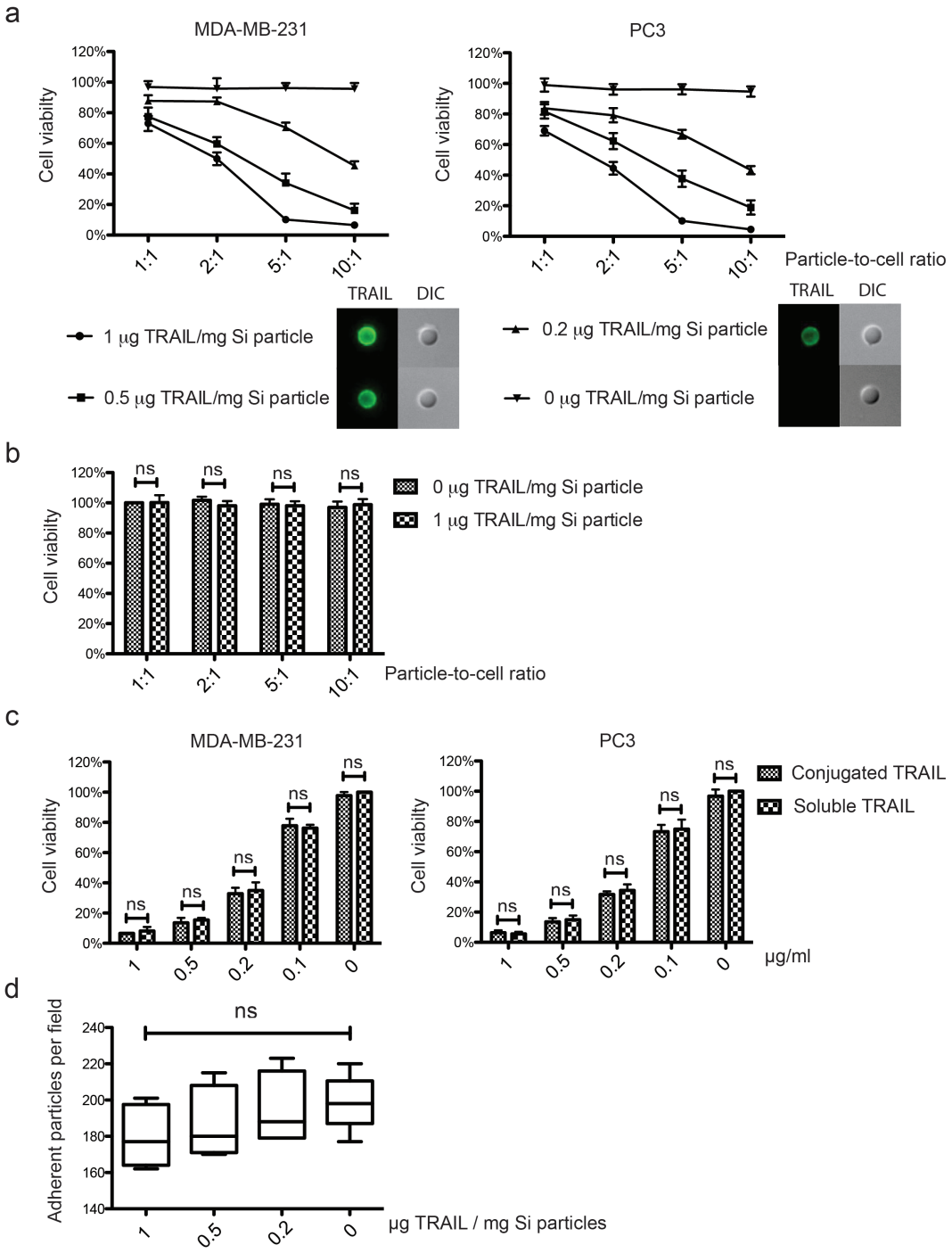

Figure 4.6. Conjugation of TRAIL to PDMV-coated Si particles induced apoptosis in cancer cells. The density of TRAIL on the surface of PDMV-coated particles was varied at 0, 0.2, 0.5, and 1 μg TRAIL/mg Si particles. (a) TRAIL was

immunostained by FITC-anti human TRAIL. PDMV-coated particles with TRAIL conjugation of varied density were incubated with breast cancer cells MDA-MB-231 and prostate cancer cells PC3 at particle-to-cell ratio of 1:1, 2:1, 5:1, and 10:1 for 24 hr. Cell viability was measured by MTT assay. (b) TRAIL conjugation on PMDV-coated Si particles was nontoxic to endothelial cells. PMDV Si particles at a conjugation density of 0 or 1 μg TRAIL/mg Si particles were incubated with HUVECs with different particle-to-cell ratios. Cell viability in each treatment group was normalized to the treatment with 0 μg TRAIL/mg Si particles at 1:1 particle-to-cell ratio. (c) Comparing efficacy of soluble TRAIL versus TRAIL immobilized to PDMV-coated Si particles in inhibition of cancer cell proliferation. PMDV-coated Si particles (1 μg TRAIL/mg silica coating density) were incubated with cancer cells at different particle-to-cell ratios and compared to soluble TRAIL at a concentration matched to respective particle-to-cell ratios. (d) TRAIL conjugation did not interfere with the ability of PDMA-coated Si particles to adhere to fibrin-immobilized surface under flow. All results are presented as the mean ± SEM, n=3; ns, no significant difference.

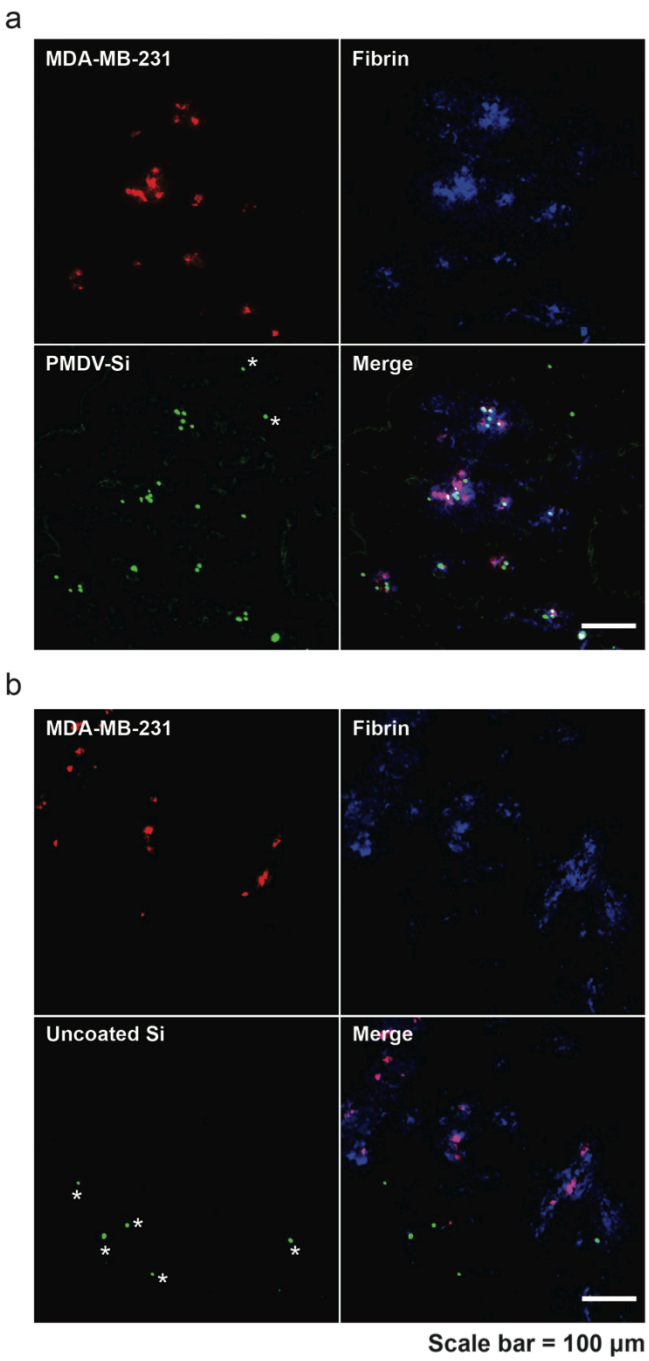

Figure 4.7. Targeting of PMDV-coated Si particles to CTC/fibrin micro-thrombi in lungs. Red fluorescent MDA-MB-231 cells were injected via tail vein to NSG mice. After 30 min, FITC-labeled (a) PMDV-Si particles or (b) uncoated Si particles were retro-orbitally injected at particle-to-cell ratio of 50:1. Thrombi were stained by anti-

fibrin conjugated with far-red dye for three-color imaging. Star symbols indicate nonspecific targeting of Si particles to fibrin/cancer cells.

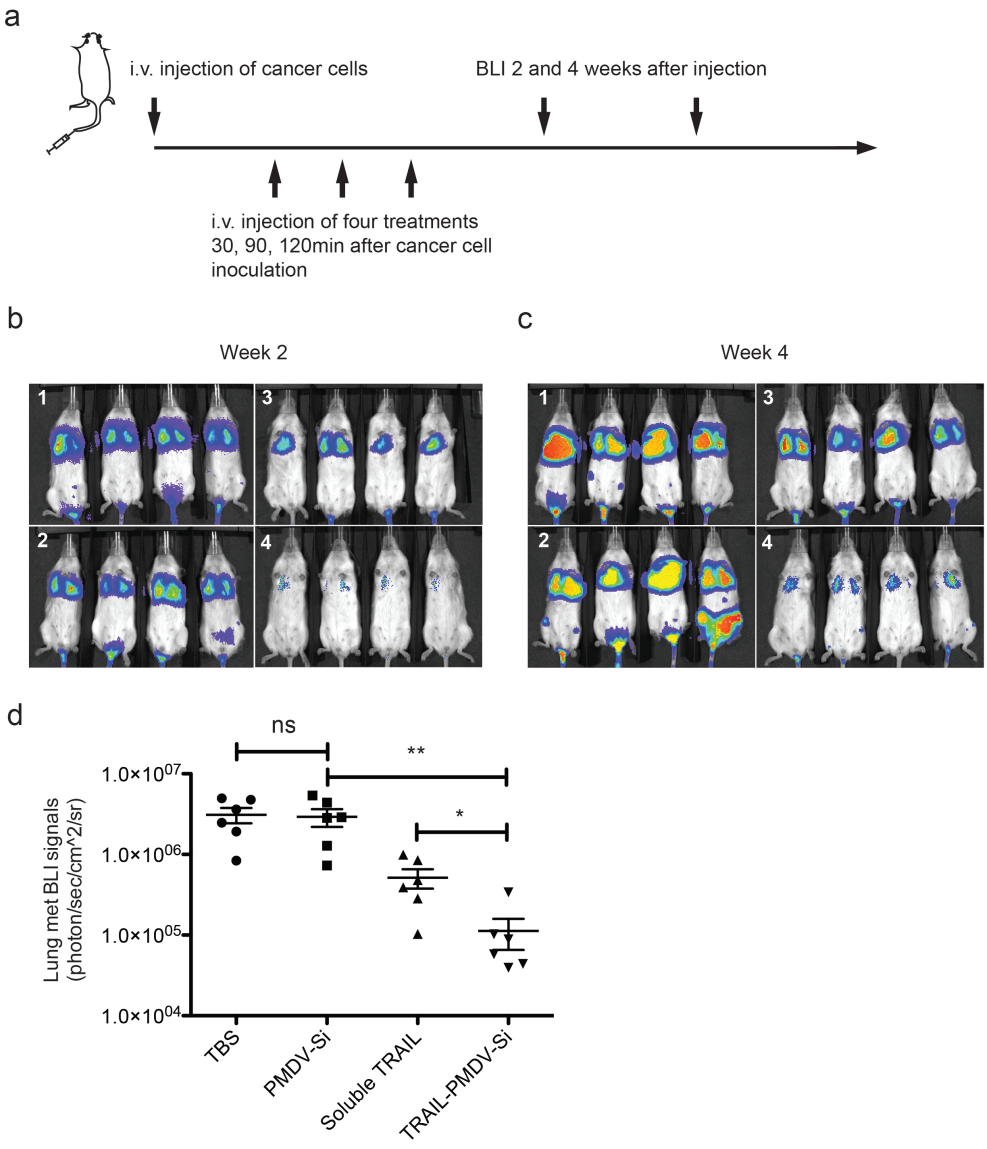

Figure 4.8. Reduction of lung metastasis by TRAIL-conjugated PMDV-Si particles. (a) Schematic of experimental protocol for lung metastasis model and therapeutic treatment. BLI at 2 weeks (b) and 4 weeks (c) after cancer cell injection. Four different treatment groups were applied: 1. TBS; 2. PMDV-Si particles; 3. Soluble TRAIL; 4. TRAIL-conjugated PMDV-Si particles. (d) Quantification of lung metastasis in different treatment groups at week 4. All results are presented as the mean ± SEM, n=6; *, $p<0.05$; **, $p<0.01$; ns, no significant difference.

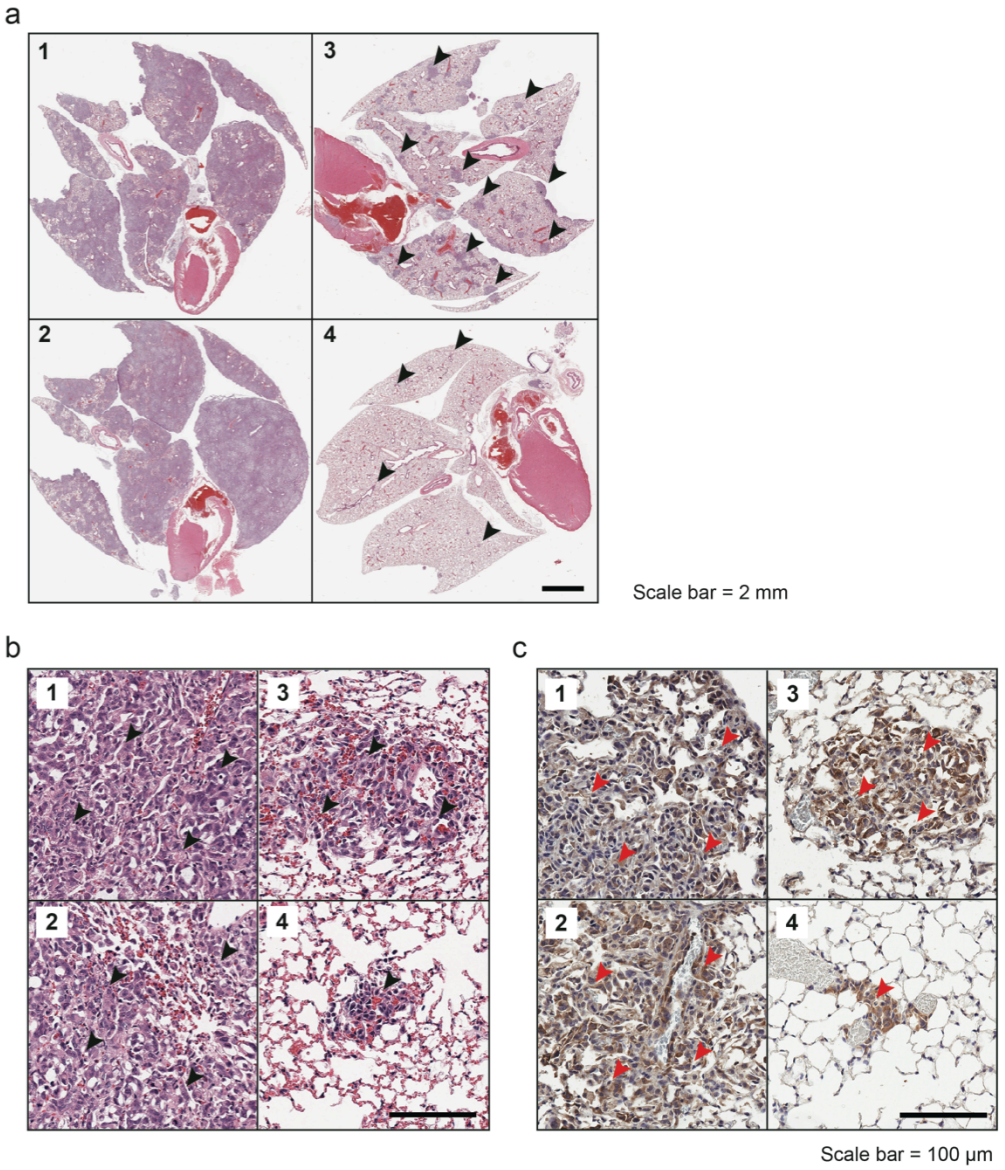

Figure 4.9. Histological examination of lung metastasis in response to TRAIL-conjugated PMDV-Si particles. Lungs were collected at the week 4 from the four different treatment groups: 1. TBS; 2. PMDV-Si particles; 3. Soluble TRAIL; 4. TRAIL-conjugated PMDV-Si particles. Images were taken at low (a) and high (b) magnifications, respectively. Arrowheads indicate tumor areas or nodules. (c) Immunohistochemistry staining of lung sections for luciferase-expressing cancer cells using anti-luciferase antibody.

Particle type	Incubation condition	Zeta potential (mV)
Uncoated Si	RPMI media with 10% FBS	-15.6 ± 2.2
Uncoated Si	Human plasma	-9.2 ± 1.1
PMDV-coated Si	RPMI media with 10% FBS	-10.5 ± 1.6
PMDV-coated Si	Human plasma	-10.8 ± 1.7

Supplemental table 4.1. Surface zeta potential measurement of Si particles in physiological conditions. Uncoated and PMDV-coated Si particles were incubated with cell culture media containing 10% fetal bone serum (FBS) or human plasma for 30 min. Following washing with TBS three times, the surface charge of particles were measured by a dynamic light scattering.

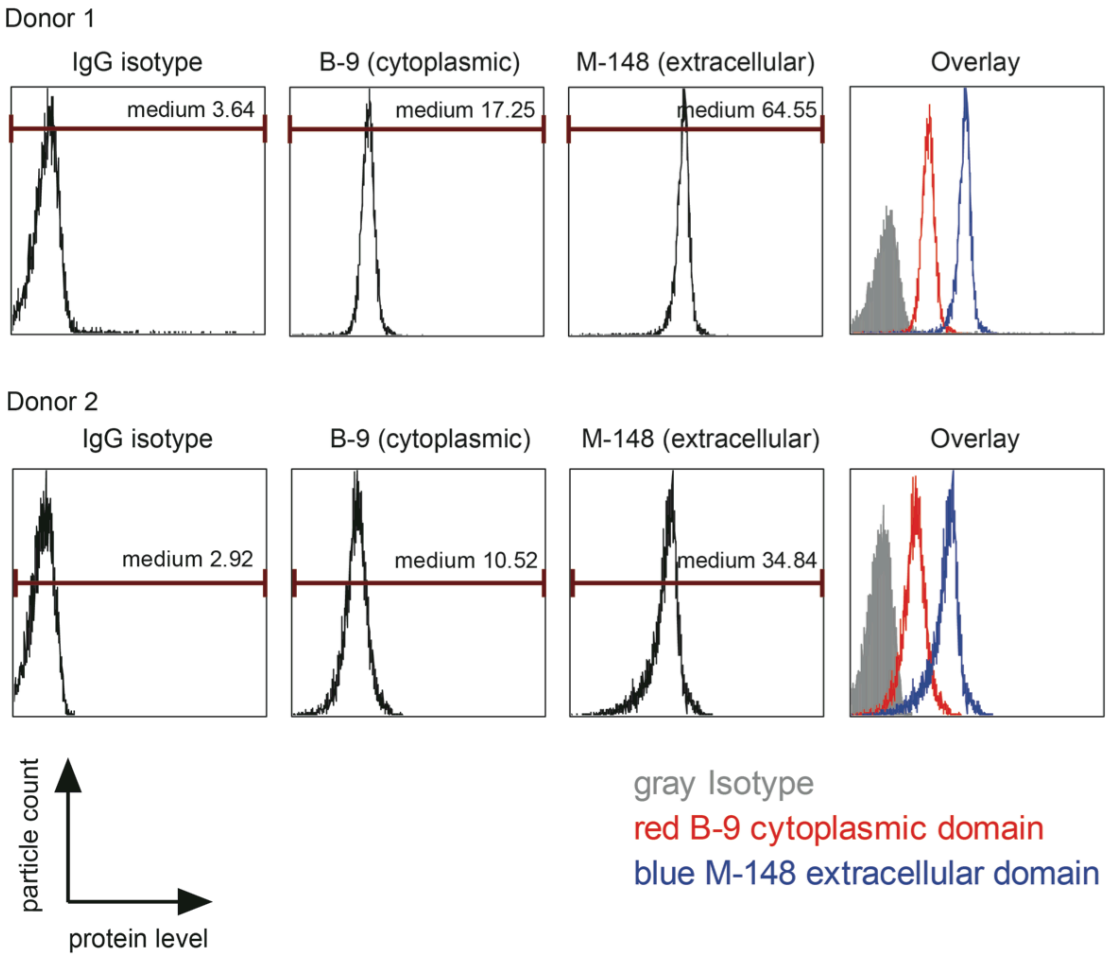

Supplemental figure 4.1. Measurement of integral membrane protein orientation on PMDV-coated Si particles. Two antibodies recognizing extracellular (M-148) and cytoplasmic (B-9) domains of CD41 were used in flow cytometry. PMDVs were prepared from two separate donors. It was found that majority of CD41 was present in an original orientation with a 4:1 ratio of extracellular to cytoplasmic domains on the outer surface of PDMV-coated Si particles.

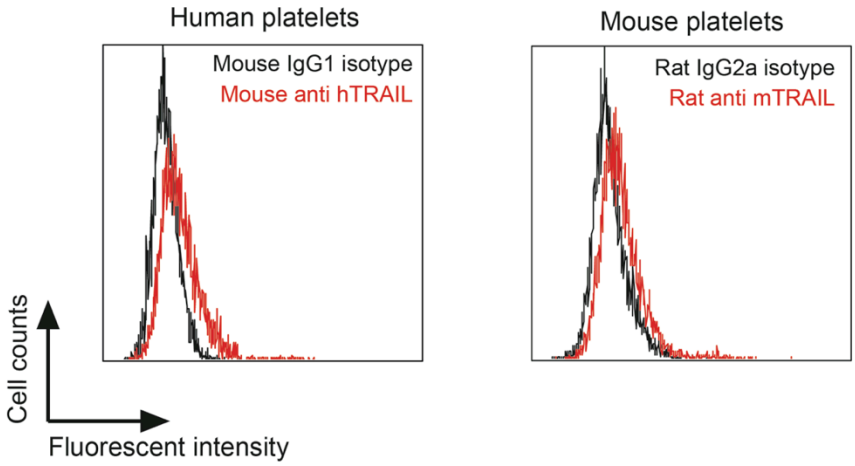

Supplemental figure 4.2. Detection of surface TRAIL on human and mouse platelets.

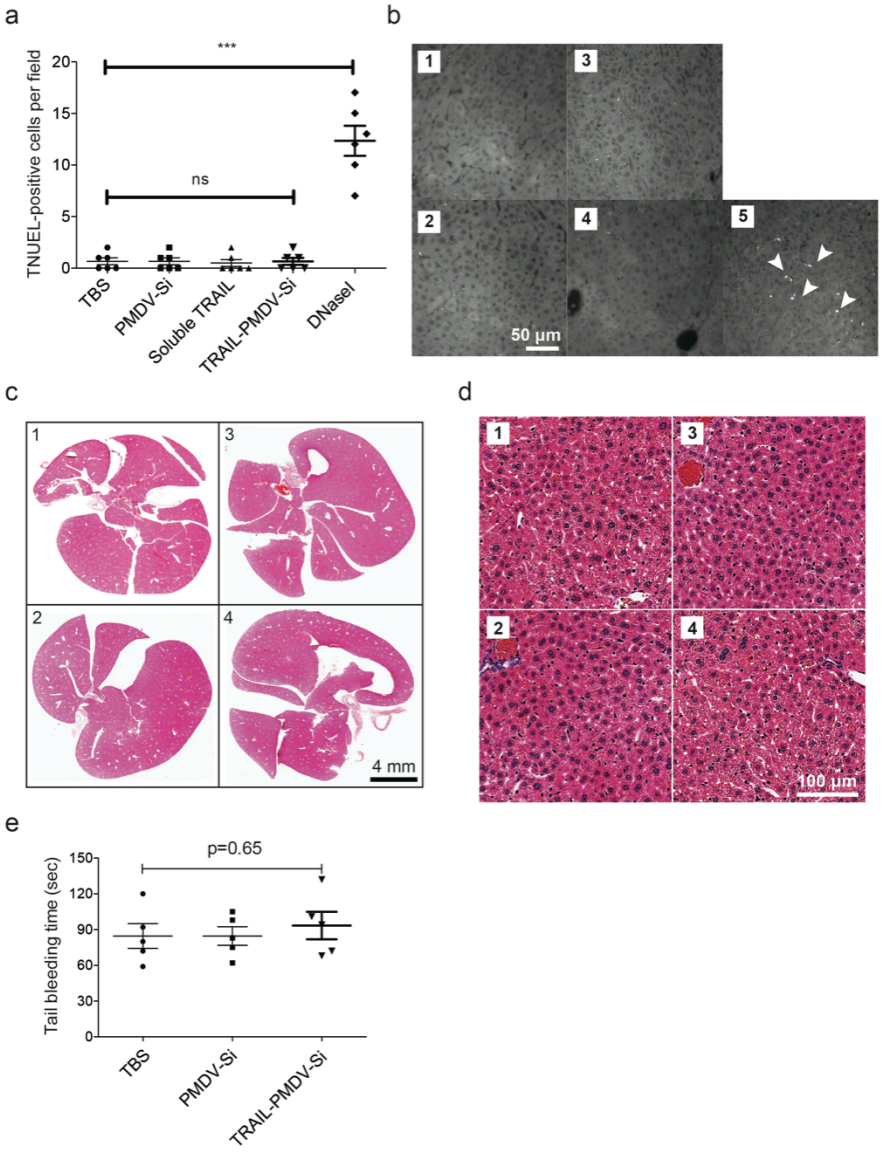

Supplemental figure 4.3. *In vivo* biological safety of TRAIL-conjugated PMDV-Si particles. Mice received three injections (0, 30, and 90 min time points) in four different treatments: 1. TBS; 2. PMDV-Si particles; 3. Soluble TRAIL; 4. TRAIL-conjugated PMDV-Si particles. After 24 hr, livers were collected. (a) TUNEL staining of liver sections. The number of apoptotic liver cells was quantified in immunofluorescence images. (b) Representative TUNEL staining images. H&E staining of liver sections at low (c) and high (d) magnifications. (e) Tail bleeding assay

of tumor-free mice receiving TRAIL-conjugated PMDV-Si particles. Results of each group are presented as the mean ± SEM, n=5. A one-way ANOVA test was performed to calculate statistic difference.

CHAPTER 5 ENGINEERING TROJAN-HORSE PLATELETS TO NEUTRALIZE CIRCULATING TUMOR CELLS

* This section is adapted from the following manuscript:

Li J, Sharkey CC, Liesveld J, King MR. Engineering Trojan-horse platelets to neutralize circulating tumor cells. (Submitted)

Mounting experimental evidence demonstrates that platelets support cancer metastasis. The activation of platelets and the coagulation system have a crucial role in the progression of cancer. Within the circulatory system, platelets guard circulating tumor cells (CTCs) from immune elimination and promote their arrest at the endothelium, supporting CTC extravasation into secondary sites. Extensive studies have explored the blockade of platelet-CTC interactions as an anti-metastatic strategy. Such an intervention approach, however, may cause bleeding disorders since the platelet-CTC interactions are inherently linked to the blood coagulation cascade including platelet activation. On the other hand, platelets have been genetically engineered to correct inherited bleeding disorders in both animal models and clinical trials through megakaryocyte lineage-targeted gene therapy in bone marrow stem cells. The successes of platelet gene therapies suggest that platelets can serve as an efficient vector to deliver cancer therapeutics. In this study, inspired by the physical association between platelets and CTCs, platelets were genetically modified to express surface-bound TRAIL, a cytokine known to induce apoptosis specifically in tumor cells. This approach is demonstrated to kill cancer cells *in vitro* and significantly reduce metastases in an experimental mouse model of prostate cancer metastasis.

5.1 Introduction

Metastasis contributes to more than 90% of cancer-associated mortality [102, 318]. It occurs after primary tumors shed circulating tumor cells (CTCs) via hematogenous dissemination to distant organs [49, 104]. Despite advancements in the understanding and detection of CTCs, effective neutralization of CTCs for the prevention of

metastasis remains clinically challenging. Previous studies have demonstrated intrinsic tumor-tropic properties of bacteria and multiple types of stem cells including mesenchymal stem cells (MSCs), neural stem cells (NSCs) and endothelial precursor cells, making them attractive candidates for the targeted delivery of anticancer biological agents [354-357]. The mechanisms of tumor tropism were found to be multifactorial including, but not limited to, gradients of hypoxia, growth factors, and inflammatory cytokines generated within solid tumors [358, 359]. The distinct transport system in the blood circulation, however, allows for rapid exchange of blood components within the vasculature. We reason that the gradients found in solid tumors are absent in circulation, which in turn makes existing cellular engineering approaches ineffective for targeting CTCs.

To explore alternative vectors for the delivery of cancer therapeutics in circulation, platelets were selected since they are capable of recognizing and interacting with CTCs immediately after the release of CTCs into circulation [106, 114]. Platelets are anuclear cytoplasmic bodies released from megakaryocytes in the bone marrow. It is estimated that one liter of blood contains about 400 billion circulating platelets [360]. In contrast to the long history of studies on the hemostatic function of platelets, their role in cancer metastasis has only recently become appreciated. It is generally believed that platelets interact with CTCs and promote metastasis via multiple mechanisms: 1. Platelet-CTC aggregates have a greater potential to become trapped in microvessels than individual CTCs. Such aggregation facilitates subsequent extravasation of cancer cells [71]; 2. Aggregation of platelets around CTCs protects against immune-mediated

clearance of CTCs largely by natural killer (NK) cells [72]; 3. CTC evasion of NK cells is not merely attributed to physical shielding of platelets. The cytotoxic activity of NK cells is guided by the principles of "missing-self" and "induced-self". Cells lacking expression of MHC class I (missing-self) and/or a stress-induced expression of ligands for activating NK receptors (induced-self) are preferentially recognized and eliminated [74]. While CTCs are often associated with a lack of MHC class I ligands, platelets can disrupt "missing self" recognition of NK cells by grafting MHC I class onto CTCs [75].

In light of the harmful association between platelets and CTCs, a variety of anti-platelet drugs have been tested to block platelet-CTC interactions or inhibit platelet activation in preclinical mouse models [326, 327, 329]. Anti-platelet therapies, however, may inevitably impair the normal hemostatic function of platelets in the presence of bleeding [326, 327]. In contrast to existing platelet intervention therapies, an alternative approach was explored in the current study by expressing the cancer cell-killing cytokine, TRAIL on the surface of platelets while maintaining the platelets' normal hemostatic function and cancer cell adhesion ability. TRAIL was selected to be ectopically expressed in platelets for four reasons: (1) TRAIL is abundantly expressed on the surface of natural killer cells and cytotoxic T cells. It is responsible for the tumoricidal activity of these immune cells [100]. (2) TRAIL exerts a tumor cell-specific apoptotic effect by recognizing death receptors (DRs) highly expressed on the surface of cancer cells [298, 328]. Previous studies have successfully modified mesenchymal stem cells (MSCs) and neural stem cells (NSCs) to express TRAIL to

kill solid tumors in mice [356, 361, 362]. (3) The adhesion and aggregation of platelets to CTCs may facilitate the DR-mediated TRAIL apoptosis signaling by clustering DRs on cancer cells [363, 364]. (4) Despite TRAIL resistances exhibited by certain cancer cells in solid tumors, it was found that these cells become more sensitive to TRAIL when they lose attachment to extracellular matrix [365]. The natural detachment of CTCs from a primary tumor likely increases their sensitivity to TRAIL.

To enable platelet-specific TRAIL expression, a platelet-targeted lentiviral transgene approach was utilized in this work through genetically engineering of hematopoietic stem and progenitor cells (HSPCs) followed by bone marrow transplantation (BMT). Such action has been successfully applied to correct genetic bleeding disorders in mice, dogs and certain human clinical trials while also meeting desired safety requirements [366-370]. The self-renewal ability of HSPCs would allow for continuous presence of TRAIL-expressing platelets upon maturation of megakaryocytes and release of platelets into the circulation. This approach can potentially enable long-term patrolling and neutralization of CTCs in circulation for the prevention or reduction of metastases.

5.2 Methods and Materials

Cell lines and mice

MDA-MB-231, PC3, 293T, Dami and MEG-01 cell lines were obtained from American Type Culture Collection (ATCC, Rockville, MD, USA). MDA-MB-231 and 293T cells were cultured in DMEM (Invitrogen, Grand Island, NY, USA) with 10% FBS. PC3 were maintained in RPMI (Invitrogen) with 10% FBS. Dami and MEG-01

were expanded in IMDM (Invitrogen) with 10% FBS. Six to eight week old NOD SCID gamma (NSG) and C57BL/6 mice were purchased from Jackson Laboratory (Bar Harbor, ME, USA). Mice were housed in a SPF barrier animal facility at Cornell University.

Chemicals and antibodies

The following chemicals or kits were used for assaying cell proliferation and apoptosis: MTT (AMRESCO, Solon, OH, USA) and TACS® Annexin V-FITC Kit (Gaithersburg, MD, USA). Reagents for TEM were obtained from Electron Microscopy Sciences (Hatfield, PA, USA): glutaraldehyde, osmium tetroxide and uranyl acetate. APC-conjugated antibodies for human and mouse CD41 and PE-conjugated antibodies for human TRAIL were purchased from Biolegend (San Diego, CA, USA). Primary antibodies for human TRAIL and β-actin were obtained from PeproTech (Rocky Hill, NJ, USA) and Santa Cruz Biotech (Santa Cruz, CA, USA). HRP-conjugated anti-mouse and anti-rabbit antibodies were from Santa Cruz Biotech.

Flow cytometry

Cells were detached with enzyme-free Gibco® Cell Dissociation Buffer (Invitrogen) and suspended at a concentration of 5×10^5 cells in 100 μL cold PBS/1% bovine serum albumin (BSA). Fluorescent primary antibodies or isotype control were incubated with cells for 30 min on ice. Following two washes with 1 mL of PBS, fluorescence measurements were collected using a Guava easyCyte™ Flow Cytometry (Millipore, Billerica, MA, USA). Data were analyzed using the Flow Express software (De Novo

Software, Los Angeles, CA, USA).

Western blotting

Western blotting was performed as previously described [134]. Briefly, whole cell lysates were prepared and separated using 10% SDS-PAGE. Membranes were incubated with primary antibodies and secondary antibodies diluted at 1:1000. Immobilized proteins were detected by using a chemiluminescent HRP substrate (Millipore, Billerica, MA, USA).

Cell proliferation assay

Cell proliferation was assayed by measuring mitochondrial dehydrogenase activity using MTT as the substrate. After treatment, cells were incubated with MTT at a concentration of 0.5 mg/mL, at 37°C for 3 hr. The purple MTT product was solubilized with DMSO and measured at 570nm using a BioTek plate reader (Winooski, VT, USA).

Isolation, lentiviral transduction and in vitro differentiation of HSPCs

To isolate mouse HSPCs (Lin^-), bone marrow mononuclear cells (MNCs) were extracted from femurs and tibias of 6-8 week old mice. Following RBC lysis, unwanted cells were targeted with biotinylated antibodies directed against non-hematopoietic stem cells and non-progenitor cells (CD5, CD11b, CD19, CD45R/B220, Ly6G/C(Gr-1), TER119) followed by removal with streptavidin-coated magnetic particles (STEMCELL TECHNOLOGIES INC, Vancouver, BC, Canada). For

lentiviral transduction, mouse Lin^- cells were cultured for 24-hr prestimulation in serum-free X-VIVO-10 (Lonza, Allendale, NJ, USA) containing 100 ng/mL mouse SCF, TPO, and flt3 ligand (Prospecbio, East Brunswick, NJ, USA). Cells were then transduced twice within 24 hr with lentivirus particles at a MOI of 50-100 in retronectin-coated plates. For *in vitro* differentiation, cells were differentiated in X-VIVO-10, 10% FBS, and 50 ng/mL mouse TPO for 10 days.

Bone marrow transplantation (BMT)

All mice were handled according to the Guide for the Care and Use of Laboratory Animals in compliance with US- and UK-based guidelines. All experimental procedures and protocols were approved by the Institutional Animal Care and Use Committee of Cornell University (Protocol No. 2012-0113). For bone marrow transplantation, 6-8 week old mice were irradiated at a dosage of 2.5 Gy. Within 24 hr of irradiation, each mouse received 1 million transduced HSPCs via retro-orbital injection.

Experimental metastasis mouse model and bioluminescence imaging

4 weeks after BMT, NSG mice received 10^4 cancer cells expressing firefly luciferase via a left ventricle injection. Bioluminescence imaging (BLI) was utilized to longitudinally monitor tumor progression. Briefly, BLI was performed with a CCD camera mounted in a light-tight specimen box (Xenogen, Waltham, MA, USA). Imaging and quantification of signals were controlled by the acquisition and analysis software Living Image® (Xenogen). Anesthetized mice were placed in the IVIS™

Imaging System and imaged from ventral views approximately 10-15 min after intraperitoneal injection of D-luciferin at 150 mg/kg body weight.

Tail bleeding assay

Tail bleeding time was determined by removing 3 mm from the tip of the distal mouse tail and immediately immersing the tail in 37°C PBS. A complete cessation of bleeding was defined as the end point of bleeding time.

Statistical analysis

All statistical analyses were performed using GraphPad Prism 5.0a for Mac OS X (San Diego, CA, USA). A one-way ANOVA followed by Tukey post test was used to compare statistical significance in the characterization of *in vitro* cell proliferation and *in vivo* experiments.

5.3 Results

Construction of lentiviral vectors with megakaryocyte-specific promoter

A self-inactivating lentiviral vector was utilized in this work due to its reported safety in gene therapies for both preclinical studies and clinical trials. To enable megakaryocyte- and platelet-specific gene expression, the human ubiquitin-C (Ubc) promoter in a self-inactivating lentiviral vector (pFUGW) was replaced by human integrin αIIβ promoter (nucleotides -889 to +35) [371, 372]. EGFP was cloned downstream of Ubc or αIIβ promoter as a reporter for examing gene transduction efficiency and tissue-specific expression. In addition, a full-length TRAIL gene

including transmembrane domain, substituted EGFP for expression of apoptosis-inducing cytokine in megakaryocyte and platelet lineages (**Figure 5.1a**). Flow cytometry measurement of gene expression indicated that both Ubc and αIIβ promoters facilitated robust EGFP and TRAIL expression in the promegakaryocyte cell line Dami. In contrast, only Ubc was able to drive gene expression in a human embryonic kidney cell line 293T (**Figure 5.1b**). This confirmed the megakaryocyte-specific activity of αIIβ promoter. Immuno-staining of TRAIL in Dami and 293T cell lines transduced with αIIβ-TRAIL or Ubc-TRAIL indicated surface-bound expression of TRAIL except for αIIβ-TRAIL in 293T (**Figure 5.1c**).

Differentiation of promegakaryocytes upregulates transgene expression in a αIIβ promoter-dependent manner

Previous studies showed that the activity of αIIβ integrin promoter increased following differentiation of promegakaryocytes [373, 374]. We reasoned that this differentiation pathway could be utilized to produce high levels of membrane-bound TRAIL. To test this hypothesis, αIIβ-EGFP and αIIβ-TRAIL were transduced into Dami cells. As shown by flow cytometry, expression of EGFP or surface-bound TRAIL was upregulated upon differentiation of Dami by phorbol 12-myristate 13-acetate (PMA) for 48 hr. In contrast, Ubc-driven transgene expression was unaffected by PMA-induced differentiation (**Figure 5.2a and b**). In addition, total TRAIL expression also increased following PMA treatment in Dami cells transduced with αIIβ-TRAIL but not Ubc-TRAIL (**Figure 5.2c**). This indicates that robust TRAIL expression can be induced following promegakaryocyte differentiation in an αIIβ promoter-dependent

manner.

Expression of TRAIL in isolated platelet-like particles

Dami and Meg-01 cells are two cell lines of megakaryoblastic origin, and are capable of spontaneously producing platelet-like particles (PLPs) [375, 376]. Consistent with previous observation, Dami cells proliferated faster, but produced fewer PLPs than Meg-01 cells (data not shown) [377]. Therefore, PLPs derived from promegakaryocytic cell line MEG-01 were examined in this study. An established protocol via differential centrifugation was adapted to isolate PLPs from MEG-01 transduced with αIIβ-EGFP or αIIβ-TRAIL (**Figure 5.3a**). These particles were found to be positive for β-actin detected by western blotting (**Figure 5.3b**). This suggested the preservation of cytoskeletal structures in PLPs similar to that of natural platelets. TRAIL-positive particles, however, can only be isolated from cells transduced with αIIβ-TRAIL but not αIIβ-EGFP vectors (**Figure 5.3b**). Both flow cytometry and immunostaining demonstrated expression of membrane-bound TRAIL on the surface of PLPs isolated from TRAIL-transduced MEG-01 cells (**Figure 5.3c and d**). Additionally, TEM examination and comparison between αIIβ-EGFP- and αIIβ-TRAIL-derived PLPs revealed no difference in particle morphology (**Figure 5.3e**).

Reduction of cancer cell viability by TRAIL-expressing megakaryocytes and PLPs

Triple-negative breast cancer (TNBC) subtypes and prostate cancer (PCa) bone metastasis represent some of the most deadly forms of metastatic cancer [243, 307]. To explore the possibility of targeting these subtypes, TNBC cell line MDA-MB-231

and PCa bone metastatic cell line PC3 were selected as target cells in co-culture experiments. Dami cells transduced with empty vector control or αIIβ-TRAIL lentiviral vectors were incubated with Calcein-AM-labeled cancer cells at a 1:1 or 5:1 ratio (effector-to-target ratio). Dead cells release their Calcein-AM dye into the medium, whereas viable cells retain their fluorescence and can be quantified using flow cytometry. It was found that the viability of both MDA-MB-231 and PC3 cells deceased with increasing effector-to-target cell ratio. Moreover, differentiation with PMA for 48 hr prior to co-culture experiments enhanced cytotoxicity of αIIβ-TRAIL-transduced Dami cells against cancer cells (**Figure 5.4a and b**). Since the co-culture experiments were unable to distinguish the origin of TRAIL-induced apoptosis (megakaryocytes, PLPs, or both), PLPs were isolated from empty vector- or αIIβ-TRAIL-transduced MEG-01 cells and incubated with cancer cells for 24 hr. It was found that PLPs from αIIβ-TRAIL-transduced MEG-01 cells were able to kill cancer cells in a dose-dependent manner (**Figure 5.4c**).

Differentiation of TRAIL-transduced HSPCs to megakaryocytes

Stable gene transduction combined with a lineage-specific promoter in haematopoietic stem and progenitor cells (HSPCs) takes advantage of self-renewal capability of stem cells to produce transgene product in a targeted blood cell lineage. C57BL/6-derived HSPCs were isolated after lineage depletion from mononuclear cells in bone marrow. After prestimulation with cytokines for 24 hr, HSPCs were transduced twice with αIIβ-TRAIL lentivirus at a MOI of ~100 within 24 hr. Transduced HSPCs were subjected to differentiation in the presence of TPO for 10 days. Double staining for

CD41 and TRAIL indicated ~57% TRAIL expression in the megakaryocyte lineage ($CD41^+$) (**Figure 5.5a and Supplemental figure 5.1**). Maturation of megakaryocytes was distinguished by their large cytoplasm relative to other lineages under examination using bright field microscopy (**Figure 5.5b**). Mature megakaryocytes were further verified by Giemsa Wright staining for endomitosis (DNA replication without cell division) in which lobulated nuclei were detectable (**Figure 5.5c**).

TRAIL overexpression does not induce apoptosis or affect replication of megakaryocytes

TRAIL signaling has been found to be involved in apoptosis of not only transformed cells but also certain immune cells for tissue homeostasis [378]. It is important to examine whether overexpression of TRAIL in the megakaryocyte lineage would induce apoptosis. Ten days after differentiation of TRAIL-transduced HSPCs in the presence of TPO, cells were stained with Annexin-V and propidium iodide (PI). Necrotic, late apoptotic and early apoptotic cell populations were double-negative for annexin-V and PI in empty vector- or TRAIL-transduced cells (**Figure 5.6a**). As megakaryocytes mature, they undergo DNA replication without cytokinesis. The DNA content was observed to increase from 2 N to 4 N, 8 N, and up to 16N (DNA ploidy) in TPO-differentiated megakaryocytes from *ex vivo* culture. Each ploidy fraction showed comparable ratio between empty vector- and TRAIL-transduced cells (**Figure 5.6b**). Therefore, we may conclude that overexpression of TRAIL is tolerable in the megakaryocyte lineage.

TRAIL expression in platelets of bone marrow transplant recipients

HSPCs from NSG mice were transduced with αIIβ-TRAIL lentivirus at a MOI of ~100 and subsequently transplanted into NSG mice that received 2.5 Gy of sub-lethal irradiation (**Figure 5.7a**). TRAIL-expressing platelets were identified as a $CD41^{+}TRAIL^{+}$ population in peripheral blood. It was found that ~40% of circulating platelets were positive for TRAIL at 4, 8, 12 and 20 weeks after BMT (**Figure 5.7b and c**). It was estimated that 10^{9} platelets expressed 10-30 ng TRAIL by semi-quantitative western blotting assay (**Supplemental figure 5.2**). Meanwhile, the average copy number of transgene in the genomic DNA of peripheral blood mononuclear cells was quantified by real-time qPCR. It was found that the average copy number of αIIβ-TRAIL cassette per cell measured by the presence of lentiviral LTR sequence in the group of recipients was not significantly different from the group receiving empty vector lentivirus over 20 weeks post BMT (**Figure 5.7d**). To examine whether TRAIL expression in megakaryocyte and platelet lineage interfered with blood coagulation, a tail-bleeding assay was performed in mice receiving empty vector- or αIIβ-TRAIL-transduced HSPCs 8 weeks after BMT. αIIβ-TRAIL-transduced mice showed no statistically significant difference in bleeding time compared to age- and sex-matched NSG mice without BMT (**Figure 5.7e**). Notably, since we were only able to achieve ~40% TRAIL-expressing platelets *in vivo*, this does not rule out the possibility that TRAIL may affect the coagulation capability within the TRAIL-expressing platelet subpopulation. Nevertheless, the bleeding assay suggests that at least the protocol which gives rise to a mixture of TRAIL-positive and -negative platelet populations does not have an adverse effect on blood clotting.

Reduction of cancer metastases via circulating TRAIL-expressing platelets

To investigate the ability of TRAIL-expressing platelets to reduce distant organ metastases, an experimental bone metastasis model was tested in the study. 10^4 human PCa cells PC3 expressing firefly luciferase were injected into NSG mice via the left ventricle 4 weeks after receiving BMT of αIIβ-TRAIL- or empty vector-transduced HSPCs. Progression of PCa metastases was monitored longitudinally by bioluminescence imaging (BLI) (**Figure 5.8a**). On day 60 after BMT, BLI revealed that mice with TRAIL-expressing platelets had significantly reduced metastases in the liver relatively to control mice receiving empty vector-transduced HSPCs (**Figure 5.8b and c**). Upon dissection, metastases were detected mainly in the liver. Relatively large tumor nodules were found in the liver of the control group (**Figure 5.8d**). H&E staining of liver sections showed that the experimental group (TRAIL-expressing platelets) had more localized tumors in liver whereas more invasive metastases developed in the control group (empty vector-transduced platelets) (**Figure 5.8e**).

5.4 Discussion

Thrombocytopenia is often associated with cancer chemotherapy clinically. It causes increased risk of bleeding, reduced dose of chemotherapy, and/or delay of treatment schedules in cancer patients [379]. Management approaches to thrombocytopenia are mainly based on platelet or plasma transfusions [380]. However, the pro-metastatic roles of platelets can possibly counteract the benefits of platelet transfusion [114, 346]. Nevertheless, this work has demonstrated a proof-of-concept in which platelets were

genetically engineered to deliver the cancer cell-specific apoptotic cytokine TRAIL. After the αIIβ promoter-driven TRAIL cDNA was inserted into the genome of HSPCs, TRAIL expression was restricted to megakaryocyte and platelet lineages following HSPC differentiation. The self-renewal ability of HSPCs allowed for continual production of TRAIL-expressing platelets in circulation. It was shown that this approach was able to significantly reduce liver metastases in an experimental prostate cancer metastasis model.

The current study requires BMT, which can be challenging in certain clinical scenarios [381]. In contrast to the traditional BMT for treating inherited blood diseases, this work requires only autologous HSPCs to be modified. The utilization of autologous HSPCs bypasses the strict criteria for donor-recipient matching. Alternatively, recent studies have indicated that following differentiation of genetically modified HSPCs to megakaryocytes *in vitro*, functional platelets can be produced upon infusion of megakaryocytes into mice [382, 383]. This approach can be a future direction for engineering TRAIL-expressing platelets to avoid the complications associated with BMT. In addition to TRAIL, previous studies have identified a variety of tumor-specific killing peptides [384, 385]. A potential direction is to utilize platelets to deliver these different peptides, as appropriate for different cancers. Such an approach can possibly overcome the drug resistance from using a single agent for the targeting of CTCs and prevention of metastatic dissemination.

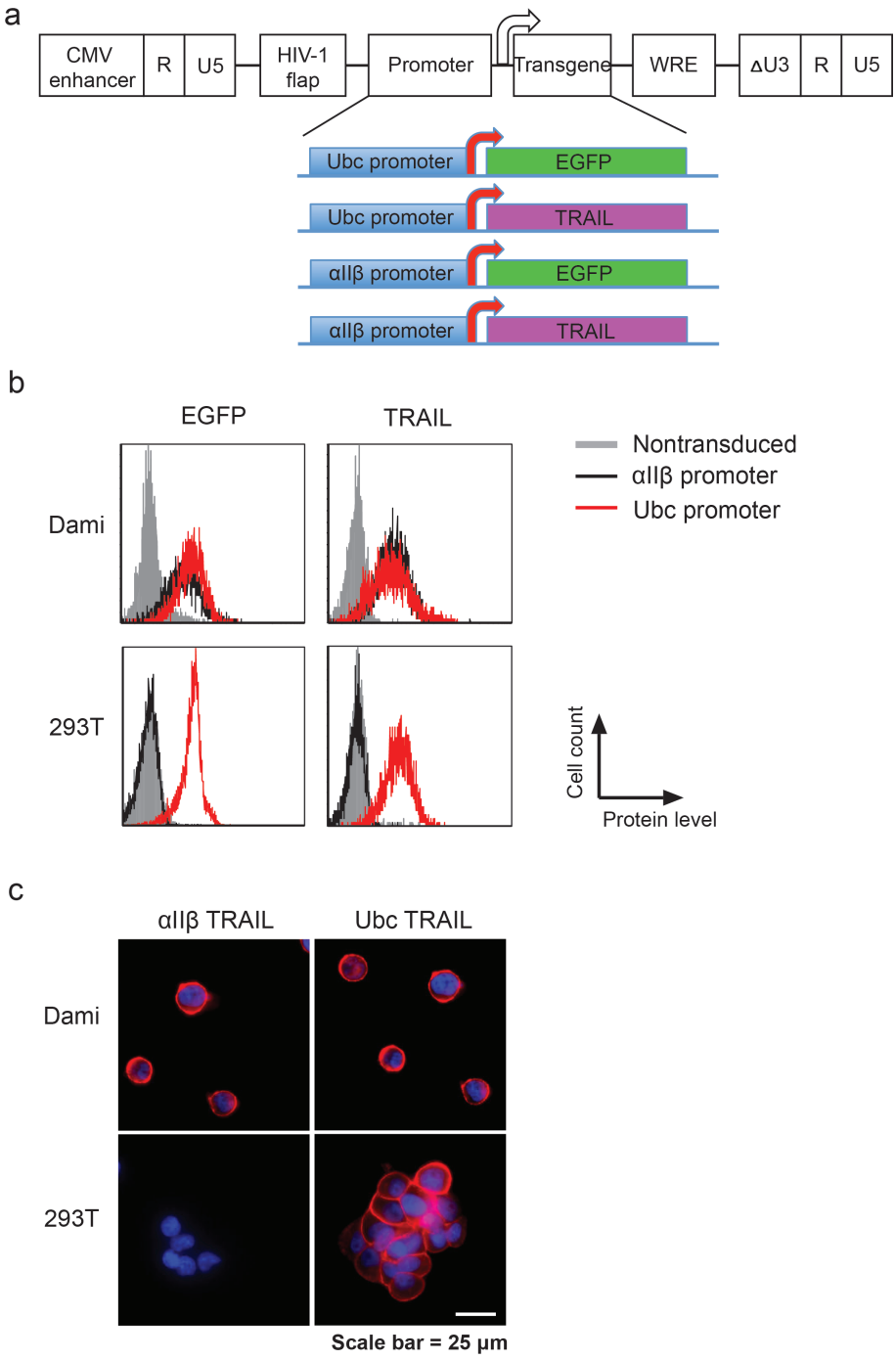

Figure 5.1. Construction and validation of megakaryocyte-specific lentiviral expression vectors. (a) Schematic of lentiviral vectors for expression of EGFP and TRAIL in megakaryocytes. (b) Flow cytometry detection of transgene expression after transduction of Ubc-EGFP, αIIβ-EGFP, Ubc-TRAIL and αIIβ-TRAIL in

promegakaryocytic cell line Dami and human embryonic kidney cell line 293T, respectively. (c) Immunofluorescence staining of surface-bound TRAIL in Ubc-TRAIL- and αIIβ-TRAIL-transduced Dami and 293T cells. Nuclei were stained with DAPI (blue).

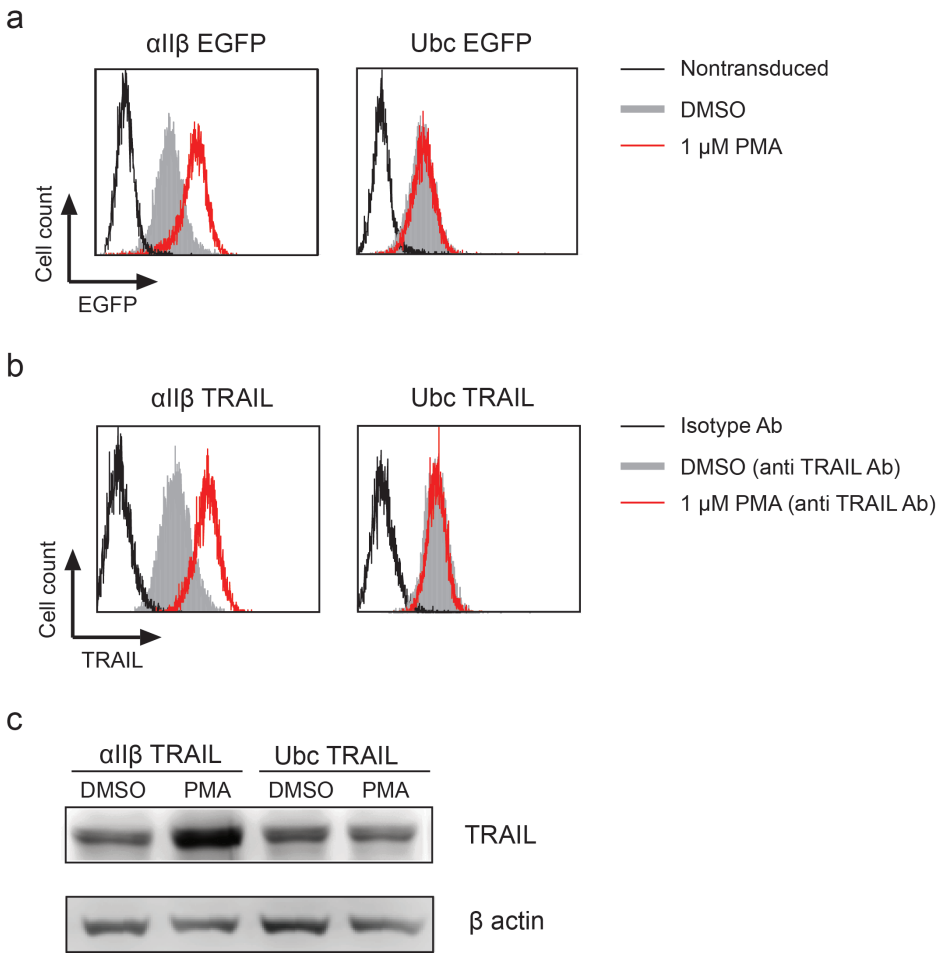

Figure 5.2. Differentiation of promegakaryocytes increases transgene expression. Histograms of (a) EGFP and (b) TRAIL expression driven by αIIβ promoter after differentiation of the promegakaryocytic cells, Dami with 1 μM PMA for 48 hr. In comparison, Ubc-driven transgene expression was not changed upon cell differentiation. (c) Western blotting of increased total TRAIL expression in αIIβ-TRAIL-transduced Dami cells after PMA-induced differentiation. In contrast, Ubc-TRAIL-transduced Dami showed no change in TRAIL expression after PMA treatment.

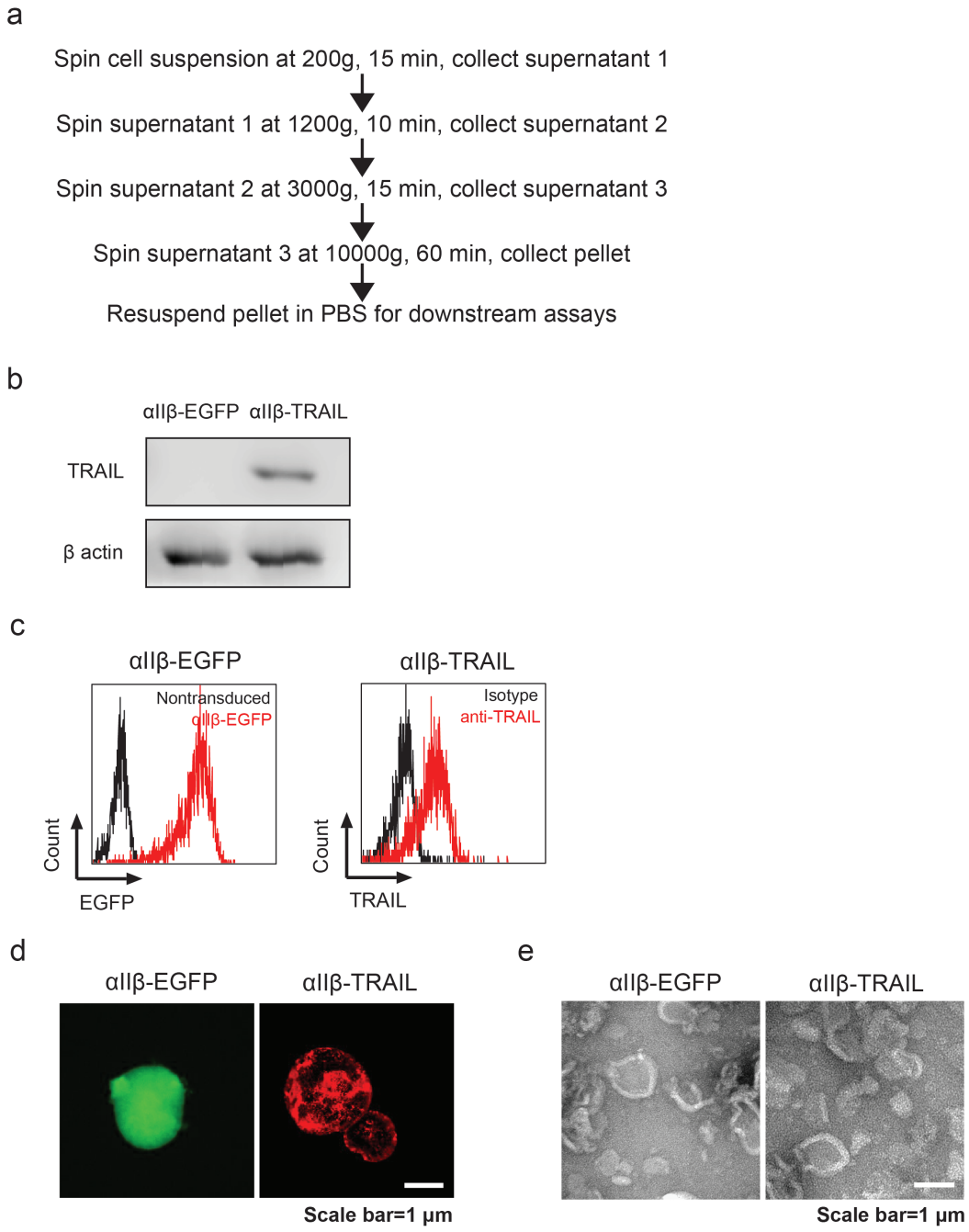

Figure 5.3. Characterization of platelet-like microparticles derived from promegakaryocytes. (a) Procedure for isolating platelet-like microparticles from MEG-01 cells. (b) Western blotting of total TRAIL and β-actin in microparticles from PMA-differentiated MEG-01 cells transduced with αIIβ-EGFP or αIIβ-TRAIL. (c)

Flow cytometry and (d) Fluorescence microscopy detection of intracellular EGFP or surface-bound TRAIL in microparticles derived from MEG-01 cells transduced with αIIβ-EGFP or αIIβ-TRAIL. (e) TEM imaging of microparticles from culture supernatant of MEG-01 transduced with αIIβ-EGFP or αIIβ-TRAIL.

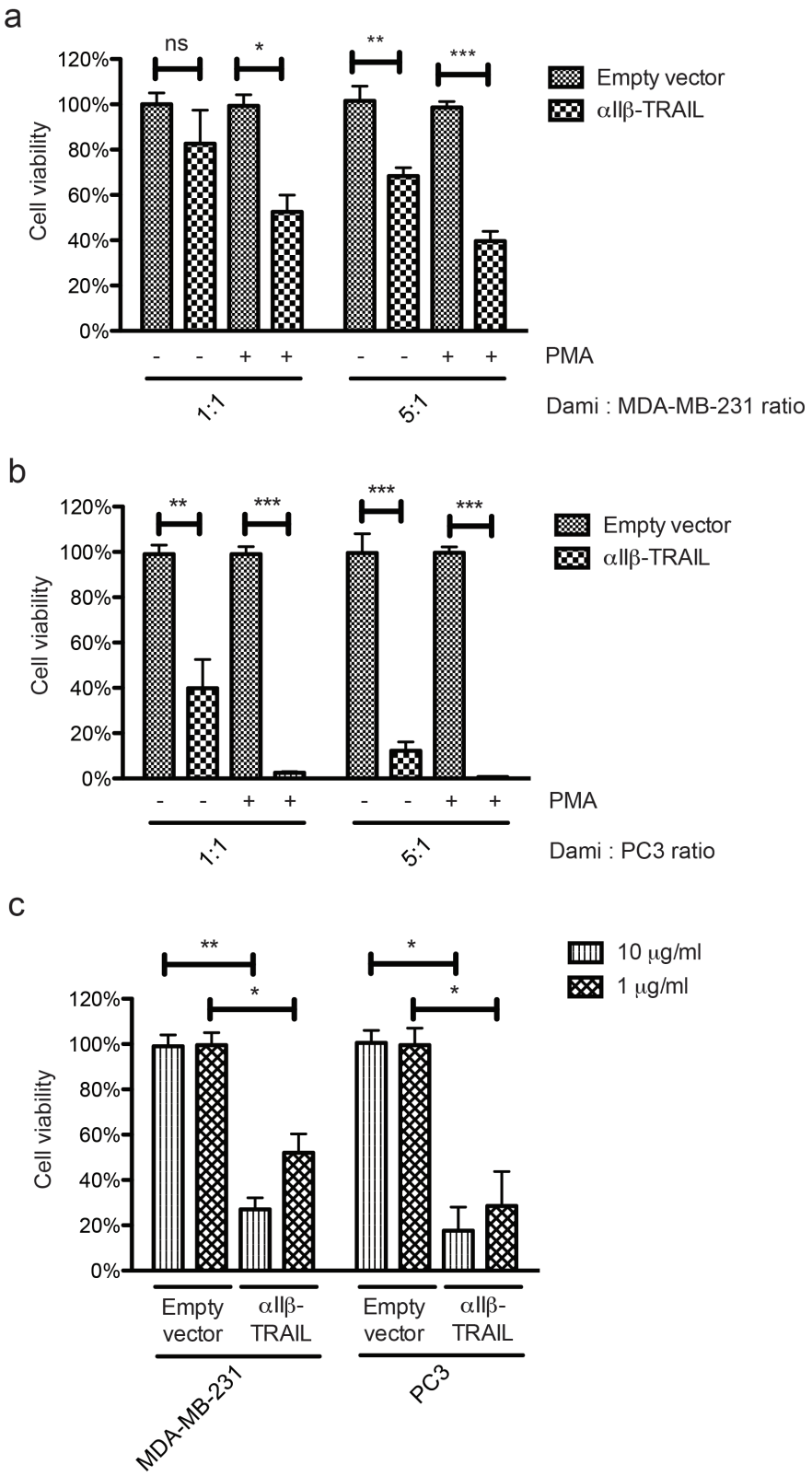

Figure 5.4. TRAIL-expressing megakaryocytes or PLPs reduce the viability of

epithelial cancer cells *in vitro*. αIIβ-TRAIL-transduced Dami cells were incubated with Calcein AM-labeled (a) MDA-MB-231 and (b) PC3 at 1:1 or 5:1 ratio for 24 hr before evaluation of cancer cell viability by flow cytometry. Pretreatment of Dami cells with PMA increased cytotoxicity of αIIβ-TRAIL-transduced Dami against cancer cells. Results are presented as the mean ± SEM; n=3; ns, no significant difference, *, $p<0.05$, **, $p<0.01$, ***, $p<0.001$. (c) Reduction of cancer cell viability by microparticles derived from αIIβ-TRAIL-transduced MEG-01 cells. Cancer cells were incubated with 10 and 1 μg/mL microparticles derived from empty vector- or αIIβ-TRAIL-transduced MEG-01 cells for 24 hr. Cell viability was measured by MTT assay. Microparticles were quantified by DC assay. Results are presented as the mean ± SEM; n = 3; *, $p<0.05$, **, $p<0.01$.

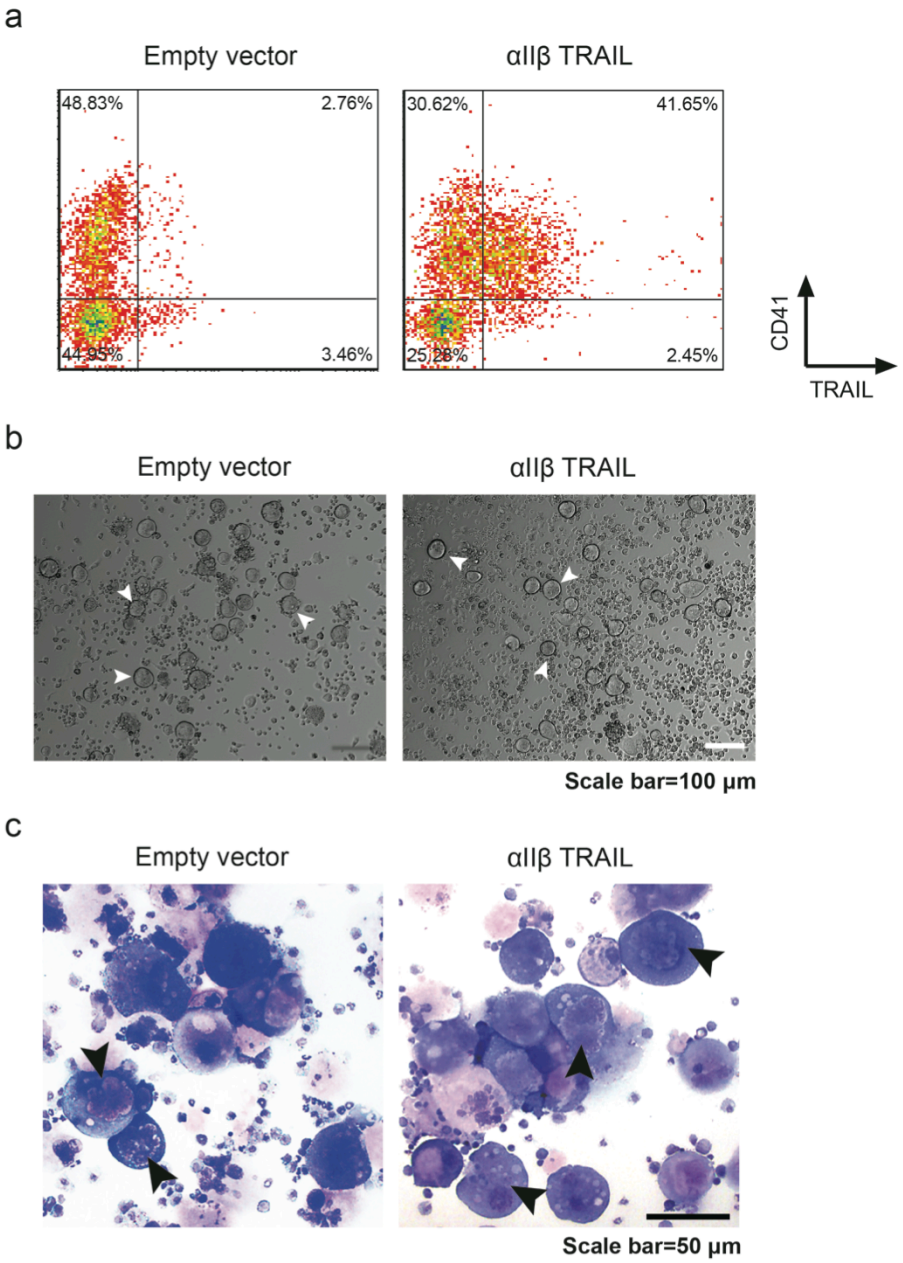

Figure 5.5. *In vitro* differentiation of αIIβ-TRAIL-transduced murine HSPCs into megakaryocytes. (a) Flow cytometry detection of TRAIL-expressing murine megakaryocytes in HSPC growth and differentiation medium 10 days post transduction. CD41 represents a marker for megakaryocyte and platelet lineage. (b) Bright field microscopy imaging of differentiated megakaryocytes transduced with

empty vector or αIIβ-TRAIL in HSPC growth and differentiation medium. Arrowheads indicate megakaryocytes. (c) Giemsa-Wright staining of differentiated megakaryocytes transduced with empty vector or αIIβ-TRAIL. Megakaryocytes are distinguished by multi-lobed nuclei and relatively large cytoplasm.

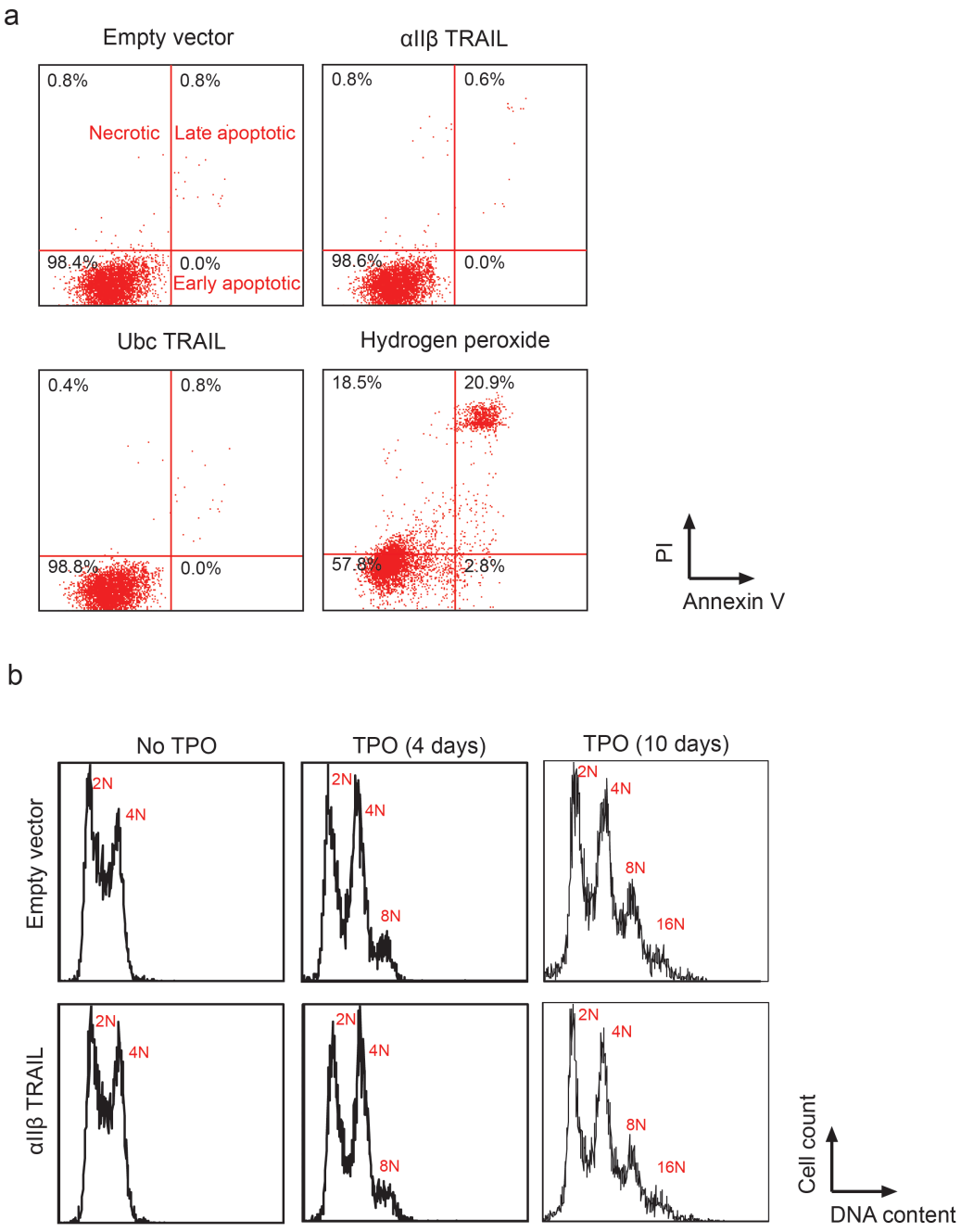

Figure 5.6. Apoptosis and cell cycle analysis in *ex vivo* culture of TRAIL-expressing megakaryocytes. (a) Annexin-V and PI staining of differentiated megakaryocytes. Mouse HSPCs were transduced with empty vector, αIIβ-TRAIL or Ubc-TRAIL and subjected to differentiation for 10 days prior to apoptosis staining.

Bone marrow mononuclear cells treated with 5 mM H_2O_2 were used as a positive control. (b) PI staining of TPO-differentiated megakaryocytes in *ex vivo* culture. After TPO treatment for 4 and 10 days, fixed and permeabilized cells were stained with PI. The vertical axis indicates the relative number of cells and the horizontal axis indicates the fluorescence corresponding to DNA ploidy. Peaks (2N, 4N, 8N, and 16N) representing each ploidy class are labeled.

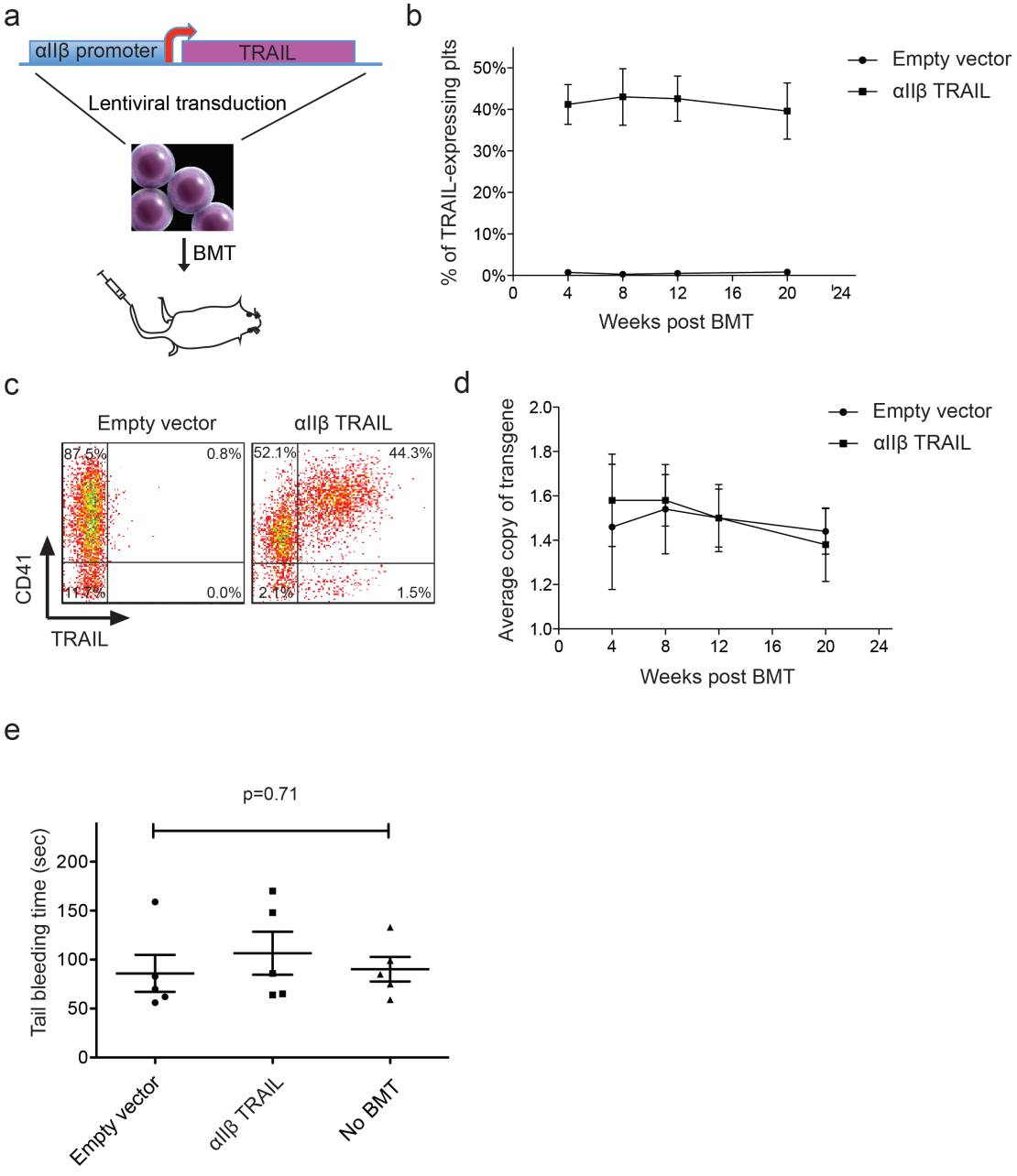

Figure 5.7. BMT of αIIβ-TRAIL-transduced HSPCs. (a) Schematic of lentiviral transduction of αIIβ-TRAIL construct into mouse HSPCs followed by BMT via tail vein injection. (b) Percentage of TRAIL-positive platelets via flow cytometry in peripheral blood of transplanted NSG mice over five months (n = 5). (c) Representative dot plots of TRAIL-expressing platelets ($CD41^+$ $TRAIL^+$) via flow

cytometry 8 weeks after BMT. (d) Quantification of transgene copy number per cell in peripheral mononuclear cells of transplanted NSG mice via qPCR (n = 5). (e) Tail-bleeding time of NSG mice 8 weeks after BMT with empty vector- or αIIβ-TRAIL-transduced HSPCs. Age- and sex-matched NSG mice without BMT were used as a control. Results are presented as the mean ± SEM (n = 5). One-way ANOVA was used to test for statistical difference (p=0.71).

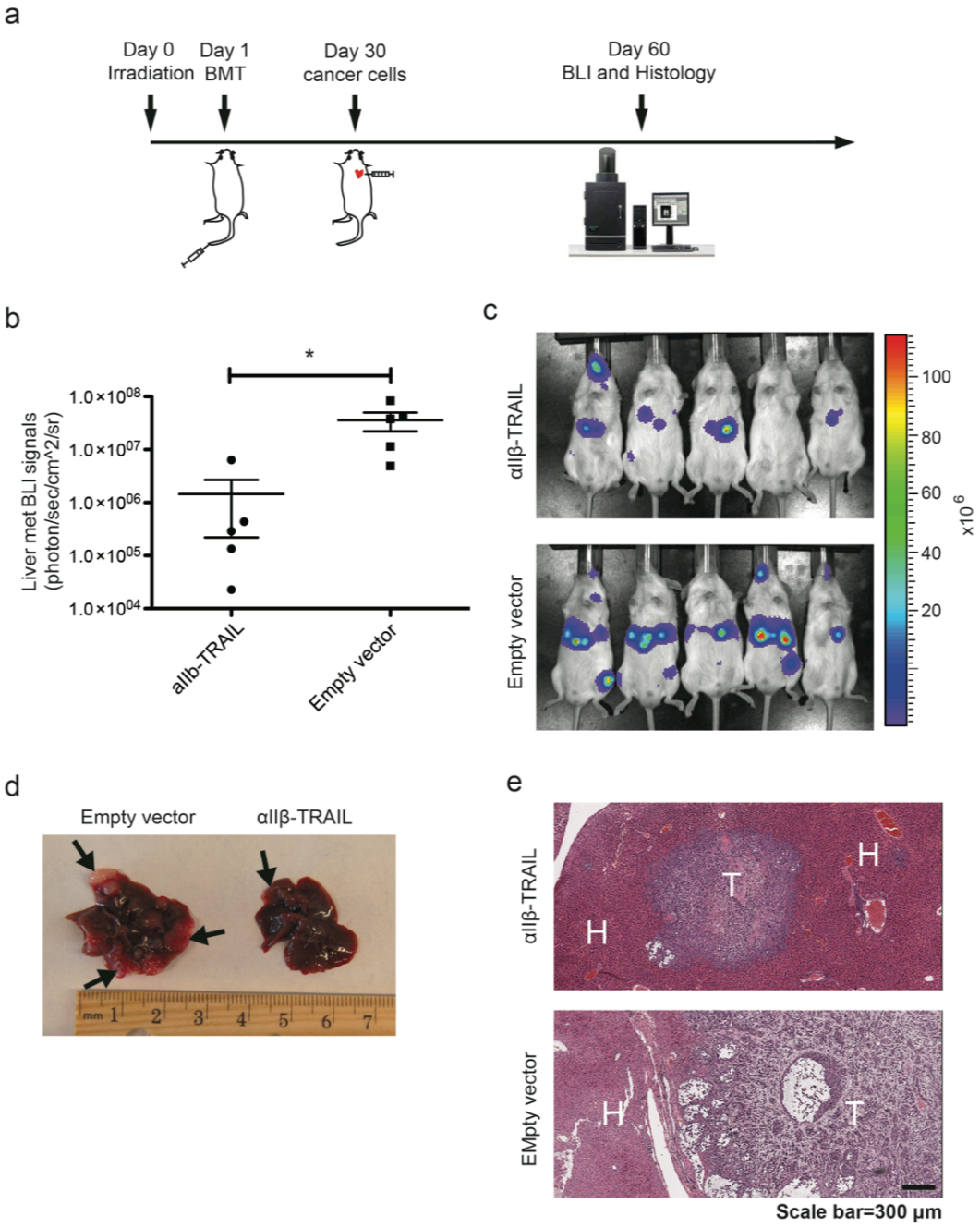

Figure 5.8. TRAIL-expressing platelets reduced systemic PCa metastases. (a) Schematic of TRAIL-expressing platelet gene therapy in a PCa experimental metastasis model. (b) Quantification of liver metastatic burden in mice with TRAIL-expressing platelets or empty vector-transduced platelets via BLI on day 60 after BMT.

Results are presented as the mean ± SEM, n = 5, *, $p<0.05$ (c) Representative BLI images of mice on Day 60 after BMT. (d) Liver samples from mice with empty vector-transduced or TRAIL-expressing platelets. Arrows point to white or pink tumor nodules. (e) H&E staining of liver sections. H: hepatocytes; T: cancer cells.

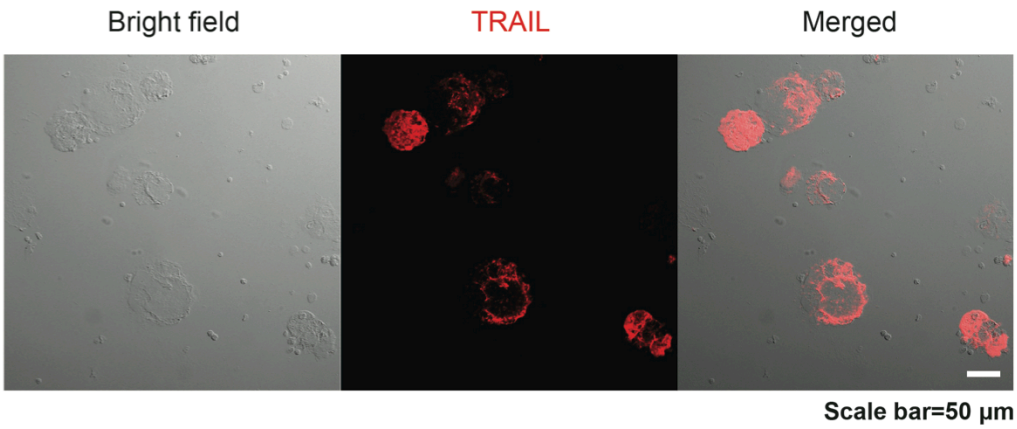

Supplemental figure 5.1. Immunofluorescent staining of αIIβ-TRAIL-transduced HSPCs for TRAIL. C57BL/6-derived HSPCs were transduced with αIIβ-TRAIL and cultured for 10 days with cytokines to allow differentiation into megakaryocytes. Cells were fixed with 4%PFA, stained with anti-TRAIL, and examined by immunofluorescence microscopy for TRAIL.

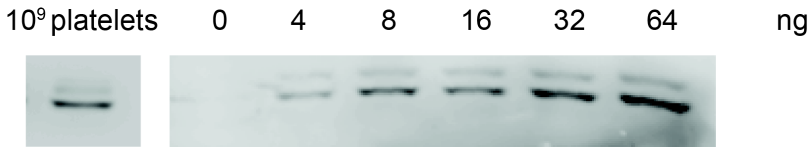

Supplemental figure 5.2. Semi-quantitative measurement of TRAIL in genetically modified platelets. A semi-quantitative measurement of TRAIL based on western blotting was performed by lysing 10^9 platelets from three individual C57BL/6 mice bearing GFP or TRAIL-expressing platelets. Recombinant TRAIL with concentrations ranging from 0 through 64 ng were utilized to plot standard curve after measuring blot intensity by Image J. Whereas GFP-expressing platelets were undetectable for TRAIL, it was estimated that 10^9 platelets carry 10-30 ng TRAIL in C57BL/6 mice with TRAIL-expressing platelets. A representative western blotting image from one TRAIL-expressing mouse is shown.

CHAPTER 6 CONCLUDING REMARKS AND FUTURE DIRECTIONS

6.1 Conclusions

Human fucosyltransferase 6 enables prostate cancer metastasis to bone

Prior studies have shown that the interaction between human PCa cells and bone marrow endothelium follows a rolling-and-adhesion cascade mediated by E-selectin ligand (ESL): E-selectin interactions. This adhesion is enabled by elevated expression of human α-1, 3 fucosyltransferases (FTs), key enzymes responsible for ESL activity in human PCa cells and leukocytes. In contrast to human, the incidence of bone metastasis in mice is rare. This may be due to lack of ESL expression found in mouse PCa cell lines. In this study we showed that overexpression of FT3, FT6 or FT7 restored ESLs and enabled mouse PCa cells to roll and adhere in E-selectin-functionalized microtubes, similar to trafficking of circulating PCa cells in bone marrow vessels. We then tested the ability of FT-overexpressing mouse PCa cells to home to bone marrow, in a manner similar to human cells. Following intracardiac inoculation with cells overexpressing one of the FT genes, FT6 cells induced robust bone metastasis in immunocompetent mice. These results indicate that ESLs induced by FTs are sufficient to direct murine PCa cells to bone marrow in an E-selectin-dependent manner. This new bone metastatic mouse model should prove to be useful for future preclinical investigations of PCa bone metastasis.

Piperlongumine and immune cytokine TRAIL synergize to promote tumor death

Malignant transformation results in increased levels of reactive oxygen species (ROS). Adaption to this toxic stress allows cancer cells to proliferate. Recently,

piperlongumine (PL), a natural alkaloid, was identified to exhibit novel anticancer effects by targeting ROS signaling. PL induces apoptosis specifically in cancer cells by downregulating several anti-apoptotic proteins. Notably, the same anti-apoptotic proteins were previously found to reduce tumor necrosis factor-related apoptosis-inducing ligand (TRAIL)-induced apoptosis in cancer cells. Therefore, we reasoned that PL would synergize with TRAIL to stimulate potent apoptosis in cancer cells. We demonstrate for the first time that PL and TRAIL exhibit a synergistic anti-cancer effect in cancer cell lines of various origins. PL resulted in the upregulation of TRAIL receptor DR5, which potentiated TRAIL-induced apoptosis in cancer cells. Furthermore, such upregulation was found to be dependent on ROS and the activation of JNK and p38 kinases. Treatment with combined PL and TRAIL demonstrated significant anti-proliferative effects in a triple-negative breast cancer MDA-MB-231 xenograft model. This work provides a novel therapeutic approach for inducing cancer cell death. Combination of PL and TRAIL may suggest a novel paradigm for treatment of primary and metastatic tumors.

Platelet membrane-functionalized particles to target tumor cell-associated micro-thrombi

Circulating tumor cells (CTCs) are responsible for metastases in distant organs via hematogenous dissemination. Fundamental studies in the past decade have suggested that neutralization of CTCs in circulation could represent an effective strategy for preventing metastasis. Learning from current paradigms of targeting cancer cells in a solid tumor, novel therapeutic approaches largely fall into two main targeting

categories: unique cancer markers (e.g. overexpression of surface receptors) and tumor-specific microenvironment (e.g. low pH, hypoxia, etc.). While relying on a surface receptor to target CTCs can be greatly challenged by cancer heterogeneity, targeting of tumor microenvironments has the advantage of recognizing a broader spectrum of cancer cells regardless of genetic differences or tumor types. The blood circulation, however, where CTCs transit through, lacks the same tumor microenvironment as that found in a solid tumor. In this study, a unique "microenvironment" was confirmed upon introduction of cancer cells of different types into the blood circulation in mice. It was found that activated platelets and fibrin were physically associated with bloodborne cancer cells forming a micro-thrombi in the vasculature. Inspired by this phenomenon, we further developed a "Trojan Horse" strategy to neutralize CTCs in circulation. Camouflaged by a platelet membrane with surface conjugation of tumor-specific apoptosis-inducing ligand cytokine, TRAIL, biomimetic silica particles were found to incorporate into micro-thrombi and dramatically decrease lung metastases in a breast cancer mouse model.

Engineering Trojan-horse platelets to neutralize circulating tumor cells

Mounting experimental evidence demonstrates that platelets support cancer metastasis. The activation of platelets and the coagulation system have a crucial role in the progression of cancer. Within the circulatory system, platelets guard circulating tumor cells (CTCs) from immune elimination and promote their arrest at the endothelium, supporting CTC extravasation into secondary sites. Extensive studies have explored the blockade of platelet-CTC interactions as an anti-metastatic strategy. Such an

intervention approach, however, may cause bleeding disorders since the platelet-CTC interactions are inherently linked to the blood coagulation cascade including platelet activation. On the other hand, platelets have been genetically engineered to correct inherited bleeding disorders in both animal models and clinical trials through megakaryocyte lineage-targeted gene therapy in bone marrow stem cells. The successes of platelet gene therapies suggest that platelets can serve as an efficient vector to deliver cancer therapeutics. In this study, inspired by the physical association between platelets and CTCs, platelets were genetically modified to express surface-bound TRAIL, a cytokine known to induce apoptosis specifically in tumor cells. This approach is demonstrated to kill cancer cells *in vitro* and significantly reduce metastases in an experimental mouse model of prostate cancer metastasis.

6.2 Future directions

The work described in this thesis presents several opportunities for proposed projects that can expand its scope.

A new PCa bone metastasis platform for screening novel inhibitors

This newly developed experimental metastasis model has several advantages over existing mouse models of bone metastasis: (1) It bypasses complicated surgical implantation of PCa cells in the bone. Moreover, the direct intraosseous implantation bypasses several crucial steps in the metastatic cascade: survival in the bloodstream, rolling and extravasation; (2) Less time-consuming than iterative selection of bone metastatic PCa cells; (3) The use of wild-type mouse allows for study of PCa development in an immunocompetent background which considers the involvement of immune system. Therefore, we reason that the new PCa bone metastasis model generated in this thesis can present a new platform for screening and identification of compounds or antibodies to prevent or treat bone metastasis.

Development of nanoparticles encapsulating TRAIL and Piperlongumine for greater in vivo efficacy

The presented *in vivo* trials involved intratumoral (i.t.) injection of TRAIL and Piperlongumine since this technique has been extensively evaluated over the past few decades [313-317]. An advantage of using this method is that i.t. injections allow for extremely high doses of drug within the tumor with minimal systemic toxicity. Additionally, this approach allows one to directly evaluate the synergistic effect of the

PL and TRAIL without the results being affected by the pharmacokinetic factors associated with intravenous injections. We acknowledge, however, that this is also a limitation because the delivery method provides little insight into the therapy's systemic effectiveness. In previous trials utilizing a systemic delivery approach, not reported here, we have found that PL did not accumulate at sufficient levels at tumors. The pharmacokinetics of the combination therapy will be the subject of future work. One direction is to encapsulate TRAIL and Piperlongumine inside long-circulating nanoparticles and improve drug accumulation within the tumor through the EPR effect.

Engineering synthetic particles that resemble more physical properties of platelets

Future investigations could engineer particles with a platelet-like disc shape (e.g. plateloid silica particles) for functionalization with platelet membrane. Plateloid particles without any targeting moiety have been demonstrated to exhibit more efficient tumoritropic accumulation in solid tumors by taking advantage of hydrodynamic forces and interfacial interactions with tumor-associated endothelium [352]. Nevertheless, it hasn't been studied whether such an advantage would also apply for targeting of CTCs in circulation. It is likely that disc-shaped particles coated with platelet membrane are more resistant to fluid shear stress when targeting fibrin-associated CTCs. In addition, an ultrasoft hydrogel with great deformability has been recently demonstrated to simulate the behavior of platelets to collapse at fibrin networks with optimal clotting effect [353]. Combining these two physical features (disc shape and deformability) with platelet membrane functionalization might form the basis for particles that more closely resemble the physical properties of platelets in

the future.

Bypassing the bone marrow transplantation for delivery of modified platelets

Recent studies have indicated that following differentiation of genetically modified HSPCs to megakaryocytes *in vitro*, functional platelets can be produced upon infusion of megakaryocytes into mice [382, 383]. This approach can be a future direction for engineering TRAIL-expressing platelets to avoid the complications associated with BMT.

Genetically modifying platelets to express cancer-killing peptides

Previous studies have identified a variety of tumor-specific killing peptides [384, 385]. A potential direction is to utilize platelets to deliver these different peptides, as appropriate for different cancers. Such an approach can possibly overcome the drug resistance from using a single agent for the targeting of CTCs and prevention of metastatic dissemination.

REFERENCES

1. Nagrath, S., et al., *Isolation of rare circulating tumour cells in cancer patients by microchip technology*. Nature, 2007. **450**(7173): p. 1235-9.
2. Lowes, L.E., et al., *Image cytometry analysis of circulating tumor cells*. Methods Cell Biol, 2011. **102**: p. 261-90.
3. Scher, H.I., et al., *End points and outcomes in castration-resistant prostate cancer: from clinical trials to clinical practice*. J Clin Oncol, 2011. **29**(27): p. 3695-704.
4. Criscitiello, C., C. Sotiriou, and M. Ignatiadis, *Circulating tumor cells and emerging blood biomarkers in breast cancer*. Curr Opin Oncol, 2010. **22**(6): p. 552-8.
5. Danila, D.C., M. Fleisher, and H.I. Scher, *Circulating tumor cells as biomarkers in prostate cancer*. Clin Cancer Res, 2011. **17**(12): p. 3903-12.
6. Lianidou, E.S. and A. Markou, *Circulating tumor cells as emerging tumor biomarkers in breast cancer*. Clin Chem Lab Med, 2011. **49**(10): p. 1579-90.
7. Hou, J.M., et al., *Evaluation of circulating tumor cells and serological cell death biomarkers in small cell lung cancer patients undergoing chemotherapy*. Am J Pathol, 2009. **175**(2): p. 808-16.
8. Yalcin, S., et al., *Determination of circulating tumor cells for detection of colorectal cancer progression or recurrence*. Hepatogastroenterology, 2010. **57**(104): p. 1395-8.
9. Cristofanilli, M., et al., *Circulating tumor cells, disease progression, and survival in metastatic breast cancer*. N Engl J Med, 2004. **351**(8): p. 781-91.
10. Cristofanilli, M., et al., *Circulating tumor cells: a novel prognostic factor for newly diagnosed metastatic breast cancer*. J Clin Oncol, 2005. **23**(7): p. 1420-30.
11. Allard, W.J., et al., *Tumor cells circulate in the peripheral blood of all major carcinomas but not in healthy subjects or patients with nonmalignant diseases*. Clin Cancer Res, 2004. **10**(20): p. 6897-904.
12. Coumans, F.A., et al., *All circulating EpCAM+CK+CD45- objects predict overall survival in castration-resistant prostate cancer*. Ann Oncol, 2010. **21**(9): p. 1851-7.
13. Aktas, B., et al., *Stem cell and epithelial-mesenchymal transition markers are frequently overexpressed in circulating tumor cells of metastatic breast cancer patients*. Breast Cancer Res, 2009. **11**(4): p. R46.
14. Theodoropoulos, P.A., et al., *Circulating tumor cells with a putative stem cell phenotype in peripheral blood of patients with breast cancer*. Cancer Lett, 2010. **288**(1): p. 99-106.
15. Toloudi, M., et al., *Correlation between Cancer Stem Cells and Circulating Tumor Cells and Their Value*. Case Rep Oncol, 2011. **4**(1): p. 44-54.
16. Iinuma, H., et al., *Clinical significance of circulating tumor cells, including cancer stem-like cells, in peripheral blood for recurrence and prognosis in patients with Dukes' stage B and C colorectal cancer*. J Clin Oncol, 2011. **29**(12): p. 1547-55.

17. Wang, J., et al., *A preliminary investigation of the relationship between circulating tumor cells and cancer stem cells in patients with breast cancer*. Cell Mol Biol (Noisy-le-grand), 2012. **58 Suppl**: p. OL1641-5.
18. Kasimir-Bauer, S., et al., *Expression of stem cell and epithelial-mesenchymal transition markers in primary breast cancer patients with circulating tumor cells*. Breast Cancer Res, 2012. **14**(1): p. R15.
19. Ghiaur, G., et al., *Cancer stem cells: relevance to clinical transplantation*. Curr Opin Oncol, 2012. **24**(2): p. 170-5.
20. Vermeulen, L., et al., *The developing cancer stem-cell model: clinical challenges and opportunities*. Lancet Oncol, 2012. **13**(2): p. e83-9.
21. Lu, J., et al., *Breast cancer metastasis: challenges and opportunities*. Cancer Res, 2009. **69**(12): p. 4951-3.
22. Toso, C., G. Mentha, and P. Majno, *Liver transplantation for hepatocellular carcinoma: five steps to prevent recurrence*. Am J Transplant, 2011. **11**(10): p. 2031-5.
23. Kim, M.Y., et al., *Tumor self-seeding by circulating cancer cells*. Cell, 2009. **139**(7): p. 1315-26.
24. Guo, W. and F.G. Giancotti, *Integrin signalling during tumour progression*. Nat Rev Mol Cell Biol, 2004. **5**(10): p. 816-26.
25. Frisch, S.M. and E. Ruoslahti, *Integrins and anoikis*. Curr Opin Cell Biol, 1997. **9**(5): p. 701-6.
26. Ley, K., *The role of selectins in inflammation and disease*. Trends Mol Med, 2003. **9**(6): p. 263-8.
27. Grailer, J.J., M. Kodera, and D.A. Steeber, *L-selectin: role in regulating homeostasis and cutaneous inflammation*. J Dermatol Sci, 2009. **56**(3): p. 141-7.
28. Larsen, G.R., et al., *P-selectin and E-selectin. Distinct but overlapping leukocyte ligand specificities*. J Biol Chem, 1992. **267**(16): p. 11104-10.
29. Kohler, S., et al., *E-/P-selectins and colon carcinoma metastasis: first in vivo evidence for their crucial role in a clinically relevant model of spontaneous metastasis formation in the lung*. Br J Cancer, 2010. **102**(3): p. 602-9.
30. Konstantopoulos, K. and S.N. Thomas, *Cancer cells in transit: the vascular interactions of tumor cells*. Annu Rev Biomed Eng, 2009. **11**: p. 177-202.
31. Geng, Y., J.R. Marshall, and M.R. King, *Glycomechanics of the metastatic cascade: tumor cell-endothelial cell interactions in the circulation*. Ann Biomed Eng, 2012. **40**(4): p. 790-805.
32. Lefer, D.J., et al., *A novel sialyl LewisX analog attenuates neutrophil accumulation and myocardial necrosis after ischemia and reperfusion*. Circulation, 1994. **90**(5): p. 2390-401.
33. Buerke, M., et al., *Sialyl Lewisx-containing oligosaccharide attenuates myocardial reperfusion injury in cats*. J Clin Invest, 1994. **93**(3): p. 1140-8.
34. Zacharowski, K., et al., *Reduction of myocardial infarct size with sCR1sLe(x), an alternatively glycosylated form of human soluble complement receptor type 1 (sCR1), possessing sialyl Lewis x*. Br J Pharmacol, 1999. **128**(5): p. 945-52.
35. Shirota, K., et al., *Anti-metastatic effect of the sialyl Lewis-X analog GSC-150*

on the human colon carcinoma derived cell line KM12-HX in the mouse. Biol Pharm Bull, 2001. **24**(3): p. 316-9.
36. Brown, J.R., et al., *Deoxygenated disaccharide analogs as specific inhibitors of beta1-4-galactosyltransferase 1 and selectin-mediated tumor metastasis*. J Biol Chem, 2009. **284**(8): p. 4952-9.
37. Hennet, T., *The galactosyltransferase family*. Cell Mol Life Sci, 2002. **59**(7): p. 1081-95.
38. Weninger, W., et al., *Specialized contributions by alpha(1,3)-fucosyltransferase-IV and FucT-VII during leukocyte rolling in dermal microvessels*. Immunity, 2000. **12**(6): p. 665-76.
39. Ding, K.F. and S. Zheng, *[Study on relationship of fucosyltransferase gene types in breast cancer with metastasis and prognosis]*. Zhonghua Wai Ke Za Zhi, 2004. **42**(9): p. 546-50.
40. Matsuura, N., et al., *Gene expression of fucosyl- and sialyl-transferases which synthesize sialyl Lewisx, the carbohydrate ligands for E-selectin, in human breast cancer*. Int J Oncol, 1998. **12**(5): p. 1157-64.
41. Barthel, S.R., et al., *Analysis of glycosyltransferase expression in metastatic prostate cancer cells capable of rolling activity on microvascular endothelial (E)-selectin*. Glycobiology, 2008. **18**(10): p. 806-17.
42. Ogawa, J., H. Inoue, and S. Koide, *Expression of alpha-1,3-fucosyltransferase type IV and VII genes is related to poor prognosis in lung cancer*. Cancer Res, 1996. **56**(2): p. 325-9.
43. Wang, Q.Y., et al., *Expressions of Lewis antigens in human non-small cell pulmonary cancer and primary liver cancer with different pathological conditions*. J Exp Clin Cancer Res, 2003. **22**(3): p. 431-40.
44. Petretti, T., et al., *Altered mRNA expression of glycosyltransferases in human gastric carcinomas*. Biochim Biophys Acta, 1999. **1428**(2-3): p. 209-18.
45. Yang, X.S., et al., *Overexpression of fucosyltransferase IV promotes A431 cell proliferation through activating MAPK and PI3K/Akt signaling pathways*. J Cell Physiol, 2010. **225**(2): p. 612-9.
46. Guo, Q., et al., *Functional analysis of alpha1,3/4-fucosyltransferase VI in human hepatocellular carcinoma cells*. Biochem Biophys Res Commun, 2012. **417**(1): p. 311-7.
47. Huang, Z. and M.R. King, *An immobilized nanoparticle-based platform for efficient gene knockdown of targeted cells in the circulation*. Gene Ther, 2009. **16**(10): p. 1271-82.
48. Joyce, J.A. and J.W. Pollard, *Microenvironmental regulation of metastasis*. Nat Rev Cancer, 2009. **9**(4): p. 239-52.
49. Chambers, A.F., A.C. Groom, and I.C. MacDonald, *Dissemination and growth of cancer cells in metastatic sites*. Nat Rev Cancer, 2002. **2**(8): p. 563-72.
50. Coussens, L.M. and Z. Werb, *Inflammation and cancer*. Nature, 2002. **420**(6917): p. 860-7.
51. Elices, M.J., et al., *VCAM-1 on activated endothelium interacts with the leukocyte integrin VLA-4 at a site distinct from the VLA-4/fibronectin binding site*. Cell, 1990. **60**(4): p. 577-84.

52. Osborn, L., et al., *Direct expression cloning of vascular cell adhesion molecule 1, a cytokine-induced endothelial protein that binds to lymphocytes*. Cell, 1989. **59**(6): p. 1203-11.
53. Minn, A.J., et al., *Genes that mediate breast cancer metastasis to lung*. Nature, 2005. **436**(7050): p. 518-24.
54. Chen, Q., X.H. Zhang, and J. Massague, *Macrophage binding to receptor VCAM-1 transmits survival signals in breast cancer cells that invade the lungs*. Cancer Cell, 2011. **20**(4): p. 538-49.
55. Kang, Y., et al., *A multigenic program mediating breast cancer metastasis to bone*. Cancer Cell, 2003. **3**(6): p. 537-49.
56. Lu, X., et al., *VCAM-1 promotes osteolytic expansion of indolent bone micrometastasis of breast cancer by engaging alpha4beta1-positive osteoclast progenitors*. Cancer Cell, 2011. **20**(6): p. 701-14.
57. Wang, Y., et al., *Gene-expression profiles to predict distant metastasis of lymph-node-negative primary breast cancer*. Lancet, 2005. **365**(9460): p. 671-9.
58. Huh, S.J., et al., *Transiently entrapped circulating tumor cells interact with neutrophils to facilitate lung metastasis development*. Cancer Res, 2010. **70**(14): p. 6071-82.
59. Roland, C.L., et al., *Tumor-derived intercellular adhesion molecule-1 mediates tumor-associated leukocyte infiltration in orthotopic pancreatic xenografts*. Exp Biol Med (Maywood), 2010. **235**(2): p. 263-70.
60. Wu, Q.D., et al., *Human neutrophils facilitate tumor cell transendothelial migration*. Am J Physiol Cell Physiol, 2001. **280**(4): p. C814-22.
61. Hoskins, M.H. and C. Dong, *Kinetics analysis of binding between melanoma cells and neutrophils*. Mol Cell Biomech, 2006. **3**(2): p. 79-87.
62. Liang, S., et al., *Two-dimensional kinetics of beta 2-integrin and ICAM-1 bindings between neutrophils and melanoma cells in a shear flow*. Am J Physiol Cell Physiol, 2008. **294**(3): p. C743-53.
63. Liang, S., M.J. Slattery, and C. Dong, *Shear stress and shear rate differentially affect the multi-step process of leukocyte-facilitated melanoma adhesion*. Exp Cell Res, 2005. **310**(2): p. 282-92.
64. Slattery, M.J. and C. Dong, *Neutrophils influence melanoma adhesion and migration under flow conditions*. Int J Cancer, 2003. **106**(5): p. 713-22.
65. Geng, Y., et al., *Vascular recruitment of human retinoblastoma cells by multi-cellular adhesive interactions with circulating leukocytes*. Cellular and Molecular Bioengineering, 2010. **3**(4): p. 361-368.
66. Rosette, C., et al., *Role of ICAM1 in invasion of human breast cancer cells*. Carcinogenesis, 2005. **26**(5): p. 943-50.
67. Gupta, G.P. and J. Massague, *Platelets and metastasis revisited: a novel fatty link*. J Clin Invest, 2004. **114**(12): p. 1691-3.
68. Liu, Y., et al., *Tissue factor-activated coagulation cascade in the tumor microenvironment is critical for tumor progression and an effective target for therapy*. Cancer Res, 2011. **71**(20): p. 6492-502.
69. Kasthuri, R.S., M.B. Taubman, and N. Mackman, *Role of tissue factor in*

cancer. J Clin Oncol, 2009. **27**(29): p. 4834-8.
70. Camerer, E., et al., *Platelets, protease-activated receptors, and fibrinogen in hematogenous metastasis*. Blood, 2004. **104**(2): p. 397-401.
71. Borsig, L., et al., *Heparin and cancer revisited: mechanistic connections involving platelets, P-selectin, carcinoma mucins, and tumor metastasis*. Proc Natl Acad Sci U S A, 2001. **98**(6): p. 3352-7.
72. Nieswandt, B., et al., *Lysis of tumor cells by natural killer cells in mice is impeded by platelets*. Cancer Res, 1999. **59**(6): p. 1295-300.
73. Lanier, L.L., *NK cell recognition*. Annu Rev Immunol, 2005. **23**: p. 225-74.
74. Moretta, L. and A. Moretta, *Unravelling natural killer cell function: triggering and inhibitory human NK receptors*. EMBO J, 2004. **23**(2): p. 255-9.
75. Placke, T., et al., *Platelet-derived MHC class I confers a pseudonormal phenotype to cancer cells that subverts the antitumor reactivity of natural killer immune cells*. Cancer Res, 2012. **72**(2): p. 440-8.
76. Kopp, H.G., T. Placke, and H.R. Salih, *Platelet-derived transforming growth factor-beta down-regulates NKG2D thereby inhibiting natural killer cell antitumor reactivity*. Cancer Res, 2009. **69**(19): p. 7775-83.
77. Amirkhosravi, A., et al., *The role of tissue factor pathway inhibitor in tumor growth and metastasis*. Semin Thromb Hemost, 2007. **33**(7): p. 643-52.
78. Amirkhosravi, A., et al., *Tissue factor pathway inhibitor reduces experimental lung metastasis of B16 melanoma*. Thromb Haemost, 2002. **87**(6): p. 930-6.
79. Wenzel, J., et al., *Inhibition of pulmonary metastasis in a human MT3 breast cancer xenograft model by dual liposomes preventing intravasal fibrin clot formation*. Breast Cancer Res Treat, 2010. **121**(1): p. 13-22.
80. Stevenson, J.L., S.H. Choi, and A. Varki, *Differential metastasis inhibition by clinically relevant levels of heparins--correlation with selectin inhibition, not antithrombotic activity*. Clin Cancer Res, 2005. **11**(19 Pt 1): p. 7003-11.
81. Koenig, A., et al., *Differential interactions of heparin and heparan sulfate glycosaminoglycans with the selectins. Implications for the use of unfractionated and low molecular weight heparins as therapeutic agents*. J Clin Invest, 1998. **101**(4): p. 877-89.
82. Hostettler, N., et al., *P-selectin- and heparanase-dependent antimetastatic activity of non-anticoagulant heparins*. FASEB J, 2007. **21**(13): p. 3562-72.
83. Wei, M., et al., *Modified heparin inhibits P-selectin-mediated cell adhesion of human colon carcinoma cells to immobilized platelets under dynamic flow conditions*. J Biol Chem, 2004. **279**(28): p. 29202-10.
84. Lee, D.Y., et al., *Antimetastatic effect of an orally active heparin derivative on experimentally induced metastasis*. Clin Cancer Res, 2008. **14**(9): p. 2841-9.
85. Borsig, L., et al., *Selectin blocking activity of a fucosylated chondroitin sulfate glycosaminoglycan from sea cucumber. Effect on tumor metastasis and neutrophil recruitment*. J Biol Chem, 2007. **282**(20): p. 14984-91.
86. Labelle, M., S. Begum, and R.O. Hynes, *Direct signaling between platelets and cancer cells induces an epithelial-mesenchymal-like transition and promotes metastasis*. Cancer Cell, 2011. **20**(5): p. 576-90.
87. Mohammad, K.S., et al., *TGF-beta-RI kinase inhibitor SD-208 reduces the*

development and progression of melanoma bone metastases. Cancer Res, 2011. **71**(1): p. 175-84.
88. Sierko, E. and M.Z. Wojtukiewicz, *Inhibition of platelet function: does it offer a chance of better cancer progression control?* Semin Thromb Hemost, 2007. **33**(7): p. 712-21.
89. Moreira, I.S., P.A. Fernandes, and M.J. Ramos, *Vascular endothelial growth factor (VEGF) inhibition--a critical review*. Anticancer Agents Med Chem, 2007. **7**(2): p. 223-45.
90. Weroha, S.J. and P. Haluska, *IGF-1 receptor inhibitors in clinical trials--early lessons*. J Mammary Gland Biol Neoplasia, 2008. **13**(4): p. 471-83.
91. Roberts, W.G., et al., *Antiangiogenic and antitumor activity of a selective PDGFR tyrosine kinase inhibitor, CP-673,451*. Cancer Res, 2005. **65**(3): p. 957-66.
92. Hughes, A.D. and M.R. King, *Use of naturally occurring halloysite nanotubes for enhanced capture of flowing cells*. Langmuir, 2010. **26**(14): p. 12155-64.
93. Hughes, A.D., et al., *Microtube Device for Selectin-Mediated Capture of Viable Circulating Tumor Cells from Blood*. Clin Chem, 2012.
94. Lawrence, M.B. and T.A. Springer, *Leukocytes roll on a selectin at physiologic flow rates: distinction from and prerequisite for adhesion through integrins*. Cell, 1991. **65**(5): p. 859-73.
95. Wild, M.K., et al., *Affinity, kinetics, and thermodynamics of E-selectin binding to E-selectin ligand-1*. J Biol Chem, 2001. **276**(34): p. 31602-12.
96. Bagge, U., A. Blixt, and K.G. Strid, *The initiation of post-capillary margination of leukocytes: studies in vitro on the influence of erythrocyte concentration and flow velocity*. Int J Microcirc Clin Exp, 1983. **2**(3): p. 215-27.
97. Goldsmith, H.L. and S. Spain, *Margination of leukocytes in blood flow through small tubes*. Microvasc Res, 1984. **27**(2): p. 204-22.
98. Iadocicco, K., L.H. Monteiro, and J.G. Chaui-Berlinck, *A theoretical model for estimating the margination constant of leukocytes*. BMC Physiol, 2002. **2**: p. 3.
99. Koschny, R., H. Walczak, and T.M. Ganten, *The promise of TRAIL--potential and risks of a novel anticancer therapy*. J Mol Med (Berl), 2007. **85**(9): p. 923-35.
100. Wang, S., *The promise of cancer therapeutics targeting the TNF-related apoptosis-inducing ligand and TRAIL receptor pathway*. Oncogene, 2008. **27**(48): p. 6207-15.
101. Rana, K., J.L. Liesveld, and M.R. King, *Delivery of apoptotic signal to rolling cancer cells: a novel biomimetic technique using immobilized TRAIL and E-selectin*. Biotechnol Bioeng, 2009. **102**(6): p. 1692-702.
102. Valastyan, S. and R.A. Weinberg, *Tumor metastasis: molecular insights and evolving paradigms*. Cell, 2011. **147**(2): p. 275-92.
103. Yin, X., et al., *Knockdown of fucosyltransferase III disrupts the adhesion of circulating cancer cells to E-selectin without affecting hematopoietic cell adhesion*. Carbohydr Res, 2010. **345**(16): p. 2334-42.
104. Mehlen, P. and A. Puisieux, *Metastasis: a question of life or death*. Nature

reviews. Cancer, 2006. **6**(6): p. 449-58.
105. Li, J. and M.R. King, *Adhesion receptors as therapeutic targets for circulating tumor cells*. Frontiers in oncology, 2012. **2**: p. 79.
106. Labelle, M. and R.O. Hynes, *The Initial Hours of Metastasis: The Importance of Cooperative Host-Tumor Cell Interactions during Hematogenous Dissemination*. Cancer discovery, 2012. **2**(12): p. 1091-9.
107. Baccelli, I., et al., *Identification of a population of blood circulating tumor cells from breast cancer patients that initiates metastasis in a xenograft assay*. Nature biotechnology, 2013. **31**(6): p. 539-44.
108. Chauhan, V.P. and R.K. Jain, *Strategies for advancing cancer nanomedicine*. Nature materials, 2013. **12**(11): p. 958-62.
109. Dawidczyk, C.M., et al., *State-of-the-art in design rules for drug delivery platforms: Lessons learned from FDA-approved nanomedicines*. Journal of controlled release : official journal of the Controlled Release Society, 2014. **187C**: p. 133-144.
110. Bertrand, N., et al., *Cancer nanotechnology: the impact of passive and active targeting in the era of modern cancer biology*. Advanced drug delivery reviews, 2014. **66**: p. 2-25.
111. Barnes, J.M., J.T. Nauseef, and M.D. Henry, *Resistance to Fluid Shear Stress Is a Conserved Biophysical Property of Malignant Cells*. Plos One, 2012. **7**(12).
112. Sheth, R.A., et al., *Barriers to Drug Delivery in Interventional Oncology*. Journal of Vascular and Interventional Radiology, 2013. **24**(8): p. 1201-1207.
113. Jain, R.K., *Normalizing Tumor Microenvironment to Treat Cancer: Bench to Bedside to Biomarkers*. Journal of Clinical Oncology, 2013. **31**(17): p. 2205-U210.
114. Gay, L.J. and B. Felding-Habermann, *Contribution of platelets to tumour metastasis*. Nature Reviews Cancer, 2011. **11**(2): p. 123-134.
115. Yu, M., et al., *RNA sequencing of pancreatic circulating tumour cells implicates WNT signalling in metastasis*. Nature, 2012. **487**(7408): p. 510-3.
116. Lohr, J.G., et al., *Whole-exome sequencing of circulating tumor cells provides a window into metastatic prostate cancer*. Nature biotechnology, 2014. **32**(5): p. 479-84.
117. Luo, X., et al., *Isolation and molecular characterization of circulating melanoma cells*. Cell reports, 2014. **7**(3): p. 645-53.
118. Earhart, C.M., et al., *Isolation and mutational analysis of circulating tumor cells from lung cancer patients with magnetic sifters and biochips*. Lab on a Chip, 2014. **14**(1): p. 78-88.
119. Armstrong, A.J., et al., *Circulating tumor cells from patients with advanced prostate and breast cancer display both epithelial and mesenchymal markers*. Molecular cancer research : MCR, 2011. **9**(8): p. 997-1007.
120. Yu, M., et al., *Circulating breast tumor cells exhibit dynamic changes in epithelial and mesenchymal composition*. Science, 2013. **339**(6119): p. 580-4.
121. Yokobori, T., et al., *Plastin3 is a novel marker for circulating tumor cells undergoing the epithelial-mesenchymal transition and is associated with*

colorectal cancer prognosis. Cancer Research, 2013. **73**(7): p. 2059-69.
122. Balasubramanian, P., et al., *Multiparameter analysis, including EMT markers, on negatively enriched blood samples from patients with squamous cell carcinoma of the head and neck*. Plos One, 2012. **7**(7): p. e42048.
123. Li, Y.M., et al., *Epithelial-mesenchymal transition markers expressed in circulating tumor cells in hepatocellular carcinoma patients with different stages of disease*. Cell death & disease, 2013. **4**: p. e831.
124. Kalluri, R. and R.A. Weinberg, *The basics of epithelial-mesenchymal transition*. The Journal of clinical investigation, 2009. **119**(6): p. 1420-8.
125. Radisky, D.C., *Epithelial-mesenchymal transition*. Journal of cell science, 2005. **118**(Pt 19): p. 4325-6.
126. Frisch, S.M., M. Schaller, and B. Cieply, *Mechanisms that link the oncogenic epithelial-mesenchymal transition to suppression of anoikis*. Journal of cell science, 2013. **126**(Pt 1): p. 21-9.
127. Ahmed, N., et al., *Epithelial mesenchymal transition and cancer stem cell-like phenotypes facilitate chemoresistance in recurrent ovarian cancer*. Current cancer drug targets, 2010. **10**(3): p. 268-78.
128. Mani, S.A., et al., *The epithelial-mesenchymal transition generates cells with properties of stem cells*. Cell, 2008. **133**(4): p. 704-15.
129. Nieto, M.A., *Epithelial plasticity: a common theme in embryonic and cancer cells*. Science, 2013. **342**(6159): p. 1234850.
130. Zarbock, A., et al., *Leukocyte ligands for endothelial selectins: specialized glycoconjugates that mediate rolling and signaling under flow*. Blood, 2011. **118**(26): p. 6743-6751.
131. Schmidt, S., M. Moser, and M. Sperandio, *The molecular basis of leukocyte recruitment and its deficiencies*. Molecular Immunology, 2013. **55**(1): p. 49-58.
132. Winkler, I.G., et al., *Vascular niche E-selectin regulates hematopoietic stem cell dormancy, self renewal and chemoresistance*. Nature medicine, 2012. **18**(11): p. 1651-7.
133. Hsu, J.W., et al., *Suppression of Prostate Cancer Cell Rolling and Adhesion to Endothelium by 1 alpha,25-Dihydroxyvitamin D-3*. American Journal of Pathology, 2011. **178**(2): p. 872-880.
134. Li, J., et al., *Human fucosyltransferase 6 enables prostate cancer metastasis to bone*. British journal of cancer, 2013. **109**(12): p. 3014-22.
135. Barthel, S.R., et al., *Alpha 1,3 fucosyltransferases are master regulators of prostate cancer cell trafficking*. Proceedings of the National Academy of Sciences of the United States of America, 2009. **106**(46): p. 19491-19496.
136. Varki, A., *Trousseau's syndrome: multiple definitions and multiple mechanisms*. Blood, 2007. **110**(6): p. 1723-9.
137. Egan, K., et al., *Platelet adhesion and degranulation induce pro-survival and pro-angiogenic signalling in ovarian cancer cells*. Plos One, 2011. **6**(10): p. e26125.
138. Labelle, M., S. Begum, and R.O. Hynes, *Platelets guide the formation of early metastatic niches*. Proceedings of the National Academy of Sciences of the

United States of America, 2014. **111**(30): p. E3053-61.
139. Wenzel, J., R. Zeisig, and I. Fichtner, *Inhibition of metastasis in a murine 4T1 breast cancer model by liposomes preventing tumor cell-platelet interactions*. Clinical & experimental metastasis, 2010. **27**(1): p. 25-34.
140. Alix-Panabieres, C., H. Schwarzenbach, and K. Pantel, *Circulating tumor cells and circulating tumor DNA*. Annual review of medicine, 2012. **63**: p. 199-215.
141. Hou, H.W., et al., *Isolation and retrieval of circulating tumor cells using centrifugal forces*. Scientific reports, 2013. **3**: p. 1259.
142. de Bono, J.S., et al., *Circulating tumor cells predict survival benefit from treatment in metastatic castration-resistant prostate cancer*. Clinical cancer research : an official journal of the American Association for Cancer Research, 2008. **14**(19): p. 6302-9.
143. Lecharpentier, A., et al., *Detection of circulating tumour cells with a hybrid (epithelial/mesenchymal) phenotype in patients with metastatic non-small cell lung cancer*. British journal of cancer, 2011. **105**(9): p. 1338-41.
144. Ksiazkiewicz, M., A. Markiewicz, and A.J. Zaczek, *Epithelial-mesenchymal transition: a hallmark in metastasis formation linking circulating tumor cells and cancer stem cells*. Pathobiology : journal of immunopathology, molecular and cellular biology, 2012. **79**(4): p. 195-208.
145. Zhang, L., et al., *The identification and characterization of breast cancer CTCs competent for brain metastasis*. Science translational medicine, 2013. **5**(180): p. 180ra48.
146. Yao, X., et al., *Functional analysis of single cells identifies a rare subset of circulating tumor cells with malignant traits*. Integrative biology : quantitative biosciences from nano to macro, 2014. **6**(4): p. 388-98.
147. Cho, E.H., et al., *Characterization of circulating tumor cell aggregates identified in patients with epithelial tumors*. Physical biology, 2012. **9**(1): p. 016001.
148. Kim, H., et al., *Development of on-chip multi-imaging flow cytometry for identification of imaging biomarkers of clustered circulating tumor cells*. Plos One, 2014. **9**(8): p. e104372.
149. Zhao, Q., et al., *Interaction between circulating galectin-3 and cancer-associated MUC1 enhances tumour cell homotypic aggregation and prevents anoikis*. Molecular cancer, 2010. **9**: p. 154.
150. Hou, J.M., et al., *Clinical significance and molecular characteristics of circulating tumor cells and circulating tumor microemboli in patients with small-cell lung cancer*. Journal of clinical oncology : official journal of the American Society of Clinical Oncology, 2012. **30**(5): p. 525-32.
151. Aceto, N., et al., *Circulating tumor cell clusters are oligoclonal precursors of breast cancer metastasis*. Cell, 2014. **158**(5): p. 1110-22.
152. Yu, M., et al., *Cancer therapy. Ex vivo culture of circulating breast tumor cells for individualized testing of drug susceptibility*. Science, 2014. **345**(6193): p. 216-20.
153. Tacar, O., P. Sriamornsak, and C.R. Dass, *Doxorubicin: an update on anticancer molecular action, toxicity and novel drug delivery systems*. The

Journal of pharmacy and pharmacology, 2013. **65**(2): p. 157-70.
154. Zhao, P. and D. Astruc, *Docetaxel nanotechnology in anticancer therapy*. ChemMedChem, 2012. **7**(6): p. 952-72.
155. Scott, A.M., J.D. Wolchok, and L.J. Old, *Antibody therapy of cancer*. Nature reviews. Cancer, 2012. **12**(4): p. 278-87.
156. Stott, S.L., et al., *Isolation and characterization of circulating tumor cells from patients with localized and metastatic prostate cancer*. Science translational medicine, 2010. **2**(25): p. 25ra23.
157. Schwarzenbach, H., et al., *Comparative evaluation of cell-free tumor DNA in blood and disseminated tumor cells in bone marrow of patients with primary breast cancer*. Breast cancer research : BCR, 2009. **11**(5): p. R71.
158. Meng, S., et al., *Circulating tumor cells in patients with breast cancer dormancy*. Clinical cancer research : an official journal of the American Association for Cancer Research, 2004. **10**(24): p. 8152-62.
159. Mitchell, L.A. and J.D. Boeke, *Circular permutation of a synthetic eukaryotic chromosome with the telomerator*. Proceedings of the National Academy of Sciences of the United States of America, 2014. **111**(48): p. 17003-10.
160. Zijlstra, A., et al., *The inhibition of tumor cell intravasation and subsequent metastasis via regulation of in vivo tumor cell motility by the tetraspanin CD151*. Cancer Cell, 2008. **13**(3): p. 221-34.
161. Livney, Y.D. and Y.G. Assaraf, *Rationally designed nanovehicles to overcome cancer chemoresistance*. Advanced drug delivery reviews, 2013. **65**(13-14): p. 1716-1730.
162. Gaitanis, A. and S. Staal, *Liposomal Doxorubicin and nab-Paclitaxel: Nanoparticle Cancer Chemotherapy in Current Clinical Use*. Cancer Nanotechnology: Methods and Protocols, 2010. **624**: p. 385-392.
163. Shapira, A., et al., *Nanomedicine for targeted cancer therapy: Towards the overcoming of drug resistance*. Drug Resistance Updates, 2011. **14**(3): p. 150-163.
164. Raemdonck, K., et al., *Merging the best of both worlds: hybrid lipid-enveloped matrix nanocomposites in drug delivery*. Chemical Society Reviews, 2014. **43**(1): p. 444-472.
165. Onyskiw, P.J. and O. Eniola-Adefeso, *Effect of PEGylation on Ligand-Based Targeting of Drug Carriers to the Vascular Wall in Blood Flow*. Langmuir, 2013. **29**(35): p. 11127-11134.
166. Rahn, J., et al., *MUC1 Mediates Transendothelial Migration in vitro by Ligating Endothelial Cell ICAM-1*. Clinical & Experimental Metastasis, 2005. **22**(6): p. 475-483.
167. Regimbald, L.H., et al., *The Breast Mucin MUC1 as a Novel Adhesion Ligand for Endothelial Intercellular Adhesion Molecule 1 in Breast Cancer*. Cancer Research, 1996. **56**(18): p. 4244-4249.
168. Palange, A.L., et al., *Lipid-polymer nanoparticles encapsulating curcumin for modulating the vascular deposition of breast cancer cells*. Nanomedicine: Nanotechnology, Biology and Medicine, 2014. **10**(5): p. 991-1002.
169. Hirai, M., et al., *Novel and simple loading procedure of cisplatin into*

liposomes and targeting tumor endothelial cells. International Journal of Pharmaceutics, 2010. **391**(1-2): p. 274-283.
170. Brigger, I., C. Dubernet, and P. Couvreur, *Nanoparticles in cancer therapy and diagnosis*. Adv Drug Deliv Rev, 2002. **54**(5): p. 631-51.
171. Alexis, F., et al., *Factors Affecting the Clearance and Biodistribution of Polymeric Nanoparticles*. Mol Pharm, 2008. **5**(4): p. 505-15.
172. Ruenraroengsak, P., J.M. Cook, and A.T. Florence, *Nanosystem drug targeting: Facing up to complex realities*. J Control Release, 2010. **141**(3): p. 265-76.
173. Gentile, F., et al., *The margination propensity of spherical particles for vascular targeting in the microcirculation*. J Nanobiotechnology, 2008. **6**: p. 9.
174. Decuzzi, P. and M. Ferrari, *The adhesive strength of non-spherical particles mediated by specific interactions*. Biomaterials, 2006. **27**(30): p. 5307-14.
175. Champion, J.A., Y.K. Katare, and S. Mitragotri, *Particle shape: a new design parameter for micro- and nanoscale drug delivery carriers*. J Control Release, 2007. **121**(1-2): p. 3-9.
176. Decuzzi, P., et al., *Size and shape effects in the biodistribution of intravascularly injected particles*. J Control Release, 2010. **141**(3): p. 320-7.
177. Jackson, S.P., *The growing complexity of platelet aggregation*. Vol. 109. 2007. 5087-5095.
178. Noguchi, H. and G. Gompper, *Shape transitions of fluid vesicles and red blood cells in capillary flows*. Proc Natl Acad Sci U S A, 2005. **102**(40): p. 14159-64.
179. Moghimi, S.M., A.C. Hunter, and J.C. Murray, *Long-circulating and target-specific nanoparticles: theory to practice*. Pharmacological reviews, 2001. **53**(2): p. 283-318.
180. Mody, N.A. and M.R. King, *Platelet Adhesive Dynamics. Part I: Characterization of Platelet Hydrodynamic Collisions and Wall Effects*. Biophys J, 2008. **95**(5): p. 2539-55.
181. Geng, Y., et al., *Shape effects of filaments versus spherical particles in flow and drug delivery*. Nat Nanotechnol, 2007. **2**(4): p. 249-55.
182. Cai, S., et al., *Micelles of different morphologies--advantages of worm-like filomicelles of PEO-PCL in paclitaxel delivery*. Pharm Res, 2007. **24**(11): p. 2099-109.
183. Gandra, N., et al., *Bacteriophage Bionanowire as a Carrier for Both Cancer-Targeting Peptides and Photosensitizers and its use in Selective Cancer Cell Killing by Photodynamic Therapy*. Small, 2013. **9**(2): p. 215-21.
184. Bruckman, M.A., et al., *Biodistribution, pharmacokinetics, and blood compatibility of native and PEGylated tobacco mosaic virus nano-rods and -spheres in mice*. Virology, 2014. **449**: p. 163-73.
185. Lee, K.L., et al., *Shape matters: the diffusion rates of TMV rods and CPMV icosahedrons in a spheroid model of extracellular matrix are distinct*. Biomater Sci, 2013. **1**(6).
186. Bianco, A., K. Kostarelos, and M. Prato, *Applications of carbon nanotubes in drug delivery*. Curr Opin Chem Biol, 2005. **9**(6): p. 674-9.

187. Yinghuai, Z., et al., *Substituted carborane-appended water-soluble single-wall carbon nanotubes: new approach to boron neutron capture therapy drug delivery*. J Am Chem Soc, 2005. **127**(27): p. 9875-80.
188. Lee, S.Y., M. Ferrari, and P. Decuzzi, *Shaping nano-/micro-particles for enhanced vascular interaction in laminar flows*. Nanotechnology, 2009. **20**(49): p. 495101.
189. Lee, S.Y., M. Ferrari, and P. Decuzzi, *Design of bio-mimetic particles with enhanced vascular interaction*. J Biomech, 2009. **42**(12): p. 1885-90.
190. Ihler, G., R. Glew, and F. Schnure, *Enzyme loading of erythrocytes*. Proc. Nat. Acad. Sci, 1973. **70**(9): p. 2663-2666.
191. Muzykantov, V.R., *Drug delivery by red blood cells: vascular carriers designed by mother nature*. Expert Opin Drug Deliv, 2010. **7**(4): p. 403-27.
192. Hu, C.M., R.H. Fang, and L. Zhang, *Erythrocyte-inspired delivery systems*. Adv Healthc Mater, 2012. **1**(5): p. 537-47.
193. Jokerst, J. and e. al., *Nanoparticle PEGylation for imaging and therapy*. Nanomedicine, 2011. **6**(4): p. 715-728.
194. Hu, C.M., et al., *Erythrocyte membrane-camouflaged polymeric nanoparticles as a biomimetic delivery platform*. Proc Natl Acad Sci U S A, 2011. **108**(27): p. 10980-5.
195. Zolnik, B.S., et al., *Nanoparticles and the immune system*. Endocrinology, 2010. **151**(2): p. 458-65.
196. Ishida, T. and H. Kiwada, *Accelerated blood clearance (ABC) phenomenon upon repeated injection of PEGylated liposomes*. Int J Pharm, 2008. **354**(1-2): p. 56-62.
197. Dams, E. and e. al., *Accelerated blood clearance and altered biodistribution of repeated injections of sterically stabilized liposomes*. JPET, 2000. **292**(3): p. 1071-1079.
198. Ishida, T., et al., *Accelerated clearance of PEGylated liposomes in rats after repeated injections*. Journal of Controlled Release, 2003. **88**(1): p. 35-42.
199. Ishida, T., et al., *PEGylated liposomes elicit an anti-PEG IgM response in a T cell-independent manner*. J Control Release, 2007. **122**(3): p. 349-55.
200. Kim, D.D. and W.C. Song, *Membrane complement regulatory proteins*. Clin Immunol, 2006. **118**(2-3): p. 127-36.
201. Oldenborg, P.A., *Role of CD47 as a Marker of Self on Red Blood Cells*. Science, 2000. **288**(5473): p. 2051-2054.
202. Hsu, Y. and e. al., *Reduced phagocytosis of colloidal carriers using soluble CD47*. Pharmaceutical Research, 2003. **20**(10): p. 1539-1542.
203. Gao, W., et al., *Surface functionalization of gold nanoparticles with red blood cell membranes*. Adv Mater, 2013. **25**(26): p. 3549-53.
204. Zocchi, E. and e. al., *Encapsulation of doxorubicin in liver-targeted erythrocytes increases the therapeutic index of the drug in a murine metastatic model*. Pro. Natl. Acad. Sci., 1988. **86**: p. 2040-2044.
205. Matherne, C.M., et al., *Clinical efficacy and toxicity of doxorubicin encapsulated in glutaraldehyde-treated erythrocytes administered to dogs with lymphosarcoma*. Am J Vet Res, 1994. **55**(6): p. 847-53.

206. Skorokhod, O. and e. al., *Doxorubicin pharmacokinetics in lymphoma patients treated with doxorubicin-loaded erythrocytes*. Hematologica, 2007. **92**: p. 570-571.
207. Skorokhod, O. and e. al., *Pharmacokinetics or erythrocyte-bound daunorubicin in patients with acute leukemia*. Med Sci Monit, 2004. **10**(4): p. PI55-64.
208. Millan, C.G., et al., *Drug, enzyme and peptide delivery using erythrocytes as carriers*. J Control Release, 2004. **95**(1): p. 27-49.
209. Alpar, H. and D. Lewis, *Therapeutic efficacy of asparaginase encapsulated in intact erythrocytes*. Biochemical Pharmacology, 1985. **34**(2): p. 257-261.
210. Kravtzoff, R. and e. al., *Erythrocytes as carriers for L-asparaginase. Methodological and mouse in-vivo studies*. J. Pharm. Pharmacol, 1990. **42**: p. 473-476.
211. DeLoach, J.R., et al., *Intraperitoneal administration of carrier erythrocytes in dogs: an improved method for delivery of L-asparaginase*. Biotechnol Appl Biochem, 1990. **12**(3): p. 331-5.
212. Updike, S.J. and R.T. Wakamiya, *Infusion of red blood cell-loaded asparaginase in monkey. Immunologic, metabolic, and toxicologic consequences*. J Lab Clin Med, 1983. **101**(5): p. 679-91.
213. Kravtzoff, R., et al., *Improved pharmacodynamics of L-asparaginase-loaded in human red blood cells*. Eur J Clin Pharmacol, 1996. **49**(6): p. 465-70.
214. Rao, C.G., et al., *Expression of epithelial cell adhesion molecule in carcinoma cells present in blood and primary and metastatic tumors*. Int J Oncol, 2005. **27**(1): p. 49-57.
215. Schulze, K., et al., *Presence of EpCAM-positive circulating tumor cells as biomarker for systemic disease strongly correlates to survival in patients with hepatocellular carcinoma*. Int J Cancer, 2013. **133**(9): p. 2165-71.
216. Muzykantov, V., *Avidin/Biotin-Mediated Conjugation of Antibodies to Erythrocytes: An Approach for in vivo Immunoerythrocyte Exploration*, in *A Laboratory Guide to Biotin-Labeling in Biomolecule Analysis*, T. Meier and F. Fahrenholz, Editors. 1996, Birkhäuser Basel. p. 167-182.
217. Modery-Pawlowski, C.L., et al., *A Platelet-Mimetic Paradigm for Metastasis-Targeted Nanomedicine Platforms*. Biomacromolecules, 2013. **14**(3): p. 910-919.
218. Yu, M., et al., *Circulating tumor cells: approaches to isolation and characterization*. Journal of Cell Biology, 2011. **192**(3): p. 373-382.
219. Miyamoto, D.T., L.V. Sequist, and R.J. Lee, *Circulating tumour cells-monitoring treatment response in prostate cancer*. Nature reviews. Clinical oncology, 2014. **11**(7): p. 401-12.
220. Joosse, S.A., T.M. Gorges, and K. Pantel, *Biology, detection, and clinical implications of circulating tumor cells*. EMBO molecular medicine, 2014.
221. Cristofanilli, M., et al., *Circulating tumor cells, disease progression, and survival in metastatic breast cancer*. The New England journal of medicine, 2004. **351**(8): p. 781-91.
222. Tewes, M., et al., *Molecular profiling and predictive value of circulating*

tumor cells in patients with metastatic breast cancer: an option for monitoring response to breast cancer related therapies. Breast cancer research and treatment, 2009. **115**(3): p. 581-90.
223. Deneve, E., et al., *Capture of viable circulating tumor cells in the liver of colorectal cancer patients*. Clinical chemistry, 2013. **59**(9): p. 1384-92.
224. Vona, G., et al., *Isolation by size of epithelial tumor cells : a new method for the immunomorphological and molecular characterization of circulatingtumor cells*. The American journal of pathology, 2000. **156**(1): p. 57-63.
225. Park, J.M., et al., *Highly efficient assay of circulating tumor cells by selective sedimentation with a density gradient medium and microfiltration from whole blood*. Analytical chemistry, 2012. **84**(17): p. 7400-7.
226. Xia, X.R., N.A. Monteiro-Riviere, and J.E. Riviere, *An index for characterization of nanomaterials in biological systems*. Nature Nanotechnology, 2010. **5**(9): p. 671-5.
227. Wang, S., et al., *Three-dimensional nanostructured substrates toward efficient capture of circulating tumor cells*. Angewandte Chemie, 2009. **48**(47): p. 8970-3.
228. Lee, S.K., et al., *Nanowire substrate-based laser scanning cytometry for quantitation of circulating tumor cells*. Nano letters, 2012. **12**(6): p. 2697-704.
229. Zhang, N., et al., *Electrospun TiO2 nanofiber-based cell capture assay for detecting circulating tumor cells from colorectal and gastric cancer patients*. Advanced materials, 2012. **24**(20): p. 2756-60.
230. Yoon, H.J., et al., *Sensitive capture of circulating tumour cells by functionalized graphene oxide nanosheets*. Nature Nanotechnology, 2013. **8**(10): p. 735-41.
231. den Toonder, J., *Circulating tumor cells: the Grand Challenge*. Lab on a Chip, 2011. **11**(3): p. 375-377.
232. Kim, D.J., et al., *Drug response of captured BT20 cells and evaluation of circulating tumor cells on a silicon nanowire platform*. Biosensors & bioelectronics, 2014.
233. Peng, F., et al., *Doxorubicin-loaded silicon nanowires for the treatment of drug-resistant cancer cells*. Biomaterials, 2014. **35**(19): p. 5188-95.
234. Shen, J., et al., *High capacity nanoporous silicon carrier for systemic delivery of gene silencing therapeutics*. ACS nano, 2013. **7**(11): p. 9867-80.
235. Zhang, L., et al., *Meta-analysis of the prognostic value of circulating tumor cells in breast cancer*. Clinical cancer research : an official journal of the American Association for Cancer Research, 2012. **18**(20): p. 5701-10.
236. Rana, K., C.A. Reinhart-King, and M.R. King, *Inducing Apoptosis in Rolling Cancer Cells: A Combined Therapy with Aspirin and Immobilized TRAIL and E-Selectin*. Molecular Pharmaceutics, 2012. **9**(8): p. 2219-2227.
237. Singh, S. and H.S. Nalwa, *Nanotechnology and health safety--toxicity and risk assessments of nanostructured materials on human health*. Journal of nanoscience and nanotechnology, 2007. **7**(9): p. 3048-70.
238. Tenzer, S., et al., *Rapid formation of plasma protein corona critically affects nanoparticle pathophysiology*. Nature Nanotechnology, 2013. **8**(10): p. 772-

U1000.
239. Monopoli, M.P., et al., *Physical-Chemical Aspects of Protein Corona: Relevance to in Vitro and in Vivo Biological Impacts of Nanoparticles*. Journal of the American Chemical Society, 2011. **133**(8): p. 2525-2534.
240. Sobczynski, D.J., et al., *Plasma protein corona modulates the vascular wall interaction of drug carriers in a material and donor specific manner*. Plos One, 2014. **9**(9): p. e107408.
241. Siegel, R., D. Naishadham, and A. Jemal, *Cancer Statistics, 2012*. Ca-a Cancer Journal for Clinicians, 2012. **62**(1): p. 10-29.
242. Wilt, T.J. and H.U. Ahmed, *Prostate cancer screening and the management of clinically localized disease*. British Medical Journal, 2013. **346**.
243. Sturge, J., M.P. Caley, and J. Waxman, *Bone metastasis in prostate cancer: emerging therapeutic strategies*. Nature Reviews Clinical Oncology, 2011. **8**(6): p. 357-368.
244. Saad, F., N. Clarke, and M. Colombel, *Natural history and treatment of bone complications in prostate cancer*. European Urology, 2006. **49**(3): p. 429-440.
245. Li, J. and M.R. King, *Adhesion receptors as therapeutic targets for circulating tumor cells*. Frontiers Oncology, 2012. **2**(79): p. 1-9.
246. Barthel, S.R., et al., *Definition of Molecular Determinants of Prostate Cancer Cell Bone Extravasation*. Cancer Research, 2013. **73**(2): p. 942-952.
247. Winkler, I.G., et al., *Vascular niche E-selectin regulates hematopoietic stem cell dormancy, self renewal and chemoresistance*. Nature Medicine, 2012. **18**(11): p. 1651-+.
248. Sackstein, R., *Glycoengineering of HCELL, the Human Bone Marrow Homing Receptor: Sweetly Programming Cell Migration*. Annals of Biomedical Engineering, 2012. **40**(4): p. 766-776.
249. Dimitroff, C.J., et al., *Identification of leukocyte E-selectin ligands, P-selectin glycoprotein ligand-1 and E-selectin ligand-1, on human metastatic prostate tumor cells*. Cancer Research, 2005. **65**(13): p. 5750-5760.
250. Dimitroff, C.J., et al., *Rolling of human bone-metastatic prostate tumor cells on human bone marrow endothelium under shear flow is mediated by E-selectin*. Cancer Research, 2004. **64**(15): p. 5261-5269.
251. de Vries, T., et al., *Fucosyltransferases: structure/function studies*. Glycobiology, 2001. **11**(10): p. 119R-128R.
252. Yin, X.Y., et al., *Knockdown of fucosyltransferase III disrupts the adhesion of circulating cancer cells to E-selectin without affecting hematopoietic cell adhesion*. Carbohydrate Research, 2010. **345**(16): p. 2334-2342.
253. Barthel, S.R., et al., *Analysis of glycosyltransferase expression in metastatic prostate cancer cells capable of rolling activity on microvascular endothelial (E)-selectin*. Glycobiology, 2008. **18**(10): p. 806-817.
254. Gingrich, J.R., et al., *Metastatic prostate cancer in a transgenic mouse*. Cancer Research, 1996. **56**(18): p. 4096-4102.
255. Bu, P., et al., *A microRNA miR-34a-regulated bimodal switch targets notch in colon cancer stem cells*. Cell stem cell, 2013. **12**(5): p. 602-15.
256. Matsumoto, M., et al., *CD43 functions as a ligand for E-selectin on activated T*

cells. Journal of Immunology, 2005. **175**(12): p. 8042-8050.
257. Granot, Z., et al., *Tumor Entrained Neutrophils Inhibit Seeding in the Premetastatic Lung*. Cancer Cell, 2011. **20**(3): p. 300-314.
258. Graves, B.J., et al., *Insight into E-Selectin Ligand Interaction from the Crystal-Structure and Mutagenesis of the Lec Egf Domains*. Nature, 1994. **367**(6463): p. 532-538.
259. Foster, B.A., et al., *Characterization of prostatic epithelial cell lines derived from transgenic adenocarcinoma of the mouse prostate (TRAMP) model*. Cancer Research, 1997. **57**(16): p. 3325-30.
260. Thompson, T.C., et al., *Multistage carcinogenesis induced by ras and myc oncogenes in a reconstituted organ*. Cell, 1989. **56**(6): p. 917-30.
261. Burdick, M.M., et al., *HCELL is the major E- and L-selectin ligand expressed on LS174T colon carcinoma cells*. The Journal of biological chemistry, 2006. **281**(20): p. 13899-905.
262. Zen, K., et al., *CD44v4 Is a Major E-Selectin Ligand that Mediates Breast Cancer Cell Transendothelial Migration*. Plos One, 2008. **3**(3).
263. Mitoma, J., et al., *The N-glycolyl form of mouse sialyl Lewis X is recognized by selectins but not by HECA-452 and FH6 antibodies that were raised against human cells*. Glycoconjugate Journal, 2009. **26**(5): p. 511-523.
264. Rana, K., J.L. Liesveld, and M.R. King, *Delivery of Apoptotic Signal to Rolling Cancer Cells: A Novel Biomimetic Technique Using Immobilized TRAIL and E-Selectin*. Biotechnology and Bioengineering, 2009. **102**(6): p. 1692-1702.
265. Narasipura, S.D. and M.R. King, *P-selectin-coated microtube for the purification of CD45+hematopoietic cells directly from human peripheral blood*. Blood Cells Molecules and Diseases, 2009. **42**(2): p. 136-139.
266. Campbell, J.P., et al., *Models of bone metastasis*. Journal of visualized experiments : JoVE, 2012(67): p. e4260.
267. Zou, M., et al., *Multiple metastases in a novel LNCaP model of human prostate cancer*. Oncology reports, 2013.
268. Draffin, J.E., et al., *CD44 potentiates the adherence of metastatic prostate and breast cancer cells to bone marrow endothelial cells*. Cancer Research, 2004. **64**(16): p. 5702-5711.
269. Rillahan, C.D., et al., *Global metabolic inhibitors of sialyl- and fucosyltransferases remodel the glycome*. Nature Chemical Biology, 2012. **8**(7): p. 661-668.
270. Sackstein, R., et al., *Ex vivo glycan engineering of membrane CD44 to create HCELL programs human mesenchymal stem cell trafficking to bone*. Blood, 2007. **110**(11): p. 72A-72A.
271. Homeister, J.W., et al., *The alpha(1,3)fucosyltransferases FucT-IV and FucT-VII exert collaborative control over selectin-dependent leukocyte recruitment and lymphocyte homing*. Immunity, 2001. **15**(1): p. 115-26.
272. Matsuura, N., et al., *Gene expression of fucosyl- and sialyl-transferases which synthesize sialyl Lewis(x), the carbohydrate ligands for E-selectin, in human breast cancer*. International Journal of Oncology, 1998. **12**(5): p. 1157-1164.

273. Thankamony, S.P. and R. Sackstein, *Enforced hematopoietic cell E- and L-selectin ligand (HCELL) expression primes transendothelial migration of human mesenchymal stem cells*. Proceedings of the National Academy of Sciences of the United States of America, 2011. **108**(6): p. 2258-2263.
274. Sackstein, R., et al., *Ex vivo glycan engineering of CD44 programs human multipotent mesenchymal stromal cell trafficking to bone*. Nature Medicine, 2008. **14**(2): p. 181-187.
275. Grivennikov, S.I., F.R. Greten, and M. Karin, *Immunity, Inflammation, and Cancer*. Cell, 2010. **140**(6): p. 883-899.
276. Barthel, S.R., et al., *Peracetylated 4-fluoro-glucosamine reduces the content and repertoire of N- and O-glycans without direct incorporation*. The Journal of biological chemistry, 2011. **286**(24): p. 21717-31.
277. McCabe, N.P., et al., *Intraosseous injection of RM1 murine prostate cancer cells promotes rapid osteolysis and periosteal bone deposition*. Clinical & Experimental Metastasis, 2008. **25**(5): p. 581-590.
278. Power, C.A., et al., *A Novel Model of Bone-Metastatic Prostate Cancer in Immunocompetent Mice*. Prostate, 2009. **69**(15): p. 1613-1623.
279. Mitchison, T.J., *The proliferation rate paradox in antimitotic chemotherapy*. Molecular Biology of the Cell, 2012. **23**(1): p. 1-6.
280. Galmarini, C.M., J.R. Mackey, and C. Dumontet, *Nucleoside analogues: mechanisms of drug resistance and reversal strategies*. Leukemia, 2001. **15**(6): p. 875-890.
281. Harbeck, N., et al., *Cardiovascular complications of conventional and targeted adjuvant breast cancer therapy*. Annals of Oncology, 2011. **22**(6): p. 1250-1258.
282. Yeh, E.T.H. and C.L. Bickford, *Cardiovascular Complications of Cancer Therapy Incidence, Pathogenesis, Diagnosis, and Management*. Journal of the American College of Cardiology, 2009. **53**(24): p. 2231-2247.
283. Yeh, E.T.H., et al., *Cardiovascular complications of cancer therapy - Diagnosis, pathogenesis, and management*. Circulation, 2004. **109**(25): p. 3122-3131.
284. Logue, J.S. and D.K. Morrison, *Complexity in the signaling network: insights from the use of targeted inhibitors in cancer therapy*. Genes & Development, 2012. **26**(7): p. 641-650.
285. Yingling, J.M., K.L. Blanchard, and J.S. Sawyer, *Development of TGF-beta signalling inhibitors for cancer therapy*. Nature Reviews Drug Discovery, 2004. **3**(12): p. 1011-1022.
286. Koivisto, P., et al., *Androgen receptor gene amplification: A possible molecular mechanism for androgen deprivation therapy failure in prostate cancer*. Cancer Research, 1997. **57**(2): p. 314-319.
287. Spector, N., et al., *Small molecule HER-2 tyrosine kinase inhibitors*. Breast Cancer Research, 2007. **9**(2).
288. Slamon, D.J., et al., *Human-Breast Cancer - Correlation of Relapse and Survival with Amplification of the Her-2 Neu Oncogene*. Science, 1987. **235**(4785): p. 177-182.

289. Trachootham, D., J. Alexandre, and P. Huang, *Targeting cancer cells by ROS-mediated mechanisms: a radical therapeutic approach?* Nature Reviews Drug Discovery, 2009. **8**(7): p. 579-591.
290. Schumacker, P.T., *Reactive oxygen species in cancer cells: Live by the sword, die by the sword*. Cancer Cell, 2006. **10**(3): p. 175-176.
291. Raj, L., et al., *Selective killing of cancer cells by a small molecule targeting the stress response to ROS*. Nature, 2011. **475**(7355): p. 231-234.
292. Wang, Y., et al., *Piperlongumine induces autophagy by targeting p38 signaling*. Cell death & disease, 2013. **4**: p. e824.
293. Komarova, N.L. and D. Wodarz, *Drug resistance in cancer: Principles of emergence and prevention*. Proceedings of the National Academy of Sciences of the United States of America, 2005. **102**(27): p. 9714-9719.
294. Tang, J., et al., *Target Inhibition Networks: Predicting Selective Combinations of Druggable Targets to Block Cancer Survival Pathways*. Plos Computational Biology, 2013. **9**(9).
295. Wang, H., et al., *Doxorubicin and Lapatinib Combination Nanomedicine for Treating Resistant Breast Cancer*. Molecular pharmaceutics, 2014.
296. Bellail, A.C., et al., *TRAIL agonists on clinical trials for cancer therapy: the promises and the challenges*. Reviews on recent clinical trials, 2009. **4**(1): p. 34-41.
297. Wang, S. and W.S. El-Deiry, *TRAIL and apoptosis induction by TNF-family death receptors*. Oncogene, 2003. **22**(53): p. 8628-33.
298. Mitchell, M.J., et al., *TRAIL-coated leukocytes that kill cancer cells in the circulation*. Proceedings of the National Academy of Sciences of the United States of America, 2014. **111**(3): p. 930-5.
299. Dimberg, L.Y., et al., *On the TRAIL to successful cancer therapy? Predicting and counteracting resistance against TRAIL-based therapeutics*. Oncogene, 2013. **32**(11): p. 1341-1350.
300. Chae, S.Y., et al., *Improved Antitumor Activity and Tumor Targeting of NH2-Terminal-Specific PEGylated Tumor Necrosis Factor-Related Apoptosis-Inducing Ligand*. Molecular Cancer Therapeutics, 2010. **9**(6): p. 1719-1729.
301. Li, J., et al., *Human fucosyltransferase 6 enables prostate cancer metastasis to bone*. British Journal of Cancer, 2013. **109**(12): p. 3014-3022.
302. Gao, F., et al., *Ulinastatin Exerts Synergistic Effects with Taxotere and Inhibits Invasion and Metastasis of Breast Cancer by Blocking Angiogenesis and the Epithelial-Mesenchymal Transition*. Cancer Biotherapy and Radiopharmaceuticals, 2013. **28**(3): p. 218-225.
303. Choo, M.K., et al., *Blockade of transforming growth factor-beta-activated kinase 1 activity enhances TRAIL-induced apoptosis through activation of a caspase cascade*. Molecular Cancer Therapeutics, 2006. **5**(12): p. 2970-2976.
304. Szegezdi, E., et al., *TRAIL sensitisation by arsenic trioxide is caspase-8 dependent and involves modulation of death receptor components and Akt*. British Journal of Cancer, 2006. **94**(3): p. 398-406.
305. Jia, Y.T., et al., *Activation of p38 MAPK by reactive oxygen species is essential in a rat model of stress-induced gastric mucosal injury*. Journal of

Immunology, 2007. **179**(11): p. 7808-7819.
306. Cowan, K.J. and K.B. Storey, *Mitogen-activated protein kinases: new signaling pathways functioning in cellular responses to environmental stress*. Journal of Experimental Biology, 2003. **206**(7): p. 1107-1115.
307. Criscitiello, C., et al., *Understanding the biology of triple-negative breast cancer*. Annals of Oncology, 2012. **23**: p. 13-18.
308. Crown, J., J. O'Shaughnessy, and G. Gullo, *Emerging targeted therapies in triple-negative breast cancer*. Annals of Oncology, 2012. **23**: p. 56-65.
309. Wang, S., et al., *Doxorubicin induces apoptosis in normal and tumor cells via distinctly different mechanisms. intermediacy of H(2)O(2)- and p53-dependent pathways*. The Journal of biological chemistry, 2004. **279**(24): p. 25535-43.
310. Praga, C., G. Beretta, and R. Labianca, *Cardiac toxicity from antitumor therapy*. Oncology, 1980. **37 Suppl 1**: p. 51-8.
311. Chlebowski, R.T., *Adriamycin (doxorubicin) cardiotoxicity: a review*. The Western journal of medicine, 1979. **131**(5): p. 364-8.
312. Cobleigh, M.A., *Other Options in the Treatment of Advanced Breast Cancer*. Seminars in Oncology, 2011. **38**(3): p. S11-S16.
313. Gochi, A., et al., *The prognostic advantage of preoperative intratumoral injection of OK-432 for gastric cancer patients*. British Journal of Cancer, 2001. **84**(4): p. 443-451.
314. Han, H.D., et al., *Enhanced localization of anticancer drug in tumor tissue using polyethylenimine-conjugated cationic liposomes*. Nanoscale Research Letters, 2014. **9**.
315. Lammers, T., et al., *Effect of intratumoral injection on the biodistribution and the therapeutic potential of HPMA copolymer-based drug delivery systems*. Neoplasia, 2006. **8**(10): p. 788-795.
316. Sersa, G., et al., *Electrochemotherapy with cisplatin: Clinical experience in malignant melanoma patients*. Clinical Cancer Research, 2000. **6**(3): p. 863-867.
317. Xie, H., et al., *Effect of intratumoral administration on biodistribution of Cu-64-labeled nanoshells*. International Journal of Nanomedicine, 2012. **7**: p. 2227-2238.
318. Li, J., et al., *Nanobiotechnology for the Therapeutic Targeting of Cancer Cells in Blood*. Cellular and Molecular Bioengineering, 2015: p. 1-14.
319. Granot, Z., et al., *Tumor entrained neutrophils inhibit seeding in the premetastatic lung*. Cancer Cell, 2011. **20**(3): p. 300-14.
320. Gul, N., et al., *Macrophages eliminate circulating tumor cells after monoclonal antibody therapy*. The Journal of clinical investigation, 2014. **124**(2): p. 812-23.
321. Aerts, J.G. and J.P. Hegmans, *Tumor-specific cytotoxic T cells are crucial for efficacy of immunomodulatory antibodies in patients with lung cancer*. Cancer research, 2013. **73**(8): p. 2381-8.
322. Palumbo, J.S., et al., *Fibrinogen is an important determinant of the metastatic potential of circulating tumor cells*. Blood, 2000. **96**(10): p. 3302-3309.
323. Biggerstaff, J.P., et al., *Soluble fibrin augments platelet/tumor cell adherence*

in vitro and in vivo, and enhances experimental metastasis. Clinical & Experimental Metastasis, 1999. **17**(8): p. 723-730.
324. Rosenberg, S.A., *IL-2: the first effective immunotherapy for human cancer*. Journal of immunology, 2014. **192**(12): p. 5451-8.
325. Rizza, P., F. Moretti, and F. Belardelli, *Recent advances on the immunomodulatory effects of IFN-alpha: implications for cancer immunotherapy and autoimmunity*. Autoimmunity, 2010. **43**(3): p. 204-9.
326. Hejna, M., M. Raderer, and C.C. Zielinski, *Inhibition of metastases by anticoagulants*. Journal of the National Cancer Institute, 1999. **91**(1): p. 22-36.
327. Amirkhosravi, A., et al., *Assessment of Anti-Metastatic Effects of Anticoagulant and Antiplatelet Agents Using Animal Models of Experimental Lung Metastasis*. Anticoagulants, Antiplatelets, and Thrombolytics, Second Edition, 2010. **663**: p. 241-259.
328. Li, J., C.C. Sharkey, and M.R. King, *Piperlongumine and immune cytokine TRAIL synergize to promote tumor death*. Scientific reports, 2015. **5**: p. 9987.
329. Zhang, W., et al., *A humanized single-chain antibody against beta 3 integrin inhibits pulmonary metastasis by preferentially fragmenting activated platelets in the tumor microenvironment*. Blood, 2012. **120**(14): p. 2889-98.
330. Bubendorf, L., et al., *Metastatic patterns of prostate cancer: an autopsy study of 1,589 patients*. Human pathology, 2000. **31**(5): p. 578-83.
331. Minn, A.J., et al., *Genes that mediate breast cancer metastasis to lung*. Nature, 2005. **436**(7050): p. 518-524.
332. Mazumder, A. and S.A. Rosenberg, *Successful immunotherapy of natural killer-resistant established pulmonary melanoma metastases by the intravenous adoptive transfer of syngeneic lymphocytes activated in vitro by interleukin 2*. The Journal of experimental medicine, 1984. **159**(2): p. 495-507.
333. Headrick, J.R., et al., *Surgical treatment of hepatic and pulmonary metastases from colon cancer*. The Annals of thoracic surgery, 2001. **71**(3): p. 975-9; discussion 979-80.
334. Labelle, M., S. Begum, and R.O. Hynes, *Direct Signaling between Platelets and Cancer Cells Induces an Epithelial-Mesenchymal-Like Transition and Promotes Metastasis*. Cancer Cell, 2011. **20**(5): p. 576-590.
335. Liu, J., et al., *Electrostatically mediated liposome fusion and lipid exchange with a nanoparticle-supported bilayer for control of surface charge, drug containment, and delivery*. Journal of the American Chemical Society, 2009. **131**(22): p. 7567-9.
336. Richter, R., A. Mukhopadhyay, and A. Brisson, *Pathways of lipid vesicle deposition on solid surfaces: a combined QCM-D and AFM study*. Biophysical journal, 2003. **85**(5): p. 3035-47.
337. Laskin, D.L., B. Weinberger, and J.D. Laskin, *Functional heterogeneity in liver and lung macrophages*. Journal of leukocyte biology, 2001. **70**(2): p. 163-70.
338. Sobota, A., et al., *Binding of IgG-opsonized particles to Fc gamma R is an active stage of phagocytosis that involves receptor clustering and phosphorylation*. Journal of immunology, 2005. **175**(7): p. 4450-4457.

339. Martinez-Sales, V., et al., *Unstimulated and thrombin-stimulated platelets binding to immobilized fibrinogen and fibrin on polystyrene supports*. Haemostasis, 1995. **25**(4): p. 158-65.
340. Meng, H.A., et al., *Engineered Design of Mesoporous Silica Nanoparticles to Deliver Doxorubicin and P-Glycoprotein siRNA to Overcome Drug Resistance in a Cancer Cell Line*. Acs Nano, 2010. **4**(8): p. 4539-4550.
341. Decuzzi, P., et al., *Size and shape effects in the biodistribution of intravascularly injected particles*. Journal of Controlled Release, 2010. **141**(3): p. 320-327.
342. Moore, T.L., et al., *Multifunctional Polymer-Coated Carbon Nanotubes for Safe Drug Delivery*. Particle & Particle Systems Characterization, 2013. **30**(4): p. 365-373.
343. Rayavarapu, R.G., et al., *In vitro toxicity studies of polymer-coated gold nanorods*. Nanotechnology, 2010. **21**(14).
344. Volkmann, X., et al., *Increased hepatotoxicity of tumor necrosis factor-related apoptosis-inducing ligand in diseased human liver*. Hepatology, 2007. **46**(5): p. 1498-508.
345. Zheng, S.J., et al., *Critical roles of TRAIL in hepatic cell death and hepatic inflammation*. The Journal of clinical investigation, 2004. **113**(1): p. 58-64.
346. Erpenbeck, L. and M.P. Schon, *Deadly allies: the fatal interplay between platelets and metastasizing cancer cells*. Blood, 2010. **115**(17): p. 3427-3436.
347. Modery-Pawlowski, C.L. and A.S. Gupta, *Heteromultivalent ligand-decoration for actively targeted nanomedicine*. Biomaterials, 2014. **35**(9): p. 2568-79.
348. Modery-Pawlowski, C.L., et al., *A platelet-mimetic paradigm for metastasis-targeted nanomedicine platforms*. Biomacromolecules, 2013. **14**(3): p. 910-9.
349. Immordino, M.L., F. Dosio, and L. Cattel, *Stealth liposomes: review of the basic science, rationale, and clinical applications, existing and potential*. International Journal of Nanomedicine, 2006. **1**(3): p. 297-315.
350. Oldenborg, P.A., et al., *Role of CD47 as a marker of self on red blood cells*. Science, 2000. **288**(5473): p. 2051-+.
351. Rodriguez, P.L., et al., *Minimal "Self" Peptides That Inhibit Phagocytic Clearance and Enhance Delivery of Nanoparticles*. Science, 2013. **339**(6122): p. 971-975.
352. van de Ven, A.L., et al., *Rapid tumoritropic accumulation of systemically injected plateloid particles and their biodistribution*. Journal of Controlled Release, 2012. **158**(1): p. 148-155.
353. Brown, A.C., et al., *Ultrasoft microgels displaying emergent platelet-like behaviours*. Nature materials, 2014. **13**(12): p. 1108-14.
354. Massa, P.E., et al., *Salmonella engineered to express CD20-targeting antibodies and a drug-converting enzyme can eradicate human lymphomas*. Blood, 2013. **122**(5): p. 705-14.
355. Stuckey, D.W. and K. Shah, *Stem cell-based therapies for cancer treatment: separating hope from hype*. Nature reviews. Cancer, 2014. **14**(10): p. 683-91.
356. Kauer, T.M., et al., *Encapsulated therapeutic stem cells implanted in the tumor*

resection cavity induce cell death in gliomas. Nature neuroscience, 2012. **15**(2): p. 197-204.
357. Balyasnikova, I.V., et al., *Intranasal Delivery of Mesenchymal Stem Cells Significantly Extends Survival of Irradiated Mice with Experimental Brain Tumors*. Molecular Therapy, 2014. **22**(1): p. 140-148.
358. Nakamizo, A., et al., *Human bone marrow-derived mesenchymal stem cells in the treatment of gliomas*. Cancer research, 2005. **65**(8): p. 3307-3318.
359. Liu, S.C., et al., *Anticancer efficacy of systemically delivered anaerobic bacteria as gene therapy vectors targeting tumor hypoxia/necrosis*. Gene Therapy, 2002. **9**(4): p. 291-296.
360. Daly, M.E., *Determinants of platelet count in humans*. Haematologica-the Hematology Journal, 2011. **96**(1): p. 10-13.
361. Deng, Q., et al., *TRAIL-secreting mesenchymal stem cells promote apoptosis in heat-shock-treated liver cancer cells and inhibit tumor growth in nude mice*. Gene Therapy, 2014. **21**(3): p. 317-27.
362. Loebinger, M.R., et al., *Mesenchymal Stem Cell Delivery of TRAIL Can Eliminate Metastatic Cancer*. Cancer research, 2009. **69**(10): p. 4134-4142.
363. Kopp, H.G., T. Placke, and H.R. Salih, *Platelet-derived transforming growth factor-beta down-regulates NKG2D thereby inhibiting natural killer cell antitumor reactivity*. Cancer research, 2009. **69**(19): p. 7775-83.
364. Wagner, K.W., et al., *Death-receptor O-glycosylation controls tumor-cell sensitivity to the proapoptotic ligand Apo2L/TRAIL*. Nature medicine, 2007. **13**(9): p. 1070-7.
365. Phipps, L.E., S. Hino, and R.J. Muschel, *Targeting cell spreading: a method of sensitizing metastatic tumor cells to TRAIL-induced apoptosis*. Molecular cancer research : MCR, 2011. **9**(3): p. 249-58.
366. Fang, J., et al., *Platelet gene therapy improves hemostatic function for integrin alphaIIbbeta3-deficient dogs*. Proceedings of the National Academy of Sciences of the United States of America, 2011. **108**(23): p. 9583-8.
367. Shi, Q., et al., *Lentivirus-mediated platelet-derived factor VIII gene therapy in murine haemophilia A*. Journal of Thrombosis and Haemostasis, 2007. **5**(2): p. 352-361.
368. Kuether, E.L., et al., *Lentivirus-mediated platelet gene therapy of murine hemophilia A with pre-existing anti-factor VIII immunity*. Journal of Thrombosis and Haemostasis, 2012. **10**(8): p. 1570-1580.
369. Biffi, A., et al., *Lentiviral hematopoietic stem cell gene therapy benefits metachromatic leukodystrophy*. Science, 2013. **341**(6148): p. 1233158.
370. Aiuti, A., et al., *Lentiviral hematopoietic stem cell gene therapy in patients with Wiskott-Aldrich syndrome*. Science, 2013. **341**(6148): p. 1233151.
371. Wilcox, D.A., et al., *Integrin alphaIIb promoter-targeted expression of gene products in megakaryocytes derived from retrovirus-transduced human hematopoietic cells*. Proceedings of the National Academy of Sciences of the United States of America, 1999. **96**(17): p. 9654-9.
372. Lois, C., et al., *Germline transmission and tissue-specific expression of transgenes delivered by lentiviral vectors*. Science, 2002. **295**(5556): p. 868-

72.
373. Fong, A.M. and S.A. Santoro, *Transcriptional regulation of alpha IIb integrin gene expression during megakaryocytic differentiation of K562 cells. Role of a silencer element*. The Journal of biological chemistry, 1994. **269**(28): p. 18441-7.
374. Zutter, M.M., et al., *Regulation of alpha 2 integrin gene expression in cells with megakaryocytic features: a common theme of three necessary elements*. Blood, 1995. **86**(8): p. 3006-14.
375. Lev, P.R., et al., *Production of functional platelet-like particles by the megakaryoblastic DAMI cell line provides a model for platelet biogenesis*. Platelets, 2011. **22**(1): p. 28-38.
376. Takeuchi, K., et al., *Production of platelet-like particles by a human megakaryoblastic leukemia cell line (MEG-01)*. Experimental cell research, 1991. **193**(1): p. 223-6.
377. Sahler, J., et al., *A novel method for overexpression of peroxisome proliferator-activated receptor-gamma in megakaryocyte and platelet microparticles achieves transcellular signaling*. Journal of thrombosis and haemostasis : JTH, 2012. **10**(12): p. 2563-72.
378. Corazza, N., et al., *TRAIL and immunity: more than a license to kill tumor cells*. Cell Death and Differentiation, 2004. **11**: p. S122-S125.
379. Elting, L.S., et al., *Incidence, cost, and outcomes of bleeding and chemotherapy dose modification among solid tumor patients with chemotherapy-induced thrombocytopenia*. Journal of Clinical Oncology, 2001. **19**(4): p. 1137-1146.
380. Benjamin, R.J. and K.C. Anderson, *What is the proper threshold for platelet transfusion in patients with chemotherapy-induced thrombocytopenia?* Critical Reviews in Oncology Hematology, 2002. **42**(2): p. 163-171.
381. Ringden, O., *Allogeneic bone marrow transplantation for hematological malignancies - Controversies and recent advances*. Acta Oncologica, 1997. **36**(6): p. 549-564.
382. Fuentes, R., et al., *Infusion of mature megakaryocytes into mice yields functional platelets*. Journal of Clinical Investigation, 2010. **120**(11): p. 3917-3922.
383. Lambert, M.P., et al., *Challenges and promises for the development of donor-independent platelet transfusions*. Blood, 2013. **121**(17): p. 3319-3324.
384. Kawamoto, M., et al., *A novel transferrin receptor-targeted hybrid peptide disintegrates cancer cell membrane to induce rapid killing of cancer cells*. Bmc Cancer, 2011. **11**.
385. Wu, D.D., et al., *Peptide-based cancer therapy: Opportunity and challenge*. Cancer Letters, 2014. **351**(1): p. 13-22.